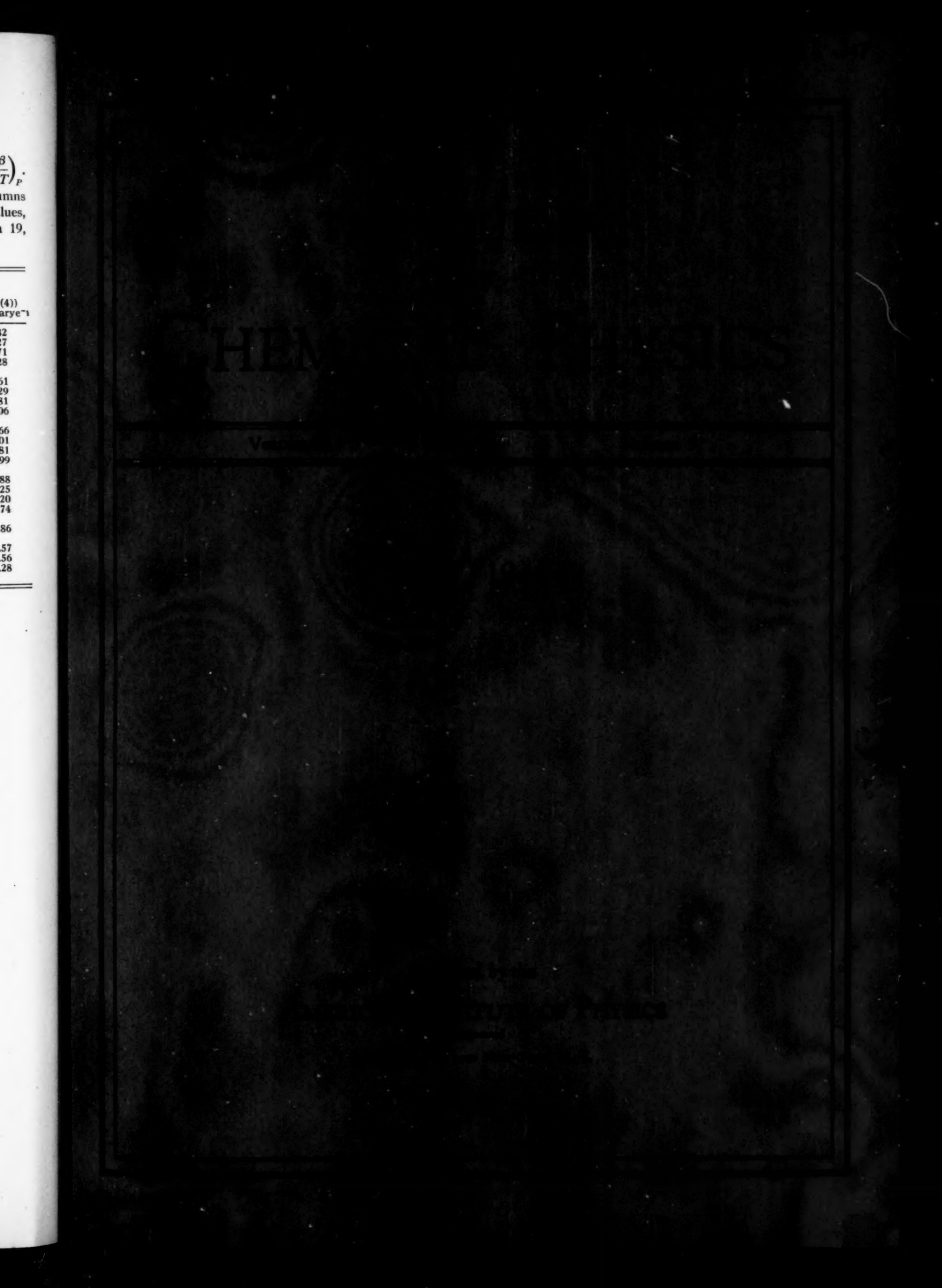

...CAL ...ICS

...

...

...

THE JOURNAL
OF
CHEMICAL PHYSICS

VOLUME 15, NUMBER 5 MAY, 1947

The Interpretation of Electron Diffraction Patterns from Hydrocarbon Films*

J. KARLE
U. S. Naval Research Laboratory, Washington, D. C.

AND

L. O. BROCKWAY
University of Michigan, Ann Arbor, Michigan

(Received January 7, 1947)

The theoretical expressions previously derived for the scattering of electrons by oriented hydrocarbon chains have been extended and applied to the calculation of characteristic diffraction patterns. These patterns are analyzed to form a basis for obtaining information about the molecular orientation. For the long chain molecules, the azimuthal direction, and the declination from the vertical may be determined independently. The orientation of the hydrocarbon chain about its own axis is less easily established, since it is determined only from the intensity distribution within the separate diffraction orders. When the declination is sufficiently large, randomness in the azimuthal directions is distinguished by the crossed-line pattern obtained. Randomness in the declination from the vertical may be estimated from the irregular spacing of the intercepts of the crossed lines. Quantitative intensity data would permit a more precise study of the angular distribution of the declination, and also of the orientation of the hydrocarbon chain about its own axis.

THE formation of films of close packed long-chain molecules on a water surface by the Langmuir technique has been known for some time, but the recent studies by Zisman *et al.*[1] of the oleophobic properties of films formed on solid surfaces by adsorption of long-chain molecules from dilute solutions have indicated the importance of adsorbed films in relation to lubrication and corrosion inhibition problems. Since the unique properties of adsorbed films of long-chain molecules appear to be related to the molecular orientations in the films, it was considered valuable to pursue an investigation of the structure of these films with the aid of electron diffraction. Several types of diffraction patterns characteristic of hydrocarbon films have already been observed,[2] and the present paper considers the detailed analysis of typical photographs in terms of the orientation of the molecules, including the effects of randomness.

The theoretical scattering functions have been

* This report concerns part of a study of films on metals authorized by the Chemistry Division of the Naval Research Laboratory under Contract No. N173s-10452 (June 15, 1945), and undertaken at the University of Michigan under the direction of the Department of Engineering Research, Project M639. The investigations included here were completed at the Naval Research Laboratory under Project No. N2002BR.

[1] W. C. Bigelow, D. L. Pickett, and W. A. Zisman, "Oleophobic Monolayers; Part I, Films Adsorbed from Solution in Non-Polar Liquids," J. Colloid Sci. 1, 513 (1946); Part II, "Effect of Temperature on Adsorption," to be published.

[2] L. O. Brockway and J. Karle, "Electron Diffraction Study of Oleophobic Films on Copper, Iron and Aluminum," to be published in J. Colloid Sci.; L. O. Brockway and R. L. Livingston," Electron Diffraction Study of Oleophobic Films on Platinum," to be published.

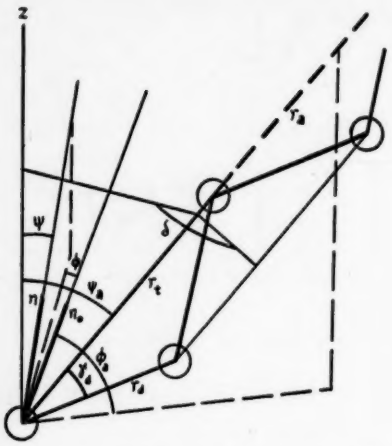

FIG. 1. The orientation of the hydrocarbon chain is determined by angles ψ_a, ϕ_a, and δ. Also shown are the internal structural parameters r_t, r_d, and γ_d, the main beam, $\bar{n}_0$, and the deviated beam, $\bar{n}$, with its polar coordinates ψ and ϕ.

developed for several cases,[3] and they are used here in the calculation of intensity contour maps which show the appearance of patterns corresponding to several different orientations. The results and conclusions based on these maps are presented below.

CALCULATION OF MAPS

The carbon atoms in the long-chain hydrocarbon molecules comprising an adsorbed film form a staggered chain and are assumed to be coplanar. There are therefore two parallel rows of carbon atoms in each chain. We may consider the row which contains the carbon atom closest to the surface as the axis of the molecule, $\bar{r}_a$ (see Fig. 1). ψ_a is the angle defining the tilt of this axis from a normal to the surface of attachment, z, and ϕ_a the angle of rotation of the $\bar{r}_a z$ plane from the $\bar{n}_0 z$ plane which is normal to the photographic plate. The angle, δ, measures the rotation of the plane of the carbon atoms about axis $\bar{r}_a$ from the $\bar{r}_a z$ plane. The orientation of the hydrocarbon chain is completely described by angles ψ_a, ϕ_a, and δ.

The internal structural parameters of the chain are r_t, the spacing of the carbon atoms along a row, r_d, the C−C bonded distance and γ_d the angle between them. Owing to the regularity of the structure of the carbon chain only two of these parameters are independent. The coordinates of a point on the scattered beam, $\bar{n}$, are: (1) r, its radial extension into space; (2) ψ, the tilt of $\bar{n}$ from the vertical axis, z; and (3) ϕ, the rotation of the $\bar{n}z$ plane from the $\bar{n}_0 z$ plane. The value of r is practically invariant over the area of a photographic plate ordinarily considered.

A formula for the intensity of electron scattering from a hydrocarbon chain must contain the orientation parameters (ψ_a, ϕ_a, and δ), the internal structural parameters (r_t and γ_d), and the coordinates of a point on the scattered beam (ψ, ϕ, and r). The formulae previously derived[3] concern various configurations of the carbon chains on the surface of attachment, that is to say special cases regarding the orientation parameters. The assumption was made in deriving the formulae that the electron scattering from the hydrogen atoms on the hydrocarbon chain is negligible. In addition the distribution of the molecules in the film was considered to be sufficiently irregular so that there arises no detectable inter-molecular interaction. In performing the calculations the value used for the bonded carbon to carbon distance in the chain was 1.54A, and the bond angle was given the regular tetrahedral value. The number of atoms in the chain, N, was assumed equal to sixteen, the value of the wave-length of the electrons, λ, equal to 0.07A, and the distance of the point of scattering from the origin of the photographic plate, L, equal to 35 cm. In the first four cases the angle of tilt of the molecular axis from the vertical to the surface was set equal to 20°, and in the fifth case it assumed random values. The formulae were expressed for convenience in terms of the cartesian coordinates x and y defined for a photographic plate by using relations (8) and (9) in reference (3). The point at which the main beam strikes is considered to be the origin, y is the axis parallel to the surface normal, z, and x is the axis parallel to the plane of the supporting surface. The intensity of electron scattering was calculated on an arbitrary scale for the contour maps and the first three orders were obtained.

The values of sines and cosines were obtained from *Tables of Sines and Cosines for Radian Arguments*, Federal Works Agency, Works Projects Administration, Project No. 765-97-3-10, New

[3] J. Karle, J. Chem. Phys. **14**, 297 (1946).

York, 1940. The values of the Bessel functions were obtained from: (a) British Association for the Advancement of Science, Mathematical Tables, Volume VI Bessel Functions, Part I Functions of orders O and unity, University Press, Cambridge, 1931; (b) G. N. Watson, *Bessel Functions* (The Macmillan Company, New York, 1944), p. 730; (c) Gray, Mathews and MacRobert, *A Treatise on Bessel Functions* (The Macmillan Company, New York, 1931), p. 286.

Case I

The molecules are fixed in space and, accordingly, angles ψ_a, ϕ_a, and δ are given specific arbitrary values. The formula for this case is

$$\frac{f_c^2 \sin^2(Nsr_t \cos\alpha_a/4)}{r^2 \sin^2(sr_t \cos\alpha_a/2)}[1+\cos(sr_d \cos\alpha_d)], \quad (1)$$

where

$$\cos\alpha_a = \cos\psi_n \cos\psi_a + \sin\psi_n \sin\psi_a \cos(\phi_a - \phi_n),$$

$$\cos\alpha_d = \cos\alpha_a \cos\gamma_d + \sin\gamma_d \cos\beta \cos\delta - \sin\gamma_d \sin\psi_n \sin(\phi_a - \phi_n) \sin\delta,$$

$$\cos\beta = \cos\psi_n \sin\psi_a - \sin\psi_n \cos\psi_a \cos(\phi_a - \phi_n),$$

$$s = 2\pi|\bar{n} - \bar{n}_0|/\lambda, \; f_c = (6 - F_c)/s^2,$$

and N, the total number of carbon atoms in the chain, is necessarily even when using (1). λ is the electron wave-length dependent upon the voltage, and F_c is the scattering factor of carbon for x-rays, which is tabulated.[4] The angle ψ_n is the tilt of the $\bar{n} - \bar{n}_0$ vector from the surface normal, z, and angle ϕ_n measures the rotation of the $(\bar{n} - \bar{n}_0)z$ plane from the $\bar{n}_0 z$ plane. The model chosen for Case I was given a rotation out of the $\bar{n}_0 z$ plane (angle ϕ_a) equal to 45°. The second row of carbon atoms was considered to hang down from axis $\bar{r}_a$, and therefore angle δ was set equal to 180°. The result is shown in Fig. 2.

The distribution of intensity along the first and second orders was studied as a function of the rotation of the molecular plane in two auxiliary calculations. For a molecule with

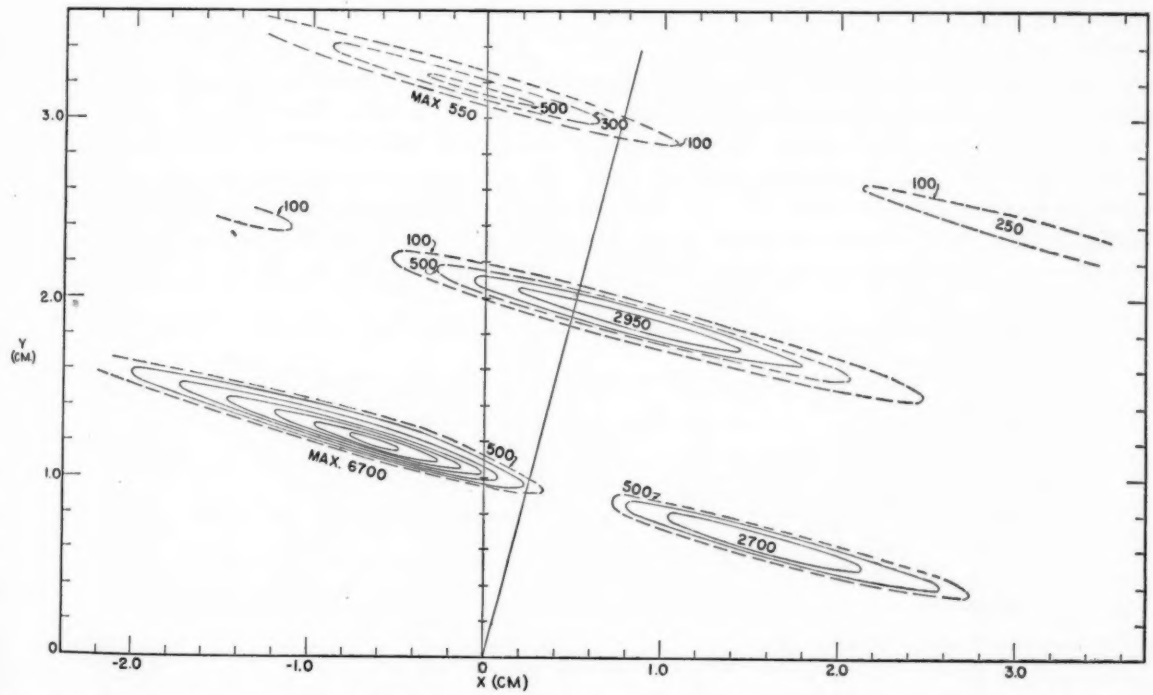

FIG. 2. Calculated pattern for Case I (formula 1). Angles $\psi_a = 20°$, $\phi_a = 45°$, and $\delta = 180°$. The solid contours are spaced by 1000 on the arbitrary scale. The line perpendicular to the successive orders is the projection of the molecular axis. The maxima of the intensity contours are indicated.

[4] *Internationale Tabellen Zur Bestimmung Von Kristallsstrukturen* (J. W. Edwards, Ann Arbor, Michigan, 1944), revised edition, Vol. II, p. 571.

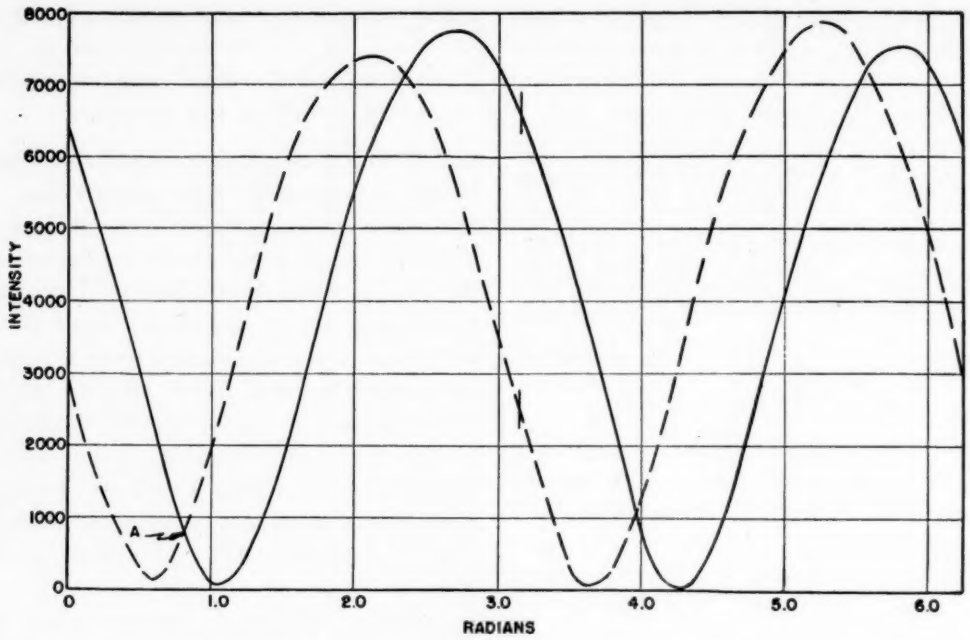

FIG. 3. Variation of intensity for two points placed symmetrically about projection of molecular axis in first order of Case I ($\psi_a=20°$ and $\phi_a=45°$) as δ varies from 0 to 2π. For solid line, $x=-0.62$, $y=1.19$ and for dotted line, $x=1.12$ and $y=0.74$. Point A corresponds to the value of δ for which the plane of the hydrocarbon chain is perpendicular to the photographic plate. Vertical lines are placed at $\delta=180°$, the value in Fig. 2.

$\psi_a=20°$ and $\phi_a=45°$ (as in Case I), the intensity was calculated at two points lying in the first order at equal distances from the projection of the molecular axis ($x=-0.62$, $y=1.19$ and $x=1.12$, $y=0.74$). The intensity at these two points is plotted as a function of δ in Fig. 3. Similar results for the second order ($x=0.30$, $y=1.97$; $x=0.70$, $y=1.87$) are shown in Fig. 4.

The effect of rotating the molecule about $\bar{r}_a$ was also calculated for the special case of a vertical molecule. Distributions along the first and second orders were obtained for the plane of the carbon chain both parallel and perpendicular to the photographic plate. An additional calculation was made for the first order distribution when the plane of the chain is tilted 45° to the

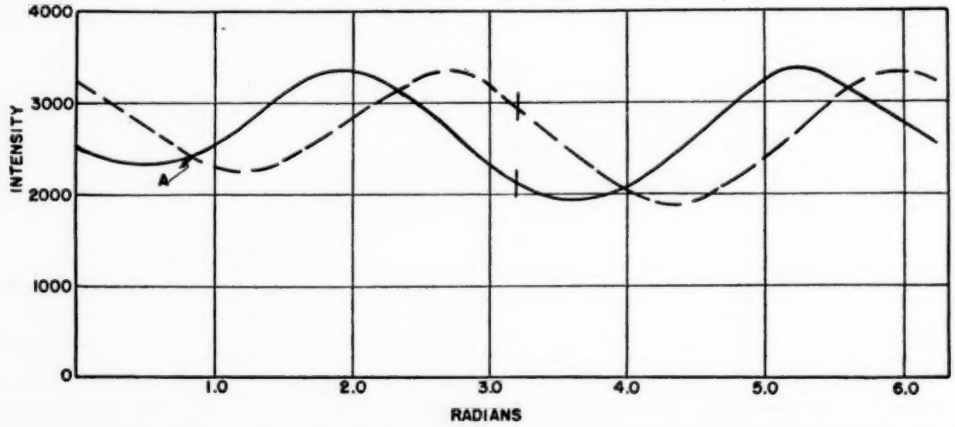

FIG. 4. Variation of intensity for two points placed symmetrically about projection of molecular axis in second order of Case I ($\psi_a=20°$ and $\phi_a=45°$) as δ varies from 0 to 2π. For solid line, $x=0.30$, $y=1.97$ and for dotted line $x=0.70$, $y=1.87$. Point A and the vertical markers have the same significance as in Fig. 3.

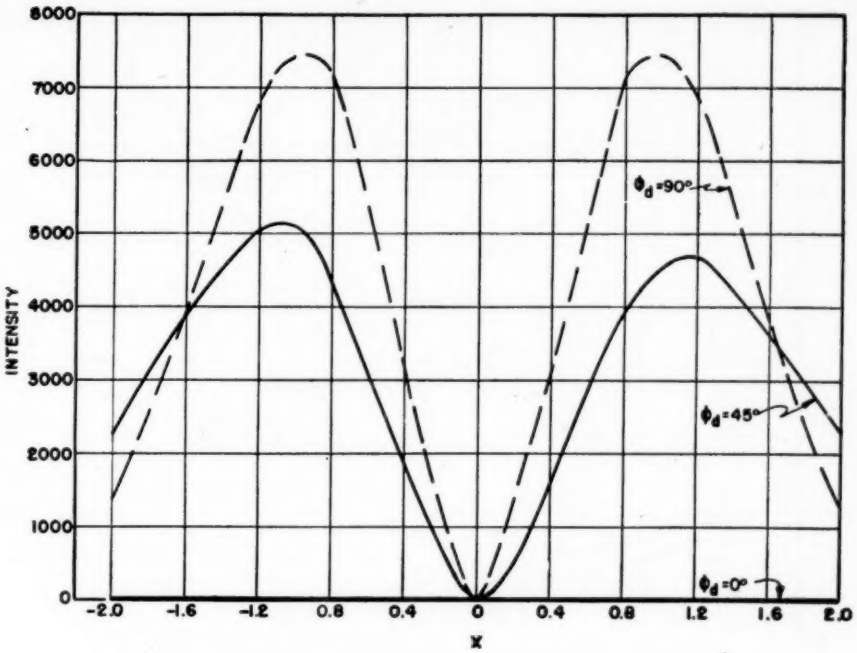

FIG. 5. Variation of intensity in first order for molecule with axis vertical and the indicated values for the orientation of the plane of the carbon chain (see text concerning ϕ_d).

photographic plate. The formula used is

$$\frac{f_e^2 \sin^2(Nsr_t \cos\psi_n/4)}{r^2 \sin^2(sr_t \cos\psi_n/2)} \times[1+\cos(r_d s \cos\psi_n \cos\gamma_d + r_d s \sin\psi_n \sin\gamma_d \cos(\phi_n-\phi_d))], \quad (2)$$

where ϕ_d measures the rotation of the plane of the molecule from the $\bar{n}_0 z$ plane. (Angle ϕ_d determines the orientation of the plane of the chain for a vertical molecule just as angle δ serves for the general case. It is necessary though to distinguish between the two since they are not similarly defined.) In performing the calculation, the value of y for which the ratio of the sine squared terms is a maximum was determined, and then the values of the function were calculated for varying values of x and the latter value of y. For the calculations in this article, the values 0°, 45° and 90° were chosen for angle ϕ_d. The results are shown in Figs. 5 and 6.

Case II

The axes of the molecules in a film are fixed in space, and the planes of the carbon chains

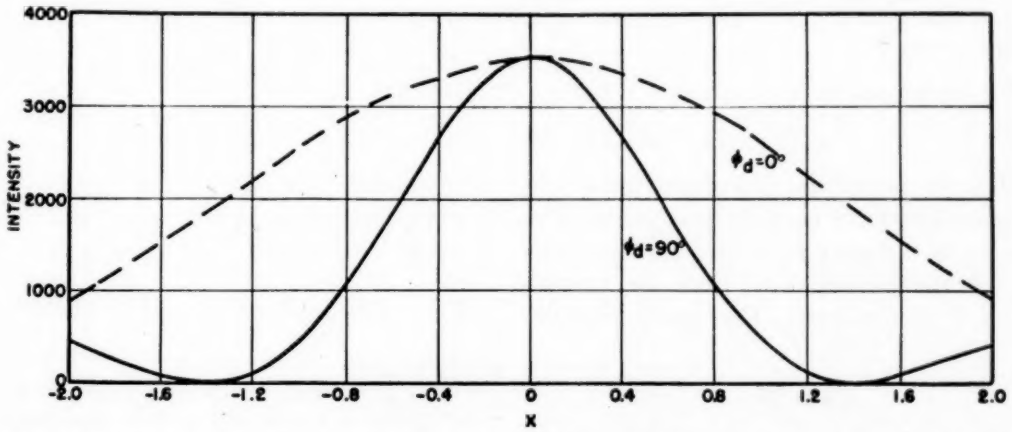

FIG. 6. Variation of intensity in second order for molecule with axis vertical and the indicated values for the orientation of the plane of the carbon chain.

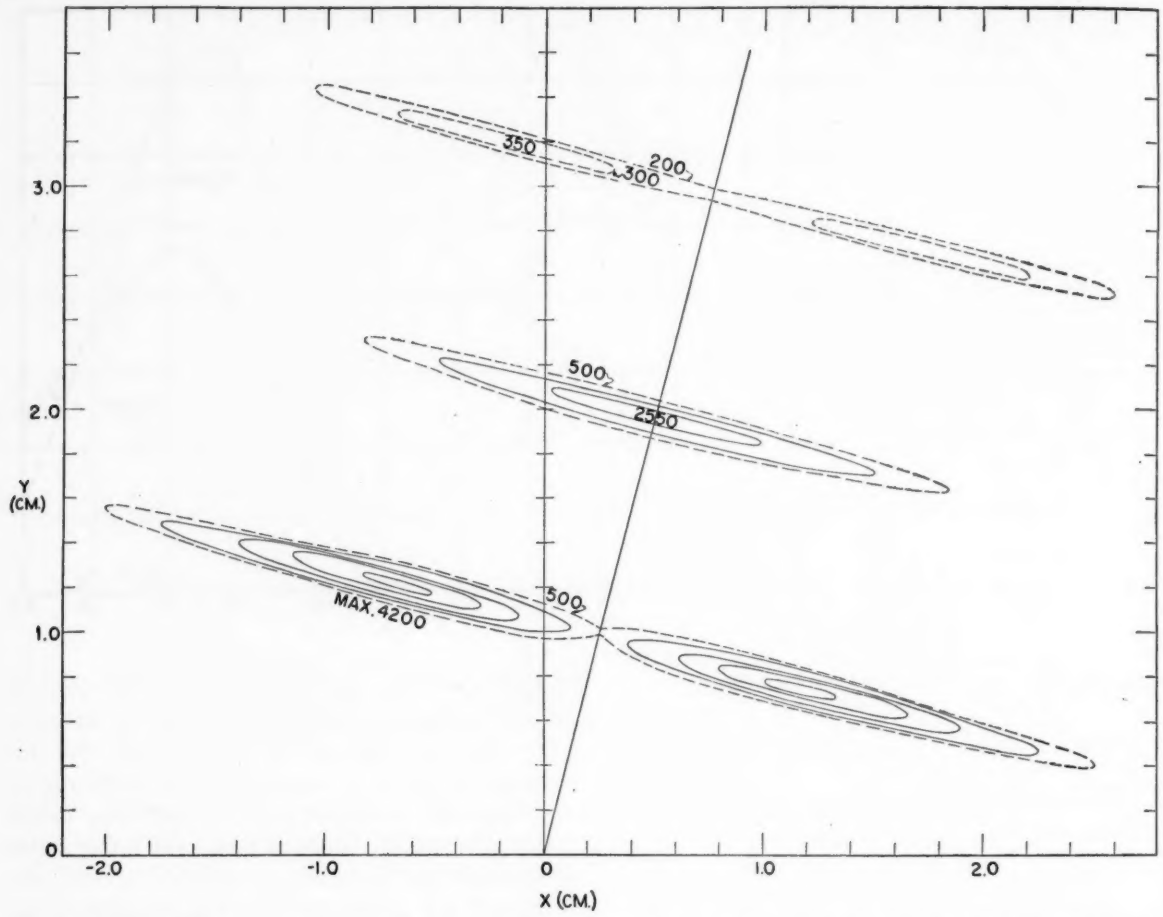

FIG. 7. Calculated pattern for Case II (formula 3). Angles $\psi_a = 20°$, $\phi_a = 45°$, and δ is random. The solid contours are spaced by 1000 on the arbitrary scale. The projection of the molecular axis and the maxima of the intensity contours are indicated.

assume random positions about these axes. The formula used is:

$$\frac{f_c^2 \sin^2(Nsr_t \cos\alpha_a/4)}{r^2 \sin^2(sr_t \cos\alpha_a/2)} \times[1+\cos(sr_d \cos\gamma_d \cos\alpha_a) \times J_0(sr_d \sin\gamma_d \sin\alpha_a)], \quad (3)$$

where J_0 is the Bessel function of zero order. The other quantities have been defined above. This calculation is different from the first one only insofar as the contribution from all possible values of δ is considered. The result is shown in Fig. 7.

Case III

The tilt of the molecular axes and the orientation of the planes of the carbon chains are arbitrarily specified. The molecules, however, assume random positions about the surface normal, z. The formula used is

$$\frac{Nf_c^2}{2r^2}+\frac{f_c^2}{r^2}\sum_{\nu=1}^{(N-2)/2} 2\nu \cos[(N/2-\nu)A] \times J_0[(N/2-\nu)B] + \frac{f_c^2}{r^2}\sum_{\mu=1}^{N/2} \mu \cos[([N+1]/2-\mu)A+C] \times J_0[([(N+1)/2-\mu]B-D)^2+E^2]^{\frac{1}{2}} + \frac{f_c^2}{r^2}\sum_{\lambda=1}^{(N-2)/2} \lambda \cos[-([N-1]/2-\lambda)A+C] \times J_0[([(N-1)/2-\lambda]B-D)^2+E^2]^{\frac{1}{2}}, \quad (4)$$

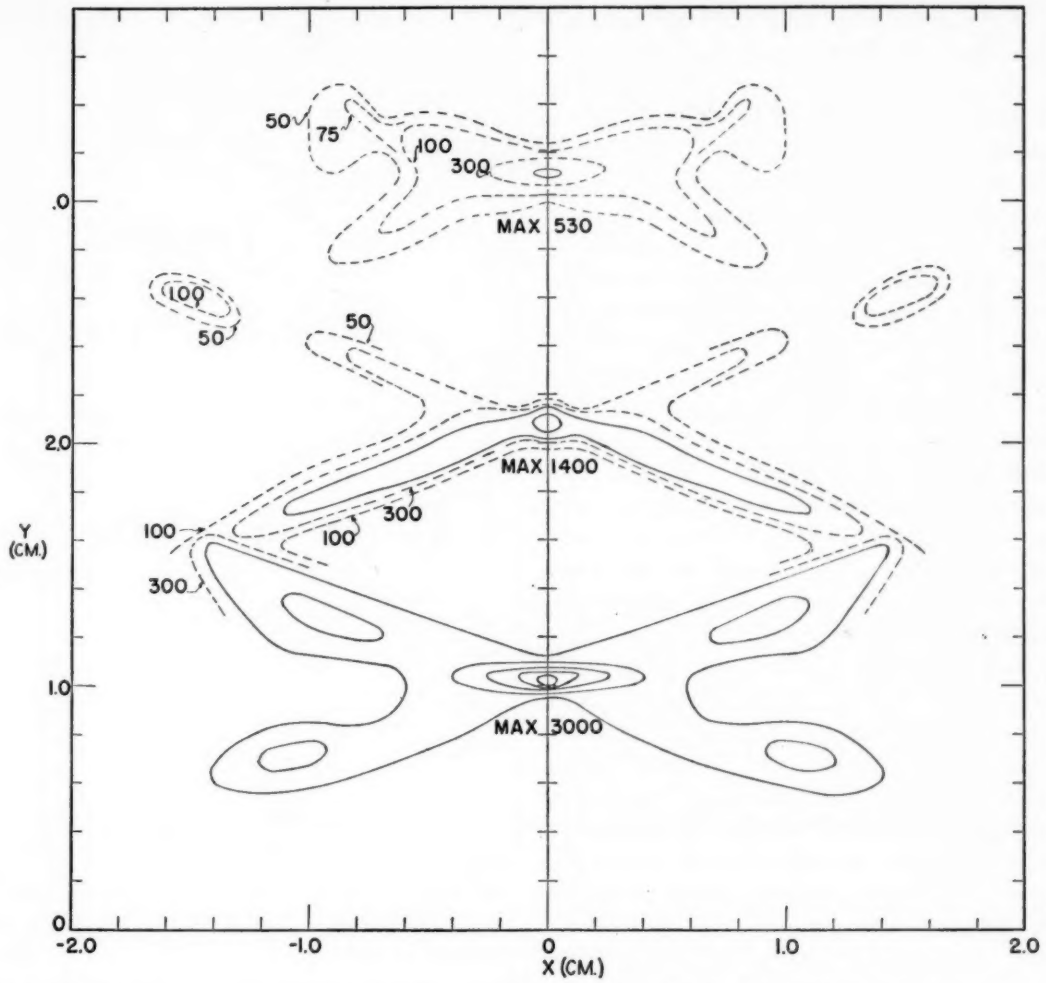

FIG. 8. Calculated pattern for Case III (formula 4). Angles $\psi_a = 20°$, $\delta = 180°$, and angle ϕ_a is random. The solid contours are spaced by 500.

where

$$A = r_t \cos\psi_a s \cos\psi_n,$$
$$B = r_t \sin\psi_a s \sin\psi_n,$$
$$C = r_0 \sin\psi_a s \cos\psi_n \cos\delta,$$
$$D = r_0 \cos\psi_a s \sin\psi_n \cos\delta,$$
$$E = r_0 s \sin\psi_n \sin\delta.$$

This calculation differs from the first one in that the contribution from all possible values of ϕ_a is considered. The result is shown in Fig. 8.

Case IV

The tilt of the axes of the molecules is arbitrarily specified. The molecules are randomly distributed about the surface normal, z, and also about their own axes. The formula used is

$$\frac{Nf_c^2}{2r^2} + \frac{f_c^2}{r^2} \sum_{\nu=1}^{(N-2)/2} 2\nu \cos[(N/2-\nu)A] \times J_0[(N/2-\nu)B]$$
$$+ \frac{f_c^2}{\mu^2} \sum_{\mu=1}^{N/2} (2\mu-1) \cos[([N+1]/2-\mu)A] \times \sum_{m=0}^{\infty} (-1)^m \epsilon_m J_{2m}(sr_0a) J_{2m}(sr_0b) \times J_{2m}[([N+1]/2-\mu)B]$$
$$+ \frac{f_c^2}{r^2} \sum_{\mu=1}^{N/2} (2\mu-1) \sin[([N+1]/2-\mu)A] \times \sum_{m=0}^{\infty} (-1)^{m+1} 2 J_{2m+1}(sr_0a) \times J_{2m+1}(sr_0b) J_{2m+1}[([N+1]/2-\mu)B], \quad (5)$$

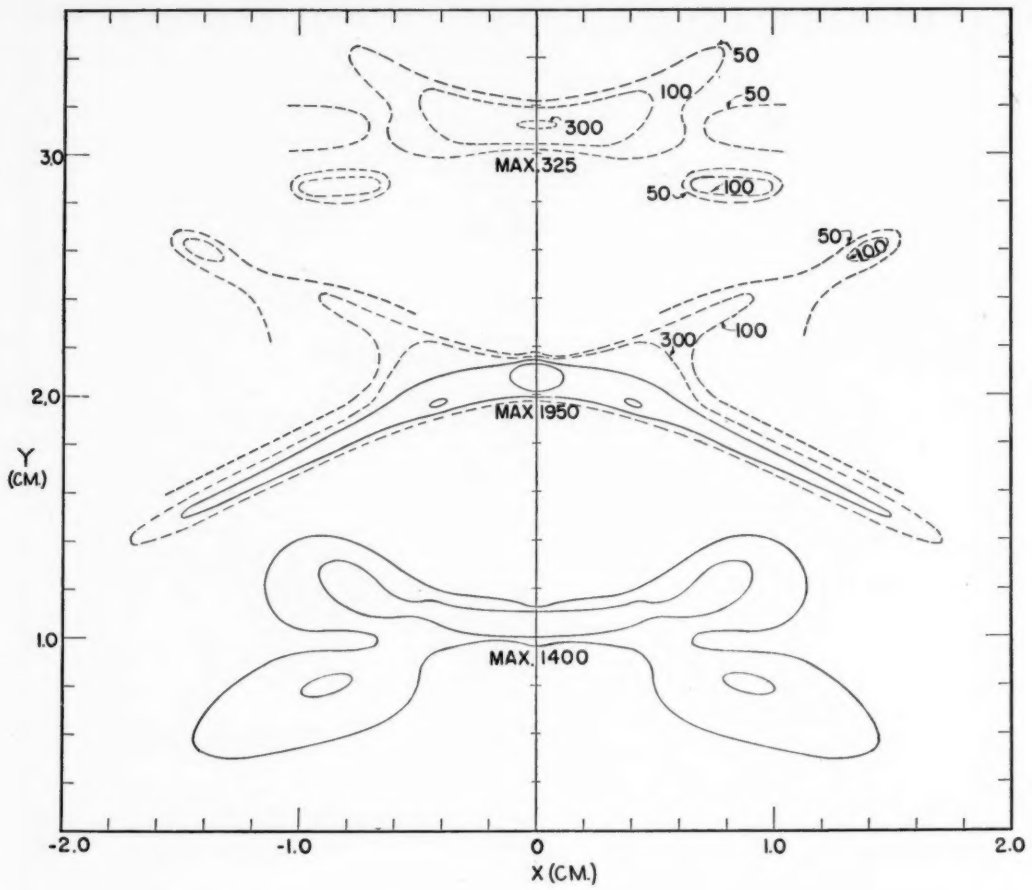

FIG. 9. Calculated pattern for Case IV (formula 5). Angle $\psi_a = 20°$, and angles ϕ_a and δ are random. The solid contours are spaced by 500.

where

$$a^2 = [P + (P^2 - Q^2)^{\frac{1}{2}}]/2,$$
$$b^2 = Q^2/[2P + 2(P^2 - Q^2)^{\frac{1}{2}}],$$
$$P = 1 - \cos^2\psi_n \cos^2\psi_a,$$
$$Q = 2\cos\psi_n \cos\psi_a \sin\psi_n \sin\psi_a,$$

$\epsilon_m = 1$ when $m = 0$, $\epsilon_m = 2$ when $m \neq 0$, and J_n is the Bessel function of order n. This calculation differs from the second one in that the contribution from all possible values of ϕ_a is considered. The result is shown in Fig. 9.

Case V

The first four calculations given in detail in reference (3) were based on various orientations in which the tilt of the molecular axis remained fixed. The effect of a variation in angle ψ_a on the position of the y-intercept of successive orders was of particular interest since it was observed that the spacings varied in some photographs. This variation was introduced into formula (4) of Case III by inserting approximations which are valid in the vicinity of the y axis and then averaging over all values of ψ_a, from 0 to 20° using the assumption that all values of ψ_a in this range are equally probable. The calculation was restricted to points along the y axis including the first four orders.

As in Case III angle δ was set equal to 180°, $N = 16$, $\lambda = 0.07$A, and $L = 35$ cm. In addition the J_0 were set equal to unity since $\sin\psi_n$ is almost zero for the region of the y axis under consideration. We may write $\cos\psi_a - 1 = \psi_a^2/2$, and $\sin\psi_a = \psi_a$ in formula (4) and then average this expression over ψ_a from 0 to 20°. The result is

$$\frac{8f_c^2}{r^2}+\frac{f_c^2}{r^2}\sum_{\nu=1}^{7}\frac{2\nu}{G}\Big(\cos H\int_0^G \cos\phi^2 d\phi + \sin H\int_0^G \sin\phi^2 d\phi\Big)$$

$$+\frac{f_c^2}{r^2}\sum_{\mu=1}^{8}\frac{\mu}{J}\Big(\cos[K+L]\int_{L^{\frac{1}{2}}}^{J+L^{\frac{1}{2}}} \cos\phi^2 d\phi + \sin[K+L]\int_{L^{\frac{1}{2}}}^{J+L^{\frac{1}{2}}} \sin\phi^2 d\phi\Big)$$

$$+\frac{f_c^2}{r^2}\sum_{\omega=1}^{7}\frac{\omega}{M}\Big(\cos[N+P]\int_{-P^{\frac{1}{2}}}^{M-P^{\frac{1}{2}}} \cos\phi^2 d\phi + \sin[N+P]\int_{-P^{\frac{1}{2}}}^{M-P^{\frac{1}{2}}} \sin\phi^2 d\phi\Big), \quad (6)$$

where

$$G=\pi(H/2)^{\frac{1}{2}}/9,$$
$$H=(8-\nu)r_t s\cos\psi_n,$$
$$J=\pi(K/2)^{\frac{1}{2}}/9,$$
$$K=(8.5-\mu)r_t s\cos\psi_n,$$
$$L=(r_0 s\cos\psi_n)^2/2K,$$
$$M=\pi(N/2)^{\frac{1}{2}}/9,$$
$$N=(7.5-\omega)r_t s\cos\psi_n,$$
$$P=(r_0 s\cos\psi_n)^2/2N.$$

The integrals involved were calculated from the related Fresnel integrals.[5] The result is shown in Fig. 10.

DISCUSSION OF CONTOUR MAPS

The contour diagrams of the intensities, all plotted on the same arbitrary scale, are shown in Figs. 2, 7, 8 and 9. The pattern in Fig. 2 from an oriented molecule shows the expected concentration of scattered electrons along a series of parallel lines normal to the projection of the molecular axis. The intensity distribution in the successive orders is characteristic of the double row of atoms in which the second is displaced relative to the first by half the identity distance along the row. The pattern from a single row of carbon atoms would show parallel lines in the same positions, but with intensity decreasing with increasing distance from the main beam, as required by the atomic scattering factor. The odd orders in Fig. 2 show a minimum near the projection of the molecular axis, and the even orders show a maximum, but the value chosen for the angle δ causes these minima and maxima to lie off the axis, with a generally asymmetric intensity distribution. In the first order the intensity on the left of the axis reaches a value about twice as great as that on the right.

In Fig. 7 calculated for random values of δ, the intensity pattern is symmetric about the projection of the molecular axis. It is therefore clear that as the value of δ changes, the intensity distribution along the layer lines varies. This is depicted in Figs. 3 and 4. It is seen that the

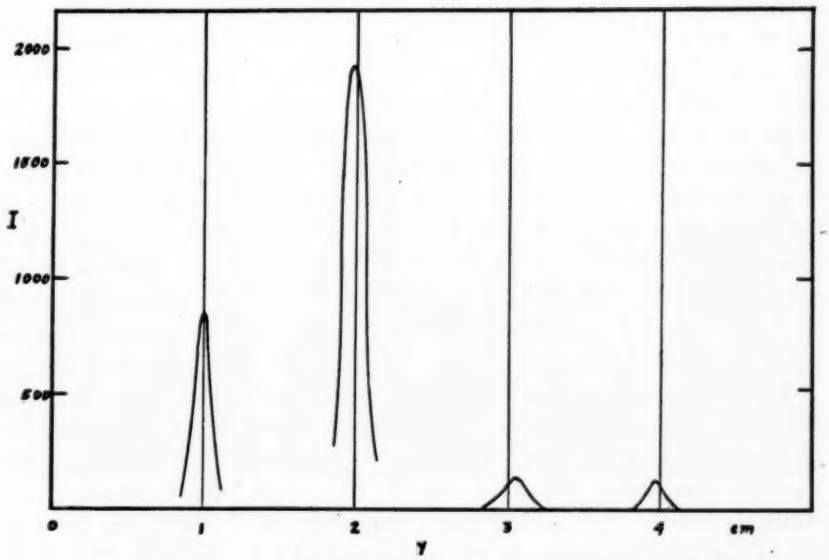

FIG. 10. Calculated pattern for Case V (formula 6). The variation of the intensity is shown along the y axis in the vicinity of the maxima of the first four orders. Angle $\delta=180°$, ϕ_a is random, and ψ_a varies from 0° to 20°.

[5] British Association for the Advancement of Science, *Calculation of Mathematical Tables*, 273 (1926).

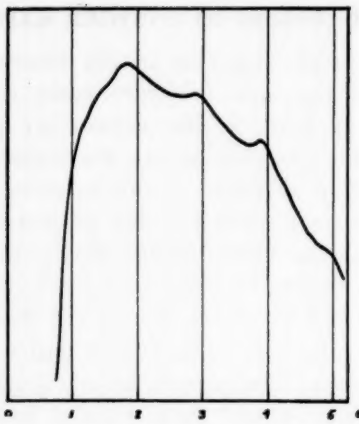

FIG. 11. Microphotometer trace of Fig. 12 along y axis showing difference in spacing between second and third, and third and fourth maxima. Position of main beam is altered by refraction.

variations in the first order are larger than those in the second order, and that the intensities at points symmetrically placed with respect to the projection of the molecular axis have the same range of values, but not in phase. This accounts for the asymmetry of the resulting patterns for particular values for the angle δ. A change by π radians in δ has little effect on the intensity. The intersection of low intensities, point A, in Fig. 3 corresponds to a value of δ, which makes the plane of the carbon chain perpendicular to the photographic plate.

The great variations of the intensity of the first order and the smaller variations in the second order with changes in angle ϕ_d are shown for a molecule with its axis vertical in Figs. 5 and 6. The intensity in the first order is lowest when the plane of the chain is perpendicular to the photographic plate and greatest when the chain is parallel. The asymmetry in the patterns for different positions of the plane of the chain about the molecular axis is very small when the axis is vertical. The greater asymmetry shown by Figs. 3 and 4 is associated with the 20° tilt of the molecular axis.

The effect on scattering from molecules assuming random positions about the surface normal instead of maintaining a fixed position may be seen by comparing Fig 8 to Fig. 2. Fig. 9. is similarly related to Fig. 7. In all these cases the tilt of the molecular axes is 20°. Figures 8 and 9 may be described roughly as crossed-line patterns. The position of the maxima on the y axis are evenly spaced and have the same intensity and position as those in Figs. 2 and 7, respectively. This was anticipated since it was pointed out previously[8] that in the region of the photographic plate ordinarily considered, the intensity along the y axis is virtually independent of angle ϕ_a. Figure 9 differs from Fig. 8 in that the second row of carbon atoms assumes random positions about the molecular axis. In both cases the first and third orders are spread out, that is, the intensity changes gradually and hence would appear weak to the eye. The second order shows a sharp change of slope and would appear dark. It should be noted that the tilt of these orders from a horizontal axis is about 14° and not 20°, the value of ψ_a. The major difference in Figs. 8 and 9 is the intensity of the maxima along the y axis.

The qualitative appearance of these maps may be compared with Fig. 12, a diffraction pattern from an oleophobic film formed on rolled platinum from a 0.05 percent cerotic acid solution in cetane. The first order that appears on the print is actually the second order. Although Fig. 12 has many of the characteristics of Figs. 8 and 9, it is apparent that the maxima along the y axis are not evenly spaced. This is borne out by the microphotometer trace in Fig. 11. It was proposed that since the maxima along the y axis are mainly determined by the angle of tilt of the molecular axis, uneven spacings may be caused by a randomness in this tilt. Calculation V was therefore performed to show the effect of this variation, and the resultant intensities along the y axis are plotted in Fig. 10. It is noted that the spacing between the second and third orders is 17 percent greater than that between the third and fourth orders, while in the photometer trace, Fig. 11, the spacing is 15 percent greater. It will be recalled that the assumption made in calculating Fig. 10 was equal probability for all positions between 0° and 20°. Analysis of Fig. 12 indicates that angle ψ_a assumes values as large as 30°. It is possible that the distribution leading to Fig. 12 resembles more closely that on the surface of a sphere, in which case the population would be proportional to $\sin\psi_a$ This type of distribution would make the contribution from the larger tilts more im-

portant and reduce the magnitude of the difference in spacings of successive orders.

INTERPRETATION OF PATTERNS

The question arises concerning what conclusions may be drawn from the analysis of the diffraction patterns of a hydrocarbon film, in view of the calculations performed above. In effect, we are concerned with determining the values of ψ_a, ϕ_a, and δ for the many molecules comprising a film. To a certain extent independent effects from these angles are obtained in the scattering patterns which allow separate evaluations of each of these orientation parameters.

The value of angle ψ_a may be determined from the positions of the intercepts of successive orders on the y axis. When angle ψ_a has a fixed value among the many molecules comprising a film, the intercepts are very nearly evenly spaced, and their separations may be expressed in terms of the carbon to carbon distance along a single row of atoms, r_t, as follows:

$$y = nL\lambda/r_t \cos\psi_a, \tag{7}$$

where n refers to the order. This expression has been used previously to determine the tilt of the axes of long chain molecules by Germer and Storks.[6] When angle ψ_a assumes a range of values the spacings of the intercepts of successive orders on the y axis do not remain constant (see Fig. 10). This result cannot be derived from expression (7). It arises from considering the scattered intensity of the entire staggered carbon chain instead of that from a single row of atoms.

For the purpose of making quantitative estimates, an average value for angle ψ_a may be obtained from expression (7) by measuring the spacings between the second and fourth orders. These latter orders are affected similarly, and to about the same extent, by variations in angle ψ_a. The spread about this average value can be approximated from the difference in spacing between the second and third, and the third and fourth orders. Some estimate of the magnitude of the spread may be based on the results obtained in Figs. 10 and 11. It should be borne in mind that the quantitative conclusions so drawn are necessarily quite rough if the investigator does not know the weight function to be applied to the angular distribution. Variations in the value of angle δ will have a small additional effect on the relative spacings. It should be noted that the foregoing remarks concerning angle ψ_a apply irrespective of whether angle ϕ_a varies or not, since, as was previously pointed out, the position and intensity of the intercepts on the y axis are independent of angle ϕ_a for the region of the photographic plate ordinarily considered.

Methods of estimating the value of angle ϕ_a may now be considered. If ϕ_a has a fixed value, the scattering pattern shows a succession of orders perpendicular to the projection of the molecular axis (Figs. 2 and 7). The value of angle ϕ_a may be obtained from the expression,

$$\frac{1}{\tan\psi_a \sin\phi_a}, \tag{8}$$

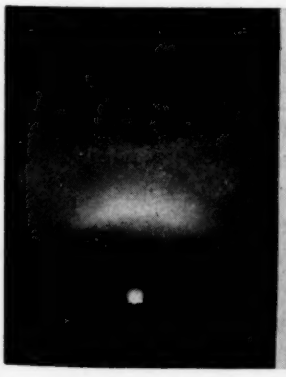

FIG. 12. Pattern from film of cerotic acid on flamed, rolled platinum foil.

FIG. 13. Pattern from film of cerotic acid on metallographically polished platinum.

FIG. 14. Pattern from film of stearic acid on cold rolled steel.

FIG. 15. Pattern from excess stearic acid crystallized on platinum foil.

[6] L. H. Germer and K. H. Storks, J. Chem. Phys. 6, 280 (1938).

which is the slope of the projection of the molecular axis on the photographic plate. This expression was used by Germer and Storks.[6] When angle ϕ_a assumes all possible values from 0 to 2π the pattern obtained is symmetric about the y axis. Random values of ϕ_a, when ψ_a is large, produce patterns similar to Figs. 8 and 9. When ψ_a is small and ϕ_a is random, the pattern is similar to the well-known patterns[7] of vertical molecules with random values of angle ϕ_d. Angle ϕ_a has no significance when angle ψ_a is zero.

For an estimation of the values of angle δ, Figs. 3, 4, 5, and 6, are very helpful as a guide. They show that if angles ψ_a and ϕ_a are fixed, the value of angle δ will determine not only the relative intensities of the odd and even orders, but also the symmetry within a particular order. When ψ_a is small (less than 10°) asymmetry effects are very small. When ψ_a is fixed and δ is random, the pattern obtained will be symmetric about the projection of the molecular axis irrespective of the value of angle ϕ_a. This symmetry does not occur for most fixed values of δ and may be checked experimentally by varying angle ϕ_a, which is accomplished by rotating the sample about a vertical axis, z. From noting the pattern asymmetry and knowing the values of angles ψ_a and ϕ_a, and inserting them into formula (1), the value of angle δ may be estimated. When angle ϕ_a is random and ψ_a is large, the question of whether δ is random or fixed is indicated from measuring the relative intensities of successive orders along the y axis. The differences which may occur are shown in Figs. 8 and 9. Additional calculations using formula (4) would need to be made to ascertain the values of the maxima along the y axis for various values of angle δ. When ψ_a is small and ϕ_a random, it is not possible to decide on the value of δ. From the calculations performed so far it is also not possible to decide on the value of δ generally when angle ψ_a assumes a range of values.

It is clear that many conclusions depend upon estimates of relative intensities. Visual estimates are quite poor, but microphotometer traces used in conjunction with the rotating-sector technique should aid considerably in estimating the intensities. The effects of incoherent scattering[8] should be included in these considerations. The neglect of the scattering from hydrogen atoms in performing the calculations will have some effect on the intensities within the orders. This should not affect the validity of the analysis, though, since the hydrogen atoms have the same vertical identity spacing as the carbon atoms and hence will not affect the positions or the general shapes of the successive orders of scattering. Intermolecular interaction, that is scattering due to a regularly close-packed assemblage, may also affect the intensities within the orders. This effect will be quite negligible in films of randomly oriented molecules. When the molecules have a fixed orientation and regular spacing, the contribution from the distances between the molecules is readily recognized as spots along the order lines (see Fig. 13).

ILLUSTRATION OF METHOD

Several types of observed diffraction patterns are illustrated in Figs. 12, 13, 14, and 15. As indicated above, the crossed line pattern in Fig. 12 arises from molecules showing random values of ϕ_a, with ψ_a ranging from 0° up to about 30°. This estimate is based on the observation that the average tilt of the molecular axis calculated from formula (7) from the spacing between the second and fourth maxima is 16°, and that the tilt of the successive orders on the pattern from a horizontal axis is about 20°. The range of orientation of the molecules giving rise to this photograph does not fix by itself the nature of the attachment of the molecule to the supporting surface. The random values for ψ_a would be accounted for in the specimen either by a variation in the angles between the molecules and the surface, or by a variation in the surface contour with all molecules fixed at this same angle at the point of attachment. Such questions have to be considered in the light of photographs taken from similar specimens using different methods of preparation. An illustration of this point is found in Fig. 13.

The pattern of horizontal lines observed in Fig. 13 indicates that the molecules are standing vertically. The effect of wide spacings between different molecules is manifested to a small degree in the intensity distribution along the first-order line. This pattern was also obtained

[7] C. A. Murison, Phil. Mag. **17**, 201 (1934).
[8] L. Bewilogua, Physik. Zeits. **32**, 740 (1931).

from cerotic acid, but on a surface which was smoothed by polishing, in contrast with the rolled surface used in Fig. 12. The differences between the molecular orientations exhibited in these two figures is associated with the difference in the method of preparing the platinum surface.

Figure 14 shows a pattern of stearic acid on iron in which the deviation from the vertical ranges over not more than 10°, while the values of ϕ_a are random. An average value of 5° was obtained for ψ_a by measuring the spacing between the second and fourth maxima and using formula (7). The upper limit of 10° was set by assuming that the average value represents the mean of a variation starting at zero degrees. This assumption is supported by the fact that the spacing between the second and third orders is about six percent larger than the spacing between third and fourth. A microphotometer trace was found to be quite useful in corroborating the visual measurements.

Figure 15 shows a pattern of tilted layer lines obtained from stearic acid crystallized on platinum. This pattern arises from molecules having constant values of ϕ_a and ψ_a, equal to 64° (or 116°) and 40°, respectively, determined from using formulas (7) and (8). The intensity distributions within the successive orders are not too clearly defined, but appear on the original negative to be symmetric with respect to a line perpendicular to them and intersecting the main beam. The odd orders are strongest on either side of this line, and the even orders are strongest at the intersections. Angle δ, therefore, probably assumes random values. As pointed out above, this can be established by taking additional photographs at various values of ϕ_a by rotating the specimen. Patterns with fixed orientation such as Fig. 15 were not observed so far for films believed to be monolayers.

The information of the kind obtained from the illustrations above has been of considerable assistance in studying the properties of oriented monolayers, and it is hoped that the information obtainable in some cases from electron diffraction photographs will advance the study of the physical and chemical properties of long chain organic molecules, especially in the adsorbed state.

ACKNOWLEDGMENT

The close interest of Dr. W. A. Zisman of the Naval Research Laboratory and the assistance of Dr. Isabella Karle are gratefully acknowledged.

THE JOURNAL OF CHEMICAL PHYSICS VOLUME 15, NUMBER 5 MAY, 1947

The Entropy of Solution of Molecules of Different Size

J. H. HILDEBRAND
Department of Chemistry, University of California, Berkeley, California

(Received February 25, 1947)

The entropy of mixing two liquids whose molecules differ in size is expressed in terms which avoid the assumption of a lattice as an artificial frame of reference, and which is not limited to linear polymers. The equation obtained is

$$\frac{\Delta S}{R}=N_1\ln\frac{V-N_1b_1-N_2b_2}{N_1(v_1-b_1)}+N_2\ln\frac{V-N_1b_1-N_2b_2}{N_2(v_2-b_2)},$$

where N_1 and N_2 denote number of moles, V the volume of the solution, v_1 and v_2 the molal volumes of the pure components and b_1 and b_2 the sum of the actual geometrical volumes of 6×10^{23} molecules. With certain simplifying assumptions, equivalent to those used by authors who have analyzed the problem for linear polymers in a lattice frame of reference, the above equation reduces to the form obtained by the latter method. Various methods of obtaining experimental values for b are outlined.

THE thermodynamic properties of solutions of long, linear molecules in the ordinary solvents have recently attracted considerable attention by reason both of the commercial importance of high polymers and of the interesting problems in the entropy of mixing which their

solutions present. Nearly all who have endeavored to formulate the entropy of mixing two such components have done so in terms of a possible arrangement in a quasi-solid lattice, in which "segments" of the polymer can occupy the same kind of sites as the molecules of the solvent. The first step was made by Meyer,[1] who discussed the problem from a qualitative standpoint. Fowler and Rushbrooke[2] gave a partial solution for the case of components occupying 1 and 2 sites, respectively. The effect of this difference in size proved to be surprisingly small. The more complete solution was furnished by Chang.[3] Miller[4] extended the treatment to molecules occupying 3 sites. The general treatment for molecules occupying any number of sites has been developed independently by Huggins,[5] and Flory,[6] and refined by Guggenheim.[7] Quite recently Zimm[8] has succeeded in avoiding the artificial assumptions of a lattice, and, proceeding upon the basis of theoretical investigations by McMillan and Mayer,[9] has formulated the osmotic pressure of dilute solutions of polymers of various sorts.

The above work agrees substantially in yielding the following equations for the partial molal free energies in athermal solutions of linear polymers.

$$\Delta\bar{F}_1/RT=\ln\phi_1+\phi_2(1-1/m)+\mu\phi_2^2 \text{ (solvent)} \quad (1)$$
$$\Delta\bar{F}_2/RT=\ln\phi_2+\phi_1(m-1)+m\mu\phi_2^2 \text{ (polymer)} \quad (1')$$

where ϕ denotes volume fraction, m, the number of "segments" in the polymer, and μ is a constant "which takes care of heat of mixing, deviations from complete randomness, and other factors."

The problem is thus essentially solved, for many practical purposes, nevertheless the result is not altogether satisfying, at least aesthetically, because the treatment of all but dilute solutions of the polymer rests upon the assumption of a lattice frame of reference which is quite artificial for the liquid state, which does not explicitly include non-integral multiples such as ethane, and pentane, and which, except for the treatment by Zimm, is limited to linear polymers. There remains the fundamental question stated by Guggenheim,[10] namely, the applicability of Raoult's law to solutions of substances whose molecules differ even moderately in size.

Now we have experimental evidence that substances of equal internal pressure, which mix without heat effect, can differ in volume without causing serious deviations from Raoult's law. One may mention chlorine in carbon tetrachloride[11] and diphenyl in benzene.[12] The formula given above, 1 and 1′, corresponds to but small departures from ideality when m is small, say, 2 or 3, and one would expect two *spherical* molecules with a volume ratio of 2 or 3 to show no greater departure from the ideal entropy of mixing.

Hildebrand and Sweny[13] reported a special case, normal hexane in normal hexadecane, which obeys Raoult's law quite closely, in spite of a length ratio of 3 to 8. The case was deliberately chosen, however, in order to favor an approximately parallel ordered molecular arrangement; the temperature range was not far above the melting point of dicetyl. It was also shown that the number of distinguishable molecular arrangements in such a system is the same as the number for two species of identical size in a fixed lattice. Brönsted[14] has quite recently made very accurate measurements on binary solutions of normal paraffins with the following numbers of carbon atoms, 6–12, 6–16, 7–16, and found the small deviations from Raoult's law that are to be expected from the failure of these solutions to conform strictly to the model.

The type of solution considered in this paper is that of molecules of different size, whose shape is not specified, and which mix without heat effect and with maximum randomness.

[1] K. H. Meyer, Zeits. f. physik. Chemie **B44**, 383 (1939).
[2] R. H. Fowler and G. S. Rushbrooke, Trans. Faraday Soc. **33**, 1272 (1937).
[3] Chang, Proc. Camb. Phil. Soc. **35**, 265 (1939).
[4] A. R. Miller, Proc. Comb. Phil. Soc. **38**, 109 (1942); **39**, 54 (1943).
[5] M. L. Huggins, J. Chem. Phys. **9**, 440 (1941); J. Phys. Chem. **46**, 151 (1942); J. Am. Chem. Soc. **64**, 1712 (1942).
[6] P. J. Flory, J. Chem. Phys. **9**, 660 (1941); **10**, 51 (1942); **13**, 453 (1945).
[7] E. A. Guggenheim, Proc. Roy. Soc. **A183**, 203 (1944); Trans. Faraday Soc. **41**, 107 (1945).
[8] B. H. Zimm, J. Chem. Phys. **14**, 164 (1946).
[9] W. G. McMillan and J. E. Mayer, J. Chem. Phys. **13**, 276 (1945).
[10] E. A. Guggenheim, Trans. Faraday Soc. **33**, 151 (1937).
[11] J. H. Hildebrand, *Solubility* (Reinhold Publishing Corporation, New York, 1936), second edition, p. 136.
[12] J. C. Warner, R. C. Scheith, and W. J. Svirbely, J. Chem. Phys. **2**, 590 (1934).
[13] J. H. Hildebrand and J. W. Sweny, J. Phys. Chem. **43**, 297 (1938).
[14] J. N. Brönsted, Kgl. Danske Vid. Sels. Math.-Fys. Medd. **22**, No. 17 (1946).

It has doubtless seemed strange to many who have thought about these matters that Raoult's law should hold in the limit for the solvent regardless of the size and nature of the solute molecules. The fact that this is a necessary consequence of the "Gibbs-Duhem" equation hardly satisfies one's curiosity as to its physical significance. An elucidation of this difficulty can contribute to a clarification of the main problem. That equation can be derived by equating the energy changes in two equivalent processes, one, $\partial\bar{F}_2/\partial N_2$, when dN_2 mole of solute is added to a solution containing N_1+N_2 moles; the other, when a portion of solution containing the same amount of solute is added and the equivalent amount of solvent, $dN_1=(N_1/N_2)dN_2$, is distilled out. The result is, $\partial\bar{F}_2/\partial N_2=-(N_1/N_2)(\partial\bar{F}_1/\partial N_2)$, or, the more familiar forms,

$$N_1\frac{\partial \ln f_1}{\partial N_1}+N_2\frac{\partial \ln f_2}{\partial N_2}=0 \quad \text{and} \quad \frac{\partial \ln f_1}{\partial \ln x_1}=\frac{\partial \ln f_2}{\partial \ln x_2},$$

where f denotes fugacity and x mole fraction.

Now, when the solution is very dilute, and the molecules of the solute do not "interfere" statistically with each other, their fugacity is proportional to their number, that is, $f_2 \propto x_2$, which is Henry's law, and when this relation holds for the solute in dilute solution, Raoult's law holds for the solvent, as is well known.[15] But the larger are the solute molecules, the more they "interfere," causing the solute to deviate from Henry's law, in the sense indicated by Zimm, and the solvent, accordingly, to deviate from Raoult's law. This is most easily appreciated by considering the volume entropy of a gas. The probability of a molecule being found at a certain instant of time at a definite point within a vessel of volume V containing a mole of the gas is proportional to the number of molecules present, A, the Avogadro number; to the volume of the individual molecules, v; and inversely to the free volume, $V-Av$, because any one molecule passes through a certain point oftener than it would if its mean free path were not shortened by the excluded volume. The probability is therefore $Av/(V-Av)$ and the "uncertainty" is its reciprocal, hence the increase in entropy is expanding the gas to the volume V' is

$$s'-s=R\ln\frac{V'-Av}{V-Av}.$$

This is identical with the expression one obtains by applying the thermodynamic equation $(\partial S/\partial V)_T=(\partial P/\partial T)_V$ to the van der Waals equation if the van der Waals $b=Av$. We obtain the correct result by defining the entropy in terms of a statistical uncertainty independent of any counting of positions in an artificial frame of reference.

Let us next apply the same reasoning to the formation of *a* solution—whether gaseous or liquid is immaterial. Let us transfer N_1 and N_2 moles of the components from the pure state, where they occupy the respective volumes, v_1 and v_2, to a solution of the composition N_1+N_2. We assume that if these molecules are polyatomic their energies of vibration, rotation, or libration will not be significantly different in the pure state and in the solution. The probability of the instant location of a single molecule of solvent around an arbitrary point in the pure state is $Av_1/(v_1-Av_1)$ and in the solution is $Av_1/(V-N_1Av_1-N_2Av_2)$, and similarly for the other component. The increase in entropy on transferring N_1 and N_2 moles of the components from pure liquid to solution is accordingly, substituting b for Av, and the gas constant, R, for A times the Boltman constant,

$$\frac{\Delta S}{R}=N_1\ln\frac{V-N_1b_1-N_2b_2}{N_1(v_1-b_1)}+N_2\ln\frac{V-N_1b_2-N_2b_2}{N_2(v_2-b_2)}. \quad (2)$$

If the volume of the solution is additive, $V=N_1v_1+N_2v_2$, and the expression becomes,

$$\frac{\Delta S}{R}=N_1\ln\frac{N_1(v_1-b_1)+N_2(v_2-b_2)}{N_1(v_1-b_1)}+N_2\ln\frac{N_1(v_1-b_1)+N_2(v_2-b_2)}{N_2(v_2-b_2)}. \quad (3)$$

Differentiating with respect to N_1 at constant N_2 gives the partial molal entropy of 1, the solvent,

[15] Cf. reference 11, p. 42ff.

in the solution, i.e.,

$$\frac{\bar{s}_1}{R}=\ln\frac{N_1(v_1-b_1)+N_2(v_2-b_2)}{N_1(v_1-b_1)}+\frac{N_2[(v_1-b_1)-(v_2-b_2)]}{N_1(v_1-b_1)+N_2(v_2-b_2)}. \quad (4)$$

If the two free volumes, $v-b$, are equal in the pure liquids, this reduces to $\bar{s}_1=-R\ln x_1$, and the solution obeys Raoult's law. If the free volumes are proportional to the molal volumes, and ϕ denotes volume fraction,

$$\frac{\bar{s}_1}{R}=-\ln\phi_1+\frac{N_2(v_1-v_2)}{N_1v_1+N_2v_2}. \quad (5)$$

Since the activity, a, and the partial molal entropy are related by the equation, $s_1=-R\ln a_1$, we can write

$$\ln a_1=\ln\phi_1+\frac{N_2(v_2-v_1)}{N_1v_1+N_2v_2}. \quad (6)$$

This is identical with Eq. (1) except for the term containing μ, which may be zero under certain conditions implicit in the derivations of that equation. This is a striking coincidence, but one which is less surprising when one recalls that the derivation here given is really not limited to spherical molecules; the probability that a molecule will include an arbitrary point within the solution is not dependent upon its shape, but only on its volume, and therefore the entropy of mixing should correspond to Eq. (2) unless the shapes of the molecules are such as to involve structural entropy, as in the special case of hexane and hexadecane, cited above.

Inasmuch as the primary purpose of this analysis has been to answer the question put by Guggenheim, namely, the validity of assuming the Raoult's law entropy for the ordinary regular solutions for which it has been assumed, let us consider several numerical values. The following ratios of molal volumes are illustrative: CCl_4 to Cl_2, 1.9; $n-C_7H_{16}$ to I_2, 2.5; $n-C_6H_{14}$ to CS_2, 2.2. If the assumptions involved in obtaining Eq. (6) from the more general Eq. (2) are valid, then the logarithm of the activity coefficient, a_1/x_1, has the values given in Table I for several ratios of v_2/v_1.

TABLE I. Values of $-\log(a_1/x_1)$.

v_2/v_1	$X_1=0.01$	0.1	0.9	0.99
1	0	0	0	0
2	.083	.073	.0019	.00002
3	.185	.168	.0068	.00008
10	.605	.572	.073	.0015

Let us next consider alternatives to the oversimplified assumption that the co-volumes, v_1-b_1 and v_1-b_2 are proportional to the volumes, v_1 and v_2. This assumption is doubtless nearest the truth for components of equal internal pressure, which yield solutions whose deviation from ideal behavior is caused by non-ideal entropy, Eq. (3), rather than non-ideal heat.[16] On the other hand, where one liquid has a higher internal pressure than the other, one may infer that it is proportionately less expanded and the above simplification is less warranted.

One method that suggests itself for evaluating $v-b$ is to set b equal to the molal volume in the solid state, extrapolated to absolute zero. Another method is to calculate b from the interatomic distances and the van der Waals radii assigned to the peripheral atoms. A third possibility, using the van der Waals equation and critical data, can hardly be expected to give consistant values in view of the well known failures of that equation in the critical region. A fourth possibility is to use experimentally determined values of $(\partial P/\partial T)_V$, such as those determined by Hildebrand and Carter,[17] and by Westwater, Frantz, and Hildebrand,[18] or as calculated from expansivity and compressivity.[19] Since $(\partial P/\partial T)_V=(\partial S/\partial V)_T$, which, for a van der Waals liquid, equals $R/(v-b)$, one can calculate values of $v-b$. A comparison of results to be obtained by these different methods will be published in a later communication.

[16] Cf. reference 8, Chap. III.
[17] J. H. Hildebrand and J. M. Carter, J. Am. Chem. Soc. **54**, 3592 (1932).
[18] W. Westwater, H. W. Frantz, and J. H. Hildebrand, Phys. Rev. **31**, 135 (1928).
[19] J. H. Hildebrand, Phys. Rev. **34**, 649 (1929).

Comments on the "Hildebrand Rule"

J. H. HILDEBRAND AND T. S. GILMAN
Department of Chemistry, University of California, Berkeley, California

(Received February 25, 1947)

According to the "Hildebrand rule," normal liquids should have the same entropy of vaporization at temperatures at which their vapors have the same molal volume. Pitzer has shown that liquids which obey the theory of corresponding states should have equal entropies of vaporization at temperatures at which their ratio of vapor volume to liquid volume is the same. He pointed out, however, that this rests upon several assumptions, including, "potential energy depending only on intermolecular distances and universal shape of potential energy curve." In this paper, two pairs of liquids with widely different liquid molal volumes but otherwise closely similar, are compared with the result that the former rule is more closely obeyed, supporting the suggestion that it is an oversimplification to regard the molecular fields of polyatomic molecules as radial from the center of the molecule. The entropy of vaporization of a van der Waals liquid, $R[\ln(V-b)-\ln(v-b)]$, where V refers to vapor and v to liquid, indicates that equal V and equal $v-b$ should give equal entropy of vaporization. In comparing ethane and diisopropyl, for example, the separation of the methyl groups is more significant than the separation of the molecular centers.

IT was early recognized that the useful "Trouton constant," i.e., the quotient of the molal heat of vaporization of a "normal liquid" by its boiling point on the absolute scale, is not strictly constant but increases slowly in going from substances with lower to those with higher boiling points. Empirical equations to take account of this drift were proposed by several.[1] The senior writer[2] examined the drift by plotting $\log P$ *vs.* $\log T$ for the vapor pressures of a number of widely boiling normal liquids. The tangents to these curves at any point multiplied by the gas constant, R, give the value of the entropy of vaporization at that point, as can readily be seen from the Clausius-Clapeyron equation, neglecting gas imperfections, which are not serious at pressures somewhat below 1 atmosphere. It was noticed that the curves became steeper in going to less volatile substances so that their tangents were by no means the same at any one pressure, such as 1 atmosphere, as demanded by the Trouton rule, but that they agreed very well if compared along lines of unit slope, $\log P = \log T$ +constant. The constant obviously has the value, $\log(R/V)$, so that the proper rule appeared to be that entropies of vaporization of normal liquids are the same if the temperatures are so chosen as to give equal molal volumes of saturated vapor.

This rule has been widely used, for it permits a simple and fairly accurate graphic construction of an entire vapor pressure curve from a single point. Its theoretical basis has accordingly invited examination by a number of writers. The usual conclusion has been[3] that the entropy of vaporization depends on $\log(V/v)$, representing the volume of the liquid, and that the rule holds as it does because the liquids compared do not differ greatly in molal volume. Pitzer[4] has shown that the theory of corresponding states leads to equal entropies of vaporization at equal ratios of V/v for liquids he has called "perfect." The necessary conditions are, "(1) The validity of classical statistical mechanics, (2) spherical or freely rotating molecules, (3) intramolecular vibration same in liquid and gas, (4) potential energy depending only on intermolecular distances, and (5) universal shape of potential curve." He has shown that argon, krypton, and xenon have the entropies of vaporization 18.67, 18.60, 18.66, respectively, when compared at $V/v = 335$, while at equal V, 10 liters, their entropies of vaporization are 19.0, 18.5, 18.0.

Guggenheim[5] has extended Pitzer's treatment

[1] W. Nernst, Göttinger Nach. (1906); E. Bingham, J. Am. Chem. Soc. **28**, 723 (1906); Forcrand, Comptes rendus **156**, 1439, 1648, 1809 (1913).
[2] J. H. Hildebrand, J. Am. Chem. Soc. **37**, 970 (1915); **40**, 45 (1918).
[3] E.g., H. Eyring and J. O. Hirschfelder, J. Phys. Chem. **41**, 249 (1937).
[4] K. S. Pitzer, J. Chem. Phys. **7**, 583 (1939).
[5] E. A. Guggenheim, J. Chem. Phys. **13**, 253 (1945).

TABLE I. Entropies of vaporization of chlorine and carbon tetrachloride.

	T°K	v(cc)	V(liters)	V/v	ΔS	Diff
Cl_2	239.1	45.4	19.1	420	20.4	+1.6
CCl_4	336.5	101.4	42.7	420	22.0	−0.8
Cl_2	221.0	44.2	42.7	965	22.8	+1.7
CCl_4	312.7	97.7	94.2	965	24.5	−0.6
Cl_2	205.9	43.3	94.2		25.1	

to other properties and in discussing vaporization said, "Neither Trouton's rule nor Hildebrand's accords with the principle of corresponding states, which requires, rather that the molar entropies of evaporation should be equal at corresponding temperatures."

It has been apparent, nevertheless, that, as stated by Halford,[6] "this definition of characteristic temperature" (i.e., that derived from corresponding states) "cannot compete in practical value with the empirical rule of Hildebrand," and Frank[7] having examined many cases, has written regarding the same point, "This does not do justice to the rule, however, for it is far more accurate than such statement would apply." Pitzer himself recognized, as reported by Halford from a private conversation, that polyatomic molecules might introduce deviations from one or more of the five essential conditions stated above. The senior author[8] suggested some years ago that it might prove more realistic in the case of certain polyatomic molecules, such as the tetrahalides, to consider the outer atoms as the main center of attraction. The range of the London, or "dispersion" forces is so short that the buried atoms contribute but little to it. Such molecules should show departures from stipulations 4 and 5 of Pitzer, above, and their free volumes might be more nearly equal than their liquid volumes, therefore showing variations from the rule derived from the theory of corresponding states in the direction of the Hildebrand rule.

Since $(\partial S/\partial V)_T=(\partial P/\partial T)_V$, a gas which obeys the van der Waals equation will increase in entropy on expanding from V to V' by

$$S'-S=\int_V^{V'}\frac{RdV}{V-b}=R\ln\frac{V'-b}{V-b}.$$

If the equation holds for the continuous van der Waals path from liquid to vapor, then, letting V refer to vapor and v to liquid, we would have, since V is very large compared to b,

$$\Delta S_{vap}=R[\ln V-\ln(v-b)].$$

The theory of corresponding states substitutes v, a larger quantity, for $v-b$, on the basis that the two liquids are proportionately expanded. The Hildebrand rule amounts to considering $\ln(v-b)$ to be substantially the same for different substances at the same "Hildebrand temperature." This could be the case for a pair such as CF_4 and SF_6 if the main attractive forces are central to the fluorine atoms instead of to the whole molecules. Light may accordingly be thrown upon the nature of forces between polyatomic molecules by comparing the entropy of vaporization of substances having the same peripheral atoms but widely different liquid volumes.

In order to make a significant test it is necessary to select two liquids whose molal volumes differ widely so that V/v shall be as different as possible for the two at temperatures where their gas volumes are equal, but which are as nearly alike as possible in all other respects. The two rules are not as different in practice as one might at first sight suppose, because the molal volumes of liquids likely to be compared seldom differ enough to require more than a few degrees change in temperature to compensate for it, corresponding to only a few tenths of an entropy unit.

We have selected, first, Cl_2 and CCl_4 as a pair of liquids with unusually large ratio of molal volumes and for which the essential data have been determined with the desired accuracy. For Cl_2 we have the vapor pressures, heat capacities and heat of vaporization by Giauque and Powell.[9]

TABLE II.

	Cl_2	ΔS for CCl_4	
T	ΔS	At same V/v as Cl_2	At same T/T_c as Cl_2
223	22.6	24.2	26.4
241	20.2	21.7	23.6

[6] R. S. Halford, J. Chem. Phys. **8**, 496 (1940).
[7] H. S. Frank, J. Chem. Phys. **13**, 493 (1945).
[8] J. H. Hildebrand, Trans. Faraday Soc. **33**, 144 (1937).

For CCl_4 we have the heat data by Pitzer and the vapor pressures equation obtained by Vold.[10] We have calculated heats of vaporization both from the vapor pressure data, correcting for gas law imperfections by means of the Berthelot equation, and from the thermal data. In only one case do the corresponding values for ΔS differ by as much as 0.2 e.u., so we report only one set of values, the one from the thermal data. The values of v, V, and ΔS are arranged in Table I in pairs with alternately equal values of V and of V/v. It is evident that the entropy of vaporization of Cl_2, at equal gas volumes, is greater than it is for CCl_4 by about 0.7 e.u. while at equal ratios of gas to liquid volumes it is less by about 1.6 e.u. We may infer from these results that the free volumes, while not equal, are more nearly so than the liquid volumes, a plausible conclusion.

Guggenheim has applied the theory of corresponding states in terms of equal fractions of critical temperatures. This suffers practically from the fact that critical temperatures have been determined for relatively few liquids. They are known for these two substances, however, and it is interesting to see how their entropies of vaporization compare at temperatures which are equal fractions of their critical temperatures, 417°K and 556°K, respectively. Results are shown in Table II, where it is seen that the discrepancy between the entropies of vaporization of the two substances is over twice as great when compared at the same T/T_c as it is at the same V/v. This will not surprise those who are familiar with the history of attempts to express the properties of polyatomic molecules as functions of the "reduced" pressures, volumes, and temperatures, P/P_c, v/v_c, and T/T_c.

In the foregoing we have neglected the other factors that might contribute to the different entropies of vaporization of the two substances, such as differences in rotational and vibrational energies in the two states. ΔC_p is -8.4 for Cl_2 at 200°K and -10.5 for CCl_4 at 300°K, not sufficiently different as to have a significant effect upon the above comparisons.

TABLE III. Entropies of vaporization of ethane and diisopropyl.

	T°K	v(cc)	V(liters)	V/v	ΔS	Diff
$(CH_3)_2CHCH(CH_3)_2$	304.7	132.3	61.15		22.7	−0.5
C_2H_6	160.0	52.2*	61.15	1170	23.2	+2.3
$(CH_3)_2CHCH(CH_3)_2$	281.8	128.2	150.2	1170	25.5	−0.3
C_2H_6	148.0	51.0*	150.2	2940	25.8	+2.5
$(CH_3)_2CHCH(CH_3)_2$	262.5	125.1	368	2940	28.3	

* Extrapolated; may be in error by one percent.

As a second pair for our comparison we have selected ethane and diisopropyl, whose liquid volumes differ by an even larger factor than Cl_2 and CCl_4, and whose peripheral groups are even more nearly identical. Table III gives values of v, V, V/v, and ΔS for this pair of liquids, arranged as in Table I to give alternatively equal vapor volumes and equal vapor-liquid volume ratios. It is seen that here again the agreement is much better when the entropies of vaporization are compared at temperatures corresponding to equal vapor volumes.

The entropies were calculated using the Clapeyron equation; values of dP/dT were obtained from reliable vapor pressure equations,[11] the liquid volumes were determined from density data,[12] and the vapor volumes were calculated by means of the Berthelot equation, using $T_c=305.2$°K and $P_c=48.8$ atmos. for ethane, and $T_c=500.5$°K and $P_c=30.6$ atmos. for diisopropyl.

[9] W. F. Giauque and T. M. Powell, J. Am. Chem. Soc. 61, 1970 (1939).

[10] R. D. Vold, J. Am. Chem. Soc. 59, 1515 (1937).

[11] "Tables of Ten Physical and Thermodynamic Properties of Hydrocarbons," A.P.I. Research Project 44 at the National Bureau of Standards (1945).

[12] For ethane: O. Maass and C. H. Wright, J. Am. Chem. Soc. 43, 1098 (1921). For diisopropyl: S. Young, Sci. Proc. Roy. Dublin Soc. 12, 374 (1910).

THE JOURNAL OF CHEMICAL PHYSICS VOLUME 15, NUMBER 5 MAY, 1947

Infra-Red Spectra of Monomeric Formic Acid and Its Deuterated Forms. I. High Frequency Region*

VAN ZANDT WILLIAMS**
Princeton University, Princeton, New Jersey
(Received January 14, 1947)

The hydrogen and deuterium stretching vibrations of the molecules HCOOH, HCOOD, DCOOH, and DCOOD have been studied with a high resolution echelette-grating infra-red spectrometer. From the rotational structure of these bands parameters which are functions of the moments of inertia have been calculated. From these parameters, previous data, and assumptions of the hydrogen bond distances and molecular planarity, the following dimensions of the molecule have been derived: O−H, 0.96±0.01A; C−H, 1.08±0.01A; C=O, 1.225±0.02A; C−O, 1.41 ±0.02A; O−C=O, 125±1°; C−O−H, 107±5°; H−C=O, 122±5°.

INTRODUCTION

BECAUSE of the limited resolving power of present day infra-red spectrographs and the half-widths of the rotational bands, complete evaluation of molecular moments of inertia from rotational band structure has been possible for only a few simple or symmetrical molecules. For some heavier molecules which are needle-shaped symmetrical top rotators, i.e., have two large equal moments of inertia and one smaller one, it is often possible to resolve the perpendicular bands even though the parallel band structure cannot be separated. This is also true for a molecule which is an approximate symmetric top, where the two large moments of inertia are comparable and the third is much smaller. Such analyses, unfortunately, offer only one datum for determining the several structural parameters of the molecule. In many cases, particularly if such molecules contain hydrogen atoms, it is possible to prepare isotopic forms for further study. Since the molecular dimensions are not appreciably changed on replacing an atom by its isotope, new data pertaining to the same structure can be obtained.

An example of a molecule to which the above method of analysis can be applied is formic acid, HCOOH. Its rotational fine structure has already been partially examined in the photographic infra-red region by Herzberg and Verleger[1] and Bauer and Badger[2] who studied the second harmonic of the O−H stretching vibration at 10,203 cm^{-1} and Thompson[3] who photographed the third harmonic of the same band at 13,287 cm^{-1}. These authors showed the structure of HCOOH to be a planar, approximate symmetrical top whose perpendicular bands were such that they could be resolved in the fundamental region. Moreover, it is possible to deuterate the molecule and have four isotopic forms, HCOOH, HCOOD, DCOOH, and DCOOD. These four molecules have been studied with an echelette-grating spectrometer in the region from 4000 cm^{-1} to 800 cm^{-1}. Since the high frequency region of the hydrogen-deuterium stretching vibrations gives all the data from which structural parameters may be calculated, the interval from 4000 to 2000 cm^{-1} forms the subject of this first paper.

EXPERIMENTAL

Instrument

An excellent, automatic recording, echelette-grating spectrometer designed and built by Dr. L. G. Smith[4] was used in this research. However, at the time of this work the instrument was not free of water vapor nor was the KBr fore-prism in use. Therefore, bands in the water region could not be studied carefully and those below 800 cm^{-1} were not considered.

* This material was presented in partial fulfillment of the requirements for the degree of Doctor of Philosophy, March, 1941. A portion of the material has also been presented before the Physical Society [Phys. Rev. **57**, 1078 (1940), and **58**, 208 (1940)].

** Present address: Stamford Research Laboratories, American Cyanamid Company, Stamford, Connecticut.

[1] G. Herzberg and H. Verleger, Physik. Zeits. **12**, 444 (1936).

[2] S. H. Bauer and R. M. Badger, J. Chem. Phys. **5**, 852 (1937).

[3] H. W. Thompson, J. Chem. Phys. **7**, 453 (1939).

[4] L. G. Smith, Rev. Sci. Inst. **13**, 54 (1942).

Preparation and Purity of Materials

The HCOOH used was obtained from Kahlbaum and purified by distillation. Its vapor pressure agreed well with the values given by Coolidge.[5]

HCOOD was prepared by repeated exchange with D_2O as described by Hofstadter.[6]

DCOOH and DCOOD were prepared as described by Herman and Williams.[7] Anhydrous oxalic acid, $(COOH)_2$, was deuterated by straight exchange and thermally decomposed to DCOOD, CO, CO_2, and D_2O. The CO and CO_2 were removed by pumping. DCOOH was then made by exchange of DCOOD with H_2O. The deuterated forms were freed of water by use of anhydrous $CuSO_4$ and purified by distillation. All reactions and purifications were carried out in vacuum.

Since two or three lots of each deuterated compound were made as needed, it was not possible to get accurate values of purity at all times. However, some mass spectrographic analyses of D/H ratio were performed by Mr. T. Mariner to determine purity and infra-red spectra and vapor pressure lowerings were used in other cases. It was estimated that HCOOD contained 3 to 4 percent HCOOH; DCOOH, a similar amount of DCOOD; and DCOOD, 6 to 7 percent of DCOOH. All the deuterated samples contained about 5 percent of water.

Cells and Techniques

The absorption cells were Pyrex cylinders with rocksalt windows sealed with Glyptal. As it was necessary to work at 150–160°C to eliminate dimer interference, these cells were contained in a furnace made of sheet metal wrapped with asbestos and a nichrome heating coil. The ends of the furnace were closed with transite slabs with rocksalt window apertures. The sample was contained in a side tube from the cell brought outside the furnace, and the vapor pressure was regulated by the temperature of the side tube. If the pressure desired was greater than could be obtained at room temperature, the side tube was heated with an auxiliary furnace. The pressures quoted are based on the temperature of this side tube. The vapor was regulated to give good spectral resolution without special regard to its absolute value.

[5] A. S. Coolidge, J. Am. Chem. Soc. **50**, 2166 (1928).
[6] R. Hofstadter, J. Chem. Phys. **6**, 540 (1938).
[7] R. C. Herman and V. Z. Williams, J. Chem. Phys. **8**, 447 (1940).

BASIS OF CALCULATIONS

An excellent summary of the theory of the slightly asymmetric top rotator has been given by Dieke and Kistiakowsky[8] in connection with their study of the formaldehyde molecule. In fact, the degree of asymmetry of HCOOH is very close to that of H_2CO so that the analogy with their results can be followed very closely. The nomenclature used in this work is the same as that of the above authors: $\gamma''\ (\text{cm}^{-1}) = h/8\pi^2 cC$, $\delta\ (\text{cm}^{-1}) = h/8\pi^2 cD$, $1/D = 1/2(1/A + 1/B)$ where A, B, and C are the large, middle, and the small moments of inertia, respectively, in gm cm^2 units. The molecular parameters derived from the perpendicular bands are $\gamma' - \delta$ and $\gamma'' - \delta$, where the single prime refers to the upper vibrational state of the transition and the double prime to the lower. It is assumed that, within the error of measurement, the δ values are the same for each state. These parameters are obtained from the difference equations,

$$\gamma' - \delta = \frac{rQ(K) - pQ(K)}{4K},$$

$$\gamma'' - \delta = \frac{rQ(K-1) - pQ(K+1)}{4K},$$

and the band center from

$$\nu(\text{cm}^{-1}) = \frac{rQ(K) + pQ(K)}{2} + K^2(\gamma'' - \gamma') - (\gamma' - \delta),$$

where $rQ(K)$ and $pQ(K)$ refer to the frequency value in cm^{-1} of the rotational bands of the r branch and p branch, respectively, arising from the Kth energy level of the lower state.

RESULTS

Table I gives a list of the fundamental bands which could be studied thoroughly in the high frequency region and the conditions under which they were observed. These characteristic absorptions are shown in Figs. 1–6. These are the

[8] G. H. Dieke and G. B. Kistiakowsky, Phys. Rev. **45**, 4 (1934).

direct photographic records obtained from the spectrograph in which the ordinates are galvanometer deflections representing absorption in an upward direction and the abscissae are cm^{-1} not corrected for vacuum. Above each peak is marked the K-value of the lower state involved in the transition.

All the spectra shown are essentially perpendicular bands consisting of $pQ(K)$ and $rQ(K)$ branches. For K greater than 3 or 4, the peaks are fairly sharp and equally spaced, but for small values of K the asymmetry of the molecule evidences itself as a "washing out" of this characteristic structure. Some of the bands show a small qQ branch at a slightly lower frequency than the computed value of ν_0 indicating a component of dipole moment change parallel to the axis of least moment of inertia. A Fortrat diagram is given (Figs. 1a, 3a–6a) when the bands could be analyzed. With each spectrum there is a table (Tables Ia, III–VI) showing the frequency position of the peaks and wherever possible, individual and average values of $\gamma'-\delta$, $\gamma''-\delta$, and ν_0.

An attempt was made to dry the instrument to permit a study of the ν(O−H) stretching vibrations of HCOOH and DCOOH. This was sufficiently successful to show that both bands were of the perpendicular type with ν_0 values of 3567 ± 3 cm^{-1}. However, it was not possible to make a band analysis or to determine whether or not a qQ branch was present.

Figure 1 shows the ν(C−H) stretching vibration of HCOOH at 2942.85 cm^{-1}. The pQ and rQ branches are quite sharp and can be traced on each side to the sixteenth member. The irregularities at the high frequency end are caused by water vapor in the instrument. There is no indication of a qQ branch, showing that the change in dipole moment involved in the transition is practically perpendicular to the axis of least moment of inertia of the molecule.

Figure 2 is the ν(C−H) vibration of HCOOD. Unlike the previous picture it does not have quite the regular symmetric appearance expected of a perpendicular band but shows evidence of some perturbing influence. While the bands on the low frequency side are sharp and regular, those on the high frequency half are indistinct and not evenly spaced. The average band separation in the pQ branch is exactly that of the typical pQ branch of ν(O−D), HCOOD, Fig. 3, but it does not have the proper convergence. By drawing a line graph of the structure of Fig. 3 and comparing it with one for Fig. 2, the tentative K assignments of Table II are made. This places ν_0 at about 2948 cm^{-1}. Because the assigned K-values are not at all certain, no attempt has been made to determine rotational constants.

Figure 3 is the ν(O−D) vibration of HCOOD. It is a regular perpendicular band for which the pQ branch shows twenty-three members and the rQ, sixteen. The large peak at 2681.3 cm^{-1} is a background band and does not belong to the main structure. The band center is at 2631.88 cm^{-1} and just below it there is a small qQ branch.

Figure 4 shows the ν(O−D) band of DCOOD. Like the preceding bands its pQ branch shows more structure than the rQ. Here there is the added difficulty to analysis that the irregular structure on the extreme high frequency side is mainly caused by the presence of D_2O in the sample. The band center is at 2632.28 cm^{-1} and again there is a small qQ branch.

Figure 5 is the ν(C−D) stretching frequency of DCOOH. The band center is at 2219.84 cm^{-1} with a fairly strong qQ branch just below it.

Figure 6 shows the spectrum of the ν(C−D) region of DCOOD. Like the ν(C−H) of HCOOD, the regular band symmetry is destroyed by some

TABLE I. Important bands studied. All spectra taken in first order.

Fig.	Molecule	$\lambda(\mu)$	$\nu(cm^{-1})$	$T(°C)$	P (mm. Hg)	Cell length (cm)	Grating lines/in.	Spectral slit width (cm^{-1})
1	HCOOH	3.40	2942.85	170	64±10	15	4800	1.1
2	HCOOD	3.40	*ca.* 2948	170	60±10	15	7500	0.9
3	HCOOD	3.80	2631.88	170	68±10	15	4800	1.1
4	DCOOD	3.80	2632.28	150	58±10	15	4800	1.0
5	DCOOH	4.51	2219.84	150	58±10	15	4800	0.9
6	DCOOD	4.48	2231.83	163	60±10	15	4800	1.0

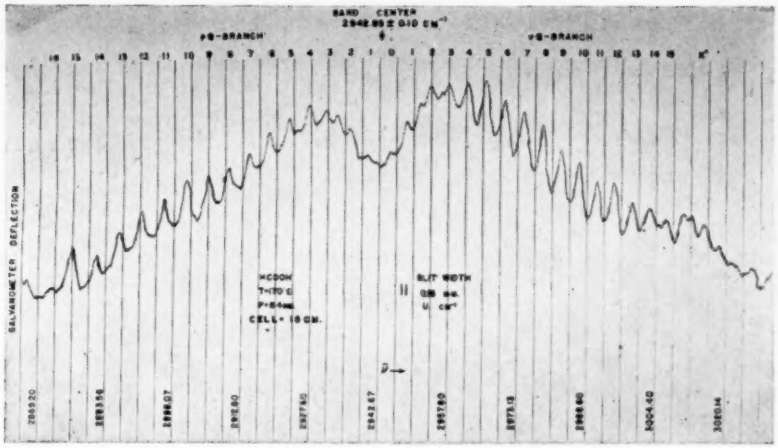

FIG. 1. ν(C−H), HCOOH.

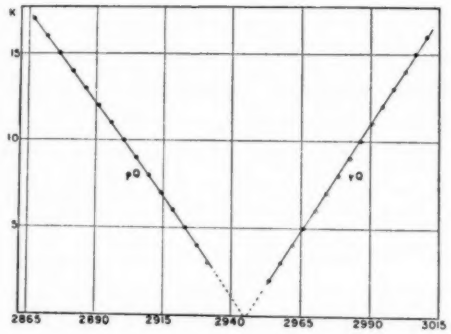

FIG. 1a. Fortrat diagram ν(C−H), HCOOH.

TABLE Ia. ν(C−H); HCOOH.

K''	ν(cm^{-1}) pQ branch	$\Delta\nu$	ν(cm^{-1}) rQ branch	$\Delta\nu$	$(\gamma'-\delta)$ (cm^{-1})	$(\gamma''-\delta)$ (cm^{-1})	ν_0 (cm^{-1})
0							
1							
2			2953.9	4.0			
3	2931.0	3.8	57.9	4.2			
4	27.2	4.3	62.1	4.0			
5	22.9	4.2	66.1	4.2	2.160	2.170	2942.90
6	18.7	4.5	70.3	4.2	150	63	2.85
7	14.2	4.4	74.5	4.3	54	61	2.88
8	09.8	4.5	78.8	4.0	56	63	3.04
9	05.3	4.6	82.8	4.2	53	69	3.01
10	00.7	4.7	87.0	3.8	58	70	3.09
11	2896.0	4.8	90.8	3.8	55	77	2.94
12	91.2	4.6	94.6	4.2	54	71	2.76
13	86.6	4.9	98.8	4.1	58	71	2.91
14	81.7	5.2	3002.9	3.7	64	84	2.89
15	76.5	4.6	06.6	4.0	68	83	2.54
16	71.9	5.0	10.6		67	82	2.68
17	66.9						
				Average:	2.158	2.172	2942.85 ±0.1

perturbing factor, but it is possible here to identify the ν(C−D) absorption band. By comparing a line graph of the ν(O−D), DCOOD, Fig. 4 structure with this band, one finds a very close correspondence if the K-assignments are made as shown. With this analysis, ν_0 can be computed to lie at 2231.83 cm^{-1} and the values of $\gamma'-\delta$, and $\gamma''-\delta$ are in close agreement with those obtained from the ν_0(O−D) band. Without a complete knowledge of the spectrum of DCOOD, one cannot with certainty account for the large band at 2195 cm^{-1} and the regular structure at lower frequency. At first the structure was thought to be due to carbon monoxide in the cell, but closer examination showed that neither the exact frequencies nor the convergence of the peaks fitted that molecule. In order to be sure, two or three runs were made with fresh samples of DCOOD, but the structure remained. A possible explanation of this region may be that a combination band of two lower frequencies at 1040 and 1171 cm^{-1} would fall at 2211 cm^{-1} about midway between the peaks of Fig. 6. There might be a slight interaction between the combination band and the ν(C−D) fundamental which would tend to spread the two peaks about the central position.

By comparing the appearance of these bands, one can see the influence of the asymmetry of the molecule. On going from HCOOH to DCOOD, the ratio of the principal moments of inertia changes from 1:7:8 to 1:4.5:5.5. In the spectra, the bands of HCOOH are sharp and well resolved,

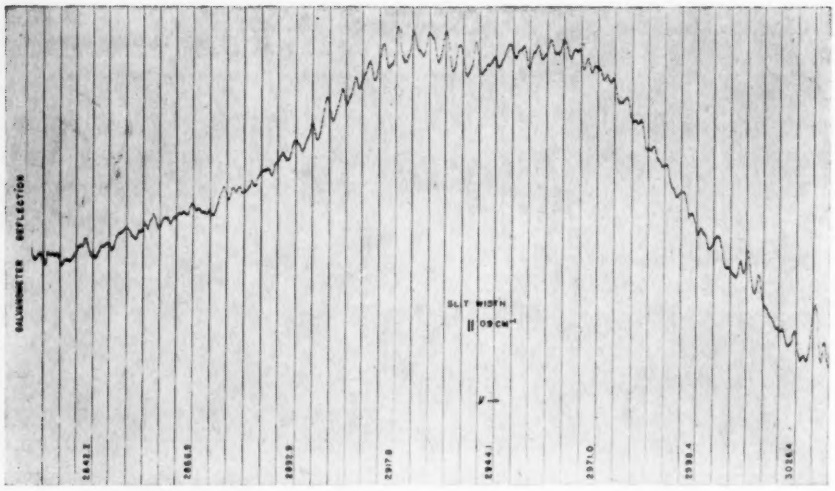

FIG. 2. ν(C−H), HCOOD.

TABLE II. ν(C−H); HCOOD.

Band center approximately		$\nu_0 = 2948$ cm^{-1}
K''	ν(cm^{-1})	$\Delta\nu$
17	2884.7	
		4.2
16	88.9	
		3.5
15	92.4	
		3.9
14	96.3	
		3.7
13	2900.0	
		3.9
12	03.9	
		3.5
11	07.4	
		3.7
10	11.1	
		3.4
9	14.5	
		3.9
8	18.4	
		4.1
7	22.5	
		4.4
6	26.9	
		4.0
5	30.9	
		3.8
4	34.7	
		4.0
3	38.7	
	43.7	
	47.7	
	51.5	
	55.1	
2	58.6	
		3.3
3	61.9	
		3.8
4	65.7	
		2.6
5	68.3	
	70.7	
	73.4	
7	75.2	
		3.3
8	78.5	
		4.1
9	82.4	
		3.7
10	86.1	
		3.5
11	89.6	
	94.3	
	96.7	
	99.8	

while those of DCOOD are smaller and more diffuse.

The values of $\gamma'-\delta$ and $\gamma''-\delta$ agree well among themselves, the spread in the values being about one percent. The average values are certainly good to one percent. The quantity $\gamma''-\delta$ for HCOOH has been previously determined by Herzberg and Verleger,[1] Bauer and Badger,[2] and Thompson.[3] Herzberg and Verleger, with lower dispersion than the other two, gave a rough value of $\gamma''-\delta=2.1$ cm^{-1}. Bauer and Badger obtain a value of 2.2106 cm^{-1} while Thompson gives an average of 2.202 cm^{-1}. These are to be compared with the value of 2.172 found in this work. Actually, Bauer and Badger had an average value of 2.196 cm^{-1}, but in fitting their data to an energy-level diagram of the form $W/hc=J(J+1)\delta+K^2(\gamma''-\delta)+\mu K^4$, this was raised to 2.2106 cm^{-1}. No attempt was made to fit the data of this work to an energy expression as the experimental positions of the peaks were not sufficiently accurate to make the resulting values of $\gamma''-\delta$ more significant than the average value. The value of 2.196 lies slightly outside the limit of error of the 2.172 determination. There is no apparent reason for this discrepancy although it must be remembered that the two values were obtained from different bands. Even so the values determined in this work for DCOOD were on different bands yet were very close, i.e., 1.328 and 1.320. It would be interesting to compare the value obtained from a study of the ν(O−H) fundamental with those of the above authors who worked on the ν(O−H) harmonics.

The spread in the values of ν_0 is approximately 0.3 cm^{-1}. The main inaccuracies in determining the frequency positions of the peaks are (1) the difficulty in setting on the point of maximum ab-

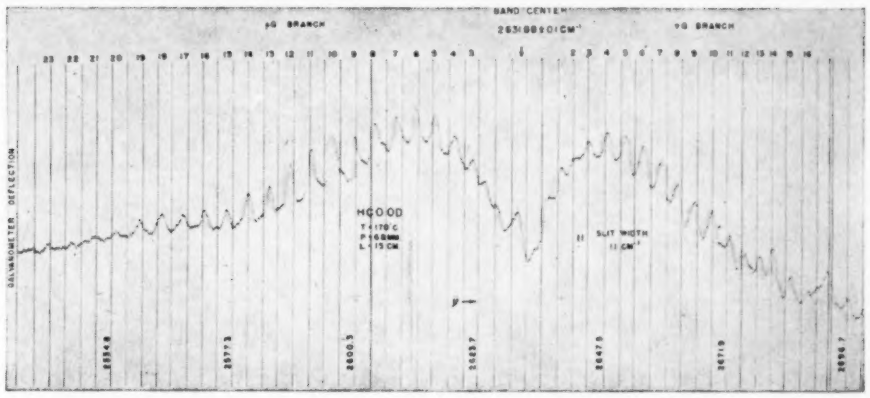

FIG. 3. ν(O−D), HCOOD.

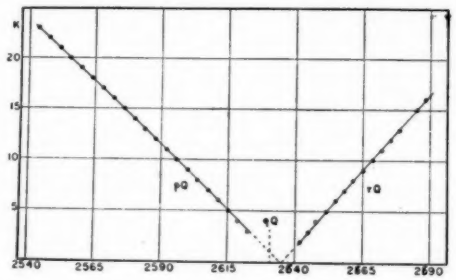

FIG. 3a. Fortrat diagram ν(O−D), HCOOD.

sorption when the peaks are not sharp, and (2) errors in calibration by use of the zero-order spectrums. Since several peaks are used in calculating ν_0, the first inaccuracy should average out leaving the second as the main source of possible error.

DISCUSSION

The results of this work give four data, the values of $\gamma''-\delta$, for the four molecules having essentially the same geometric structure. A fifth datum is given by the $\delta=0.348$ cm^{-1} value of Bauer and Badger.[2] Since there are more structural parameters than there are data, certain assumptions must be made.

The first assumption is the natural one that the molecule is planar. The C−H, C=O, and C−O bonds must lie in a plane because the structure

is known to be planar. Pauling[9] has shown that there is resonance in the carboxyl group between the two carbon oxygen bonds which would tend to prevent free rotation of the hydroxyl bond. Moreover the observed vibrations for ν(O=H) at 3567 cm^{-1} and ν(O−D) at 2632 cm^{-1} are lower than the normal frequencies at 3680 and 2720 cm^{-1} in spite of the fact that the partial double bond character of the C−O link would

[9] L. Pauling, *The Nature of the Chemical Bond* (Cornell University Press, Ithaca, New York, 1939).

TABLE III. ν(O−D); HCOOD.

K''	ν(cm^{-1}) pQ branch	$\Delta\nu$	ν(cm^{-1}) rQ branch	$\Delta\nu$	$(\gamma'-\delta)$ (cm^{-1})	$(\gamma''-\delta)$ (cm^{-1})	ν_0 (cm^{-1})
qQ	2630.8						
0							
1							
2							
3	2622.5		2644.6				2631.85
		3.7		3.3			
4	18.8		47.9		1.819	1.838	1.74
		3.6		3.7			
5	15.2		51.6		20	20	1.91
		3.7		3.4			
6	11.5		55.0		13	21	1.90
		3.6		3.4			
7	07.9		58.4		04	25	1.97
		4.0		3.3			
8	03.9		61.7		06	22	1.82
		3.8		3.5			
9	00.1		65.2		08	25	1.89
		4.1		3.6			
10	2596.0		68.8		20	28	1.88
		3.9		3.5			
11	92.1		72.3		23	32	1.96
		3.9		3.3			
12	88.2		75.6		21	38	1.87
		4.1		3.1			
13	84.1		78.7		19	37	1.78
		4.0					
14	80.1					30	
		3.9		6.5			
15	76.2		85.2		17		1.81
		4.1		3.4			
16	72.1		88.6		20	30	1.86
		4.0					
17	68.1					31	
		4.0					
18	64.1						
		4.2					
19	59.9						
		4.3					
20	55.6						
		3.8					
21	51.8				Average: 1.816	1.829	2631.88 ±0.1
		4.2					
22	47.6						
		4.2					
23	43.4						

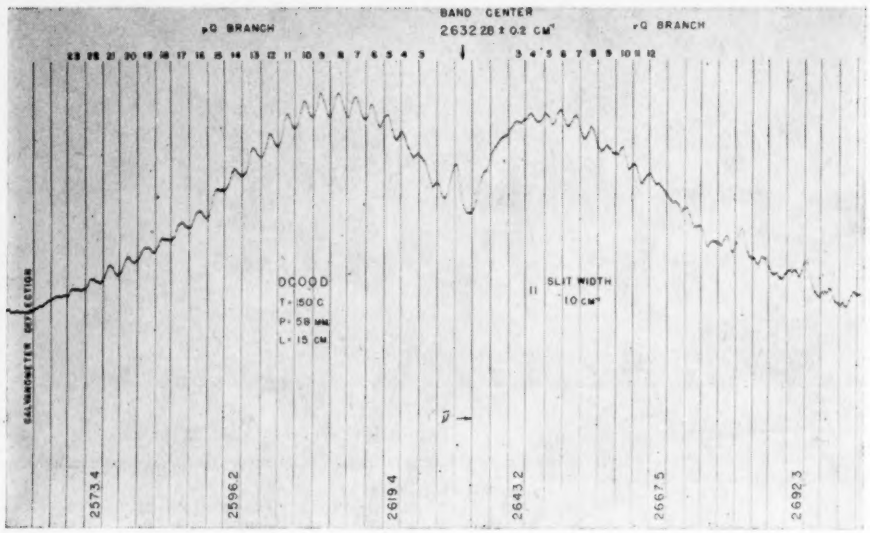

FIG. 4. ν(O−D), DCOOD.

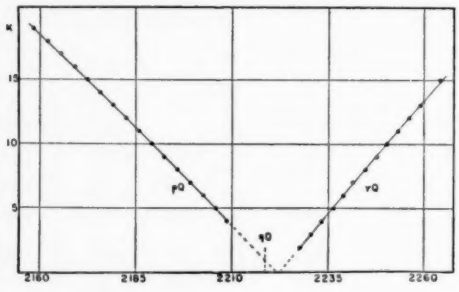

FIG. 4a. Fortrat diagram ν(O−D), DCOOD.

tend to increase these frequencies. This decrease implies a weakening of the O−H bond which could be caused by an attraction between the hydroxyl hydrogen and the double bond oxygen. Coop, Davidson, and Sutton,[10] using dipole moment data for HCOOH, infer for the monomer a *cis*- and *trans*-position for the hydroxyl group with the *cis* the dominant form. This *cis*-position of the hydroxyl is strongly supported by the perpendicular band character of the ν(O−H) and ν(O−D) absorptions. If this linkage were in the *trans*-position, these would be more nearly parallel bands. Karle and Brockway[11] doing electron diffraction studies postulate a planar structure for the monomer. Hence all the data, spectroscopic, dipole moment, resonance, and electron diffraction are in agreement on the planarity.

[10] I. E. Coop, N. R. Davidson, and L. E. Sutton, J. Chem. Phys. 6, 905 (1938).
[11] J. Karle and L. O. Brockway, J. Am. Chem. Soc. 66, 574 (1944).

TABLE IV. ν(O−D); DCOOD.

K''	ν(cm^{-1}) pQ branch	$\Delta\nu$	ν(cm^{-1}) rQ branch	$\Delta\nu$	$(\gamma'-\delta)$ (cm^{-1})	$(\gamma''-\delta)$ (cm^{-1})	ν_0 (cm^{-1})
qQ	2631.5						
0							
1							
2	2628.4						
		2.8					
3	25.6		2641.9				
		2.9		2.2			
4	22.7		44.1				
		2.6		2.5			
5	20.1		46.6		1.325	1.330	2632.19
		2.6		2.3			
6	17.5		48.9		08	17	.13
		2.5		2.7			
7	15.0		51.6		07	14	.32
		2.9		2.7			
8	12.1		54.3		19	22	.33
		2.8		2.7			
9	09.3		57.0		25	28	.40
		2.8		2.6			
10	06.5		59.6		28	35	.43
		2.9		2.2			
11	03.6		61.8		23	39	.23
		2.9		2.7			
12	00.7		64.5		29	31	.29
		2.8					
13	2597.9					37	
		2.9					
14	95.0						
		2.9					
15	92.1						
		2.9					
16	89.2						
		3.0					
17	86.2						
		3.0					
18	83.2						
		2.8					
19	80.4				Average: 1.321	1.328	2632.28 ±0.2
		2.9					
20	77.5						
		2.9					
21	74.6						
		3.0					
22	71.6						
		3.0					
23	68.6						

With this assumption there are seven parameters, four bond distances and three angles, for

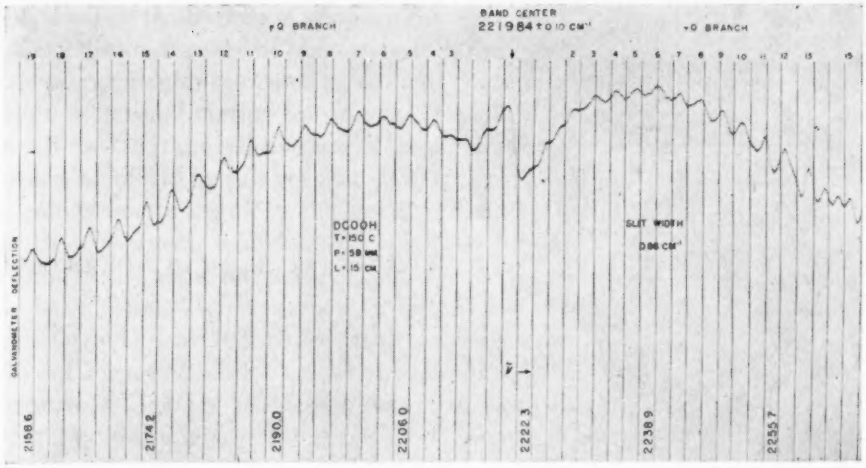

FIG. 5. ν(C−D), DCOOH.

TABLE V. ν(C−D); DCOOH.

K''	ν(cm^{-1}) pQ branch	$\Delta\nu$	ν(cm^{-1}) rQ branch	$\Delta\nu$	$(\gamma'-\delta)$ (cm^{-1})	$(\gamma''-\delta)$ (cm^{-1})	ν_0 (cm^{-1})
qQ	2218.7						
0							
1							
2			2227.7				
				2.9			
3			30.6				
				2.8			
4	08.9		33.4		1.531	1.544	2219.86
		3.0		2.8			
5	05.9		36.2		15	45	19.90
		3.4		2.8			
6	02.5		39.0		21	38	19.76
		3.2		2.9			
7	2199.3		41.9		21	39	19.81
		3.4		2.8			
8	95.9		44.7		25	44	19.73
		3.4		3.0			
9	92.5		47.7		33	42	19.79
		3.3		2.7			
10	89.2		50.4		30	48	19.77
		3.4		3.0			
11	85.8		53.4		36	41	19.89
		3.2		2.9			
12	82.6		56.3		35	46	20.08
		3.4		3.0			
13	79.2		59.3		40	46	
		3.3					
14	75.9					48	20.55
		3.3					
15	72.6		64.8		37		
		3.5					
16	69.1					52	
		3.6					
17	65.5						
		3.5					
18	62.0						
		3.6					
19	58.4						
					Average: 1.529	1.544	2219.84 ± 0.2

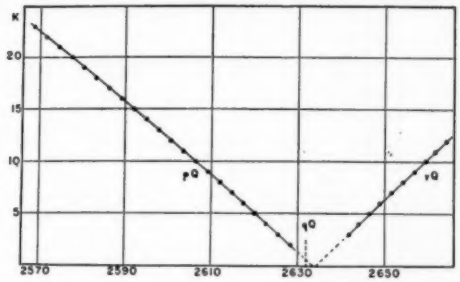

FIG. 5a. Fortrat diagram ν(C−D), DCOOH.

which there are five data. The two obvious values to assume are the hydrogen bond distances. The C−H distance is assumed to be 1.08A. It will be shorter than the 1.09A of methane because the carbon is unsaturated but it will be longer than the 1.07A of ethylene because the ν(C−H) frequency is 2943 cm^{-1} rather than greater than 3000 cm^{-1} as for a typical H−C= linkage. The O−H distance is considered to be 0.96–0.97A. The normal hydroxyl distance is 0.96A and Badger's rule,[12] using the frequency lowering, brings this value to 0.97A. With these assumptions the problem is reduced to five data and five parameters.

The remaining parameters were obtained by calculating the constants δ and $\gamma''-\delta$ for various tentative structures. The moments of inertia of the assumed structures were first calculated for arbitrary axes in the plane of the molecule, converted to principal moments by principal axes transformation, δ and $\gamma''-\delta$ calculated and compared with the experimental data which were considered good to ±1 percent. A structural model was found which would give good agreement between calculated and experimental results. Individual parameters were then varied over a plus and minus range from this model to determine the effect on δ and $\gamma''-\delta$ of each

[12] R. M. Badger, J. Chem. Phys. **3**, 710 (1935).

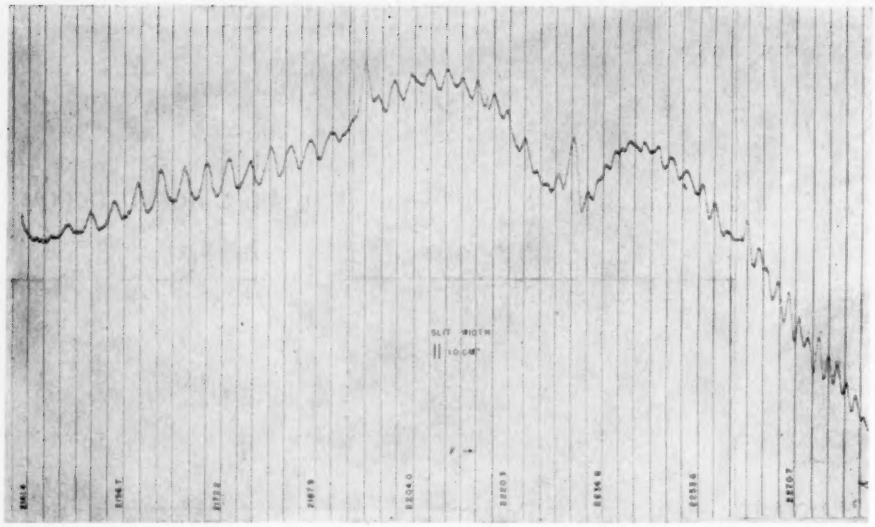

FIG. 6. ν(C−D), DCOOD.

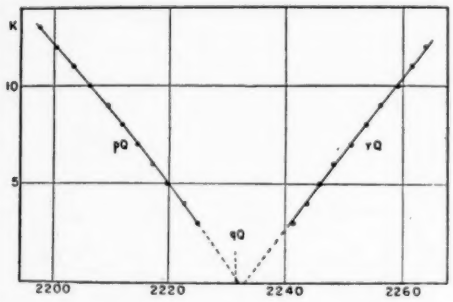

FIG. 6a. Fortrat diagram ν(C−D), DCOOD.

parameter separately. With this knowledge, it was possible to combine various values of these parameters which would give calculated results within the limits of error. In general, the final structure was chosen to be the median value of the possible variations of these parameters and the extreme values fixed the limits of error. The effect of these variations is given in some detail, and reference to Fig. 7, the final model chosen, will be of aid in following the discussion. In these considerations it should be noted that although the evaluation of $\gamma''-\delta$ involves all three moments of inertia (A, B, and C), the least moment (C) is the governing factor as a change of six or seven percent in δ represents about one percent change in $\gamma''-\delta$.

The Angles H−C=O and C−O−H

It can be seen that variations in these angles will have but slight effect on the values of $\gamma''-\delta$. Their contribution to C enters as the sine of the

TABLE VI. ν(C−D); DCOOD.

K''	ν(cm^{-1}) pQ branch	$\Delta\nu$	ν(cm^{-1}) rQ branch	$\Delta\nu$	$(\gamma'-\delta)$ (cm^{-1})	$(\gamma''-\delta)$ (cm^{-1})	ν_0 (cm^{-1})
qQ	2231.2						
0							
1							
2							
3			2241.3				2231.79
4	2222.7		43.6	2.3	1.306		1.95
5	19.6	3.1	45.8	2.2	310	1.320	1.56
6	17.2	2.4	48.3	2.5	296	04	1.69
7	14.5	2.7	51.1	2.8	307	04	1.83
8	11.8	2.7	53.9	2.8	316	06	1.99
9	09.3	2.5	56.2	2.3	303	25	2.00
10	06.2	3.1	59.4	3.2	330	23	2.19
11	03.3	2.9	61.7	2.3	327	41	2.03
12	00.4	2.9	64.0	2.3	325	38	1.90
13	2197.5	3.1					
	2195.6 (Large peak)						
	90.6	3.7					
	86.9	3.3					
	83.6	3.3					
	80.3	3.5			Average: 1.313	1.320	2231.83 ±0.2
	76.8	3.5					
	73.3	3.5					
	69.8	3.5					
	66.3	3.7					
	62.6	3.7					
	58.9	3.6					
	55.3	3.7					
	51.6	3.8					
	47.8						

angle which the hydrogen bonds make with the C axis. This angle must be very close to 90° to give the perpendicular bands observed and the sine is not a sensitive function for an angle near 90°. It was hoped that the relative size of the qQ branches would be of aid in this respect. If the change in dipole moment lies along the bond, the strength of the qQ branch would be proportional to the cosine of the angle formed by the hydrogen bond and the C axis—a very sensitive function when this angle is near 90°. Unfortunately, consideration of Figs. 1, 5, and 7 quickly blasts this hope, because ν(C−H) of HCOOH shows no qQ branch (Fig. 1) while ν(C−D) of DCOOH shows a relatively strong (but absolutely weak) one (Fig. 5). It can be seen from Fig. 7 that the carbon hydrogen lies very close to the B axis, so close that a change in its mass from 1 unit in 46 to 2 units in 47 could not possibly rotate the principal axes enough to produce the qQ branch difference shown, assuming the total magnitude of dipole moment change in each case to be similar. Evidently the dipole moment change does not lie strictly along the bond and the qQ branch can be used only as evidence that the bonds must be fairly close to 90° with respect to the C axis.

The value of the H−C=O angle was taken as 122° for which the CH bond makes an angle of 0° with the B axis for HCOOH. The variation is taken as ±5° to accord with the weak qQ branches. Values of δ for the other three molecules would not help in this determination because the hydrogen is too close to the B axis to produce much variation in δ on isotopic substitution.

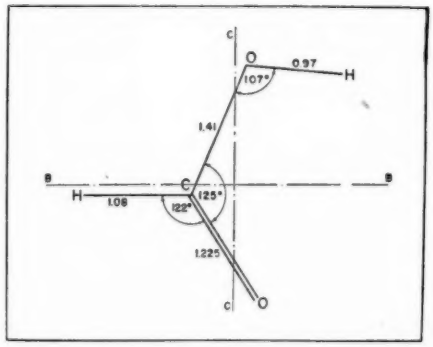

FIG. 7. Structure of the planar molecule HCOOH with principal axes B and C shown.

TABLE VII. Values of various constants of monomeric formic acids.

Molecule	Constant	Experimental values	Model of Fig. 7	Model of Karle and Brockway[11]
	Moments of inertia ($\times 10^{40}$ g cm^2)			
HCOOH	A	86.38	85.99	83.46
	B	75.27	74.89	70.39
	C	11.11	11.10	13.07
HCOOD	A		89.84	
	B		76.88	
	C		12.96	
DCOOH	A		89.70	
	B		74.92	
	C		14.78	
DCOOD	A		93.71	
	B		76.94	
	C		16.76	
	Parameters δ and $\gamma-\delta$ (cm^{-1})			
HCOOH	δ	0.348*	.350	
	$\gamma''-\delta$	2.172	2.172	
HCOOD	δ		.338	
	$\gamma''-\delta$	1.829	1.822	
DCOOH	δ		.343	
	$\gamma''-\delta$	1.544	1.550	
DCOOD	δ		.331	
	$\gamma''-\delta$	1.328	1.339	
	Angles between C−H, O−H and B axis			
HCOOH	CH		10′	
	OH	4°*	5° 40′	
HCOOD	CH		1° 55′	
	OH		3° 55′	
DCOOH	CH		30′	
	OH		5° 20′	
DCOOD	CH		2° 25′	
	OH		3° 25′	

* Values taken from Bauer and Badger.[2]

The value of the C−O−H angle was taken as 107° with a variation of ±5°. An angle of 112° would be large if the hydrogen were attracted to the double bond carbon, and an angle of 102° would show greater qQ branches. Here the other values of δ would be of some aid because this isotopic substitution has a noticeable effect (about 1 percent for 5°) in the intermediate moment.

The Distances C−O and C=O

These distances were varied according to Pauling's rule[9] for single-double bond interaction. The values considered were 1.22A and 1.43A for zero-interaction; 1.225 and 1.40 for 1/20 mixing; and 1.23 and 1.38 for 1/10 mixing. It was found that these bonds could not exceed the limits of 1/10 mixing. Variation over this range produced a 3 percent change in δ so again the other values

of δ would be of importance in fixing the results. The distances chosen were, C=O, 1.225±0.02A and C−O, 1.41±0.02A.

The O−C=O Angle

The values of $\gamma''-\delta$ were exceptionally sensitive to this angle for a 7 percent change results in a variation from 124° to 126°. In fact the variation between the Bauer and Badger value of 2.2106 cm^{-1} and this value of 2.172 cm^{-1} is just the difference between 126° and 125°. Therefore the value of this angle is fairly accurately determined as 125±1°.

The structure of the HCOOH monomer is shown in Fig. 7 with the best values designated. The position of the principal axes B and C are shown. This structure is in fairly good agreement with that given by Bauer and Badger[2] although it is felt that the present values are more accurate because of the greater number of data available for the calculations. The structure is considerably different from that obtained by Karle and Brockway[11] from electron diffraction data as their results fall considerably outside the limits of error judged for this work. To illustrate this difference, Table VII compares the A, B, and C moments of inertia according to experimental results, the model derived in this work, and that of Karle and Brockway. Table VII also includes the various values for δ, $\gamma''-\delta$ and the angles which the hydrogen bonds make with the B axis.

ACKNOWLEDGMENTS

The author wishes to acknowledge his indebtedness to Dr. L. G. Smith for advice and encouragement and to the Calco Chemical Division of the American Cyanamid Company for financial support.

Infra-Red Spectra of Monomeric Formic Acid and Its Deuterated Forms. II. Low Frequency Region (2200–800 cm^{-1})*

VAN ZANDT WILLIAMS**
Princeton University, Princeton, New Jersey
(Received January 14, 1947)

High resolution infra-red studies have been made of monomeric HCOOH, HCOOD, DCOOH, and DCOOD in the region 2200 cm^{-1} to 800 cm^{-1}. Consideration is given to the possibility of the existence of a *trans*-form of the molecule. The bands observed are not sufficiently regular in appearance or absorption frequency to permit assignment of vibrational modes without further knowledge of the spectra.

INTRODUCTION

PREVIOUS workers[1,2,3] have made infra-red studies of the deuterated forms of monomeric formic acid from 4000 cm^{-1} to 650 cm^{-1} with a low dispersion instrument. They had hoped that vibrational modes associated with the O—C=O core of the molecule would maintain fairly constant frequencies of absorption with deuteration while those arising from a motion of the hydrogen atoms would shift by a predictable amount. If this had proved true it might have been possible to assign some of the observed frequencies to characteristic modes. As such behavior was not observed in the low dispersion studies, the spectra from 3700 cm^{-1} to 800 cm^{-1} were studied under high resolution in the hope that the additional band structure would be of further aid in the assignments.

EXPERIMENTAL

The instrument used, the preparation of samples, and the instrumental techniques have been given in paper I.[4] Table I gives a list of the bands studied, together with the conditions under which each spectrum was observed. Figure 1 shows a schematic summary of all the bands observed (including those in the high frequency region). In Fig. 1, as in all subsequent figures, absorption is shown upward on the ordinate and frequency in cm^{-1} on the abscissa. In the

TABLE I. Important bands studied. All spectra taken in first order except Fig. 9 which was in the second order.

Fig.	Molecule	$\lambda(\mu)$	ν(cm^{-1})	T(°C)	P(mm Hg)	Cell length (cm)	Grating lines/in.	Spectral slit width (cm^{-1})
1	HCOOH	8.3		165	55±10	15	1800	1.1
2	HCOOH	9.06	1105.3	163	10±1	15	1800	1.3
3	HCOOH	9.69	1033.2	165	65±10	15	1800	0.8
4	HCOOD	8.50	1178.0	163	25±3	15	1800	1.4
5	HCOOD	9.94 10.28	1007.0 972.5	165	25±3	15	1800	1.0
6	DCOOH	8.76	1142.7	163	50±10	8	1800	1.3
7	DCOOH	10.30	970.6	165	30±3	8	1800	1.1
8	DCOOD	8.54	1171.3	163	15±2	15	1800	1.1
9	DCOOD	9.62	1040.2	165	50±10	15	1440	0.7
10	DCOOD	10.59	945.5	165	25±3	15	1800	1.2
11	HCOOH	4.55	2199.8	163	400±50	15	7500	0.7
12	HCOOD	4.62	2142.4 2178.8	165	400±50	15	7500	0.7
13	DCOOD	11.45	873.2	165	300±50	15	1800	1.0

* This material was presented in partial fulfillment of the requirement for the degree of Doctor of Philosophy, March, 1941.
** Present address: Stamford Research Laboratories, American Cyanamid Company, Stamford, Connecticut.
[1] L. G. Bonner and R. Hofstadter, J. Chem. Phys. **6**, 531 (1938).
[2] R. Hofstadter, J. Chem. Phys. **6**, 540 (1938).
[3] R. C. Herman and V. Z. Williams, J. Chem. Phys. **8**, 447 (1940).
[4] V. Z. Williams, J. Chem. Phys. **15**, 232 (1947).

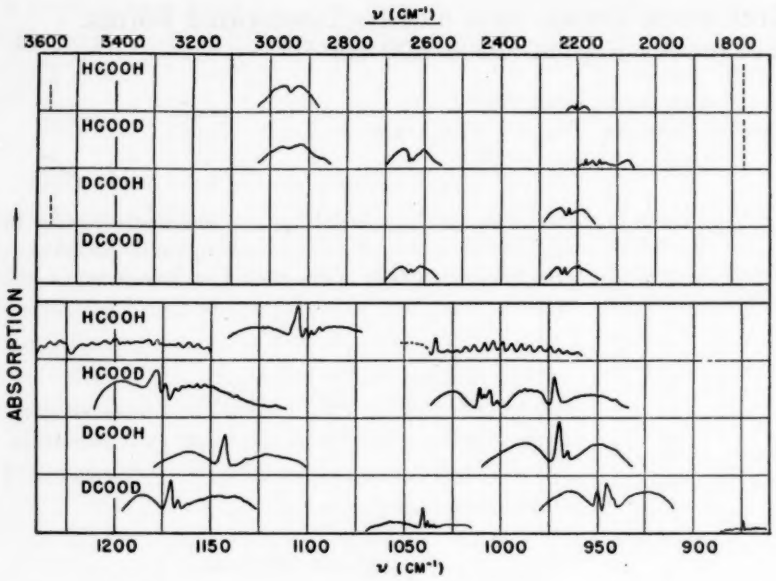

FIG. 1. Schematic representation of the absorption bands of HCOOH, HCOOD, DCOOH, DCOOD 3700–800 cm^{-1}.

schematic drawing height is roughly proportioned to intensity. Actually an attempt was made to regulate the pressure so that the strongest absorption for each band was of the order of 50–80 percent. This fact combined with the pressures and cell lengths of Table I gives a more accurate conception of relative intensities. The actual recorded spectra of the principal low frequency bands are shown in Figs. 2–11 and are discussed in some detail below. These bands were studied with a fixed fore-prism slit which gave a background energy distribution greater in the middle than at the extremes. This tends to flatten out the observed absorption and is corrected roughly in Fig. 1. An interesting feature of many of these bands is the occurrence of a sharp satellite very near the qQ branch of the main band. Whenever possible, these bands were studied at room temperature and the intensity of the satellite was observed to decrease appreciably.

Although the absorption of atmospheric water vapor was very strong from 1900 cm^{-1} to 1300 cm^{-1} an attempt was made to study this region. The only bands observed were the expected C=O frequencies. The point of maximum absorption for HCOOH and HCOOD seemed to be about 1770 cm^{-1}. These bands (like the ν(O−H) bands) are shown as dotted lines in

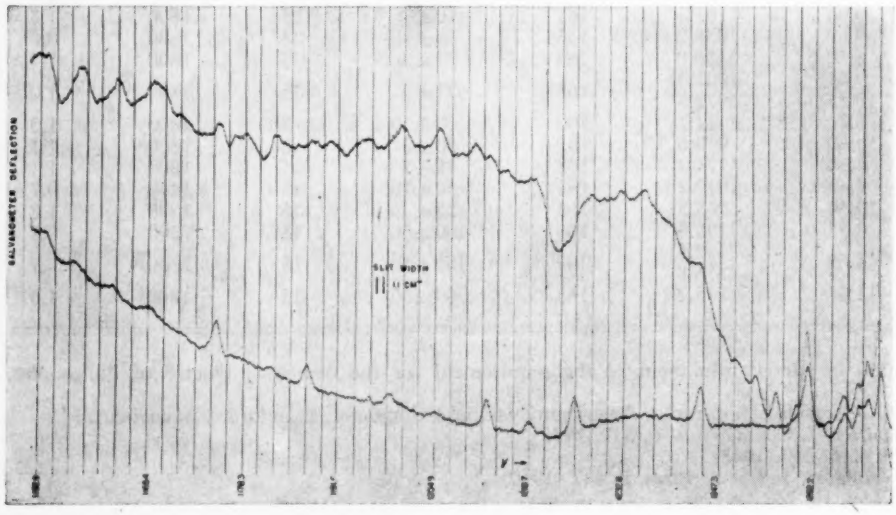

FIG. 2. Absorption of HCOOH *ca.* 1200 cm^{-1}.

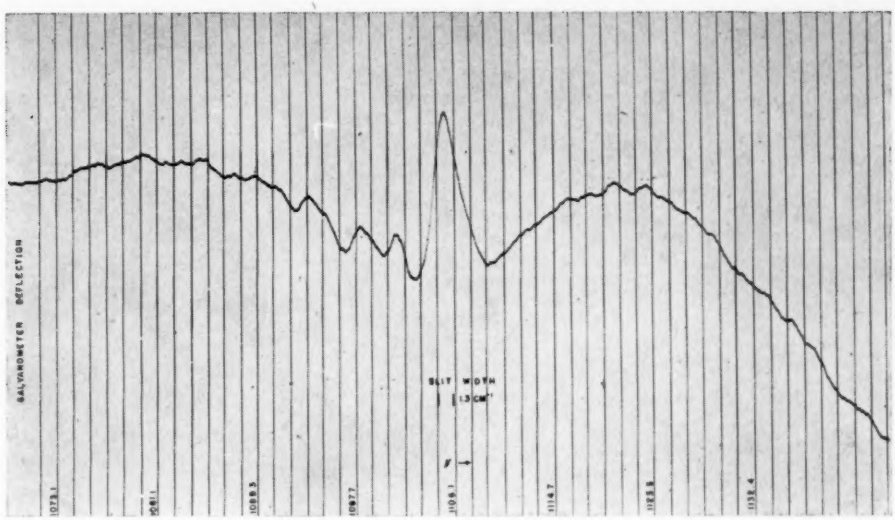

FIG. 3.
HCOOH, 1105.3 cm^{-1}

Fig. 1. No tentative values could be determined for the ν(C=O) of DCOOH or DCOOD.

HCOOH

HCOOH has three regions of absorption, *ca.* 1200 cm^{-1}, 1105 cm^{-1}, and 1033 cm^{-1} between 1700 cm^{-1} and 800 cm^{-1}. Figure 2 shows the absorption band of HCOOH in the 1200 cm^{-1} region and the background with the cell evacuated. The spectrum was not continued to lower frequency because of the intense absorption of the adjacent band at the pressure used. The structure is highly irregular and does not conform to the expected pattern of a parallel and/or perpendicular band. Frequency values of the irregularly spaced HCOOH peaks are given in Table II(a). This band could not be studied at low temperature because the dimer has strong absorption in the same region. However, the structure of Fig. 2 results from the monomer because the dimer band is quite regular and shows no structure.

The strong band at 1105.3 cm^{-1} shown in Fig. 3 is predominantly a parallel band because of the strong *qQ* branch. There is some irregular structure (Table II(b)) superimposed on the *P* and *R* branches which may arise from a perpendicular component. Of particular interest are the two sharp peaks at 1101.1 cm^{-1} and 1098.1 cm^{-1} just to lower frequency of the main *qQ* branch. Certainly the 1101-cm^{-1} peak cannot be a *pQ* peak for the bands in the high frequency

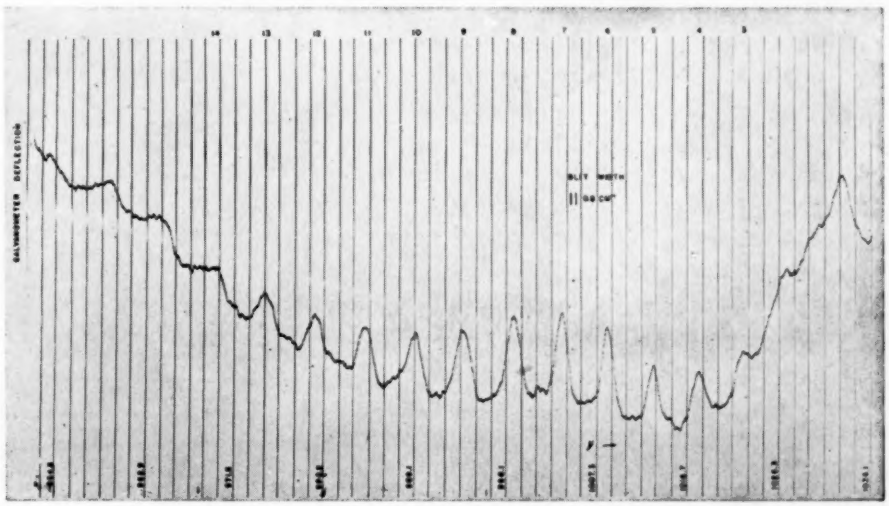

FIG. 4.
HCOOH, 1033.2 cm^{-1}.

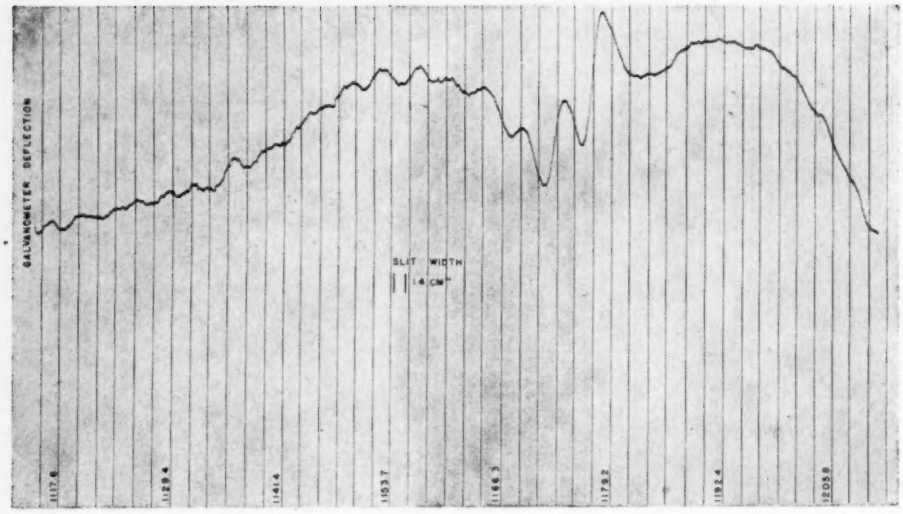

FIG. 5.
HCOOD, 1178 cm^{-1}.

region show that the asymmetry does not permit such a distinct peak so near the band center. Moreover, a study of this band at room temperature shows the higher satellite greatly decreased in intensity with respect to the main qQ branch so that it must arise from some other transition. The lower satellite seems to decrease also although it is not so obvious because the background slope changes. In addition the main qQ branch itself becomes sharper because of the loss of the shoulder on its high frequency side.

The third band of HCOOH, Fig. 4, seems to be a combined perpendicular and parallel type with its qQ branch at 1033.2 cm^{-1}. Thirteen members of its pQ branch are identified by the K-values above the peaks. The seeming lack of background in the P branch is caused by an intensity anomaly in the grating used. The R branch could not be studied because of the strong absorption of the 1105.3-cm^{-1} band. The frequency values of the $pQ(K)$ peaks are given in Table II(c). The spacings seem somewhat larger than in the ν(C−H) band but, without the rQ values, it is not possible to determine its significance in terms of the rotational constants.

HCOOD

HCOOD also shows three bands in this low frequency region. The spectrum of Fig. 5 is predominantly a parallel band with its qQ branch at 1178.0 cm^{-1}. There is definite structure in the P branch at 1168.6, 1164.5, 1160.6, 1156.9,

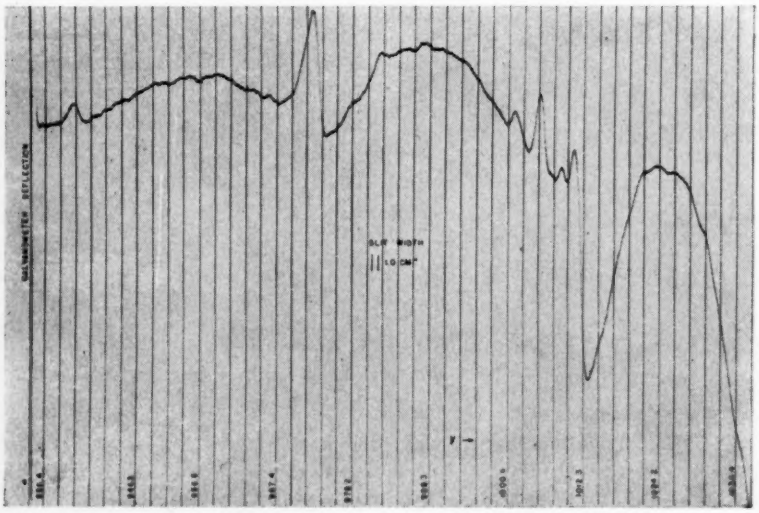

FIG. 6. HCOOD,
1007 cm^{-1} and 972.5 cm^{-1}.

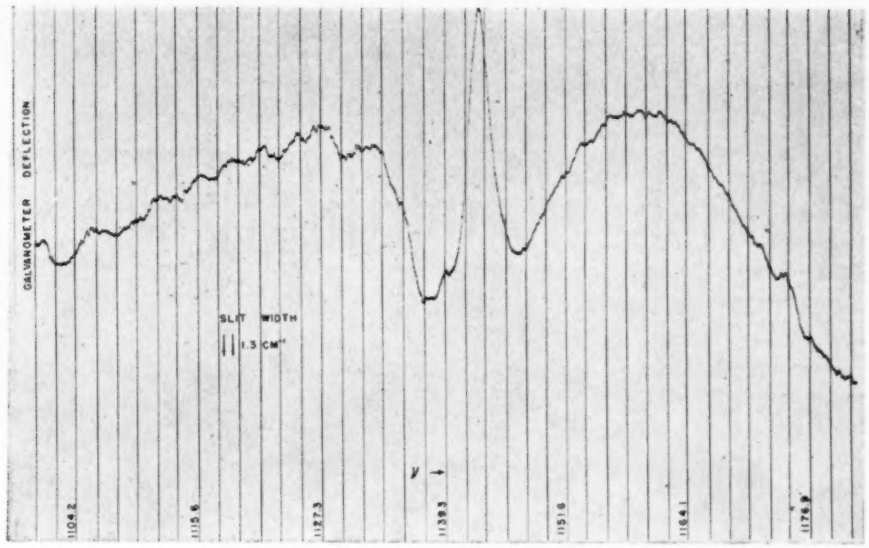

FIG. 7.
DCOOH, 1142.7 cm^{-1}.

1152.8, and 1148.6 cm^{-1} whose fairly regular separation of 4 cm^{-1} agrees with the value obtained from the ν(O−D) band and implies a perpendicular component. As in the 1105.3 cm^{-1} band of HCOOH there is a lower frequency satellite at 1173.6 cm^{-1} which decreases greatly in intensity as the temperature of the vapor is lowered.

Figure 6 shows two other bands of HCOOD, one with a qQ branch at 972.5 cm^{-1} with no satellite and the other with two qQ branches at 1005.4 and 1010.7 cm^{-1} each of which has a lower frequency satellite at 1001.5 and 1008.9 cm^{-1}, respectively. These satellites are greatly weakened at room temperature. The appearance of this second band is distorted by the above-mentioned intensity anomaly and a better idea of its appearance is gained from Fig. 1. The double peak may be caused by a resonance splitting. The origin of the 940 cm^{-1} peak is not known.

DCOOH

DCOOH shows only two bands in the region considered. Figure 7 is a parallel band at 1142.7 cm^{-1} with no appreciable satellite but some evidence of structure in its P branch. This band is essentially unchanged at lower temperature

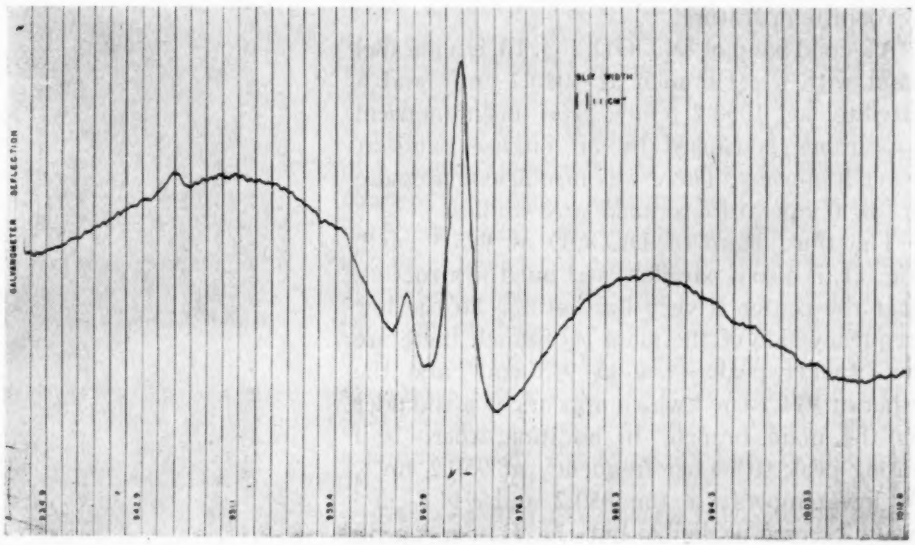

FIG. 8.
DCOOH, 970.6 cm^{-1}.

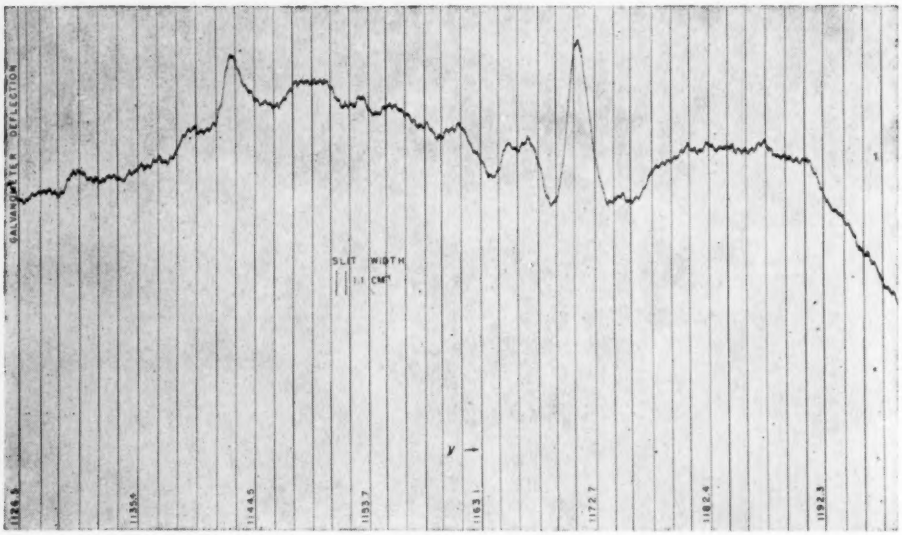

FIG. 9.
DCOOD, 1171.3 cm^{-1}.

(80°C). Figure 8 with its qQ branch at 970.6 cm^{-1} is an excellent example of a parallel band except for the satellite at 965.7 cm^{-1} and the small peak at 945.7 cm^{-1} which results from DCOOD impurity. It was not possible to study this band at room temperature because of dimer interference.

DCOOD

DCOOD again shows three bands in this region. The spectrum of the 1171.3 cm^{-1} parallel band of Fig. 9 is somewhat obscured by the D_2O impurity background and the DCOOH impurity peak at 1142.7 cm^{-1}. Again there is a satellite at 1167.0 cm^{-1} overlaid by a D_2O peak at 1165.3 cm^{-1}. The 1167-cm^{-1} peak practically disappears at room temperature.

A second band of DCOOD, Fig. 10, is a parallel band with a qQ branch at 1040.2 cm^{-1} and a satellite at 1038.2 cm^{-1}. Its unsymmetrical appearance is caused by an intense band at lower frequency. There was insufficient pressure at low temperature to make any studies.

The third band of DCOOD at 945.5 cm^{-1}, Fig. 11, is also a parallel band but the structure near the center is very interesting. To the low frequency side of the main qQ branch there are two weaker peaks—one at 943 cm^{-1} and the other at 944.7 cm^{-1} which appears as a shoulder on the main branch. In addition, there is a strong peak to higher frequency at 950.2 cm^{-1}. At low temperature the 950.2 and 944.7-cm^{-1} peaks become negligible but the 943-cm^{-1} peak remains. The peak at 970.6 cm^{-1} is a DCOOH impurity.

The above bands are all thought to be fundamentals by reason of their intensity. A careful search was made for overtone or combination bands. Three of these were found (see Fig. 1), a parallel band in HCOOH at 2199.8 cm^{-1} which is probably the first overtone of the 1105.3-cm^{-1} band; two close lying parallel bands of HCOOD at 2142 and 2179 cm^{-1} which may be combination bands of the lower frequency fundamentals; and a parallel band of DCOOD at 872.2 cm^{-1} for

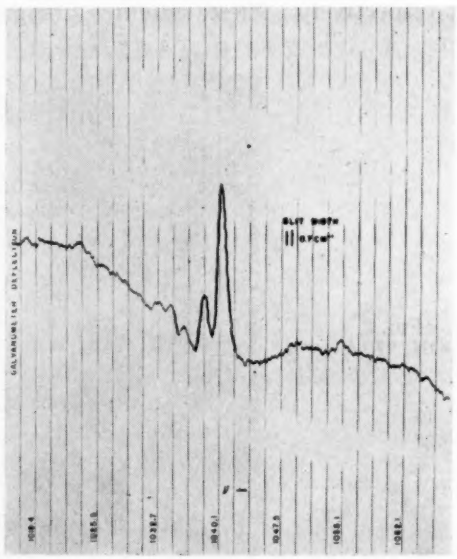

FIG. 10. DCOOD, 1040.2 cm^{-1}.

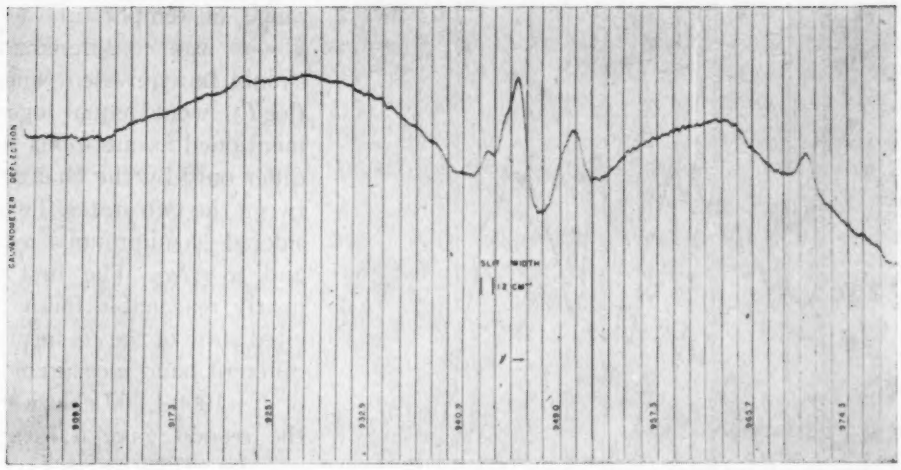

FIG. 11.
DCOOD, 945.5 cm^{-1}.

which only the qQ branch could be observed because of the intense absorption of the adjacent fundamental.

ORIGIN OF SATELLITE BANDS

Two possible explanations could be given for these satellite bands. They may arise from a quantum transition similar to the main band but having an excited vibration state as a lower state. This lower state could be the first excited level of the adjacent fundamental or of some lower frequency fundamental. As postulated by Coop, Davidson, and Sutton,[5] they might also be caused by a *trans*-isomer of HCOOH, in which the hydroxyl hydrogen is bent away from the carbonyl oxygen.

An attempt was made to study the variation of relative intensity of the main and satellite bands in order to determine the energy (or frequency) difference between the states giving rise to the two bands. The expression used for this determination was $\log(\log T_1)/(\log T_2) = \log\alpha_1/\alpha_2 - (E/k)(1/T)$, where T_1 and T_2 are the percent transmission of the satellite and main qQ branches above the background absorption of the bands; α_1, and α_2 are the absorption coefficients of the two respectively; $E=hc\nu$ is the energy difference, and T the absolute temperature. The values $\log(\log T_1)/(\log T_2)$ *vs.* $1/T$ should give a straight line from whose slope E or ν can be determined. The pairs of bands used were 1174, 1178 cm^{-1} of HCOOD, 1167, 1171 cm^{-1}, and 950, 945 cm^{-1} of DCOOD over a temperature range from 25°C to 172°C. A portion of this study is illustrated in Fig. 12 where the change in intensity of the two bands is quite marked even over the short range of temperature shown. The use of the above formula is not absolutely correct for the α-term is itself a function of temperature since the population distribution of the rotational levels of a given vibrational state changes with increasing temperature and causes a change in α. However, experiments with the 3015-cm^{-1} band of methane

TABLE II. HCOOH.

a	b		c		
1200 cm^{-1}	qQ branch 1105.3 cm^{-1}		qQ branch 1033.2 cm^{-1}		
ν(cm^{-1})	P branch ν(cm^{-1})	R branch ν(cm^{-1})	K''	Pq branch ν(cm^{-1})	$\Delta\nu$ (cm^{-1})
1151.4	1101.1	1116.0	0		
56.2	1098.1	18.0	1	1027.1	4.6
61.1	93.6	20.0	2	22.5	4.6
66.1	90.9	22.8	3	17.9	4.6
72.0	89.2		4	13.3	4.9
78.1	87.4		5	08.4	4.7
82.8	84.6		6	03.7	4.9
87.7	80.2		7	998.8	4.9
89.8	76.0		8	93.9	4.8
94.4	72.3		9	89.1	5.0
99.9			10	84.1	4.9
1205.3			11	79.2	4.9
10.6			12	74.3	4.8
14.9			13	69.5	
27.8					
32.6					
35.5					
50.0					
52.9					
56.3					
59.6					

[5] I. E. Coop, N. R. Davidson, and L. E. Sutton, J. Chem. Phys. 6, 905 (1938).

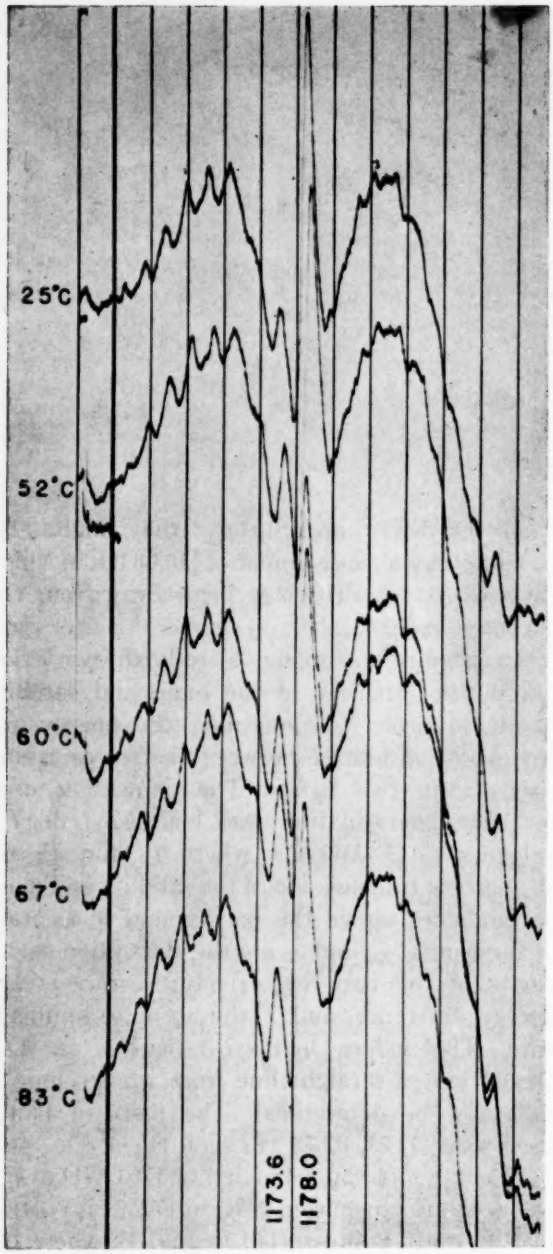

FIG. 12. Disappearance of the 1174 cm^{-1} satellite of HCOOD with decrease in vapor temperature.

shows that α can be expressed approximately as $\alpha = Ke^{-B/T}$. If this is true for HCOOH and B is approximately the same for each molecule or state, the above formula can be used.

The points obtained with the bands studied scattered badly but even by choosing extreme points the greatest difference obtained was 1400 calories (500 cm^{-1}). In order to broaden the range of temperature available the point for $T = \infty$ was considered. Here the populations should be equivalent and the term $\log(\log T_1)/(\log T_2)$ would equal $\log\alpha_1/\alpha_2$. With the above-mentioned assumptions for α, α_1 and α_2 should differ only by the change in dipole moment between the two states. Two possibilities were considered—a minimum of α_1(satellite) $= \alpha_2$(main qQ) and $\alpha_1 = 2\alpha_2$. The first possibility (the more nearly reasonable for a transition from an excited state of the *cis*-form) combined with twelve different band measurements gave a mean value of $E = 1000 \pm 200$ calories (360 ± 70 cm^{-1}), while the second gave a mean value of 1600 ± 230 calories (570 ± 80 cm^{-1}).

Of the two possible explanations for the origin of the satellite bands, the upper stage transition seems the more logical because in most cases the satellite appears at slightly lower frequency than the main band as would be expected from the usual second-order interaction terms. Although the energy difference measurements obtained from the temperature range studies are very rough, they imply an upper stage of a fundamental at much lower frequency than the adjacent one. The difficulties with this explanation are that there seems to be both lower and higher frequency satellites of the 1105 cm^{-1} band of HCOOH and of the 945 cm^{-1} band of DCOOD while some bands show no satellite at all.

Some calculations were made with the data of Coop, Davidson, and Sutton[5] to determine the energy difference between the *cis*- and *trans*-forms. The efforts were not particularly successful because of the limits of error shown, but it was evident that the *trans*-form must have a large permanent dipole and its population must increase rapidly with temperature in order to overcome the natural decrease in polarization with increasing temperature. Quantitatively, therefore, the low energy difference obtained from a measurement of relative band intensities seems in agreement with the isomer hypothesis. Qualitatively, however, this explanation does not seem so likely. It is difficult to believe that an entirely different molecule such as *trans*-HCOOH would give bands so consistently near, and similar to, those of the *cis*-form. Another argument against the *trans*-form is the appearance of the high frequency regions. The ν(O−D) of

trans-HCOOD and DCOOD would have a strong parallel component whose qQ branch should appear within 100 cm^{-1} of the *cis*-bands. No such effects were observed.

INTERPRETATION OF SPECTRA

Assuming HCOOH to be a planar molecule there will be a total of nine fundamental vibrations, seven planar and two out of the plane motions. If it were possible to assign the modes to specific atomic motions, the seven planar motions would be four stretching vibrations, O–H, C–H, C=O, and C–O, and three angular motions, two hydrogen bending and one

O bending. The two out of the plane vibrations would be essentially hydrogen motions in one of which the two hydrogens move in opposite directions and in the other in the same direction. If the vibrations were so specific, those associated with the hydrogens would give definite shifts on deuteration while those associated with the heavier core of the molecule would maintain fairly constant absorption frequency independent of deuteration. Moreover, the hydrogen stretching and the two out of the plane motions would be essentially perpendicular bands, the in-plane hydrogen bendings would be of a parallel type, and the others would be of mixed structure.

The hydrogen and carbonyl stretching vibrations are easily identified and, within limits of observation, appear as predicted. For the remaining bands these are observed in this work: HCOOH, *ca.* 1200, 1105, and 1033 cm^{-1}; HCOOD, 1178, 1007, and 973 cm^{-1}; DCOOH, only two, 1143 and 971 cm^{-1}; DCOOD, 1171, 1040, and 946 cm^{-1}. The possible resonance splitting in HCOOD may imply a fundamental near 500 cm^{-1} and the possible overtone at 875 cm^{-1} in DCOOD may mean a band near 440 cm^{-1}. In addition, there are the low dispersion results of a band in HCOOH at 667 cm^{-1} [1] and in DCOOH at 678 cm^{-1}.[3]

As pointed out from the low dispersion results the observed spectra, so far as frequency of absorption is concerned, do not fit the results predicted from the hypothesis of assigning fundamental modes to specific parts of the molecule. The high dispersion results, giving band structure, do not seem to clarify the picture further—neither the position nor the appearance of the bands correspond to the crude vibrational analysis. The peculiar absorption of HCOOH near 1200 cm^{-1} and the fact that DCOOH shows only two absorptions in the region seem anomalous. Also there may be the possibility that some of the bands denoted as fundamentals in this work may be caused by a *trans*-form of the molecule.

Evidently, explanation of these spectra must await the extension of infra-red and Raman observation, together with careful studies of relative band intensities *vs.* temperature to make certain which bands may be assigned to a single molecular species.

A Calculation of the Energy of Activation for the Racemization of 2,2′-Dibromo-4,4′-Dicarboxydiphenyl

F. H. WESTHEIMER
Department of Chemistry, University of Chicago, Chicago, Illinois

(Received January 27, 1947)

In a recent article J. E. Mayer and the author presented a method of calculating the energy of activation for the racemization of optically active diphenyl derivatives from known force constants and from the van der Waals repulsion between ortho substituents. In the present paper, the calculation of this activation energy is carried through in detail for the racemization of 2-2′-dibromo-4,4′-dicarboxydiphenyl. The value obtained is 18 kcal./mole. The experimental value is not known, but the free energy of activation for the same process is 19.5 kcal./mole. In the discussion of probable errors, it is shown that the calculated energy of activation is unlikely to be in error by as much as 7 kcal./mole, and that the probable error is only about 4 kcal./mole. The racemization involves distorting the various angles and stretching the various bonds in the molecule, as well as forcing the ortho substituents to approach one another so that the distance between them is less than the sum of their van der Waals radii. In the present treatment, all these deflections and stretchings are computed; that is to say, an accurate model for the activated complex is obtained.

INTRODUCTION

IN a recent article, J. E. Mayer and the author[1] presented a method for calculating the energy of activation for the racemization of optically active diphenyl derivatives. The calculation makes use of the force constants for the "normal" vibrations of the diphenyl derivative in question and requires a knowledge of the van der Waal's repulsion between the non-bonded[2] ortho substituents which must pass one another during the racemization process. The present article presents the details of the calculation of the activation energy for the racemization of 2,2′-dibromo-4,4′-dicarboxydiphenyl. Racemization processes of the type indicated are especially favorable for the calculation of the energy of activation, since in these reactions, no bonds are formed or broken. It is to be noted that the present computation, although approximate, involves no arbitrary parameters.

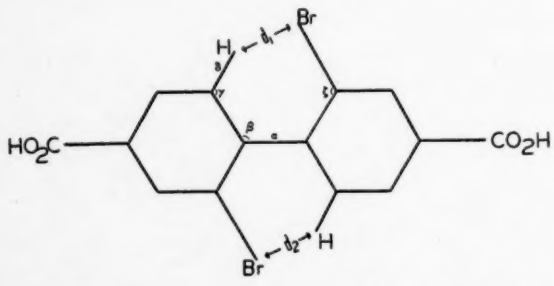

FIG. 1. The planar model of a rigid molecule of 2,2′-dibromo-4,4′-dicarboxydiphenyl.

During the racemization, the molecule passes through a planar configuration (Fig. 1), which is the activated complex for the reaction. Further, it is assumed[1] that the energy of this planar form exceeds that of the usual, non-planar one by the amount of energy, E, given in Eq. (1)

$$E=\sum_i \tfrac{1}{2}a_i q_i^2+2A\exp(-d/\rho). \qquad (1)$$

Here a_j is the force constant associated with the normal coordinate q_j; the exponential term is an approximation, over the limited range which is of interest, to the van der Waals repulsion between two non-bonded bromine and hydrogen atoms separated by the distance, d_v; A and ρ are constants. Since some of the vibrations of the diphenyl molecule are unsymmetrical, they do not affect the separation of the two bromine-hydrogen pairs equally; hence, the two distances, d_1 and d_2 (Fig. 1) must be considered individually. The distance d_1 between the first pair of bromine and hydrogen atoms and the distance d_2 between the second pair of bromine and hydrogen atoms are given approximately by Eqs. (2) and (2′),

[1] F. H. Westheimer and J. E. Mayer, J. Chem. Phys. **14**, 733 (1946).

[2] "Non-bonded" substituents are atoms or groups which are not bonded to each other; they are, of course, bonded to the carbon atoms of the benzene rings.

respectively.

$$d_1 = d_0 + \sum_i b_i q_i, \tag{2}$$

$$d_2 = d_0 + \sum_i b_i' q_i. \tag{2'}$$

In these equations, d_0 is the separation between bromine and hydrogen atoms which would obtain in the rigid planar molecule (i.e., if there were no deformations of bond angles and no changes in bond lengths). The constants b_j and b_j' are proportionality factors (calculable from the geometry of the molecule) which relate the increase in the distances d_1 and d_2 to the magnitude of the displacements q_j.

The previous paper[1] gives a method of finding the minimum value of E with respect to all possible variations in all the normal coordinates. This minimum value, E_0, which is the activation energy for the racemization, can be expressed in terms of a parameter Z, as shown in Eq. (3).

$$E_0 = \frac{2Z^2}{\rho^2} \sum_i \frac{B_i^2}{a_i} + 2Z \tag{3}$$

where $B_j = \frac{1}{2}(b_j + b_j')$. Z in turn can be determined by the numerical solution of Eq. (4)

$$Z = E_{d_0} \exp - \left(\frac{2Z}{\rho^2} \sum_i B_i^2/a_i \right) \tag{4}$$

where

$$E_{d_0} = A e^{-d_0/\rho}. \tag{4'}$$

E_{d_0} is then the value of the van der Waals repulsion between bromine and hydrogen atoms separated by a distance d_0 (i.e., where the planar molecule is rigid).

In order to calculate the activation energy for the racemization of 2,2′-dibromo-4,4′-dicarboxydiphenyl, it is necessary and sufficient to know the force constants, a_i, for the normal vibrations of the molecule, to calculate the geometric factors b_i and b_i' for these same vibrations, and to evaluate the constants A and ρ in the equation $U = Ae^{-d/\rho}$. This equation gives approximately the van der Waals potential, U, of a bromine and a hydrogen atom in the region where the energy involved is largely that of repulsion. From a_i, b_i, b_i', A, and ρ the activation energy can be calculated by means of Eqs. (3) and (4).

THE VIBRATIONS OF THE MOLECULE

In the computation of E_0, some approximations are necessary. The normal vibrations of substituted diphenyl molecules are unknown, and if they were known, they would be too complex for convenient use. However, as was previously pointed out,[1] a complete set of "normal" coordinates for the diphenyl molecule is unnecessary. Any set of coordinates in which the potential energy, E, can be expressed as a sum of squares of the form q_i^2 (as in Eq. 1) without any cross-product terms $q_i q_j$, is adequate. Although true normal coordinates would be such that the kinetic energy could also be expressed as a sum of squares of the form $\dot{q}_i^2$, this additional property is not essential for the problem at hand. Actually, even the thirty normal vibrations of benzene are too complex for convenient use; hence, the set of "bastardized" coordinates suggested in the previous paper is here used.

The normal vibrations of benzene were worked out by E. B. Wilson,[3] and the corresponding vibration frequencies were developed by him in terms of six force constants: (1) a stretching constant, K, for the carbon-carbon bond; (2) a stretching constant q, for the carbon-hydrogen bond; (3) a constant k for the deformation of a ring angle in the plane of the ring; (4) a constant H for the deformation of the C−C−H angle in the plane of the ring; and (5 and 6) two constants related to the non-planar vibrations of the ring atoms. Although this formulation of the problem may be oversimplified for very precise work, it has proved to be adequate for the purpose at hand.

In the present paper, the six carbon atoms of the benzene ring are considered as a unit, and the problem is simplified by omitting the motions (considered by Wilson) of the hydrogen atoms. The coordinates of the carbon atoms are R, for

TABLE I. Force constants, a_i, for vibrations 1, 12, 14, and 19.

Vibration No.	Force constant
1	$6K$
12	$72k$
14	$18K$
19a and 19b	$9(K+k)$

[3] E. B. Wilson, Phys. Rev. **45**, 706 (1934).

radial displacement away from the center of the ring, and Y, for displacement in the plane of the ring perpendicular to R; Y is positive for motion clockwise around the ring. The normal coordinates are given in the equations of set (5).

$$
\begin{aligned}
q_1 &= R_1+R_2+R_3+R_4+R_5+R_6,\\
q'_{6a} &= R_1-R_3+R_4-R_6,\\
q'_{6b} &= 1/\sqrt{3}(R_1-2R_2+R_3+R_4-2R_5+R_6),\\
q'_{8a} &= -1/\sqrt{3}(Y_1-2Y_2+Y_3+Y_4-2Y_5+Y_6),\\
q'_{8b} &= Y_1-Y_3+Y_4-Y_6,\\
q_{12} &= R_1-R_2+R_3-R_4+R_5-R_6,\\
q_{14} &= Y_1-Y_2+Y_3-Y_4+Y_5-Y_6,\\
q_{19a} &= 2R_1+R_2-R_3-2R_4-R_5+R_6\\
&\qquad +\sqrt{3}(Y_2+Y_3-Y_5-Y_6),\\
q_{19b} &= \sqrt{3}(R_2+R_3-R_5-R_6)\\
&\qquad -(2Y_1+Y_2-Y_3-2Y_4-Y_5+Y_6).
\end{aligned}
\tag{5}
$$

The above coordinates are closely related to Wilson's, and his numbering is retained throughout. The non-planar vibrations of the ring are omitted for reasons explained below. Coordinates q_{19a} and q_{19b} refer to a degenerate pair of vibrations. Coordinates q'_{6a} and q'_{8a} must be combined to find two true normal coordinates; and coordinates q'_{6b} and q'_{8b} must be similarly treated. The four vibrations thus derived form two degenerate pairs.

The coordinates in set (5) differ from Wilson's in two respects. First, the coordinates R and Y here refer simply to distance and not, as Wilson's do, to distance divided by the square root of the mass of the carbon atom. Second, the normalization factors $-1/\sqrt{3}$ and $1/\sqrt{3}$ have been included in the respective expressions for q_{8a}' and q_{6b}'. Although these factors are not necessary (the same vibration frequencies are obtained with or without them), unless they are included, the members of a pair of degenerate vibrations do not have the same force constant.

TABLE II. Force constants for the benzene ring (Kohlrausch).

Type	Force constant
Stretching C−C bond	$K=7.65\times10^5$ dynes/cm
Stretching C−H bond	$q=5.02\times10^5$ dynes/cm
Bending ring angle (in plane of ring)	$k=0.642\times10^5$ dynes/cm
Bending C−C−H angle (in plane of ring)	$H=0.737\times10^5$ dynes/cm

The potential energy and the force constant for each of the vibrations listed above can be found in terms of the stretching and bending force constants K and k. Each vibration causes a change in the length of some of the carbon-carbon bonds in the ring, or a change in some of the internal angles of the ring, or both; these changes in length and angle can be found from the geometry of the molecule and the equations of set (5). Following Wilson's procedure, the potential energies and the force constants for vibrations 1, 12, 14, 19a and 19b are written in terms of K and k. (Table I.)

Coordinates q_6' and q_8' must be combined to find normal modes of vibration. For both combinations, the Lagrangian, L, is given by Eq. (6)

$$
L=T-V=2M\dot{\psi}^2+2M\dot{\omega}^2-K/2(\psi+3\omega)^2 -k/2(3\sqrt{3}\psi+\sqrt{3}\omega)^2. \tag{6}
$$

Here ψ is the magnitude of the displacement q_6' and ω is the magnitude of the displacement q_8'; M is the mass of the carbon atom.

The classical equations of motion in Lagrangian form, (7), were then applied to the function

$$
\frac{d}{dt}\frac{\partial L}{\partial \dot{q}}-\frac{\partial L}{\partial q}=0, \tag{7}
$$

L of Eq. (6). The resulting differential equations were simplified by introducing the assumption that the motions in question are harmonic. This means that $\psi=A\sin\lambda t+B\cos\lambda t$ (where λ is the vibration frequency), and that therefore,

$$
\frac{d^2\psi}{dt^2}=-\lambda^2\psi. \tag{8}
$$

Similarly,

$$
\frac{d^2\omega}{dt^2}=-\lambda^2\omega. \tag{8'}
$$

The same value of λ is used in Eqs. (8) and (8'), since the modes of motion in question are just those for which q_6' and q_8' have the same frequency. Combining (6), (7), (8), and (8') leads to

two simultaneous linear equations, (9), in ψ and ω.

$$\begin{aligned} -4M\lambda^2\psi+K(\psi+3\omega)+3\sqrt{3}k(3\sqrt{3}\psi+\sqrt{3}\omega)=0,\\ -4M\lambda^2\omega+3K(\psi+3\omega)+\sqrt{3}k(3\sqrt{3}\psi+\sqrt{3}\omega)=0. \end{aligned} \quad (9)$$

These equations can both be valid only under the condition that (10) is satisfied.

$$4M\lambda^2=5K-15k\pm[(5K+15k)^2-192Kk]^{\frac{1}{2}}. \quad (10)$$

The appropriate numerical values of K and k (see below) are then substituted in (10); two values of $4M\lambda^2$ are thus computed. When these values are substituted in Eq. (9), the two negative reciprocal ratios of ψ to ω are obtained. These values are -0.481 and -2.08. The two coordinates which result from the combination of q_6' and q_8' are then

$$\begin{aligned} q_{6+8}&=q_6'-0.481q_8',\\ q_{6+8}{}^*&=q_6'+2.08q_8'. \end{aligned} \quad (11)$$

In order to obtain Eqs. (11) and in order to obtain numerical values for the force constants of the benzenoid vibrations, numerical values for the force constants K and k are needed. Concordant values of K, k, q, and H have been obtained by Kohlrausch[4] and later by Lord and Andrews.[5] Both investigations were based on Wilson's potential functions for the benzene ring, and both led to values of the force constants from which the observed infra-red and Raman frequencies of benzene were predicted with moderate accuracy. The values here used are Kohlrausch's. (Table II.)

From the data in Tables I and II, and from Eqs. (6) and (11), the force constants for all the deformations of the benzene ring have been computed (Table III).

In addition to the deformations of the ring, the following deformations (see Fig. 1) have been considered: (I) the stretching of the interannular bond, α; (II) the deformation of the angles, β, between the interannular and the ring bonds; (III) the deformation of the angles, γ, between the ring bonds and the bonds to the ortho-hydrogen atoms; (IV) the stretching (contraction) of the carbon to hydrogen bonds, δ; (V) the stretching (contraction) of the carbon to bromine bonds, ϵ; and (VI) the deformation of the angles, ζ, between the ring bonds and the bonds to the bromine atoms.

TABLE III. Values of the force constants,* a_i.

Vibration No.	Type	a_i
I	Stretching interannular bond, α	5.5×10^5 dynes/cm
II	Deforming C−C−C angle, β	1.13×10^{-11} dynes cm/radian^2
III	Deforming C−C−H angle, γ	0.86×10^{-11} dynes cm/radian^2
IV	Stretching ring to H bond, δ	5.0×10^5 dynes/cm
V	Stretching ring to Br bond, ϵ	5.0×10^5 dynes/cm
VI	Deforming C−C−Br angle, ζ	1.07×10^{-11} dynes cm/radian^2
1	Vibrations of the Benzene Ring	45.9×10^5 dynes/cm
(6+8)		13.7×10^5 dynes/cm
(6+8)*		450×10^5 dynes/cm
12		46.2×10^5 dynes/cm
14		138×10^5 dynes/cm
19		74.6×10^5 dynes/cm

* It is interesting that computations based on Wilson's equations and Kohlrausch's constants lead to vibration frequencies for the six carbon atom unit which agree well with those obtained in the experiments with models performed by Murray, Dietz, and Andrews (J. Chem. Phys. 3, 180 (1935)). The vibration frequencies obtained by these investigators are given in arbitrary units; only the relative magnitudes of the vibrations of the model can be compared with the values calculated for the carbon ring.

Vibration frequencies of a benzene ring stripped of hydrogen.

Vibration No.	Frequency Calc., cm^{-1}	Frequency Model, arbitrary units	Ratio
(6+8)	625	575	1.09
1	1040	840	1.24
12	1045		
19	1325	1045	1.27
(6+8)*	1730	1330	1.30
14	1805	1470	1.23

The force constant H for the bending of the carbon to hydrogen bonds and the force constant q for the stretching of these bonds are taken from Kohlrausch. The force constant for the stretching of the interannular bond in diphenyl was taken to be 5.5×10^5 dynes/cm, a value somewhat in excess of the corresponding force constant in aliphatic compounds.[6] The value of the force constant for the stretching of the carbon to bromine bonds was arbitrarily chosen as 5×10^5 dynes/cm; actually, the value for this force constant does not affect the calculation. (See Table VI.) No good value of the force constant for the bending of the carbon to bromine bonds in aromatic compounds is available; this value was therefore estimated in the following manner: The force constant, H, for the bending of the carbon to hydrogen bond was accepted as a first approximation to the desired constant. Then this force

[4] K. W. F. Kohlrausch, Zeits. f. physik. Chemie **B30**, 305 (1935).

[5] R. C. Lord and D. H. Andrews, J. Phys. Chem. **41**, 149 (1937).

[6] See G. Herzberg, *Infra-Red and Raman Spectra* (D. Van Nostrand Company, Inc., New York, 1945).

TABLE IV. Bond lengths used in calculating b and b'.

Bond	Position	Length, $\times 10^8$ cm
C–C	In ring	1.39
C–C	Between rings	1.54
C–H		1.08
C–Br		1.86

constant, H, was increased in the ratio of the force constants for the corresponding bonds in aliphatic compounds (i.e., in the ratio of the force constant for the deformation of the C–C–Br angle to the force constant for the deformation of the C–C–H angle in aliphatic compounds).[7] The corrected value of H was then further increased by 10 percent. A similar procedure was used for the force constant for the deformation of the angle β. In each instance, the additional ten percent was added to take into account the stiffening of the bonds caused by resonance.[8] The force constants obtained by the methods outlined are listed in Table III.

THE GEOMETRIC FACTORS

Each of the vibrations under consideration (see Table III) changes the distance (d_1 or d_2) between the members of at least one pair of ortho-bromine and ortho-hydrogen atoms. As a first approximation and for small amplitudes, the increase or decrease in the bromine-hydrogen distance is proportional to the amplitude of the vibration in question. The proportionality factors b and b' (see Eqs. 2 and 2′) may be derived from the geometry of the diphenyl molecule, the bond lengths, and the equations of set (5) for the normal vibrations of the ring. It was assumed that, in the planar but undeformed diphenyl molecule, both rings are hexagons and that the C–C–C, C–C–H, and C–C–Br angles are all 120°.

Some of the vibrations of the benzene ring involve changes in the ring angles at the position of the interannular bond or the positions ortho to it. In order to calculate b and b', it was necessary to make some assumption about the nature of these vibrations. It was, therefore, assumed that such vibrations always take place so that the center of the substituent (bromine or hydrogen or the second ring) remains upon the bisector of the ring angle at the point where the substituent is attached. It was further assumed that the length of the interannular bond was unchanged except during vibration I. Since the individual vibrations of the benzene ring are comparatively unimportant, these assumptions are unlikely to lead to large errors.

For those vibrations which do not change the distance between bromine and hydrogen atoms, the values of b and b' are zero. It has been shown[1] that vibrations for which both b and b' are zero need not be considered in the determination of the activation energy of racemization. As a first approximation, the non-planar vibrations do not change the bromine-hydrogen distances; they are therefore disregarded.

The bond lengths here used are given in Table IV. They require no comment, except for the value (1.54A) assigned to the length of the interannular bond. This value is slightly in excess of that found experimentally for diphenyl.[9] As previously pointed out,[1] resonance between the two rings may, as a first approximation, be neglected if the longer bond length is used.

The geometric factors b_i, b_i', and B_i (where $B_i=(b_i+b_i')/2$) are given in Table V.

THE VAN DER WAALS POTENTIAL

The solution of the problem under consideration requires a knowledge not only of the force constants (Table III) and the geometric factors

TABLE V. Values of the geometric factors.

Vibration No.	b	b'	B
I	0.91	0.91	0.91
II	2.01×10^{-8}	-2.65×10^{-8}	-0.32×10^{-8}
III	0.62×10^{-8}	0.00×10^{-8}	0.31×10^{-8}
IV	−0.82	0.00	−0.41
V	−0.09	0.00	−0.05
VI	1.89×10^{-8}	0.00×10^{-8}	0.95×10^{-8}
1	0.090	0.82	0.45
(6a+8a)	1.10	1.91	1.50
(6a+8a)*	2.19	7.15	4.67
(6b+8b)	1.31	−1.28	0.01
(6b+8b)*	−2.43	0.77	−0.83
12	1.72	1.00	1.36
14	−0.15	1.42	0.63
19a	1.14	0.25	0.70
19b	−0.41	1.71	0.65

[7] B. L. Crawford and S. R. Brinkley, J. Chem. Phys. 9, 69 (1941).

[8] G. W. Wheland, *The Theory of Resonance* (John Wiley and Sons, Inc., New York, 1944).

[9] I. L. Karle and L. O. Brockway, J. Am. Chem. Soc. 66, 1974 (1944).

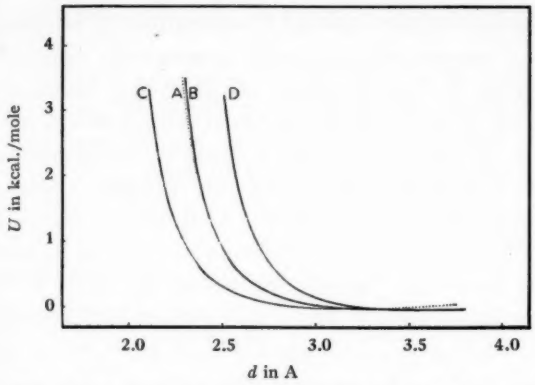

FIG. 2. The van der Waals potential function. Curve *A* is the modified neon potential of Bleick and Mayer, curve *B* is the exponential approximation used in the complete computation. Curves *C* and *D* have been displaced from *B* in opposite directions by 0.2A.

(Table V), but also of the energy of repulsion between non-bonded bromine and hydrogen atoms. No really good potential function for this energy of repulsion is available; it is, therefore, necessary to approximate one. The form of the expression for the energy of repulsion between atoms with closed electron shells is assumed to be roughly independent of the nature of the atoms involved. The van der Waals potential may be considered to be the sum of two effects: one of attraction and one of repulsion. These combine to give a total potential with a flat, shallow minimum at some inter atomic distance d_v. Most of the available experimental data for the van der Waals potential deals with the region near the minimum of the curve; the data for argon,[10] for example, are probably valid for that part of the curve where the energy is within 500 small calories of the minimum. Unfortunately, to solve the present problem, it was necessary to know the potential function for an energy region about 3 kcal. above the minimum. Since no experimental values of the van der Waals potential for this region were available, it was necessary to use a theoretical value.

Bleick and Mayer,[11] on the basis of quantum mechanical considerations, have computed the van der Waals repulsion between two neon atoms. It was hoped that the mutual repulsion between two neon atoms would approximate that between one bromine and on ehydrogen atom. Bleick and Mayer's computation for the repulsion effect in the potential should be very nearly precise in the region where $U \lesssim 5$ kcal. (i.e., in the region of interest for the present problem). Their computation of the attraction effect in the potential is, as they admitted, crude, and comparison with experimental values of the potential near the minimum[12] suggests that their attraction effect should be doubled. Since the repulsion, in the region under consideration, is almost ten times the attraction, the correction introduced by doubling the latter is small. One slight further modification was also made. The minimum value of the neon potential falls where the distance between neon atoms is 3.2A.[13] The precise distance between bromine and hydrogen atoms at the minimum of the van der Waals potential is not known, but Pauling[14] has suggested that the van der Waals radius of bromine is 1.95A and that of hydrogen 1.2A. The distance, d_v, between a bromine and a hydrogen atom (non-bonded) at the potential minimum, is thus approximately 3.15A. The potential curve for neon was therefore shifted through 0.05A, in order that the minimum might fall at 3.15A. For convenience, the minimum potential was set equal to zero. The resulting potential curve (see Fig. 2) may be approximated by the exponential expression

$$U = 2.45\times10^{-7}e^{-d/0.165\times10^{-8}} \text{ ergs/molecule.} \quad (11)$$

A comparison of Eq. (11) with Eq. (1), shows that

$$A = 2.45\times10^{-7}, \quad \text{and} \quad \rho = 0.165\times10^{-8}.$$

When

$$d = d_0 = 1.61A,$$
$$U = E_{d_0} = 1.44\times10^{-11} \text{ erg/molecule.}$$

THE ENERGY OF ACTIVATION

In the preceding sections, the values of a_i, B_i, A, ρ, and E_{d_0} are all determined. When these values are substituted in Eq. (4), the value of Z is found to be 2.02×10^{-13} ergs/molecule, or 2.9 kcal./mole. It should be noted that, in forming

[10] O. K. Rice, J. Am. Chem. Soc. **63**, 3 (1941); private communication from O. K. Rice.

[11] W. E. Bleick and J. E. Mayer, J. Chem. Phys. **2**, 252 (1934).

[12] See J. E. Leonard-Jones, Proc. Phys. Soc. **43**, 461 (1931).

[13] See S. B. Hendricks, Chem. Rev. **7**, 431 (1930); M. L. Huggins, *ibid.* **10**, 427 (1932).

[14] L. Pauling, *The Nature of the Chemical Bond* (Cornell University Press, New York, 1939).

the sum $\sum_i B_i^2/a_i$ (Eq. 4), the vibrations of both benzene rings must be taken into account. Thus the term B_i^2/a_i corresponding to each vibration listed in Table V (except vibration I) must be used twice. When the value of Z (and the values of a_i and B_i previously determined) are substituted in Eq. (3), the energy of activation is found to be 18 kcal./mole.

The experimental value of the energy of activation for the racemization of 2,2′-dibromo-4,4′-dicarboxydiphenyl has not yet been determined, but the free energy of activation[15] is 19.5 kcal./mole. However, for the racemization of other optically active diphenyl derivatives[16] and related compounds,[17] both the energy and the free energy of activation are known; they never differ by more than a few kilocalories. The experimental value for the energy of activation for 2,2′-dibromo-4,4′-dicarboxydiphenyl remains to be determined in the future, but probably it will not differ by more than a few kilocalories from the free energy of activation (19.5 kcal./mole).

LIMITS OF ERROR

The largest uncertainty in the foregoing computation of the activation energy arises from uncertainties as to the van der Waals potential function. The calculated slope of this function is determined by ρ; the particular value (0.165×10^{-8}) here assigned to this constant is somewhat less than the value (0.2091×10^{-8}) used by Bleick and Mayer[11] in their equation for the repulsion between neon atoms. The effect of including attraction as well as repulsion is to diminish ρ. Furthermore, the value of ρ appropriate to neon is considerably smaller than the value (0.345×10^{-8}) found by Born and Mayer for the ions in alkali halides,[18] and recently used by Dostrovsky, Hughes, and Ingold in their study of steric effects in substitution reactions.[19] It seems likely that the larger alkali ions and the halide ions are considerably more easily compressed than are hydrogen atoms; hence the steepness of the van der Waals potential between neon atoms seems a more appropriate approximation to that between bromine and hydrogen atoms than any other approximation now available. In any event, the position of the potential curve is more critical for the present computation than is its slope. A function ($U=2.1\times10^{-10}e^{-d/0.33\times10^{-8}}$) was chosen so that, as before, the van der Waals potential is 2.0×10^{-13} ergs/molecule (2.9 kcal./mole) when the bromine and hydrogen atoms are 2.30A apart; note, however, that in this function the value of ρ has been doubled, thus halving the slope of the function. It is unlikely that the chosen value (0.165×10^{-8}) of ρ is in error by such a large amount; the change, moreover, decreases the computed value of E_0 only by 1.5 kcal./mole.

Although the value of ρ is not in doubt by an amount which is important for the computation of E_0, the position of the potential curve is important. Admittedly, the van der Waals radii of bromine and hydrogen atoms are uncertain. Pauling rounded off his values to the nearest 0.05A; hence, the sum of the radii here used is uncertain by at least that amount. In order to set some reasonable limit of error to the calculated value of E_0, it was assumed that the position of the potential minimum may be in error (within the region here to interest) by 0.1A, i.e., it was assumed that the sum of the van der Waals radii for bromine and hydrogen lies between 3.05 and 3.25A. The computation with the smaller sum (3.05A) gives an activation energy of 15 kcal./mole; the calculation with the larger sum (3.25A) gives an activation energy of 22 kcal./mole. There is no guarantee that these limits are sufficiently wide, but they appear reasonable; the probable error in the calculation is then about three or four kilocalories. If, however, it is assumed that the position of the minimum may be in error by 0.2A (i.e., that the sum of the van der Waals radii for bromine and hydrogen lies between 2.95A and 3.35A) then the calculated activation energy lies between 12 and 26 kcal./mole. These wider limits for the sum of the van der Waals radii appears to the author to be ample, and probably too large. Thus the uncertainity in the computed value of E_0 which is caused by the uncertainty in the van der Waals

[15] W. I. Patterson and R. Adams, J. Am. Chem. Soc. **57**, 762 (1935).
[16] G. B. Kistiakowsky and W. R. Smith, J. Am. Chem. Soc. **58**, 1043 (1936).
[17] W. H. Mills and R. M. Kelham, J. Chem. Soc. 274 (1937).
[18] M. Born and J. E. Mayer, Zeits. f. Physik **75**, 1 (1932).
[19] I. Dostrovsky, E. D. Hughes, and C. K. Ingold, J. Chem. Soc. 173 (1946).

repulsion is unlikely to exceed 7 kilocalories per mole.

The errors in E_0 which might arise from possible errors in the force constants are much smaller; they may in fact be neglected. Of all the individual force constants, the one for the bending of the carbon-bromine bond is by far the most important. If this force constant has been underestimated by 20 percent, then the calculated activation energy is 1 kcal./mole too low.

The calculated energy of activation represents the saddle-point in the potential energy diagram for the substituted diphenyl molecule. Some other points on this diagram are also of interest, particularly those which correspond to planar configurations of the substituted diphenyl molecule other than the one of minimum energy. One of these configurations is that of a planar molecule in which all of the bond angles and lengths are respectively identical with those in the unstrained, non-planar molecule. For this model, the energy is determined solely by the van der Waals repulsion; it amounts to twice E_{d_0}, or about 400 kcal./mole. Another interesting configuration is the planar one in which the bromine and hydrogen atoms are separated by 3.15A, the sum of their van der Waals radii. Here, the stretching of the various bonds and the distortions of the various angles is such as to increase the bromine-hydrogen distance from 1.61A to 3.15A; the energy for this configuration exceeds 50 kcal./mole.

Finally, it is of interest to determine the minimum energy for a planar model in which the carbon-bromine bonds can bend, but the molecule is otherwise rigid. This particular model is important because it takes account only of the deflections of the carbon-bromine bonds, which, in the full calculation, account for half of the term $\sum_i B_i^2/a_i$ in Eqs. (3) and (4). These deflections are by far the most important deformations of the whole molecule. For the calculation in question, the van der Waals potential function was approximated (as before) by $U=2.45\times10^{-7}e^{-d/0.165\times10^{-8}}$ erg/molecule. The minimum energy thus calculated is 26 kcal./mole. Although this value is higher than the one obtained in the complete calculation, it exceeds the latter only by about 50 percent. The result here obtained suggests a rapid method of approximate calculation for similar cases.

An additional uncertainty in E_0, related to the assumption (Eq. (1) and elsewhere) that all the vibrations are harmonic, is discussed in the next section.

THE ACTIVATED COMPLEX

On the basis of the computations already presented, it is possible to visualize what actually happens during the racemization of 2,2′-dibromo-4,4′-dicarboxydiphenyl. How much each bond is stretched (or contracted), how much each angle is deformed, how much energy is associated with each vibration, and how much energy of activation is caused by repulsion, may all be estimated. The exact assignments may be somewhat inaccurate, but the limits of error discussed in the previous section show that the general solution here presented is essentially correct.

For each coordinate q_i, the displacement which occurs in the activated complex is called q_i^0. It has already[1] been shown that this displacement is equal to $2ZB_i/\rho a_i$. Since the values of Z, B_i, and ρ and a_i are all known, the values of q_i^0 can be computed; they appear in column 2 of Table VI. The expression $b_i q_i^0$ gives the amount by which each displacement associated with one benzene ring increases the distance d_1 between the ortho bromine and hydrogen atoms. The same displacement increases the distance d_2 between the second set of bromine and hydrogen atoms by an amount $b_i' q_i^0$. Displacements in the two rings are symmetrical about the mid-point of the interannular bond. The total increase in d_1 caused by a displacement of a given type (combining the

TABLE VI. The displacements and energy of the activated complex.

Vibration No.	q_i^0	Increase in d_1 or d_2, in A	Energy, kcal./mole
I	0.040×10^{-8} cm	0.037	0.65
II	−0.069 radian	.044	.78
III	0.088 radian	.055	.96
IV	-0.020×10^{-8} cm	.016	.30
V	0.004×10^{-8} cm	.000	.00
VI	0.216 radian	.409	7.22
1	0.002×10^{-8} cm	.002	.04
(6a+8a)	0.027×10^{-8} cm	.081	1.42
(6a+8a)*	0.002×10^{-8} cm	.024	.42
(6b+8b)	0.000×10^{-8} cm	.000	.00
(6b+8b)*	-0.003×10^{-8} cm	.006	.10
12	0.007×10^{-8} cm	.020	.34
14	0.001×10^{-8} cm	.001	.02
19a	0.002×10^{-8} cm	.002	.06
19b	0.002×10^{-8} cm	.002	.06

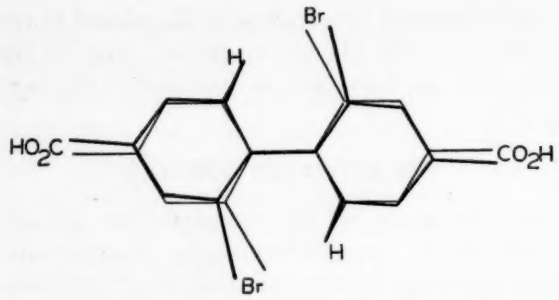

FIG. 3. The activated complex in the racemization of 2,2′-dibromo-4,4′-dicarboxydiphenyl. The light lines show the planar, rigid model (cf. Fig. 1); the heavy lines show the positions of the atoms in the activated complex.

effects of the two displacements associated with the rings) is $2B_iq_i^0$. The only exception to this rule is the stretching of the interannular bond, where, since there is only one vibration of this type, the increase is only $B_iq_i^0$. The increases in d_1 caused by the various displacements are given (according to bond type) in column 3 of Table VI.

The energies involved in the various displacements are given in the last column of Table VI; here again, the listing is according to the bond type. The value of 7.22 kcal./mole for the bending of the carbon-bromine bond refers to the energy of bending of both the carbon-bromine bonds at once; the value of 0.65 kcal./mole for stretching the interannular bond refers to only one bond.

The sum of the van der Waals radii for bromine and hydrogen is 3.15A; the value of d_0 is 1.61A. Table VI shows that, in the activated complex, the bromine and hydrogen atoms are 2.31A apart (a distance 0.84A less than the sum of the radii). Here the various bonds are stretched (and the various angles deformed) so as to increase the distance between the bromine and hydrogen atoms by 0.70A. The difference between the sum of the van der Waals radii and d_0 is thus accounted for in roughly equal amounts by deformations of the molecule and by a "climbing" of the van der Waals potential curve. A picture of the activated complex is presented in Fig. 3.

The energy of activation is divided roughly into three parts; the van der Waals energy of repulsion accounts for 6 kcal., the deflections of the two carbon to bromine bonds accounts for 7 kcal.; all the rest of the deformations account for about 5 kcal./mole. It is of interest that the energy contributed by all the deformations of the benzene rings amounts to only about 2.5 kcal./mole.

Table VI also shows that the carbon-bromine bond in the activated complex is deflected through 0.22 radian, or about 12°. This is so large an angle that the energy of the vibration in question probably cannot be closely approximated by a simple quadratic term, $\frac{1}{2}a_iq_i^2$. The anharmonicity in this vibration, although its value is unknown, is not likely to have a large effect upon the energy of activation. It has previously been pointed out that an increase of 20 percent for the force constant in question increases the computed energy of activation only by about 1 kcal./mole.

Since the uncertainties in the force constants are small for the molecules of the sort here treated, it may prove desirable to reverse the procedure here employed, and to use the rates of racemization of optically active diphenyl derivatives to determine van der Waals potential functions.

ACKNOWLEDGMENT

The author wishes to thank Professor Joseph E. Mayer for his invaluable help and advice in the research here described.

Calculation of Equilibrium Constants for Isotopic Exchange Reactions

JACOB BIGELEISEN AND MARIA GOEPPERT MAYER
Argonne National Laboratory, Chicago, Illinois and Institute for Nuclear Studies, University of Chicago*
(Received February 5, 1947)

It is pointed out that the possibility of chemical separation of isotopes is a quantum effect. This permits a direct calculation of the difference in the free energies of two isotopic molecules. Tables and approximation methods are given which permit a rapid calculation of equilibrium constants if the frequency shifts on isotopic substitution are known. Several applications are discussed.

INTRODUCTION

THE possibility of calculating equilibrium constants for isotopic exchange reactions from spectroscopic data alone was first pointed out by Urey and Rittenberg.[1] Since then numerous calculations have appeared in the literature. All these calculations can be greatly simplified. The final equilibrium constants can be calculated (except for molecules containing hydrogen) without any knowledge of the moments of inertia of the molecules.

THE METHOD OF CALCULATION

The natural logarithm of the equilibrium constant, K, at any temperature T for any chemical reaction is the difference in the standard free energies of the reactants and products divided by RT. For gaseous substances the free energy is connected to the partition function by the relation

$$F=-RT\ln Q/N, \tag{1}$$

where Q is the partition function of the molecule. According to the quantum-mechanical treatment the partition function is defined as

$$Q=\sum_n e^{-\epsilon_n/kT}, \tag{2}$$

where the summation extends over all quantum states (counting a k-fold degenerate level as k states). The energies of the molecular states, ϵ_n, have to be measured from a suitable reference zero. It follows that the equilibrium constant is

$$K=\frac{\Pi Q \text{ products}}{\Pi Q \text{ reactants}}. \tag{3}$$

A calculation of the Q's allows the calculation of equilibrium constants for chemical reactions.

For reactions involving the exchange of isotopes, K is of the order of unity. The free energies of the different isotopic molecules are almost equal and $\ln K$ is the small difference between large numbers. The calculation of $RT\ln K$ as the difference of the total free energies of the reactants and products is likely to lead to, and has in several instances led to, significant errors (even reversing the direction of the reaction). A much simpler and more accurate method is obtained by calculating the differences in the free energies or the ratios of the partition functions directly.

It is well known that the chemical separation of isotopes is a quantum-mechanical effect. The classical partition function is

$$h^fQ=\frac{1}{s}\int\int\int\cdots\int\int e^{-H(p,q)/kT}dp\cdots dq, \tag{4}$$

where s is the symmetry number and H is the Hamiltonian of the momenta p and the coordinates q of the constituent atoms. The momenta occur in the kinetic energy only, in the form $p^2/2m$. The integration over the p's may be performed leading to

$$Q=\frac{1}{s}\Pi_i\left(\frac{2\pi m_i kT}{h^2}\right)^{\frac{1}{2}} \times\int\int\int\cdots\int e^{-u/kT}dq_1\cdots dq_k. \tag{5}$$

The potential energies for molecules differing only in isotopic constituents are alike. The ratio of the partition functions of two isotopic molecules is, therefore, seen to reduce to the inverse

* This document is based on work performed under Contract No. W-31-109-eng-38 for the Manhattan Project at the Argonne National Laboratory.
[1] H. C. Urey and D. Rittenberg, J. Chem. Phys. 1, 137 (1933).

ratio of the symmetry numbers multiplied by the mass ratio of the different isotopes raised to the three-halves power.

$$\frac{Q}{Q'}=\frac{s'}{s}\left(\frac{m}{m'}\right)^{\frac{3}{2}}. \tag{6}$$

The ratio of the masses of the isotopes will cancel in any chemical reaction. The ratio of the symmetry numbers, no matter what its value, will not lead to isotopic enrichment since it merely represents the relative probabilities of forming symmetrical and unsymmetrical molecules.

In calculating the equilibrium constant of isotopic exchanges the useless classical ratio $(m/m')^{\frac{3}{2}}$ is best omitted. This omission amounts to calculating the ratio of the equilibrium constants for the dissociation of the two isotopic molecules into atoms. We shall accordingly define

$$f=\frac{Q}{Q'}\Pi_i\left(\frac{m_i'}{m_i}\right)^{\frac{3}{2}}. \tag{7}$$

In classical mechanics $(s/s')f$ is equal to one. A value of one for the $(s/s')f$ means no separation of isotopes.

In quantum mechanics the partition function may in a first approximation be written as a product of translational, rotational, and vibrational partition functions. The translational partition function is equal to the classical one at all temperatures. The rotational partition function in all cases except hydrogen, which we shall treat separately, is classical at room temperature. The form of the vibrational partition function neglecting anharmonicity is

$$Q_{\text{vib}}=\Pi_i\frac{e^{-u_i/2}}{1-e^{-u_i}}, \tag{8}$$

where

$$u_i=\frac{h\nu_i}{kT} \tag{9}$$

and the product is to be taken over the different vibrational frequencies ν_i of the molecule counting an n-fold degenerate frequency n times. We have chosen the zero of the energy scale at the minimum in the potential energy curve which is appropriate since it is the same for the two isotopic molecules.

At high temperatures or low u, Q_{vib} reduces to $\Pi_i(1/u_i)$, which is identical with the classical expression. In the quantity f these limiting values as well as the rotational and the translational parts cancel, leaving only the ratio of the symmetry numbers.[2]

The value of f depends upon the vibrations only and is of the form

$$\frac{s}{s'}f=\Pi_i\frac{u_i}{u_i'}\frac{e^{-u_i/2}/(1-e^{-u_i})}{e^{-u_i'/2}/(1-e^{-u_i'})}. \tag{10}$$

We shall write $u_i'=u_i+\Delta u_i$, where the primed molecule is the lighter one. Then Δu_i is always positive and

$$\frac{s}{s'}f=\Pi_i\frac{u_i}{u_i+\Delta u_i}e^{\Delta u_i/2}\frac{(1-e^{-(u_i+\Delta u_i)})}{(1-e^{-u_i})}. \tag{11}$$

If we calculate the free energy of formation of two isotopic molecules from their respective gaseous atoms, then the difference in the free energy of formation of the two isotopic molecules will be

$$\frac{\Delta F^0-\Delta F^{0'}}{RT}=\sum_i\left[-\tfrac{1}{2}\Delta u_i+\ln\left(1+\frac{\Delta u_i}{u_i}\right)+\ln\frac{(1-e^{-u_i})}{(1-e^{-(u_i+\Delta u_i)})}\right]+\ln\frac{s}{s'}. \tag{11'}$$

If Δu is small which is the case for everything except the isotopes of hydrogen

$$\frac{s}{s'}f=1+\sum_i\left(\frac{1}{2}-\frac{1}{u_i}+\frac{1}{e^{u_i}-1}\right)\Delta u_i, \tag{11a}$$

or

$$\frac{\Delta F^0-\Delta F^{0'}}{RT}=-\sum_i\left(\frac{1}{2}+\frac{1}{e^{u_i}-1}-\frac{1}{u_i}\right)\Delta u_i+\ln\frac{s}{s'}. \tag{11'a}$$

If, in addition, u_i itself is small, then

$$\frac{s}{s'}f=1+\sum_i\frac{\Delta u_i u_i}{12}=1+\sum_i\frac{\Delta(u_i^2)}{24}. \tag{11b}$$

Since Δu_i is positive, $(s/s')f$ will always be greater than 1. The heavy isotope is more stable in the molecule. The lighter isotope favors the

[2] This could also have been deduced from the product rule which states the invariance under isotopic substitution of the expression $\Pi_i\nu_i{}^2\Pi_i m_i{}^3/M^3I_AI_BI_C$ where the I's are the moments of inertia and M's the molecular weight.

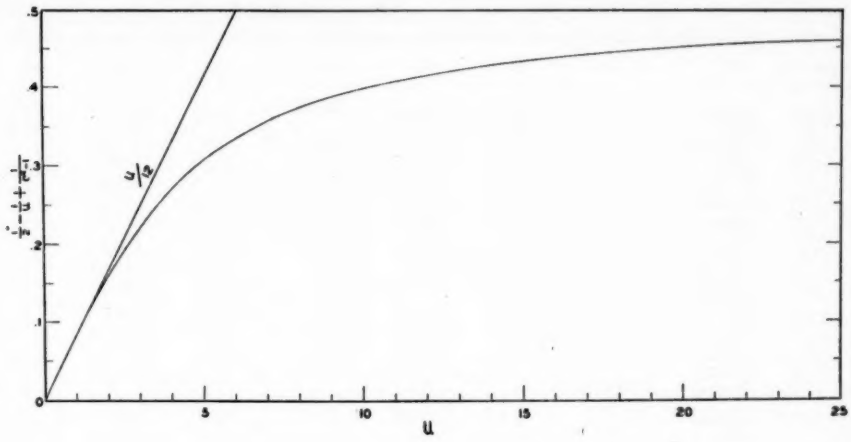

FIG. 1. The separative effect in the free energy per unit shift in u, plotted against $u=hc\omega/kT$.

separated atoms. In all isotopic exchange reactions partial cancellation of the separative effect must occur.

For low temperatures and high frequencies the bracket in (11a) approaches $\frac{1}{2}$ and the difference in the free energies approaches the difference in zero point energies. For very high temperatures formula (11b) becomes applicable to all molecules and it is seen that $(s/s')f$ approaches one as $1+k/T^2$ so that the separative effect disappears.

For most cases the separative effect, $(s/s')f$, can be calculated from the function appearing under the summation sign in (11a) or (11'a)

$$G=\frac{1}{2}-\frac{1}{u}+\frac{1}{e^u-1}. \tag{12}$$

In Fig. 1 we have plotted G against u. Table I gives values of G from $u=0$ to $u=25$.

To test the range of validity of the very simple formula (11b) it may be noted that for $u=3$, $G(u)$ is 0.218 whereas the approximate expression $u/12$ in (11b) is 0.250. This corresponds to a frequency of 625 cm^{-1} at 300°K. For $u=4$, the discrepancy between the two expressions is already 25 percent.

The fundamental approximation made was the neglection of interaction between rotation and vibration as well as anharmonicity of the vibrations. Here again we have to consider merely the ratio of the quantum mechanical to classical correction to the partition function for each of the molecules. For diatomic molecules in which the rotation-vibration spectrum is analyzed this can be worked out explicitly.[3] In general, these corrections are very small if the frequency in the ground state and the zero point energy is correctly chosen.

[3] See Mayer and Mayer, *Statistical Mechanics* (John Wiley & Sons, New York, 1940), Chapter 7.

THE ISOTOPES OF HYDROGEN

The frequency shifts for different hydrogen isotopes are so large that as a rule the unexpanded formula (11) for the vibrational contribution to f has to be used. The rotation of hydrogen molecules is not quite classical even at room temperature. The classical expression for Q_{rot} would be σ^{-1} where

$$\sigma=\frac{hcB}{kT}=\frac{h^2}{8\pi^2IkT}. \tag{13}$$

I is the moment of inertia and B is the rotational constant in cm^{-1}, which is most frequently tabulated in the literature. For small σ the rotational contribution to the quantum-mechanical partition function may be expanded to give

$$\sigma Q_{\text{rot}}=\left(1+\frac{\sigma}{3}+\frac{\sigma^2}{15}+\frac{4\sigma^3}{315}+\cdots\right). \tag{14}$$

Since f is defined such that the classical contribution σ^{-1} is cancelled, Eq. (11a) has to be modified simply by the ratio of the right-hand side of (14) for the two isotopic molecules. For small σ this is

$$1+\frac{\sigma-\sigma'}{3}+\frac{1}{18}(\sigma-\sigma')^2+\frac{1}{90}(\sigma^2-\sigma'^2). \tag{15}$$

The numerical values for the isotopic hydrogen molecules taking into account the interaction

TABLE I.

u	G	$\Delta G/\Delta u$	u	G	$\Delta G/\Delta u$	u	G	$\Delta G/\Delta u$	u	G	$\Delta G/\Delta u$
0.00	.00000		2.50	.18943	.0630	5.00	.30679	.0334	9.00	.38901	.0123
.05	.004165		2.55	.19253	.0620	5.05	.30844	.0330	9.10	.39022	.0121
.10	.008415		2.60	.19561	.0616	5.10	.31007	.0326	9.20	.39140	.0118
.15	.01265		2.65	.19866	.0610	5.15	.31168	.0322	9.30	.39256	.0116
.20	.01671		2.70	.20168	.0604	5.20	.31327	.0318	9.40	.39370	.0114
.25	.02075		2.75	.20465	.0594	5.25	.31484	.0314	9.50	.39481	.0111
.30	.02496		2.80	.20761	.0592	5.30	.31638	.0308	9.60	.39590	.0109
.35	.02910	.0832	2.85	.21051	.0580	5.35	.31790	.0304	9.70	.39697	.0107
.40	.03326	.0824	2.90	.21339	.0576	5.40	.31940	.0300	9.80	.39802	.0105
.45	.03738	.0824	2.95	.21625	.0572	5.45	.32088	.0296	9.90	.39904	.0102
.50	.04150	.0822	3.00	.21906	.0562	5.50	.32234	.0292	10.00	.40005	.0101
.55	.04561	.0818	3.05	.22184	.0556	5.55	.32378	.0288	10.10	.40103	.0098
.60	.04970	.0818	3.10	.22459	.0550	5.60	.32520	.0284	10.20	.40200	.0097
.65	.05379	.0816	3.15	.22731	.0544	5.65	.32660	.0280	10.30	.40294	.0094
.70	.05787	.0812	3.20	.22999	.0536	5.70	.32798	.0276	10.40	.40388	.0094
.75	.06193	.0808	3.25	.23264	.0530	5.75	.32934	.0272	10.50	.40479	.0091
.80	.06597	.0804	3.30	.23526	.0524	5.80	.33068	.0268	10.60	.40568	.0089
.85	.06999	.0804	3.35	.23785	.0518	5.85	.33200	.0264	10.70	.40656	.0088
.90	.07401	.0798	3.40	.24041	.0512	5.90	.33330	.0260	10.80	.40743	.0087
.95	.07800	.0796	3.45	.24294	.0506	5.95	.33458	.0256	10.90	.40828	.0085
1.00	.08198	.0790	3.50	.24544	.0500	6.00	.33583	.0250	11.00	.40911	.0083
1.05	.08593	.0788	3.55	.24790	.0492	6.10	.33831	.0252	11.10	.40993	.0082
1.10	.08987	.0782	3.60	.25032	.0484	6.20	.34075	.0244	11.20	.41072	.0079
1.15	.09378	.0780	3.65	.25271	.0478	6.30	.34311	.0236	11.30	.41151	.0079
1.20	.09768	.0774	3.70	.25508	.0474	6.40	.34541	.0230	11.40	.41229	.0078
1.25	.10155	.0770	3.75	.25741	.0466	6.50	.34766	.0225	11.50	.41305	.0076
1.30	.10540	.0764	3.80	.25972	.0462	6.60	.34984	.0218	11.60	.41380	.0075
1.35	.10922	.0760	3.85	.26200	.0456	6.70	.35198	.0214	11.70	.41454	.0074
1.40	.11302	.0756	3.90	.26425	.0450	6.80	.35406	.0208	11.80	.41526	.0072
1.45	.11680	.0750	3.95	.26647	.0444	6.90	.35608	.0202	11.90	.41598	.0072
1.50	.12055	.0746	4.00	.26866	.0438	7.00	.35805	.0197	12.00	.41668	.0070
1.55	.12428	.0738	4.05	.27082	.0432	7.10	.35998	.0193	12.10	.41736	.0068
1.60	.12797	.0734	4.10	.27295	.0426	7.20	.36186	.0188	12.20	.41803	.0067
1.65	.13164	.0728	4.15	.27505	.0420	7.30	.36369	.0183	12.30	.41870	.0067
1.70	.13528	.0722	4.20	.27712	.0414	7.40	.36547	.0178	12.40	.41935	.0065
1.75	.13889	.0716	4.25	.27919	.0408	7.50	.36722	.0175	12.50	.42000	.0065
1.80	.14247	.0712	4.30	.28119	.0402	7.60	.36892	.0170	12.60	.42063	.0063
1.85	.14603	.0704	4.35	.28318	.0398	7.70	.37058	.0166	12.70	.42126	.0063
1.90	.14955	.0700	4.40	.28515	.0394	7.80	.37220	.0162	12.80	.42187	.0061
1.95	.15305	.0694	4.45	.28709	.0388	7.90	.37379	.0159	12.90	.42248	.0061
2.00	.15652	.0688	4.50	.28901	.0384	8.00	.37534	.0155	13.00	.42308	.0060
2.05	.15996	.0678	4.55	.29090	.0378	8.10	.37684	.0150	13.10	.42366	.0058
2.10	.16335	.0674	4.60	.29276	.0372	8.20	.37832	.0148	13.20	.42424	.0058
2.15	.16672	.0668	4.65	.29460	.0368	8.30	.37977	.0145	13.30	.42481	.0057
2.20	.17006	.0662	4.70	.29641	.0362	8.40	.38117	.0140	13.40	.42537	.0056
2.25	.17337	.0654	4.75	.29820	.0358	8.50	.38255	.0138	13.50	.42593	.0056
2.30	.17665	.0648	4.80	.29997	.0354	8.60	.38390	.0135	13.60	.42647	.0054
2.35	.17989	.0642	4.85	.30172	.0350	8.70	.38523	.0133	13.70	.42701	.0054
2.40	.18310	.0636	4.90	.30343	.0342	8.80	.38651	.0128	13.80	.42754	.0053
2.45	.18628		4.95	.30512	.0338	8.90	.38778	.0127	13.90	.42806	.0052

of rotation and vibration are given in Table II. It is seen from these figures that at room temperature the rotational correction is small.

For non-linear polyatomic molecules containing hydrogen the moments of inertia are generally high enough so that no rotational correction need be made.

As an example we have calculated the equilibrium constants for the reaction

$$H_2+2DI=D_2+2HI \qquad (16)$$

at various temperatures. The constants used in the calculations are given in Table III. The results of the calculations, which include a correction for the non-classical rotation, are given in Table IV and Fig. 2.

This equilibrium has been calculated previously.[4] Our results are in good agreement with those of Urey and Rittenberg at the four temperatures for which they have made the calculation considering the fact that we have used a slightly

[4] H. C. Urey and D. Rittenberg, J. Chem. Phys. 1, 137 (1933). J. C. L. Blagg and G. M. Murphy, J. Chem. Phys. 4, 631 (1936).

TABLE I.—*Continued.*

u	G	$\Delta G/\Delta u$	u	G	$\Delta G/\Delta u$	u	G	$\Delta G/\Delta u$	u	G	$\Delta G/\Delta u$
		.0051			.0036			.0026			.0020
14.00	.42857	.0051	16.80	.44048	.0035	19.60	.44898	.0026	22.40	.45536	.0020
14.10	.42908	.0050	16.90	.44083	.0035	19.70	.44924	.0025	22.50	.45556	.0019
14.20	.42958	.0049	17.00	.44118	.0034	19.80	.44949	.0026	22.60	.45575	.0020
14.30	.43007	.0049	17.10	.44152	.0034	19.90	.44975	.0025	22.70	.45595	.0019
14.40	.43056	.0047	17.20	.44186	.0034	20.00	.45000	.0025	22.80	.45614	.0019
14.50	.43103	.0048	17.30	.44220	.0033	20.10	.45025	.0025	22.90	.45633	.0019
14.60	.43151	.0046	17.40	.44253	.0033	20.20	.45050	.0024	23.00	.45652	.0019
14.70	.43197	.0046	17.50	.44286	.0032	20.30	.45074	.0024	23.10	.45671	.0019
14.80	.43243	.0046	17.60	.44318	.0032	20.40	.45098	.0024	23.20	.45690	.0018
14.90	.43289	.0044	17.70	.44350	.0032	20.50	.45122	.0024	23.30	.45708	.0018
15.00	.43333	.0044	17.80	.44382	.0031	20.60	.45146	.0023	23.40	.45726	.0019
15.10	.43377	.0044	17.90	.44413	.0031	20.70	.45169	.0023	23.50	.45745	.0018
15.20	.43421	.0043	18.00	.44444	.0031	20.80	.45192	.0023	23.60	.45763	.0018
15.30	.43464	.0042	18.10	.44475	.0030	20.90	.45215	.0023	23.70	.45781	.0017
15.40	.43506	.0042	18.20	.44505	.0031	21.00	.45238	.0023	23.80	.45798	.0018
15.50	.43548	.0042	18.30	.44536	.0029	21.10	.45261	.0022	23.90	.45816	.0017
15.60	.43590	.0041	18.40	.44565	.0030	21.20	.45283	.0022	24.00	.45833	.0018
15.70	.43631	.0040	18.50	.44595	.0029	21.30	.45305	.0022	24.10	.45851	.0017
15.80	.43671	.0040	18.60	.44624	.0028	21.40	.45327	.0022	24.20	.45868	.0017
15.90	.43711	.0039	18.70	.44652	.0029	21.50	.45349	.0021	24.30	.45885	.0017
16.00	.43750	.0039	18.80	.44681	.0028	21.60	.45370	.0022	24.40	.45902	.0016
16.10	.43789	.0038	18.90	.44709	.0028	21.70	.45392	.0021	24.50	.45918	.0017
16.20	.43827	.0038	19.00	.44737	.0027	21.80	.45413	.0021	24.60	.45935	.0016
16.30	.43865	.0037	19.10	.44764	.0028	21.90	.45434	.0021	24.70	.45951	.0017
16.40	.43902	.0037	19.20	.44792	.0027	22.00	.45455	.0020	24.80	.45968	.0016
16.50	.43939	.0037	19.30	.44819	.0026	22.10	.45475	.0020	24.90	.45984	.0016
16.60	.43976	.0036	19.40	.44845	.0027	22.20	.45494	.0021	25.00	.46000	
16.70	.44012		19.50	.44872		22.30	.45516				

different spectroscopic assignment. It will be seen from Fig. 2 that at high temperatures $K=1+k/T^2$. At low temperatures, the calculation can only be made by summing the rotational states, giving each state its proper statistical weight taking into account the nuclear spin. These methods are well known and need not be elaborated further.

ISOTOPES OF THE HEAVY ELEMENTS

In considering exchange reactions of two polyatomic molecules containing isotopes of a heavy element, it may be possible to calculate the equilibrium constant sufficiently accurately by means of Eq. (11b). If these conditions are fulfilled then it is possible to make an approximate calculation without a complete knowledge of the vibrational frequencies of the molecules. The sum of the squares of all the frequencies of a molecule has the form

$$4\pi^2 \sum_i \nu_i^2 = \sum_{n=1}^{N} \frac{A_n}{m_n}, \tag{17}$$

where the summation on the right-hand side extends over all atoms in the molecule and the A's depend on force constants only. Then

$$\Delta \sum_i \nu_i^2 = \frac{\Delta m}{mm'} \frac{1}{4\pi^2} A, \tag{18}$$

where A is to be computed in the following manner. Let all the atoms in the molecule except the one which is to be isotopically substituted be fixed in position. A is then the sum of the three

TABLE II.*

	σT in °K
H_2	85.387
D_2	43.032

* Taken from Herzberg, *Molecular Spectra and Molecular Structure* (Prentice-Hall, Inc., New York, 1939).

TABLE III.*

	ω_e	$X_{\omega\omega}$	B_0	σT
H_2	4405.30	125.325	59.338	85.387
D_2	3117.05	63.034	29.904	43.032
HI	2309.53	39.73	6.459	9.295
DI	1640.18	20.04	3.258	4.688

* The vibrational frequencies for H_2 and D_2 are those reported by G. K. Teal and G. E. MacWood, J. Chem. Phys. **3**, 760 (1935). The B_0 values are calculated from the tables in Herzberg (footnote to Table II). The vibration frequency for HI is taken from Herzberg also and was used to calculate the frequency for DI.

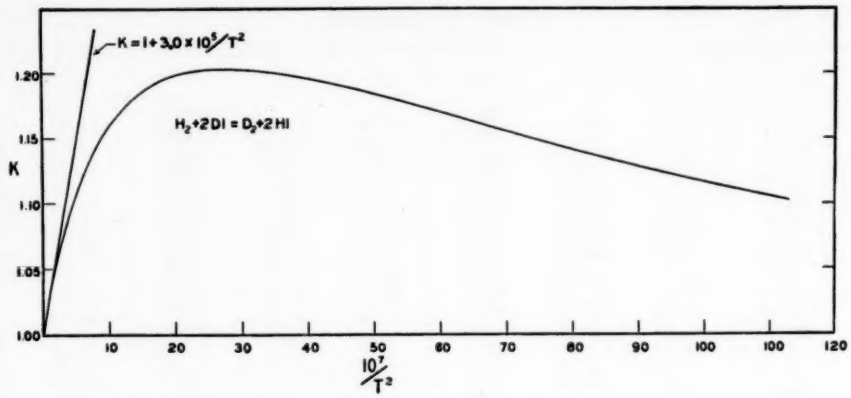

FIG. 2. The equilibrium constant for the reaction $H_2+2DI=D_2+2HI$ as a function of temperature.

restoring force constants corresponding to the displacement of the isotopic atom in three mutually perpendicular directions.

The following consideration will show that the above definition will give A. Let the atoms in the molecule be numbered from 1 to N; the isotopic atom will be 1. The force constants are denoted by $a_{i,j}{}^{x,y}(i,\ j=1\cdots N)$; the masses of the atoms by m_i and m_j; m_1 is written as M. The frequencies are determined by the equation

$$0=\begin{vmatrix} \frac{a_{11}{}^{xx}}{M}-4\pi^2\nu^2 & \frac{a_{11}{}^{xy}}{M} & \frac{a_{11}{}^{xz}}{M} & \frac{a_{12}{}^{xx}}{(Mm_2)^{\frac{1}{2}}} & \frac{a_{12}{}^{xy}}{(Mm_2)^{\frac{1}{2}}} & \frac{a_{12}{}^{xz}}{(Mm_2)^{\frac{1}{2}}} & \cdots & \frac{a_{1N}{}^{xz}}{(Mm_N)^{\frac{1}{2}}} \\ \frac{a_{11}{}^{yx}}{M} & \frac{a_{11}{}^{yy}}{M}-4\pi^2\nu^2 & \frac{a_{11}{}^{yz}}{M} & \frac{a_{12}{}^{yx}}{(Mm_2)^{\frac{1}{2}}} & \frac{a_{12}{}^{yy}}{(Mm_2)^{\frac{1}{2}}} & \frac{a_{12}{}^{yz}}{(Mm_2)^{\frac{1}{2}}} & \cdots & \frac{a_{1N}{}^{yz}}{(Mm_N)^{\frac{1}{2}}} \\ \frac{a_{11}{}^{zx}}{M} & \frac{a_{11}{}^{zy}}{M} & \frac{a_{11}{}^{zz}}{M}-4\pi^2\nu^2 & \frac{a_{12}{}^{zx}}{(Mm_2)^{\frac{1}{2}}} & \frac{a_{12}{}^{zy}}{(Mm_2)^{\frac{1}{2}}} & \frac{a_{12}{}^{zz}}{(Mm_2)^{\frac{1}{2}}} & \cdots & \frac{a_{1N}{}^{zz}}{(Mm_N)^{\frac{1}{2}}} \\ \frac{a_{21}{}^{xx}}{(Mm_2)^{\frac{1}{2}}} & \frac{a_{21}{}^{xy}}{(Mm_2)^{\frac{1}{2}}} & \frac{a_{21}{}^{xz}}{(Mm_2)^{\frac{1}{2}}} & \frac{a_{22}{}^{xx}}{m_2}-4\pi^2\nu^2 & \frac{a_{22}{}^{xy}}{m_2} & \frac{a_{22}{}^{xz}}{m_2} & \cdots & \frac{a_{2N}{}^{xz}}{(m_2m_N)^{\frac{1}{2}}} \\ \cdot & \cdot & \cdot & \cdot & \cdot & \cdot & & \cdot \\ \cdot & \cdot & \cdot & \cdot & \cdot & \cdot & & \cdot \\ \frac{a_{N1}{}^{xz}}{(Mm_N)^{\frac{1}{2}}} & \cdot & \cdot & \cdot & \cdot & \cdot & & \frac{a_{NN}{}^{zz}}{m_N}-4\pi^2\nu^2 \end{vmatrix}. \quad (19)$$

The sum of all roots of this equation is the trace, or sum of all diagonal elements, of the matrix of force constants. Consequently

$$4\pi^2\sum_i\Delta(\nu_i)^2=\frac{\Delta M}{MM'}(a_{11}{}^{xx}+a_{11}{}^{yy}+a_{11}{}^{zz})$$
$$\simeq\frac{\Delta M}{M^2}(a_{11}{}^{xx}+a_{11}{}^{yy}+a_{11}{}^{zz}). \quad (20)$$

If the central atom of mass M or $M+\Delta M$ is symmetrically surrounded by n identical atoms of mass m, a useful approximation may be derived. In the first approximation, all force constants except those arising from the stretching of the bonds with the central atom, a, may be neglected. In that case, A in Eq. (18) becomes na. The force constant may be estimated from the totally symmetric frequency, ν_1, which is usually known from Raman spectra and which obeys the equation $4\pi^2\nu_1{}^2=a/m$. One obtains

TABLE IV.

$T°K$	$f D_2/H_2$	$f(DI)/(HI)$	$K=\frac{D_2}{H_2}\left(\frac{HI}{DI}\right)^2$
0			0.0
300	13.744	3.5207	1.109
400	6.5481	2.3654	1.170
500	4.1972	1.8709	1.199
600	3.1214	1.6079	1.207
700	2.5285	1.4497	1.203
800	2.1616	1.3465	1.192
900	1.9160	1.2753	1.178
1000	1.7425	1.2238	1.164
1100	1.6147	1.1854	1.149
1200	1.5126	1.1564	1.135
1300	1.4422	1.1333	1.123
1400	1.3815	1.1150	1.112
1500	1.3327	1.0999	1.102
2000	1.1867	1.0555	1.066

then the rough approximation

$$\frac{s}{s'}f=1+\frac{\Delta M_m}{24M^2}u_1^2 n. \qquad (21)$$

Of course, the force constants arising from the bending of bonds and interaction between outer atoms are not actually negligible. The values of ν_1^2 and $\sum_i \Delta(\nu_i)^2$ are both greater than computed by this rough estimate. Equation (21) which merely equates the sum of the force constants of the center atom with ν_1^2 is somewhat more accurate than the neglections indicate.

We are now in a position to make a rough estimate of the enrichment factor to be expected for two typical exchange reactions of the heavy elements. The reactions chosen are

$$Si^{28}F_4+Si^{30}F_6^{=}=Si^{30}F_4+Si^{28}F_6^{=}, \qquad (22)$$

$$Sn^{120}Cl_4+Sn^{118}Cl_6^{=}=Sn^{118}Cl_4+Sn^{120}Cl_6^{=}. \qquad (23)$$

The results for 300°K are tabulated in Table V.

In both of these exchange reactions the cancellation of the separative effect is over ninety

TABLE V.

Molecule	ω_1	f	K
SiF_4	800[a]	1.111	1.002
$SiF_6^{=}$	600[b]	1.109	
$SnCl_4$	367[c]	1.00256	1.00025
$SnCl_6^{=}$	314[b]	1.00281	

[a] Yost, Lassettre, and Gross, J. Chem. Phys. **4**, 325 (1936).
[b] Redlich, Kurz, and Rosenfeld, Zeits. f. physik. Chemie **B 19**,231 (1932).
[c] Daure, Comptes rendus **187**, 940 (1928).

percent. This large cancellation is caused by the fact that although there are more bonds in the octahedral ions contributing to the restoring force constant for the central atom, the bonds have become weaker than those in the tetrahedral molecules and the total restoring force is approximately unchanged. This is usually the case of acid-base exchange equilibria. To get a large separative effect it is necessary to equilibrate one compound which has high frequencies and large frequency shifts on isotopic substitution with another compound (preferably the gaseous atom) with low frequencies and small frequency shifts.

Addendum: After this paper had been completed, Professor W. F. Libby kindly called a paper by L. Waldmann[5] to our attention. In this paper, Waldmann discusses briefly the fact that the chemical separation of isotopes is a quantum effect. He gives formulae which are equivalent to our (11′) and (11a) and discusses qualitatively their application to two acid base exchange equilibria. These are the exchange between NH_3 and NH_4^+ and HCN and CN^- studies by Urey[6] and co-workers.

[5] L. Waldmann, Naturwiss. **31**, 205 (1943).
[6] H. G. Thode and H. C. Urey, J. Chem. Phys. **7**, 34 (1939). C. A. Hutchison, D. W. Stewart, and H. C. Urey, J. Chem. Phys. **8**, 532 (1940).

THE JOURNAL OF CHEMICAL PHYSICS VOLUME 15, NUMBER 5 MAY, 1947

A Raman Apparatus for Quantitative Polarization Measurements*

BRYCE L. CRAWFORD, JR. AND WILLIAM HORWITZ
School of Chemistry, University of Minnesota, Minneapolis, Minnesota

(Received February 26, 1947)

An apparatus for quantitative measurement of the depolarization factors of Raman lines is described. It is a modification of Edsall and Wilson's method, using polaroid cylinders. Short exposure times result from the use of eight exciting lamps. No apparatus corrections are needed. Alignment is not overly critical. Performance is reported on the Raman lines of CCl_4, $CHCl_3$, and C_6H_6.

INTRODUCTION

IT is generally agreed nowadays that no serious study of the Raman spectrum of a molecule is complete without depolarization measurements, at least on the stronger lines. Such information is most helpful in the vibrational analysis, and certainly all possible help is usually needed in establishing an unambiguous vibrational assignment. Moreover, it is worth while to make these measurements *quantitatively;* i.e., so that one obtains numerical values of the depolarization factors rather than a mere labelling of the lines as polarized, partly polarized, or depolarized. In the first place, there are instances in which a clear distinction between complete depolarization ($\rho=0$) and partial depolarization ($\rho<6/7$) enables one to establish the symmetry of the molecule studied. In the second place, numerical values of the depolarization factor give a much better sense of the reliability of the result; the very real difference between the results $\rho=0.40$ and $\rho=0.70$ is lost in the lumping together of such results as "partly polarized."

At the same time, in seeking to design equipment for quantitative polarization measurements, one must not lose sight of the fact that the primary need in Raman spectroscopy is a high intensity of illumination. Also, since the Raman effect is essentially a simple experiment, it is well to avoid complicated apparatus or set-ups involving delicate alignment.

The scheme we have used for Raman observation seems to us to combine rather satisfactorily the desirable qualities of intense illumination, insensitivity to alignment, and good quantitative measurement of the depolarization factors. It is a modification of the first method of Edsall and Wilson.[1] In this paper we shall describe our apparatus, give data on its performance, and list some of its defects which we are planning to improve.

METHODS OF DEPOLARIZATION MEASUREMENT

Methods for measuring depolarization factors fall naturally into two types: those involving a single Raman exposure and those involving two exposures. In the single-exposure apparatus, the scattering substance is illuminated in a single plane by parallel radiation, and the scattered light is observed in a direction strictly perpendicular to the incident light. Deviations from this requirement of perpendicularity give rise to "convergence error." The beam of scattered light is resolved into its two polarized component beams which are slightly separated spatially. Preferential reflection of the polarized beams at optical surfaces (apparatus error) must be eliminated, usually by depolarizing the component beams; finally the component beams are recorded simultaneously, one above the other, on the photographic plate. In the double-exposure method, the two polarized beams are obtained in two successive exposures, with a rotation of some part of the apparatus (lamp, nicol prism, or polaroid) through 90° between exposures.

Of the earlier apparatuses, some of which have been described by Glockler and Baker,[2] those of

* This paper is drawn, in large part, from a thesis to be submitted by William Horwitz to the Graduate School of the University of Minnesota, in partial fulfillment of the requirements for the degree of Doctor of Philosophy. Some other studies whose results are partially reported here have been supported by a grant from the Research Fund of the Graduate School of the University of Minnesota. For this support and for the purchase of the recording microphotometer, the senior author is most grateful.

[1] J. T. Edsall and E. B. Wilson, Jr., J. Chem. Phys. 6, 124 (1938).

[2] G. Glockler and H. T. Baker, J. Chem. Phys. 11, 446 (1943).

Cabannes and Rousset,[3] and of Reitz[4] stand out as being constructed with elaborate precautions to eliminate possible sources of error. Indeed, these arrangements are often referred to as "ideal." These were both of the single-exposure type, as are most of the more recent arrangements. Glockler and Baker[2] used a split-field polaroid, backed by half-wave mica plates for the component resolution and depolarization. The half-wave plates were later eliminated[5] by placing the resolving polaroids in such a manner that their line of contact was 45° off the vertical axis of the spectrograph. Cleveland[6] also used a split-field polaroid for the resolution but did not depolarize the resolved components. Empirically determined factors were applied to the observed data to correct for the apparatus and convergence errors. A double-exposure apparatus, with polaroid as the resolving element, was described by Rank, Pfister, and Grimm[7] in connection with the application of their photoelectric technique to the measurement of depolarization factors of Raman lines; they also used empirical correction factors.

The single-exposure methods of obtaining depolarization factors have the obvious inherent advantage of being independent of changes in the experimental conditions during a run. Because of theoretical considerations, the exciting radiation must be confined to a single plane. Therefore a maximum of two lamps can be used with this type of apparatus. This condition seriously limits the speed of the apparatus, and, as a rule, relatively long exposure times are required for the polarization spectra. Further, very precise alignment of the Raman tube, lamps, and optical components is necessary, and the Raman tube window must be strain-free. For example, Reitz reported that after several months of use his apparatus showed a residual apparatus correction of 1.065 (instead of 1.000) which was traced to the warping of a wooden support.

A double-exposure apparatus is usually simpler and requires a less critical alignment of parts than a single-exposure arrangement. If polarized light is used for the excitation, lamps can be arranged axially around the Raman tube so that their number and intensity are limited only by the physical dimensions of the lamps and the apparatus (and by the laboratory's facilities for supplying electrical power and for dissipating heat). While one must guard against the danger of conditions changing from the first to the second exposure, improvements in the control of high-intensity mercury lamps to provide intensity stability have advanced to a point where the double-exposure method can compete successfully in accuracy with the single-exposure method.

The possibility of obtaining high incident intensity and relatively short exposure times, was the major consideration which led us to the construction of our double-exposure apparatus.

APPARATUS

Our apparatus is, as mentioned above, a modification of that used by Edsall and Wilson.[1] In their apparatus, they used a cylindrical "light furnace" in which the Raman tube was surrounded by four symmetrically placed mercury arcs; in this manner the radiation field in which the Raman tube was immersed was axially symmetric. In one exposure, the Raman tube was surrounded by a cylinder of polaroid with its optical axis parallel to that of the Raman tube; thus the axially symmetric radiation field was composed of polarized light, the planes of vibration passing through the Raman tube axis. For the comparison exposure, no Polaroid was used and the intensity of the lamps was reduced to provide an approximately correct comparison for the depolarized lines. Edsall and Wilson, of course, intended their set-up only for qualitative polarization studies; for quantitative purposes, it is better to make the comparison exposure using tangentially polarized illumination. The suggestion of using appropriately oriented Polaroid on both exposures was again made by Cleveland and Murray[8] in their discussion of the method of Edsall and Wilson. This suggestion corresponds essentially to our design.

[3] J. Cabannes and A. Rousset, Ann. de physique [X] **19**, 229 (1933).
[4] A. W. Reitz, Zeits. f. physik. Chemie **B33**, 368 (1936); **B38**, 275 (1937).
[5] G. Glockler, J. F. Haskin, and C. C. Patterson, J. Chem. Phys. **12**, 349 (1944).
[6] F. F. Cleveland, J. Chem. Phys. **13**, 101 (1945).
[7] D. H. Rank, R. J. Pfister, and H. H. Grimm, J. Opt. Soc. Am. **33**, 31 (1943).
[8] F. F. Cleveland and M. J. Murray, J. Chem. Phys. **7**, 396 (1939).

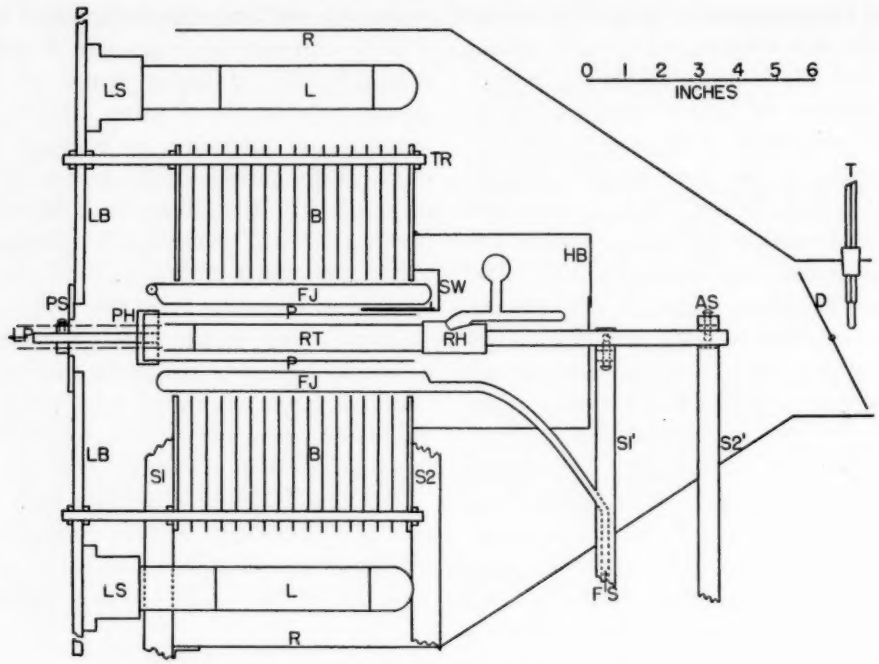

FIG. 1. Side view of the Raman apparatus.

AS	Alignment screws
B	Baffles
BB	Base board
D	Damper
FJ	Filter jacket
FS	Filter solution inlet
HB	Hinged box
L	Lamp
LB	Lamp board
LP	Light path
LS	Lamp socket
P	Polaroid
PH	Polaroid holder
PS	Polaroid holder support
R	Reflector
RH	Raman tube holder
RT	Raman tube
S1, *S2*	Illuminator supports
S1', *S2'*	Raman tube holder supports
SW	Thermal safety switch
T	Thermometer
TR	Tie rods
TS	Tripod adjustment screws

The general outline of our apparatus is shown in side and rear views in Figs. 1 and 2. Like Edsall and Wilson, we use a cylindrical light furnace with appropriate baffles and filters. For polarization measurements, we take two exposures. In the first, the Raman tube is surrounded by a cylinder of polaroid with its axis parallel to that of the Raman tube; in the second, a cylinder of polaroid is used with its axis tangentially around the Raman tube.

If we denote the intensities of a given Raman line in the first and second exposures by $I_{\parallel}$ and $I_{\perp}$, respectively, then, as Edsall and Wilson discussed, the ratio $(I_{\parallel}/I_{\perp})$ is equal to the depolarization ratio ρ as usually defined, with values between 0 and 6/7. Since the beam of scattered light is not polarized, no apparatus correction need be made. We calculated our "convergence error" by an appropriate modification of the method of Gans;[9] with the baffles we use, the correction to be subtracted from the observed ρ is not over 0.01, and accordingly it was neglected.

Spectrograph

A three-prism $f:3$, Steinheil spectrograph, having a dispersion of 32A/mm at 4358A, was used with this apparatus. The resolution at the usual slit width of 0.1 mm was such that the carbon tetrachloride doublet at 762–790 cm^{-1} was just resolved.

Illuminator

The cylindrical illuminator or light furnace contains the baffles and filter jacket. The cham-

[9] Gans, Physik. Zeits. **28**, 661 (1927); also in Bhagavantam, *Scattering of Light and the Raman Effect*, Waltair, 1940, Appendix II.

ber inside the jacket contains the polaroid filter, Raman tube, and a bimetallic safety switch which, operating through a relay, will open the lamp circuit if the jacket chamber becomes too warm. The illuminator is connected by a cone-shaped adapter to a blower which ejects the hot air from the room. The damper is placed just in front of the blower, together with a thermometer for indicating the air-stream temperature. The adapter chamber also contains supports for the Raman-tube holder and a hinged, insulated box which keeps the hot air and stray light from entering the center portion of the apparatus. The reflector and the adapter are split along a horizontal diameter for easy access to the interior in changing Raman tubes and in making alignment adjustments.

Lamps

Eight General Electric type A-H2 (250 watt) mercury lamps arranged in a circle and backed by a chromium-plated reflector provide the exciting illumination. These are very intense, self-starting lamps, operating off the usual a.c. power lines through auto-transformers. They have the disadvantages that the mercury spectrum is accompanied by a moderate continuous background in the neighborhood of 4358A,[10] and that the intensity is somewhat sensitive to voltage and temperature fluctuations. Polarization exposures were run at times of day when the line voltage was expected to be rather constant. The lamp temperatures were controlled by a manually operated damper in the cooling air stream. Very little attention was required to maintain the air temperature within plus or minus one degree after an initial half-hour warm-up period. Figure 3 shows the intensity variation of the lamps in density units per minute when the apparatus is uncontrolled (U), and controlled by the damper (C), after an initial warm-up period. It was obtained by taking successive Raman exposures of short duration, and plotting the resulting density per minute of a Raman line against the exposure number. This stability was considered satisfactory at the present stage of development of the apparatus but it will be improved by the addition of voltage stabilizers.

Filters

An alcoholic solution of Rhodamine 5 GDN Extra[11] is circulated through a cylindrical filter jacket, and a cooling coil immersed in running tap water. This filter is a modification of the one used by Edsall and Wilson.[1] The p-nitrotoluene of their filter has been replaced by a Wratten 2A gelatin filter which is wrapped around the Polaroids. The gelatin filter is reported[12] to transmit less than 1 percent at 4047, and about 80 percent at 4358.

Polaroid-filter tubes

These tubes consist of successive layers of type H Polaroid,[13] Wratten 2A gelatin filter, and

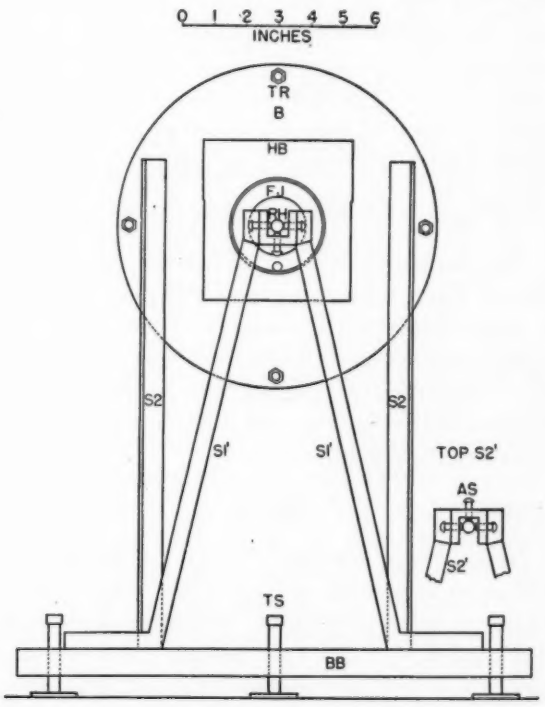

FIG. 2. Rear view of Raman apparatus. Reflector, lamps, and polaroid omitted. See Fig. 1 for legend.

[10] The type A-H11, discussed below, give less background and are less sensitive to temperature variations. All the work reported here was done with A-H2 lamps. We are indebted to Dr. Foil A. Miller for suggesting the use of these lamps, and for many other suggestions during the construction of this apparatus.

[11] We are indebted to E. I. duPont deNemours for this dye.

[12] *Wratten Light Filters*, 16th Edition (Eastman Kodak Company, Rochester, New York, 1940).

[13] We are indebted to Mr. C. D. West of the Polaroid Corporation for the Polaroid used. This type H film transmits 34.2 percent of 4358 with a degree of polarization

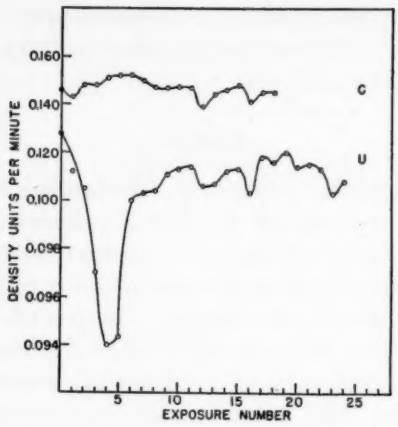

FIG. 3. Intensity stability of the mercury AH-2 lamps as measured by the Raman line density of successive exposures. *C*, air stream temperature maintained at 80 ±2°C by means of a damper; *U*, air stream temperature uncontrolled.

protective Cellophane, wrapped around a glass cylinder, and secured with Scotch Tape. Two such cylinders were constructed, identical except that the optical axis of the polaroid on one was perpendicular to the axis of the polaroid on the other. These cylinders are concentric with the Raman tube and are easily changed between exposures from the front of the apparatus.

Raman tubes

The Raman tubes are of conventional Wood design. Each tube is permanently cemented into a brass holder with plaster of Paris; tube and holder are aligned in V-blocks during the cementing. This method allows free interchange of Raman tubes in the illuminator without the necessity of realignment.

Speed

No generally accepted measure of the speed of a Raman apparatus seems to be in use; yet this factor is quite important. We have some work still under way on this matter, and we shall report here that an exposure of about 30 minutes, using the standard conditions described, and a standard plate and development, will bring the 314 cm^{-1} line of CCl_4 to a photographic density of 1.0; an exposure of about 13 minutes will bring the 992 cm^{-1} line of C_6H_6 to this density.

of 0.996, and was used throughout the work reported here. The Polaroid Corporation has since replaced type H with a similar film designated as type K on ABC support.

PHOTOMETRY

Eastman 103a-0 and 103a-J plates, with antihalation backing, were used throughout this study. They were chosen primarily because of their low reciprocity-law failure; their high speed is also advantageous in Raman work. Plates were developed for two minutes at 17°C in D-8, diluted 1 part of developer to two parts of water; this formula gives less fog than the usual D-19. The resulting gamma is about 2.4.

A series of calibration spectra was impressed upon each plate using a small, coiled-filament bulb operated from a constant-voltage transformer. A blue glass filter and a piece of ground glass were placed in the optical path. Ten calibration exposures were made, using rotating sector disks cut so that the logarithm of the intensity was decreased in steps of 0.2. The calibration exposures were each 2 minutes, compared with Raman exposures on the order of an hour.

We felt that reciprocity-law failure could be ignored for two reasons. First, the plates used were specifically designed to reduce this effect to a minimum. Second, as Reitz[4] pointed out, the time difference between the two spectra will not introduce a serious error since we require relative, and not absolute data. The desired information is the ratio of the two Raman intensities, and these exposures are of the same duration.

Line densities were obtained with a Leeds & Northrup recording microphotometer and were

TABLE I. Depolarization factors for carbon tetrachloride from individual plates.

	Line			
Plate No.	218	314	459	762–90
H-19	0.86	0.83	0.03	0.80
H-20	0.82	0.78	<0.05	0.88
H-21	0.83	0.85	0.06	0.89
H-22	0.85	0.85	<0.04	0.91
H-23	0.80	0.84	0.03	0.92
H-24	0.78	0.77	0.04	0.88
H-25	0.86	0.82	<0.04	0.81
H-33a	0.88	0.85	<0.08	—
H-33b	0.81	0.80	<0.05	—
H-35a	0.86	0.85	—	—
H-35b	0.83	0.82	—	—
H-35c	0.83	0.82	—	—
H-36	0.78	0.76	0.06	0.93
H-37	0.86	0.90	<0.04	0.85
Average	0.83	0.82	0.04_4	0.88
Std. dev.	0.03	0.04	0.01_4	0.04
Accepted values	0.857	0.857	0.046	0.857

transformed into relative intensities by means of a characteristic curve constructed from the calibration marks.

The continuous background deserves special attention. Our studies show it to be the greatest single source of error, exceeding even the residual intensity fluctuations of our lamps. Fortunately, the background is polarized and is absent in most of the "parallel" exposures. In cases of relatively strong lines, close together and near the exciting line, background troubles may be complicated by the Eberhard effect.

We used the usual method of correcting for background, transforming background density into intensity from the characteristic curve, and subtracting the result from the line intensity. Strock[14] maintains that even this method provides a spurious, or at best only a partial, correction. He adds, quite correctly, that the only cure for background is to eliminate it. Since we could not achieve this, we determined the proper choice of background on our microphotometer tracings by some studies on carbon tetrachloride. These experiments indicated that, to obtain the accepted values for the carbon tetrachloride lines, the background minimum just in front of the line (i.e., closest to the exciting line; see Fig. 4) should be taken as representing the line background. When this procedure was applied consistently to carbon tetrachloride, the results were acceptable, although slightly low (see Table I). The results could be improved by taking a somewhat higher point as the actual background, but this was not considered advisable since there was no other point on the microphotometer tracing which could be logically and consistently taken as a measure of background. The same choice of background which was worked out for carbon tetrachloride was applied successfully to several other compounds.

We have found that the background can be reduced by using the new General Electric mercury-vapor lamps, type A-H11. These lamps are identical with the type A-H2 except for a reduction in the amount of mercury used. Our preliminary experiments indicate that, for exposures giving equal Raman line densities, the A-H11

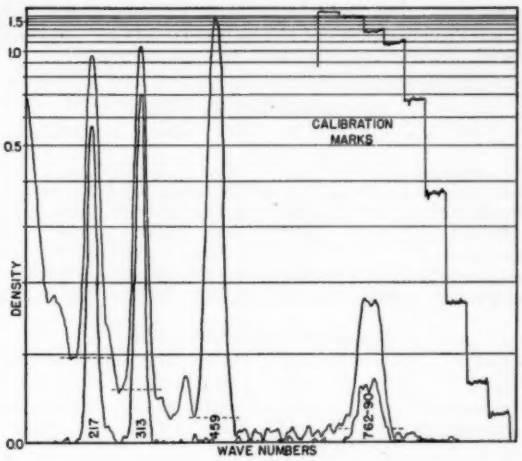

FIG. 4. Microphotometer tracing of the polarized Raman spectra of carbon tetrachloride. The upper tracing is the perpendicular spectrum; the lower is the parallel spectrum. The dashed horizontal lines indicate the background density used for calculating the background correction.

lamps give less than half the background density of the A-H2 lamps. The reduction in background, however, is accomplished at the sacrifice of half of the operating lamp intensity; i.e., the Raman exposures must be twice as long for the same line density. A further reduction in the background could be obtained by running the lamps at a lower operating temperature, but this decreases the lamp intensity still further.

PERFORMANCE

Figure 4 shows a typical tracing of a plate taken to determine the depolarization factors of the stronger lines of carbon tetrachloride. The upper tracing represents the perpendicular spectrum and the lower, the parallel. The calibration marks have been compressed. Particular features to be noted are the complete absence of background in the parallel spectrum, and the complete absence of the parallel component of the 459 line, although the perpendicular component of this line excited by 4348 is plainly visible. (The ratio of the intensities of 4348 to 4358 is about 0.08.)

Table I gives the actual results with carbon tetrachloride for two series of runs. Only one plate was rejected; on this exposure there was an error in the calibration marks caused by slipping of the rotating sectors.

On approximately half the plates, the parallel

[14] L. W. Strock, Proc. 7th Spect. Con. 134 (1940); J. Opt. Soc. Am. **32**, 103 (1942).

TABLE II. The average, average deviation, and maximum deviation of the depolarization factors for the Raman lines of carbon tetrachloride from various sources.

Author	Line 218	314	459	762	790
Average depolarization factors					
Reitz-I (5)†	0.854	0.872	0.045	0.742	0.777
Reitz-II (17)	0.84	0.87	0.04	0.89	0.84
Cleveland (5)	0.853	0.867	0.072	0.847	0.832
This research	0.83	0.82	0.044	0.88	
Theory or accepted	0.857	0.857	0.045	0.857	0.857
Average deviation from the mean					
Reitz-I	0.021	0.030	0.015	0.055	0.028
Reitz-II	0.06	0.07	0.02	0.06	0.08
Cleveland	0.017	0.020	0.057	0.023	0.044
This research	0.03	0.03	0.013	0.03	
Maximum deviation from the mean					
Reitz-I	0.048	0.062	0.027	0.111	0.043
Reitz-II	0.12	0.13	0.05	0.13	0.15
Cleveland	0.035	0.047	0.072	0.036	0.078
This research	0.05	0.08	0.015	0.08	

† Number of observations in parentheses; our calculations are based on the observations recorded in Table I, *viz.*, 14 observations on the 218 and 314 lines, 5 on the 459 line, and 9 on the doublet.

component of 459 was undetectable; in such cases we could only estimate a maximum value of ρ based on the relative intensity of the perpendicular component. Only the five observations which led to a significant result were used in the calculation of the precision measures in Tables I and II. On short-exposure plates, the factor is omitted both for this line and for the doublet. The results on this compound agree with the accepted or theoretical values within the standard deviation.

We present in Table II a comparison of the precision of our results on CCl_4 with that obtained by a few other workers. (Very few investigators report enough data for a precision estimate.) "Reitz-I" refers to his fundamental work,[4a] and "Reitz-II" refers to his control results;[4b] "Cleveland" refers to the paper cited above.[6] The deviations in our data compare favorably even with those of Reitz's fundamental paper.

TABLE III. Depolarization factors for chloroform and benzene.

Chloroform line cm^{-1}	found	accepted††	Benzene line cm^{-1}	found	accepted††
262	0.86	6/7	606	0.8	0.81
366	0.18	0.20	849	0.8	0.77
668	0.08	0.06	992	0.04	0.07
760	0.92	0.80	1177	0.8	0.70
1214	0.9	6/7	1585–1606	0.9	6/7
3020	0.4	0.31	3046–3063	0.3	D 0.4

†† M. Magat, *Tables Annuelles* (Hermann and Cie, Paris, 1937).

Additional results on chloroform and benzene are given in Table III. The values for the depolarization factors of benzene are given only to one place since a background correction had to be applied to the parallel spectrum as well as to the perpendicular one. The last two lines of chloroform are reported in the same manner because they were weak.

The advantages of the present apparatus are numerous. Eight high intensity lamps are used, a number impossible with single-exposure methods. The addition of eight more lamps to the present apparatus is contemplated to reduce the already short exposure times. The apparatus is simple, and the optical alignment is not delicate. The polarizing cylinders are easily prepared and are inexpensive. Most important, no "apparatus corrections" are necessary. (The usual photographic-background correction may, of course, cover a multitude of photometric sins.)

The most important disadvantages of this apparatus are not too formidable. The stability of the light source can be improved. The continuous background, which is common to any method, can be reduced by the use of an improved type of lamp.

Heat-Capacity Lag Measurements in Various Gases*

PAUL W. HUBER AND ARTHUR KANTROWITZ**
National Advisory Committee for Aeronautics, Langley Field, Virginia
(Received February 17, 1947)

The impact-tube method of measuring relaxation times for the transfer of molecular energy from translational to internal degrees of freedom has been introduced in a previous report. This method has been applied to a series of gases to make measurements of relaxation times which would be difficult to measure quantitatively by sonic methods. Measurements of the relaxation times of the vibrational energy of H_2O, N_2, N_2 catalyzed by H_2O, and CCl_2F_2 are presented. The existence of a measurable lag in the adjustment of the rotational heat capacity of H_2 has been confirmed, and measurements of its relaxation time are presented.

INTRODUCTION

IN a previous report,[1] the impact-tube method of measuring the relaxation time of gases was introduced. In this method, measurements are made of the entropy change in a single cycle of adiabatic expansion and compression of the gas. The gas is expanded from a chamber through a nozzle, and compressed at the nose of an impact tube aligned with the jet from the nozzle (see Fig. 1 of reference 1). If the apparatus is large enough so that the portion of the stream which interacts with the impact tube is outside the boundary layer of the nozzle, then the process is adiabatic. If this apparatus is properly constructed and adjusted and a gas without internal heat capacity, such as helium is used, the pressure measured at the impact tube is found to be very close to the chamber pressure. In this case, practically no dissipation of energy occurs in this flow. Therefore, this apparatus provides a sensitive and accurate method of detecting dissipations caused by a lag in the adjustment of the internal heat capacity of a gas, to external conditions.

The energy dissipations involved are nearly always small compared to the kinetic energy of the gas in the jet, and so it is possible to calculate the thermal energy of the gas as a function of time from conventional hydrodynamics neglecting the heat-capacity lag effects. This calculation can be simplified by choosing shapes for the nozzle and the impact tube for which hydrodynamic solutions are already available. Next, it is assumed that the rate of change of the internal molecular energy is directly proportional to its departure from equilibrium. Thus, only one type of lagging heat capacity with a single relaxation time is considered. Assuming a value for the relaxation time, it is then possible to calculate the departure from equilibrium at all times during a flow process, for which the thermal energy is known as a function of time from the hydrodynamic solution.

When a gas is not in equilibrium, a process analogous to heat conduction occurs in which heat flows from a temperature, which is appropriate to the internal energy of the molecules, to a temperature which corresponds to the translational energy. Now, when the departure from equilibrium and the relaxation time of the gas are known, the entropy increase in this "heat-conduction" process can be computed readily. In the case of the nozzle-impact-tube flow process, this entropy increase means that the stagnation pressure, measured by the impact tube, will be lower than the pressure of the gas in the chamber. The energy of the gas is, of course, identical with that of the chamber since these processes are adiabatic. The entropy, and the energy of the gas at stagnation conditions at the impact tube are thus known, and its pressure can readily be computed from standard thermodynamic formulae.

Method for Short Relaxation Times

If the impact tube is made very small (of the order of 0.005 inch in diameter), the time in-

* This work was done at the Langley Memorial Aeronautical Laboratory of the National Advisory Committee for Aeronautics. A somewhat more complete version was first published as a Restricted Bulletin No. L4E29 by the NACA. The restriction has since been removed, and the authors are grateful to the NACA for permission to publish this report.
** Now at the Graduate School of Aeronautical Engineering, Cornell University, Ithaca, New York.
[1] A. Kantrowitz, J. Chem. Phys. 14, 150 (1946).

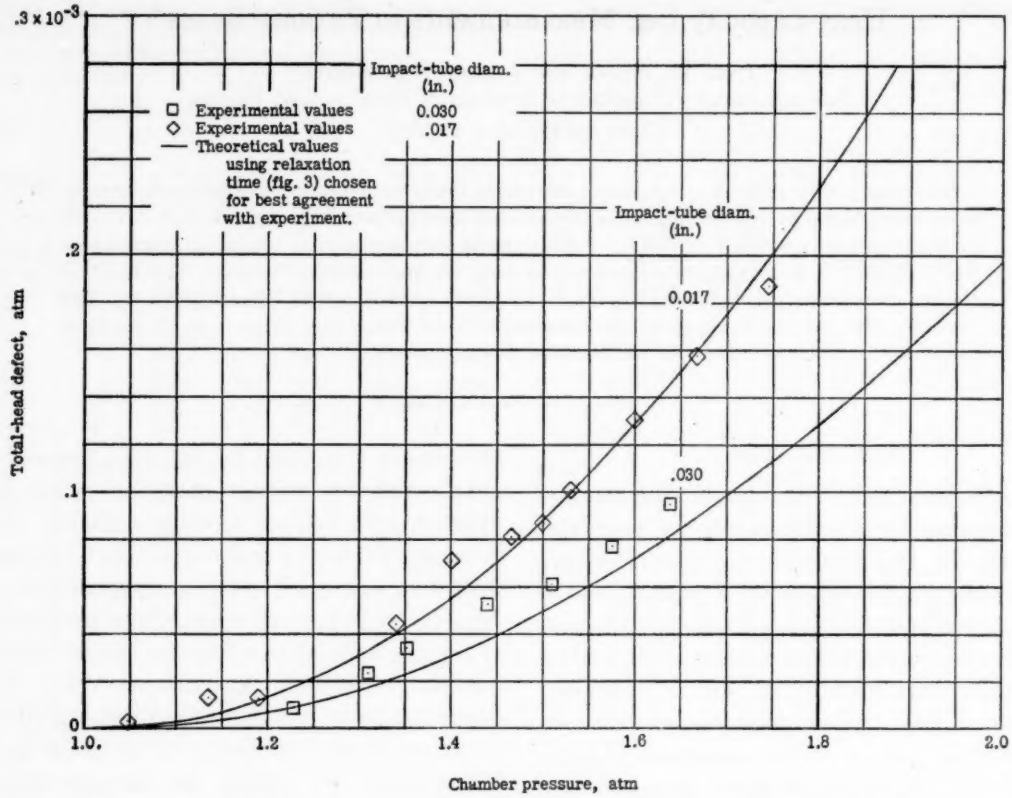

FIG. 1. Total-head defect of water vapor for chamber temperature of 585°K. From the departure of the experimental points from the theoretical curves, it can be concluded that the accuracy of these measurements is about ±20 percent. Points taken with a total-head defect less than 0.02×10^{-3} atmos. were used only to establish the zero reading of the manometer.

volved in the compression at the nose of the impact tube can be made very short (of the order of 1 microsecond). On the other hand, the nozzle can be made long (e.g., 2 inches), so that the expansions take place in times of the order of $\frac{1}{2}$ millisecond. Now, if the relaxation time of a gas is very short (compared to $\frac{1}{2}$ millisecond), the internal energy will follow the expansion in the nozzle very closely, and the gas approaching the impact tube will be very close to equilibrium. Thus, only the departures from equilibrium and the dissipation in the compression process at the nose of the impact tube need be considered.

In reference 1, calculations of the total-head defect (that is, the difference between chamber pressure and impact-tube pressure) were made for the case where an equilibrium gas approaches a "source-shaped" impact tube. The calculations were made assuming various ratios K of the diameter of the impact tube, to the distance traveled by the undisturbed gas in its relaxation time. Now, if it is desired to measure the relaxation time of a gas, known to have a short relaxation time compared to the time required for the expansion through the nozzle, experimental values of the total-head defect can be compared with these computations. Thus, values of K can be found for which the theoretical and experimental values of the total-head defect agree. In this way, a single measurement of the total-head defect yields a value of the relaxation time of the gas. If now a series of such measurements are made with different chamber pressures and different impact-tube sizes, the consistency of this method can be tested.

In this way measurements of the relaxation time of carbon dioxide were made. It was found that fairly consistent results for two impact tubes, and for a range of chamber pressures were obtained, thus establishing the general validity of this procedure.

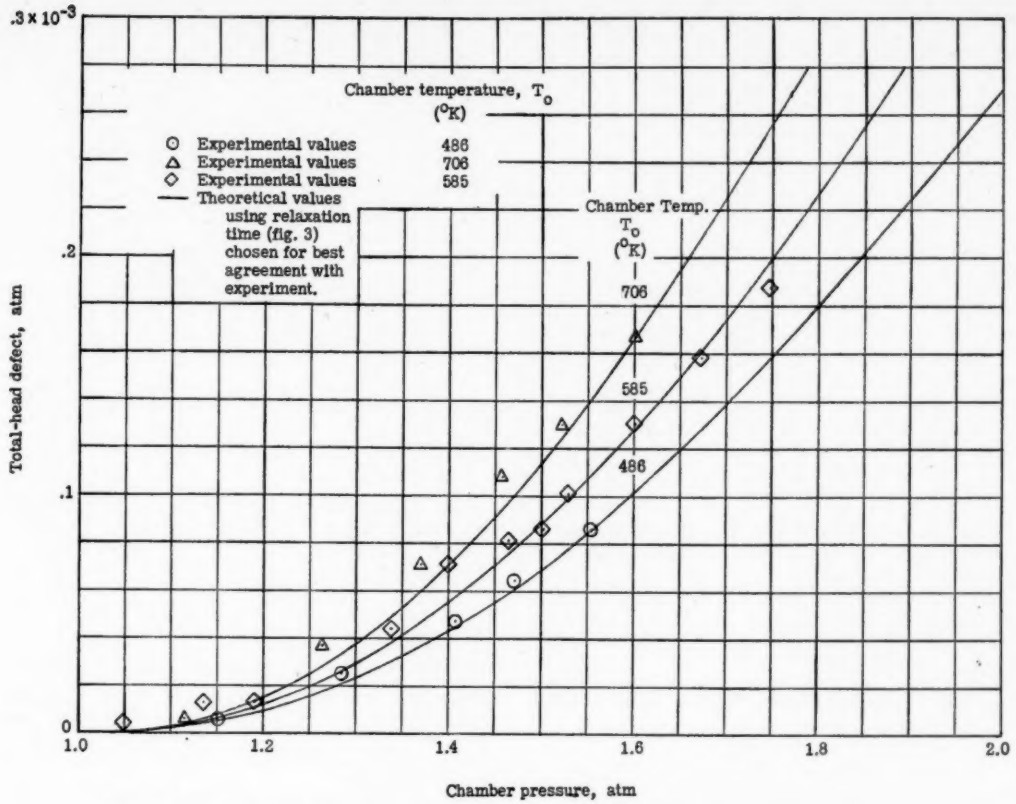

FIG. 2. Variation of total-head defects in water vapor with chamber temperature for 0.017-inch diameter impact tube.

Method for Long Relaxation Times

If the relaxation time of a gas is very long compared to the time during which compressions take place at the nose of the impact tube, then the relaxation time cannot be obtained by the foregoing method. In this case, only negligible changes in the internal energy of the gas take place during the compression process, and the gas adjusts after the compression is over. The entropy increase and total-head defect will then be independent of the time of compression and, thus, of the impact-tube diameter.

If the relaxation time is long compared to both the times required for the expansion and the compression, no adjustment of the lagging internal energy will take place during the entire cycle. In this case, no entropy increase and no total-head defect will be observed. If, however, the relaxation time is long compared to the compression time but is comparable with the time required for expansion through the nozzle, then some adjustment of the lagging internal energy will take place in the nozzle. In this case, an entropy increase will occur and, by measuring the resultant total-head defects, the relaxation time can be compared with the time required for the gas to flow through the nozzle. In this way, relaxation times up to the order of 0.01 second can be measured. This extension of the impact-tube method has been reported.[2] The necessary calculations together with some experimental details which may be helpful to those intending to apply impact-tube methods are given in the appendix.

WATER VAPOR

An electric boiler and super heater were constructed which produced enough steam for an hour's run. The water-vapor boiler was carefully cleaned and then heated in a vacuum for some time before it was used. Distilled water was used at all times in the boiler, and only the middle

[2] A. Kantrowitz and P. W. Huber, NACA Restricted Bulletin No. L4E29 (1944).

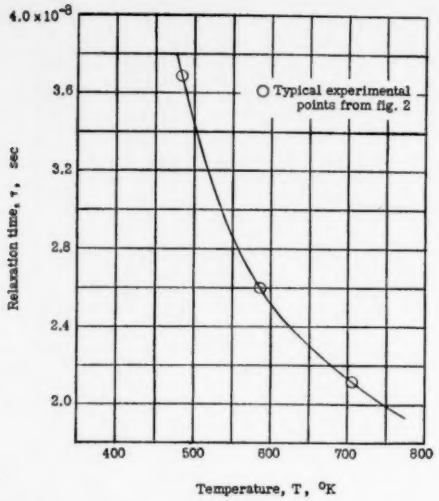

FIG. 3. Temperature variation of the relaxation time of water vapor (1 atmos.) chosen to give best agreement with measured total-head defects.

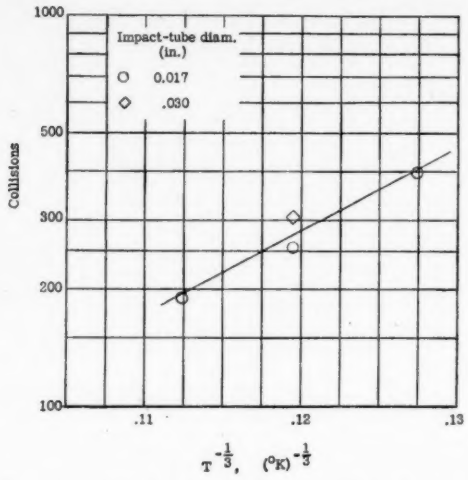

FIG. 4. Logarithmic plot of the relaxation time of water vapor in molecular collisions against $T^{-\frac{1}{3}}$. The theory of Landau and Teller (reference 3) indicates that a straight line should be obtained.

two-thirds of the water vapor generated was used in these experiments.

Total-head defects in water vapor were measured at three different temperatures and with two "source-shaped" impact tubes over a range of chamber pressures (see Figs. 1 and 2). It will be seen from Fig. 1 that the total-head defect is roughly inversely proportional to the impact-tube diameter. This fact, and the fact that the defects observed were small, means that water vapor has a relaxation time which is short compared with the compression time at the nose of the impact tubes. The relaxation times were then calculated by employing the method for short relaxation times discussed in the introduction. It was assumed that the total-head defects were caused by a lag in the vibrational heat capacity of water vapor and it was assumed that all of the vibrational heat capacity adjusted with a single relaxation time.

Choosing three typical experimental points, the relaxation times shown in Fig. 3 were found. Using these experimental values of relaxation time and the theory of reference 1, and presuming that the collisions responsible for the adjustment of vibrational energy are bimolecular (relaxation time τ inversely proportional to pressure), we computed the theoretical total-head defects shown in Figs. 1 and 2. The agreement between the theoretical variations with chamber pressure, and impact-tube diameter with these measurements, may be taken as an index of the accuracy of these results, which are probably of the order of ± 20 percent for relaxation time. Some experimental relaxation times for steam are shown in Table I. It can be seen that a very few collisions—of the order of 300—are required for adjustment of the vibrational energy.

Inasmuch as the water vapor employed probably had only slight impurities, and the adjustment involved only a few hundred molecular collisions, it seems very unlikely that these results could be appreciably affected by impurities. These measurements may therefore be presumed to apply to pure water vapor. The possibility exists that a part of the total-head defects measured may be attributable to a lag in the rotational heat capacity of water vapor, but vibrational and rotational effects cannot be separated in measurements of this kind (since both relaxation times are apparently very short compared to the compression time, $K \simeq 50$). If the total-head defects measured were partially caused by a lag in the rotational heat capacity, then less than 300 collisions are required for the adjustment of vibrational heat capacity in water vapor.

The results shown in Table I are next compared with the theory of Landau and Teller.[3] This theory indicates that the logarithm of the number of collisions necessary to transmit a

[3] L. Landau and E. Teller, Physik. Zeits. Sowjetunion 1, 34 (1936).

TABLE I. Experimental relaxation times of water vapor, hydrogen, and nitrogen.

Relaxation times for water vapor and hydrogen were calculated as shown in the tables* on page 161 of reference 1, using the theory for very short relaxation times where the approximation $K=1.743/\Delta S'$ is valid. Relaxation times for the nitrogen points were calculated in a similar manner, but using the value of K from the part of the curve in Fig. 8 for long relaxation times. The relaxation times for hydrogen were reproducible to about ±5 percent using different impact tubes. The relaxation times for water vapor were only reproducible to about ±20 percent because of the very small total-head defects. The water-vapor content of the nitrogen was not measured closer than ±10 percent.

Type and percent of impurities in gas	Diameter of impact tube (in.)	Temperature $\overline{T}$ (°K)	Relaxation time, τ (sec.) at $\overline{T}$ and converted to 1 atmos.	Type of collision considered effective for adjustment	No. of collisions per molecule per sec. of the effective type (at 1 atmos. and converted to $\overline{T}$)	No. of molecular collisions required for adjustment	No. of observations
				Water Vapor			
Negligible	0.017	486	3.7×10^{-8}	Bimolecular (13.92×10^{9}	10.74×10^{9}	4.0×10^{2}	5
Negligible	.017	585	2.6	H_2O with H_2O per mole-	9.78	2.6	8
Negligible	.030	585	3.1	cule per second at 1	9.78	3.1	6
Negligible	.017	706	2.1	atmos. and 288°K)**	8.89	1.9	5
				Normal Hydrogen			
0.5 O_2	0.0175	285	1.04×10^{-8}	Bimolecular (1.48×10^{10}	1.49×10^{10}	1.55×10^{2}	10
0.5	.029	287	1.09	H_2 with H_2 per molecule	1.48	1.61	5
0.5	.064	284	1.15	per second at 1 atmos.	1.50	1.72	3
0.5	.0175	207	1.18	and 288°K)**	1.74	2.05	5
				Nitrogen			
0.05 H_2O	0.060	556	5.9×10^{-3}	Bimolecular (74.3×10^{8}	5.35×10^{9}	3.1×10^{7}***	6
.05	.060	680	2.9	N_2 with N_2 per molecule	4.84	1.4***	5
.05	.060	686	2.7	per second at 1 atmos.	4.82	1.3***	5
.05	.060	694	3.4	and 288°K)**	4.79	1.6***	6
.05	.060	761	2.6		4.58	1.2***	5
3.5 H_2O	0.017	413	1.2×10^{-4}	N_2 with H_2O (1.04×10^{8}	30.8×10^{7}	3.6×10^{4}	5
1.33	.060	560	3.7	N_2 with H_2O per N_2	9.51	3.5	5
.66	.060	561	6.2	molecule, per percent	4.72	3.0	5
1.99	.017	575	2.3	H_2O, per second at 1	14.70	3.4	5
2.97	.017	708	1.4	atmos. and 288°K)**	19.70	2.9	6
1.41	.060	709	2.8		9.37	2.7	5
.97	.060	712	3.9		6.43	2.5	5
1.45	.017	733	2.6		9.46	2.4	5

* $\tau=d/Uk$ in column 8 of these tables should read $\tau=d/UK$.
** Collisions per molecule per second at 1 atmosphere and 288°K were obtained from E. H. Kennard, *Kinetic Theory of Gases* (McGraw-Hill Book Company, Inc., New York, 1938), and were assumed to vary with $T^{-\frac{1}{2}}$ and P.
*** Adjustment computed as resulting from collisions of N_2 with N_2 even though it is thought that the small amount of water vapor present was important.

vibrational quantum is inversely proportional to the cube root of the absolute temperature T. The number of collisions required for the relaxation of water vapor is plotted against $T^{-\frac{1}{3}}$ in Fig. 4. The results presented herein, as well as those of other recent investigations on pure gases (see reference 1, p. 162), have been shown to fit the theory of reference 3 within experimental accuracy.

HYDROGEN

The existence of anomalous absorption and dispersion of the velocity of sound in hydrogen have been reported by various workers.[4–6] These effects have been attributed to a lag in the rotational heat capacity of hydrogen. Van Itterbeck and his collaborators found a relaxation time for the transfer of energy from translation to rotation of the order of 2×10^{-8} second at 1 atmosphere and 288°K from absorption measurements. Stewart[6] found relaxation times ranging from 1.1 to 3.6×10^{-8} second from velocity of sound measurements for the same conditions. Since the rotational heat capacity is a large fraction of the total heat capacity of hydrogen, it would be expected that considerable total-head defects (several cm of alcohol) would result from

[4] A. Van Itterbeck and P. Mariens, Physica **4**, 609 (1937); A. Van Itterbeck and L. Thys, Physica **5**, 889 (1938); and A. Van Itterbeck and R. Vermaelen, Physica **9**, 345 (1942).

[5] J. L. Stewart, Dissertation, Johns Hopkins University (1943); Rev. Sci. Inst. **17**, 59 (1946).

[6] E. S. Stewart, Dissertation, Johns Hopkins University (1946); Phys. Rev. **69**, 632 (1946).

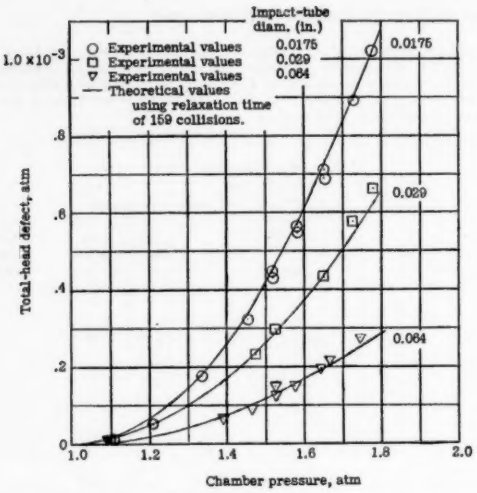

FIG. 5. Total-head defect of hydrogen for chamber temperature of 304°K. From the departure of the experimental points from the theoretical curves, it can be concluded that the accuracy of these measurements is about ±5 percent. Points taken with a total-head defect less than 0.15×10^{-3} atmos. were used only to establish the zero reading of the manometer.

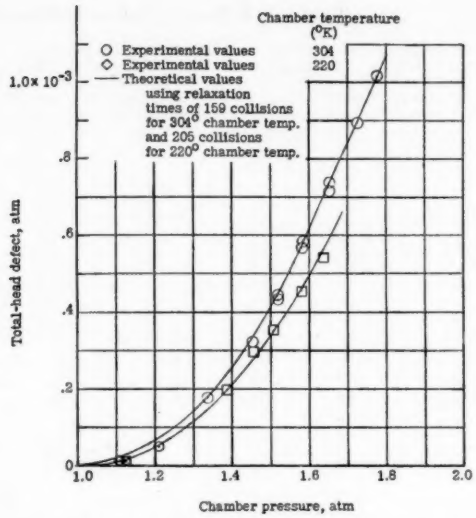
Chamber temperature (°K)
Experimental values 304
Experimental values 220
Theoretical values using relaxation times of 159 collisions for 304° chamber temp. and 205 collisions for 220° chamber temp.
1.0x 10⁻³
Total-head defect, atm
Chamber pressure, atm

FIG. 6. Variation of total-head defects in hydrogen with chamber temperature for 0.0175-inch diameter impact tube.

these lags. It seemed quite likely, therefore, that accurate values of the relaxation time could be obtained from the impact-tube method, and so a series of measurements was made on hydrogen.

The gas used was commercial hydrogen and the manufacturers reported that impurities were of the order of 0.5 percent of oxygen by volume, and perhaps 0.1 percent of nitrogen. The velocity of sound in this gas was measured at 1000~, and was found to be 4 percent below the value which would be expected for pure hydrogen. This agrees roughly with the impurity estimates.

Total-head defects were measured with three impact tubes over a range of chamber pressures at room temperature, and are given in Fig. 5. (A few measurements were also made at 207°K with the smaller impact tube, and are given in Fig. 6.) It can be seen (Fig. 5) that the total-head defect is inversely proportional to the impact-tube diameter, which shows that the method for short relaxation times should be used. Relaxation times for rotational heat capacity computed from each of these points averaged 1.07×10^{-8} second at 285°K, and 1.18×10^{-8} second at 207°K converted to atmospheric pressure on the assumption that the effective collisions were bimolecular. (The rotational heat capacities used were for equilibrium hydrogen, $\frac{3}{4}$ ortho $+\frac{1}{4}$ para, and were taken from Fowler and Guggenheim.[7]) These computations were made on the assumption that all of the rotational heat capacity adjusted with a single relaxation time. This relaxation time was converted to molecular collisions and we obtained 159 collisions for the relaxation time at 285°K and 205 collisions at 207°K. Using 159 collisions, theoretical values for the total-head defect at 285°K for the three impact tubes were computed, and are plotted as solid lines in Fig. 5. The reproducibility of our measurements of the relaxation time can be estimated from the departure of individual points from the theoretical curves. Since an error in the relaxation time results in an error of the same percentage in the total-head defect in this case ($K\gg1$), it can be seen from Fig. 5 that the relaxation-time measurements are consistent to ±5 percent. A few rough experiments were made to examine the effects of the impurities in our hydrogen. Several percent of nitrogen and then oxygen were added to the hydrogen and no large effect on the total-head defect was found. This indicates that our results were probably not affected by the presence of these impurities.

NITROGEN

The nitrogen used was commercial dry, 99 percent pure, obtained in high pressure cylinders.

[7] R. H. Fowler and E. A. Guggenheim, *Statistical Thermodynamics* (University Press, Cambridge, 1939), p. 92.

Analysis of a sample of this nitrogen showed that it contained less than 0.1 percent oxygen by volume and less than 0.25 percent carbon dioxide. Passage of the gas through a dew point instrument indicated that roughly 0.05 percent water vapor was present. Additional water vapor was added to the nitrogen in some of the experiments by passing the gas through the boiler used in the water-vapor experiments. It was considered that the water-vapor content measurements were not accurate to better than ± 10 percent.

Total-head defects in nitrogen were measured at temperatures from 413 to 760°K over a range of chamber pressures with two different impact tubes. No change in total-head defect was found with change of diameter of the impact tube from 0.017 inch to 0.060 inch. This result indicated that the relaxation time of nitrogen was long compared with the compression time at the nose of the impact tubes used. The addition of small amounts of impurities in order to shorten the relaxation time, resulted in much larger total-head defects, and further established the fact that the relaxation time of nitrogen is of the same order as the time required for the expansion through the nozzle. The relaxation times were then calculated by employing the method for *long* relaxation times discussed in the introduction, assuming that all the vibrational heat capacity adjusted with a single relaxation time.

The relaxation times found for commercial nitrogen and nitrogen with various amounts of added water vapor are shown in Table I. It is clear from this data that not more than 1 collision in 10^7 between nitrogen molecules is effective in transforming translational energy into vibrational energy. Water vapor seems to be an effective catalyst for this transformation and about 1 collision in 30,000 between water vapor and nitrogen molecules is effective. As has been observed with some other gases,[8] the dependence of the number of collisions for relaxation on temperature is much smaller for a gas with impurities than for a relatively pure gas. Some evidence can be seen from the results in Table I, however, that the relaxation time in collisions decreases as the temperature increases.

An attempt was made to find evidence of a lag in the rotational heat capacity of nitrogen from the very small total-head defects (of the order of 0.002 percent of the dynamic pressure) measured at room temperature. No component of these total-head defects which varied with the square of the dynamic pressure could be isolated. This indicates that the rotational relaxation time is shorter than 10^{-9} second at room temperature and atmospheric pressure.

DICHLORODIFLUOROMETHANE

A few total-head defect measurements were made on dichlorodifluoromethane and have been reported.[9] Assuming that all the vibrational heat capacity lagged with a single relaxation time, a relaxation time of the order of 2×10^{-8} second at 297°K and 1 atmosphere was found.

APPENDIX

Symbols

l—nozzle length;
d—diameter of impact tube;
U—final velocity in nozzle;
u—velocity;
u'—non-dimensional velocity (u/U);
t—time;
t'—non-dimensional time $\left(\frac{t}{l/U} \text{ or } \frac{t}{d/U}\right)$;
τ—relaxation time at average temperature and pressure of flow;
K—non-dimensional constant of flow referred to impact tube $(d/U\tau)$;
K_N—non-dimensional constant of flow referred to nozzle $(l/U\tau)$;
ϵ'—excess of internal energy over that of equilibrium at the translational temperature (non-dimensional);
$\Delta S'$—non-dimensional entropy increase;
r—radius of nozzle cross section;
x—distance along nozzle axis;
T—temperature;
λ—constant $\left(\frac{du'^2}{dt'}\right)$ (non-dimensional);
ν—kinematic viscosity;
δ^*—boundary-layer displacement thickness.

Measurements of Heat-Capacity Lag for Gases with Long Relaxation Times by Means of a Nozzle of Special Design

In the measurements of heat-capacity lag of gases with the apparatus shown in Fig. 5 of reference 1, a nozzle is employed in which the gases expand and accelerate before meeting the impact tube. If the relaxation time of a gas

[8] L. Küchler, Zeits. f. physik. Chemie **41**, 199 (1938).

[9] P. W. Huber, NACA Technical Note No. 1024 (1946).

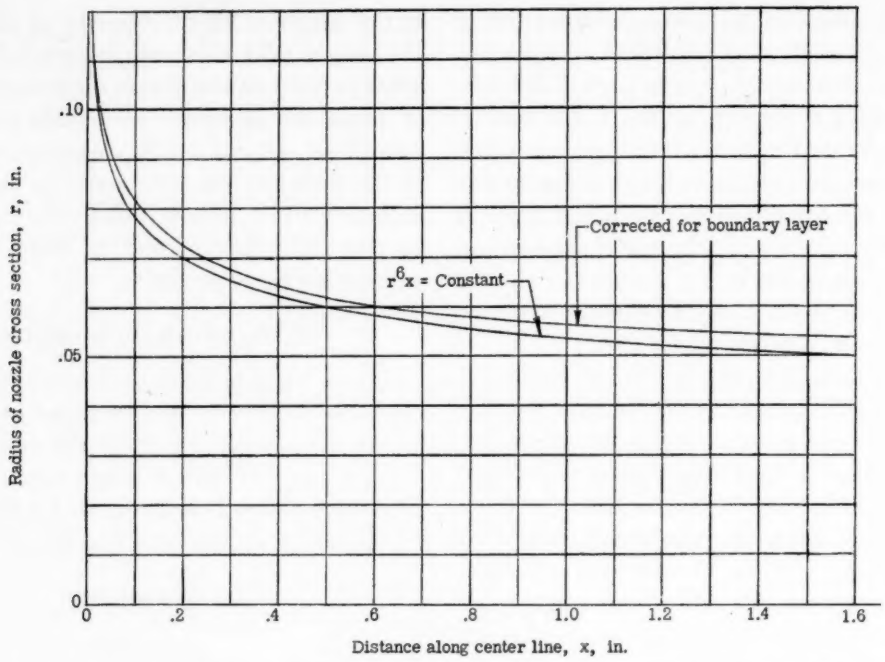

FIG. 7. Shape of nozzle, radius against distance along center line. Boundary-layer correction was computed as explained in the appendix.

is long enough to be of the same order as the expansion time through this nozzle, an entropy increase occurs in the nozzle. For ease of calculation, the nozzle used in these tests was so designed that

$$\frac{du^2}{dt}=\text{constant}. \tag{1}$$

The shape of a nozzle, of circular cross section, to meet the condition of Eq. (1) can be readily found if low velocity flow—that is, constant density—is assumed. When the velocity is assumed constant across the cross section, continuity yields

$$ur^2=\text{constant}. \tag{2}$$

Also,

$$udt=dx. \tag{3}$$

Combining Eqs. (1) to (3) gives

$$r^6x=\text{constant}. \tag{4}$$

Equation (4) must be corrected for the presence of a boundary layer along the walls of the nozzle. The displacement thickness of this boundary layer—that is, the distance the streamlines just outside the boundary layer are displaced by its presence—can be found by standard methods.[10] It was assumed that this boundary layer would be laminar. Equation (1) of reference 10 was thus used to calculate the displacement thickness. This equation is an approximate formula for the laminar boundary-layer displacement thickness and is given as

$$\delta^*=1.73\sqrt{\frac{\nu s}{U}},$$

where

$$s=\int_0^x\left(\frac{u}{U}\right)^{8.17}dx.$$

For these calculations $\nu/U=2.7\times10^{-5}$ cm was used. The distance δ^* was then added to the nozzle radius. The radius of the nozzle cross section is plotted against the distance along the center line in Fig. 7.

We will now calculate the entropy increase in a nozzle of this design. It can be shown from definition that $\lambda=\frac{2}{3}$. From Eq. (11) of reference 1,

$$\epsilon'=\exp(-K_Nt')\times\left(\int_0^{t'}\tfrac{2}{3}\exp(K_Nt')dt'+\text{constant}\right),$$

where $t'=0$ is taken at the start of the expansion when $\epsilon'=0$. The constant is then zero and integration yields

$$\epsilon'=\frac{2}{3K_N}[1-\exp(-K_Nt')]. \tag{5}$$

From Eq. (16) of reference 1 for the change in entropy as t' changes from 0 to $t'_{\max}$

$$\Delta S'=2K_N\int_0^{t'_{\max}}\epsilon'^2dt'$$

$$=2K_N\frac{4/9}{K_N^2}\int_0^{t'_{\max}}[1-\exp(-K_Nt')]^2dt'.$$

From Eq. (1), the non-dimensional time $t'_{\max}$ for the gas to pass through the nozzle is $\frac{1}{\lambda}=\frac{3}{2}$; hence,

$$\Delta S_N'=\frac{4}{3K_N}-\frac{16}{9K_N^2}[1-\exp(-\tfrac{3}{2}K_N)]$$

$$+\frac{4}{9K_N^2}[1-\exp(-3K_N)].$$

[10] A. E. von Doenhoff, NACA Technical Note No. 671 (1938).

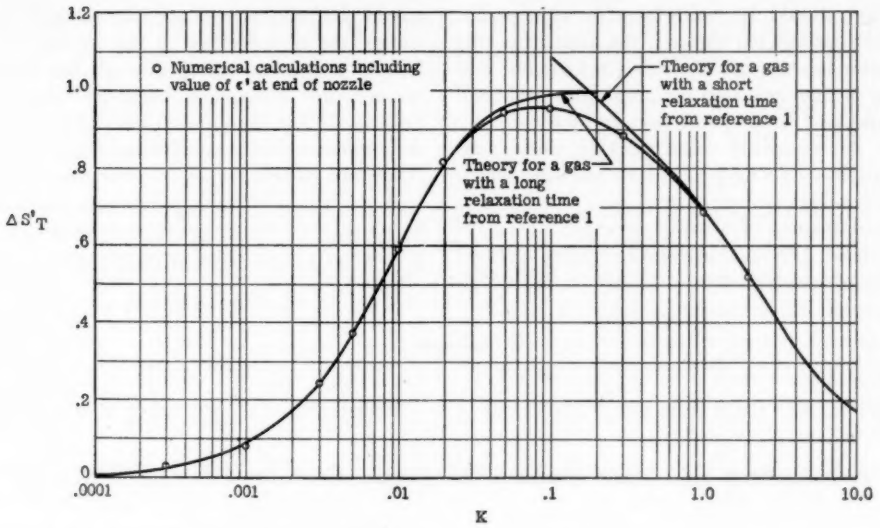

FIG. 8. The total non-dimensional entropy increase in nozzle and impact tube. $\Delta S'_T = \Delta S'_{\text{tube}} + \Delta S'_N$; $K = d/U\tau$; $K_N = 94.1 \times K = (l/d)K$.

This entropy increase in the nozzle must be added to the increase at the impact tube in order to obtain the total entropy increase in an expansion through a nozzle of this type, followed by a compression at the nose of a source-shape impact tube.

For the calculations of the entropy increase at the impact tube in reference 1, it was presumed that $\epsilon' = 0$ initially. This assumption does not hold, however, for a gas with a long relaxation time which has reached a non-equilibrium condition at the end of the nozzle; consequently, the equations of reference 1 must be modified to fit this case as follows: In Eq. (22) of reference 1, for the variation of ϵ' with time at the impact tube, the constant was zero because ϵ' was assumed zero before compression. For a gas with a long relaxation time, the constant becomes Eq. (5) with $t' = \frac{3}{2}$, which is the value of ϵ' at the end of expansion. This assumes that the impact tube is placed so close to the end of the nozzle that compression starts immediately after the gas leaves the nozzle. Equation (22) of reference 1 now becomes

$$\epsilon'(t') = -\exp(-Kt') \times \left[\int_{t_0'}^{t_1'} 16u'^2(1-u')^{\frac{1}{2}} \exp(Kt')dt' - \frac{2}{3K_N}(1-\exp[-\tfrac{3}{2}K_N]) \right]. \quad (6)$$

By integrating Eq. (6) by Simpson's rule and Eq. (16) of reference 1 by the planimeter, both between $t' = 0$ and $t' = \infty$, the entropy increase in the compression at the impact tube is obtained for a gas with any relaxation time. The total entropy increase becomes

$$\Delta S_T' = \Delta S_{\text{tube}}' + \Delta S_N',$$

which is plotted against K in Fig. 8 and compared with the theory of reference 1.

Experimental Methods and Apparatus Details

It is apparent that the accuracy with which total-head defects caused by heat-capacity lag can be measured, depends to a great extent on how well total-head defects caused by other factors can be eliminated. It might be helpful to list several sources of other effects on the total-head, and their method of elimination for the convenience of those intending to apply this measurement technique. The apparatus used in these experiments is essentially that shown in Fig. 5 of reference 1.

In constructing the apparatus, it is important to guard against high turbulence levels in the chamber which result in total-head defects. We found that these effects could be greatly reduced by the provision of two 200-mesh screens spaced 1 inch apart. Care must be taken to insure that the screens cover the whole chamber so that no jets, for example, are formed around the edges. The gas should be let into the chamber through small orifices which tend to smooth out fluctuations in the chamber pressure, which would otherwise lead to unsteadiness of the alcohol manometer. It is important to insure that no temperature differences exist in the gas, or between the gas and the chamber. Our practice was to run the gas around the chamber in spaces provided by two or three concentric liners, and further, to measure the temperature of the chamber and of the incoming gas, and to equalize these two temperatures by varying the electric heater currents. The nozzle, of course, should be made very smooth and the entrance should be well faired to the top of the chamber.

The technique for grinding the impact tube is essentially the same as that reported in reference 1, but perhaps it might be well to point out here that it is important that the end of the impact tube be flat and free from nicks.

The impact tube must be accurately aligned with the jet. It is convenient to provide an adjustment mechanism which keeps the end of the impact tube centered in the jet, while permitting the adjustment of its alignment in two perpendicular planes. A gas, such as nitrogen at room temperature, which shows no total-head defects caused by

heat-capacity lag, should be used for this adjustment. While the nitrogen is flowing through the apparatus, the alcohol manometer is observed through a microscope and the impact tube is then adjusted for minimum total-head defect. It is important to keep the impact tube carefully centered in the jet, especially when working with gases, such as hydrogen, having a high kinematic viscosity which results in thick nozzle boundary layers.

For the measurements of steam, an ethyl phthalate manometer was used. The manometer was heated to above the boiling point of steam to prevent condensation which would produce spurious pressure readings. It was necessary to find the zero position of this manometer while a small flow of steam was going through the apparatus, because temperature differences occurred when no steam was flowing. It has been found that this procedure of taking zero readings with a small flow of gas generally gives more consistent results also in measurements of other gases.

When all of these adjustments are properly made, it is possible to reduce the total-head defect to about 0.002 percent of the dynamic pressure, using room temperature nitrogen.

THE JOURNAL OF CHEMICAL PHYSICS VOLUME 15, NUMBER 5 MAY, 1947

A Relation Between Bond Order and Covalent Bond Distance

H. J. BERNSTEIN
Division of Chemistry, National Research Council Ottawa, Canada
(Received February 26, 1947)

A relation between covalent bond distance and bond order of the form $R=R_1[2/3+1/3\times(n-1/n+1)^{p/2}]$ is proposed and tested against the available experimental data. A suitable expression for all covalent bond distances between atoms of the first row of the periodic table of the form $R=Z-A/Z-B[2/3+1/3(1/3)^{p/2}]$ is also proposed. The agreement between calculated and observed values is well within the limits of the experimental errors.

A GREAT number of measurements of the CC bond distance[1] in different molecules show that it may have any value intermediate between 1.55A, the single bond distance, and 1.205A, the triple bond distance. These intermediate bond distances have been discussed on the basis of a quantum-mechanical treatment by Lennard-Jones,[2] Penney,[3] and Coulson.[4] These authors have introduced the concept of bond order, designated by p, where p is defined as zero for a single bond, one for a double bond, and two for a triple bond, and may have any intermediate value for bonds of so-called fractional order. In molecules such as benzene and napthalene, for example, where the electrons are considered to be non-localized or mobile the links have intermediate lengths[1] corresponding to bonds of fractional order. In their papers the above authors have calculated the bond orders of various links by the method of molecular orbitals and also by the bond pair method; practically identical values are obtained. From their definition of p which depends linearly on the interaction energy, values for the bond energies, and thus for the resonance energy, may be calculated. Also, as Coulson[4] points out, vibrational frequencies may be estimated.

Lennard-Jones[2] and Coulson[4] have derived a relation for the length of a link of order p in the form

$$R_p=R_1-\frac{R_1-R_2}{1+\left(\frac{1-p}{p}\right)\frac{K_1}{K_2}}, \qquad (1)$$

where R_p is the length of the link of order p; R_1 is the length of the link of order $p=0$, i.e., the single bond distance; R_2 is the double bond distance; and K_1, K_2 are the single and double bond force constants, respectively.

Kavanau[5] has proposed an empirical relation

[1] J. M. Robertson, J. Chem. Soc. 131 (1938). L. R. Maxwell, J. Opt. Soc. Am. **30**, 374 (1940).
[2] J. E. Lennard-Jones, Proc. Roy. Soc. London **A158**, 280 (1937).
[3] W. G. Penney, Proc. Roy. Soc. London **A158**, 306 (1937).
[4] C. A. Coulson, Proc. Roy. Soc. London **A169**, 413 (1939).
[5] J. L. Kavanau, J. Chem. Phys. **12**, 467 (1944).

between bond distance and bond order of the form

$$R_p = a + b\left(\frac{n_1+n_2-1}{n_1+n_2+1}\right)^{p+1}, \qquad (2)$$

where a and b are constants and n_1 and n_2 are the principal quantum numbers of the valence electrons of the bonded atoms. Both of these relations require the knowledge of two data before they can be applied.

Recently Lagemann[6] has attempted to extend the applicability of Kavanau's relation by assuming that a and b of Eq. (2) have the form $K_1/(Z_1+Z_2)$ and $K_2(Z_1+Z_2)$, respectively. K_1, K_2 are constants for atoms of the same row of the periodic table and Z_1, Z_2 are the atomic numbers of the bonded atoms. Suitable values of K_1, K_2 were found by Lagemann for the first row atoms.

Since the total variation from the single to the triple bond distance is only about 1/4 of the single bond distance, it is apparent that any function which varies slowly enough with its argument is bound to have reasonable success in representing the experimental data. The final choice for the form of the function can be made only by reasons of a fundamental theoretical nature. Lacking these, however, it would not seem worth while to propose yet another relation of this nature unless it succeeded in simplifying the present position of the problem and has sufficiently wide applicability.

A relation which seems to accomplish this for symmetrical linkages is

$$R = R_1\left[2/3+1/3\left(\frac{n-1}{n+1}\right)^{p/2}\right], \qquad (4)$$

where R_1 is the single bond distance; R is the bond distance for a bond of order p; and n is the principal quantum number of the valence electrons of a bonded atom. (See Appendix for the reasons for proposing this expression.) By use of the additivity rule, *viz:* $R_{AB} = (1/2)R_{AA} + (1/2)R_{BB}$ where R_{AB}, R_{AA}, and R_{BB} are the distances between atoms A−B, A−A, and B−B, respectively, of links AB, AA, BB, the bond distances for non-symmetrical linkages are obtained. Equation (4) then becomes

$$R = R_{AA,1}\left[2/3+1/3\left(\frac{n_A-1}{n_A+1}\right)^{p/2}\right] + R_{BB,1}\left[2/3+1/3\left(\frac{n_B-1}{n_B+1}\right)^{p/2}\right], \qquad (5)$$

where $R_{AA,1}$ and $R_{BB,1}$ are the single bond distances of the links AA and BB, respectively, and n_A, n_B are the principal quantum numbers of the valence electrons of the bonded atoms A and B. Equation (4) requires but one observational datum in order to be applicable as compared with the two data which are required before either of Eqs. (1) or (2) can be used.

TABLE I.

	Calc. Eq. (4)	Pauling	Calc. Eq. (4)	Pauling	Calc. Eq. (4)	Pauling	Calc. Eq. (4)	Pauling	Calc. Eq. (4)	Pauling
	B		C		N		O		F	
Single-bond radius	.88*	.88	.772	.77	.707	.70	.66*	.66	.64*	.64
Double-bond radius	.767	.76	.664	.67	.609	.61	.567	.57	.551	.55
Triple-bond radius	.684	.68	.60*	.60	.55*	.55	.513	.51		
			Si		P		S		Cl	
Single-bond radius			1.17*	1.17	1.11	1.10	1.04*	1.04	.99*	.99
Double-bond radius			1.06	1.07	1.01	1.00	.95	.95	.90	.90
Triple-bond radius			.98	1.00	.93*	.93	.87	.88		
			Ge		As		Se		Br	
Single-bond radius			1.22*	1.22	1.21*	1.21	1.17	1.17	1.14*	1.14
Double-bond radius			1.13	1.12	1.12	1.11	1.08*	1.08	1.05	1.05
			Sn		Sb		Te		I	
Single-bond radius			1.40*	1.40	1.41*	1.41	1.36	1.37	1.33*	1.33
Double-bond radius			1.31	1.30	1.32	1.31	1.28*	1.28	1.25	1.24

[6] R. T. Lagemann, J. Chem. Phys. **14**, 743 (1946).

TABLE II.

Molecule	Bond order p	Bond distance calc. Eq. (4)	obs.
Acetylene	2	1.205	1.205[7]
Ethylene	1	1.33	1.33[7]
Ethane	0	1.55	1.55[7]
Benzene	2/3[a]	1.39	1.39[1]
Graphite	.55[b]	1.417	1.42[1]
Napthalene	.55[b]	1.417	1.41[1]

[a] Bond order calculated by Coulson, see reference (4).
[b] Average of all bond orders calculated for the CC bonds in napthalene by Penney, see reference (3).

The validity of Eq. (4) may be tested by comparing the covalent bond radii calculated from it with the values given by Pauling[7] (see Table I). In the table the values marked with an asterisk were considered the most reliable and were used to calculate the other radii. The first, second, and third rows are the single, double, and triple bond covalent radii, respectively. The agreement exclusive of hydrogen is well within the average experimental error of ±.02A in the bond distance determined by x-ray or electron diffraction methods.

In the following subsections the bond distances of particular linkages are discussed in more detail.

C—C BONDS

The CC bonds in ethane, ethylene, and acetylene are considered as usual to be pure single, double, and triple bonds, respectively, with bond orders $p=0$, 1, 2, respectively. The bond orders of benzene, graphite, and napthalene are calculated from quantum-mechanical considerations to be 2/3[4], .55[3] and .55[3], respectively.

From the value of the triple bond distance in acetylene (1.205A) and the above bond orders the following table of calculated [by Eq. (4)] and observed CC bond distances may be drawn up (Table II).

N—N BONDS

The N_2 molecule in the $^1\Sigma_g^+$ ground state is considered to be a pure triple bond with length 1.095A.[8] The calculated single and double bond distances are 1.41A and 1.21A, respectively. The observed NN distance in H_2N-NH_2 at 1.47A[9] corresponds then to a bond of order $p=-0.22$, i.e., 78 percent of a single bond. The fact that the NN bond energy in hydrazine is extremely low[10] may be taken as supporting evidence for this value of the bond order.

O—O BONDS

The O_2 molecule is in a $^3\Sigma_g^-$ ground state and as considered by Pauling[7] has one single bond and two three electron bonds giving it a fractional order between a single and double bond. Using 1.32A[7] as the single bond distance the bond order for O_2 is calculated as $p=0.588$. Here again the observed distance in HO—OH at 1.48A[11] would correspond to a bond of order $p=-0.56$, i.e., 44 percent of a single bond, corresponding to the very low bond energy observed for this bond.[10]

C—N, C—O, N—O BONDS

Having obtained the single, double, and triple bond distances for C—C, N—N, O—O bonds, the multiple bond distances for C—N, C—O, N—O are calculated by means of the additivity rule, and in the cases where indicated the appropriate bond orders are calculated.

	p	Calc.	Obs.
C—N	1	1.48	1.47[12]
C=N	2	1.27	
C≡N	3	1.15	1.15[7]
C—O	1	1.43	1.43[7]
C=O	2	1.23	
C≡O	3	1.15	
CO	1.88	1.13[8]	1.13[8]
N—O	1	1.36	
N=O	2	1.17	
N≡O	3	1.065	
NO	1.16	1.15[8]	1.15[8]

P—P BONDS

The P_2 molecule in the $^1\Sigma_g^+$ ground state is triply bonded with a bond distance of 1.89A.[8] The single and double bond distances are calcu-

[7] L. Pauling, *The Nature of the Chemical Bond* (Cornell University Press, Ithaca, New York, 1939).
[8] G. Herzberg, *Diatomic Molecules* (Prentice-Hall, Inc., New York, 1939).
[9] P. A. Giguere and V. Schomaker, J. Am. Chem. Soc. **65**, 2025 (1943).
[10] See reference (7) and O. K. Rice, *Electronic Structure and Chemical Binding* (McGraw-Hill Book Company, Inc., New York, 1940).
[11] P. A. Giguere, Ann. A. C. F. A. S. **9**, 88 (1943).
[12] G. W. Wheland, *The Theory of Resonance* (John Wiley and Sons, Inc., New York, 1945).

lated as 2.27A and 2.04A, respectively. Penney[3] has shown that four similar atoms at the corners of a regular tetrahedron have bonds between them of order $p=1/3$, so the calculated P−P distance in P_4 for $p=1/3$ is 2.21A. These calculated values of 2.21A and 2.27A agree very well with the observations in P_4 where the P−P distance is found to be 2.21±.02A,[13] and in amorphous red and black phosphorous where the P−P distance is found to be 2.28±.02A.[14] It seems probable that the difference between these experimental values is real and not to be attributed to experimental error.

S—S BONDS

S_2 is in a $^3\Sigma$ ground state and should be similar to O_2 in its bondings. Since the S−S bond distance has been measured in H_2S_2, $(CH_3)_2S_2$, and S_8 and found to be 2.04±.02A[7] in all three molecules, the bond order is apparently the same, but does not necessarily correspond to that of a single bond. Again the bond distance in the S_2 molecule is accurately known to be 1.89A,[8] but its bond order is unknown. A plausible set of distances is obtained by assuming the bond order in S_2 to be 0.75. The single bond distance is then calculated to be 2.05, and the double and triple bond distances are 1.85, 1.71, respectively.

As—As BONDS

The As−As distance observed in the crystal is 2.50A,[7] and in As_4 it is 2.44A.[7] Again the bond order for As_4 as for P_4 is $p=1/3$. Taking 2.44A as corresponding to a bond of order $p=1/3$ the calculated single, double, and triple bond distances are 2.50A, 2.32A, and 2.16A, respectively. Again the difference between the values of 2.50A and 2.44A for the As−As distance would appear to be real and not to be attributed to experimental errors. Since the vibrational frequency and internuclear distance of both Se_2, Br_2 are known for atoms of this row of the periodic table, Badger's rule[7] may be employed to estimate the bond distance in As_2 where the vibrational frequency is known.[8] The value 2.13A is obtained for the triply bonded As−As distance which is in as good agreement as can be expected with the value 2.16A calculated above.

Se—Se AND Te—Te BONDS

Since the ground states of these molecules are $^1\Sigma$[8] it would appear reasonable to suppose that the molecules have double bonds. Using the observed values[8] of 2.16A and 2.59A for the doubly bonded Se_2 and Te_2 molecules, respectively, the single bond distances have been calculated as 2.34A and 2.76A. Pauling[7] gives these distances from x-ray measurements as 2.32A and 2.76A, respectively.

Unfortunately there is a lack of known multiple bond distances with which to test Eq. (4) any further but the agreement so far obtained between calculated and observed distances is within 1 percent.

GENERAL EXPRESSION FOR COVALENT BOND DISTANCE OF THE ATOMS OF THE FIRST ROW OF THE PERIODIC TABLE

By assuming a reasonable relation for the single bond distances of the first row atoms in terms of the atomic numbers of the bonded atoms it is possible to express the bond distance in the form

$$R=\left(\frac{Z-1.50}{Z-3.10}\right)[2/3+1/3(1/3)^{p/2}]$$

for all the symmetrical linkages of the first row atoms. The bond distances for unsymmetrical links may be calculated by means of the additivity rule. This equation fits all the reliable data to within 1 percent. The extensive table which may be drawn up to show this agreement is omitted for the sake of brevity.

DISCUSSION

Substituting the value for R_2 obtained in terms of p for the C−C double bond from Eq. (4) into Eq. (1) and equating Eqs. (4) and (1) it is found that

$$\frac{K_1}{K_2}=\frac{p}{1-p}\cdot\frac{(1/3)^{p/2}-(1/3)^{1/2}}{1-(1/3)^{p/2}}.$$

Evaluating K_1/K_2 for values of p between -1 and 2 it is found that K_1/K_2 has values from

[13] L. R. Maxwell, S. B. Hendricks, and V. M. Mosley, J. Chem. Phys. **3**, 698 (1935).

[14] C. D. Thomas and N. S. Gingrich, J. Chem. Phys. **6**, 659 (1938). R. Hultgren, N. S. Gingrich, and B. E. Warren, J. Chem. Phys. **3**, 351 (1935).

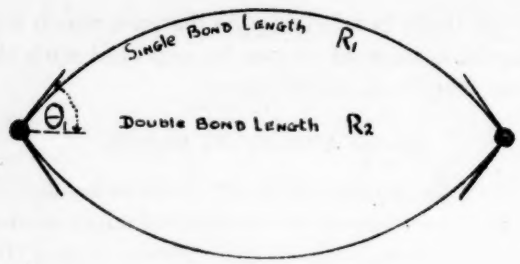

FIG. 1.

.790−.740 with the average value of 0.764, where the average deviation is ±0.015 and greatest deviation ±0.025. In the theoretical development of Eq. (1) the energy was taken as a first approximation to be a parabolic function of the displacement from the equilibrium position, so that K_1/K_2 is the force constant ratio for harmonic oscillators. Pauling[7] on the basis of Badger's rule employs a value of 1/3 for the ratio. Lennard-Jones[2] uses the value 0.507 which was derived from the infra-red vibration spectra values of the fundamental modes of ethane and ethylene, and the use of suitable potential functions for the molecules. Coulson[4] uses the value 0.765 which is obtained by substituting the value of the observed distance in acetylene in Eq. (1). Coulson justifies his choice of constant on semi-empirical grounds. Whereas Eq. (1) with Pauling's or Lennard-Jones's constants give calculated triple bond distances which are a good deal too high, use of the constant 0.765 fits the data accurately. Since this ratio appears in the part of Eq. (1) which is at most 1/4 of the total bond distance, the greatest difference between the value of K_1/K_2 obtained above and the value used by Coulson introduces an error of about 0.8 percent in the bond distance calculations. It is difficult to believe that this agreement is entirely fortuitous, in fact the agreement obtained seems to justify in a rather indirect manner both the suitability of Coulson's choice of 0.765 for the K_1/K_2 ratio and our choice for the relationship between bond distance and bond order.

A serious objection to relation (4) exists in as much as it makes the hydrogen—hydrogen bond distances independent of bond order. That the expression is not valid for hydrogen is to be expected, however, since most approximations of this kind become more accurate with increasing atomic number.

APPENDIX

Since the tetrahedral angle is extremely well preserved in a wide variety of substituted methanes and ethanes[7] it is not unreasonable to assume, as a first approximation, that this angle is also preserved in a double or triple bond. As an *ad hoc* model for double bond formation one may consider two normal single C−C bonds to be bent in circles* with the tetrahedral angles preserved at the nuclei as is shown in the figure. It is readily seen from the geometry of the figure that

$$R_2 = R_1 \frac{\sin\theta_1}{\theta_1} \tag{1}$$

where θ_1 is half the value of the tetrahedral angle. Similarly for the triple bond, for which the angle θ_2 is (π-tetrahedral angle), there is the relation

$$R_3 = R_1 \frac{\sin\theta_2}{\theta_2}. \tag{2}$$

The angles θ_1 and θ_2 are related by the expression

$$\sin\theta_2 = [2/3(1-\cos 2\theta_1)]^{\frac{1}{2}}. \tag{3}$$

The general expression

$$R = R_1 \frac{\sin\theta}{\theta} \tag{4}$$

is thus indicated. Now let $\cos\theta = M^p$ where p is the bond order and M is some quantity independent of R. This choice for $\cos\theta$ satisfies Eq. (4) for $p=0$. For $p=1$, $\cos\theta_1 = M$ and for $p=2$, $\cos\theta_2 = M^2$. Substituting these values in (3) it is found that $M=(1/3)^{\frac{1}{2}}$ and thus $\cos\theta = (1/3)^{p/2}$. Expanding $\sin\theta$ and $\cos\theta$ in terms of θ and neglecting powers of θ greater than the second, Eq. (4) becomes

$$R = R_1[2/3 + 1/3(1/3)^{p/2}]. \tag{5}$$

It would seem that this crude multiple CC bond model has been adequate for evaluating M and the first two coefficients of a very probable general expression for the bond distance which has the form $R = R_1(a_0 + a_1 M^p + a_2 M^{2p} + \cdots)$.

Equation (5) may be tested for CC bonds by assuming the accurately known triple bond distance 1.205A[7] and calculating the double and

* A rod or spring having stretching and bending force constants is reasonably approximated by a circle when equal bending movements are applied at its ends.

single CC bond distances. The calculated values are 1.33A and 1.55A for the double and single bond distances, respectively. The experimental values are also 1.33A[7] and 1.55A,[7] respectively.

This very good agreement makes it of interest to attempt a more general expression for M which would then provide an expression suitable for all multiple bond distances. The form of Kavanau's relation [Eq. (2) of the text] indicates the choice $M=(n-1/n+1)^{\frac{1}{2}}$ which is satisfied for CC bonds where $n=2$. The relation $R=R_1[2/3+1/3(n-1/n+1)^{p/2}]$ is thus obtained.

Another relation which may be derived from this crude model is that between force constants of multiple CC bonds.

The potential energy of the double bond may be written as $(K_2/2)\Delta R_2^2$ for small displacements from the equilibrium position, where K_2 is the force constant of the double bond. From the figure, the energy can also be written as $(2K_1/2)\Delta R_1^2$ (since the tetrahedral angles are preserved) where K_1 is the single bond force constant. From (1) $\Delta R_1/\Delta R_2=\theta_1/\sin\theta_1$ whence $K_2=2K_1(\theta_1/\sin\theta_1)^2$. Similarly for triple bonds $K_3=3K_1(\theta_2/\sin\theta_2)^2$, where K_3 is the triple bond force constant. Putting in the values of θ_2 and θ_1 of 70.5° and 54.75° one obtains $K_3:K_2:K_1=5:2.7:1$ which is of the same order of accuracy as the ratio derived from Badger's rule,[7] *viz:* $K_3:K_2:K_1=5:2.5:1$.

That the circular bond notion with preserved tetrahedral angles is internally consistent is further demonstrated by the bond energy/bond distance relation which can be derived from it. (See Letter to the Editor, this Journal.)

Though this model was useful in obtaining relations which apparently represent the data, its success is totally unwarranted on the basis of present day valence theory. The author can suggest no reason for the apparent physical significance of this model.

The author takes pleasure in acknowledging the helpful discussions with members of the Yerkes Observatory of the University of Chicago.

THE JOURNAL OF CHEMICAL PHYSICS VOLUME 15, NUMBER 5 MAY, 1947

The Mechanism of the Luminescence of Solids*

FERD E. WILLIAMS**
RCA Laboratories, Princeton, New Jersey

AND

HENRY EYRING***
Princeton University, Princeton, New Jersey

(Received March 3, 1947)

In this paper, effort is directed toward explaining various diverse luminescent properties of solids in terms of a simple model of potential energy *versus* configuration coordinate. Three states of different multiplicities—a normal, metastable and an emitting state—are involved. The luminescent process consists of the excitation of an electron to the metastable level, the activated release of the electron to the emitting level, and a forbidden transition between the emitting and the ground state. With high excitation energy, the metastable state is bypassed. At high temperatures, the electron in the metastable state surmounts a larger potential barrier to undergo radiationless recombination with the activator atom.

Among those significant phenomena that have been measured experimentally and treated quantitatively by calculations based on this model are the temperature dependence of luminescent efficiency and the effect of type and wave-length of excitation on this temperature dependence; the three types of phosphorescence—spontaneous, metastable, and recombination phosphorescence; the phenomena of two-stage afterglow and the effect of type of excitation and temperature on the two stages; the

* Part of a dissertation submitted by Ferd E. Williams to Princeton University in partial fulfillment for the degree of Doctor of Philosophy. Portions of this article are based upon work performed for the Office of Scientific Research and Development under Contract NDCrc-150 and Contract OEMsr-440. Presented in part at the American Physical Society Meeting in New York in January, 1946.

** Now Assistant Professor of Chemistry, University of North Carolina, Chapel Hill, North Carolina.
*** Now Dean of the Graduate School, University of Utah, Salt Lake City, Utah.

relationship between buildup and afterglow kinetics; and the release of electrons from metastable states by thermal energy. The concept of the Absolute Rate theory are used to clear up the essential criteria for the different types of afterglow.

A detailed theoretical analysis of "glow curves" is presented and quantitatively applied to improved glow curves obtained at linear rates of heating 100 times slower than those previously reported. The slower rates of heating allow one metastable level to be operative at a time. Both monomolecular and bimolecular mechanisms are treated, and it is concluded that glow curves result from discrete metastable states that are emptied thermally by predominantly monomolecular kinetics. The explicit expressions for the specific rate constants involved in the release of electrons from metastable states are calculated.

I. INTRODUCTION

INORGANIC crystalline luminescent solids, commonly referred to as "phosphors," possess the property of absorbing energy of a certain frequency and re-emitting part of the absorbed energy as radiant energy of another frequency. If, on removing the excitation, emission ceases within the time required for an ordinary atomic transition, the phenomenon is called fluorescence. If the emission persists longer, the phenomenon is called phosphorescence. Most phosphors are prepared by crystallizing at 600 to 2000°C highly purified substances to which 0.001 to a few percent of a foreign substance, or "activator," has been added.

Phosphors belong to the class of solids known as electronic semi-conductors. Electrons in a crystal move in a potential which is periodic in three dimensions. Bloch[1] and Wilson[2] have studied such a system, and neglecting the exchange forces between the electrons, the energy levels consist of broad bands of allowed energies, separated by broad bands of forbidden energies. In their states of lowest energy the electrons which do not form a complete valence group should be tightly bound and exactly fill up one of the bands of allowed energies in order that a substance be an electronic semi-conductor. More precise energy diagrams[3] contain narrow continuous bands lying in the forbidden region between the Bloch-Wilson bands. In these states, which are computed by the Heitler-London approximation, the excited electron and the positive hole it leaves in the lowest band—together called an "exciton"—are closely coupled and move together, transporting no charge.

Impurities and crystal defects dominate the electrical properties of electronic semi-conductors.[4] An electron from a discrete impurity level just below the conduction band is more likely to be thermally excited to the conduction band than is an electron from the filled band. On introducing impurity ions into the lattice, the energies of the electrons on the ions are modified by the crystal field depending on the wave function for the state of each electron. Splitting[5] into sublevels according to symmetry considerations occurs. The interaction of levels of the impurity with lattice levels leads to the possibility of the formation of potential "wells" for trapping electrons.[3] Other proposed schemes for trapping electrons include trapping at crystal surfaces[6] and Landau trapping in which the electron essentially "digs its own hole."[7]

On exciting the impurity, there is no atomic rearrangement during the absorption process. After the absorption, the excited atom will have a different distribution of electronic charge, and

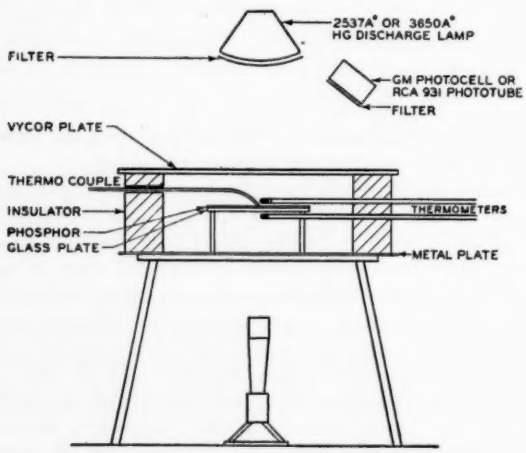

FIG. 1. Apparatus to measure the temperature dependence of efficiency of luminescence.

[1] F. Bloch, Zeits. f. Physik **52**, 555 (1928–29).
[2] A. H. Wilson, Proc. Roy. Soc. London **133**, 458 (1931).
[3] F. Seitz, J. Chem. Phys. **6**, 150 and 454 (1938).
[4] A. H. Wilson, Proc. Roy. Soc. London **134**, 277 (1932).
[5] H. Bethe, Ann. d. Physik **3**, 133 (1929).
[6] I. Tamm, Phys. Zeits. d. Sowjetunion **1**, 733 (1932).
[7] D. Blochinev, Comptes Rendus Acad. Sci. U.R.S.S. **2**, 79 (1934).

so, the atoms will shift to new equilibrium positions in the new force field, simultaneously radiating the excess energy as elastic waves. To describe completely this atomic rearrangement would require energy contours in a configuration space having three times as many coordinates as there are particles involved in the rearrangement. A useful simplification consists of defining a "center" as the excited atom plus the group of neighboring atoms involved in the rearrangement, and then specifying to a first approximation the coordinates of the center by an average configuration coordinate. Diagrams of potential energy *versus* configuration coordinate have been applied by Gurney and Mott,[8] Pringsheim,[9] and Seitz[3] to the phenomenon of luminescence of solids.

II. TEMPERATURE DEPENDENCE OF LUMINESCENT EFFICIENCY

The variation with temperature of the emission intensity under continuous excitation is a measure of luminescent efficiency and provides a key to the mechanism of luminescence. Such data obtained with ultraviolet excitation are simpler to measure experimentally and to interpret theoretically, and therefore, will be discussed first.

The measurements above and below 25°C were made on different apparatus. Figure 1 shows the furnace used for the measurements above 25°C. The emission intensity and temperature of the phosphor were simultaneously measured as the furnace was heated at a rate slow enough to keep the thermometers, above and below the sample, within 1C° of each other. The sulfide phosphors were excited by the 3650A G.E. E-H-4 100-watt lamp doubly-filtered with Corning 5840 and 5874. The borate, germanate, silicate, and tungstate phosphors were excited by the 2537A G.E. 8-watt germicidal lamp filtered with Corning 9863. Both lamps were operated from a voltage regulator to insure constant excitation intensity. The measurements were checked by taking points on the cooling curve as well as on the heating curve to test for any hysteresis effect. Runs were made with different Wratten filters on the photo-cell to determine whether

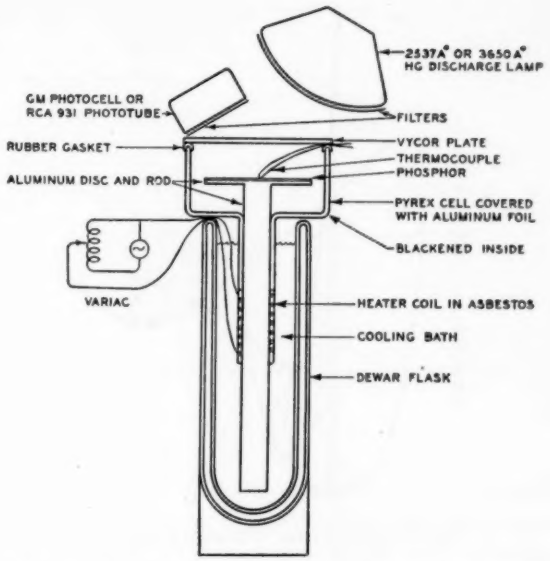

FIG. 2. Apparatus to measure "glow curves" and the temperature dependence of luminescent efficiency at low temperatures.

the emission spectrum has appreciable temperature dependence.

Figure 2 shows the apparatus used below 25°C. The lamps and filters were identical with the above. Before starting a run, the cell was desiccated by cooling by conduction with the liquid air in the Dewar flask. The phosphor on the aluminum disk was then inserted, the thermocouple dipped into the powder, and the apparatus allowed to attain thermal equilibrium. The Dewar flask was slowly lowered and with the current controlled by the Variac, a linear heating rate was approximated. The heating was continued above 25°C to allow a 50 C° overlap with the data taken on the high temperature apparatus.

The results may be summarized as follows: Above a rather critical temperature the luminescent efficiencies of the phosphors examined decrease rapidly and continuously with increasing temperature. The (Zn, Cd)S:Ag phosphors start to decrease in efficiency at 25°C and at 200°C the emission intensity is reduced to 10 percent. The (Zn, Cd)S:Cu phosphors increase in efficiency with increasing temperature until 225°C whereupon the efficiency starts to decrease and at 400°C has decreased to 10 percent of the efficiency at 25°C. The temperature-dependence curves of the borate, silicate, sulfoselenide, and

[8] R. W. Gurney and N. F. Mott, Trans. Faraday Soc. 35, 69 (1939).
[9] P. Pringsheim, Rev. Mod. Phys. 14, 132 (1942).

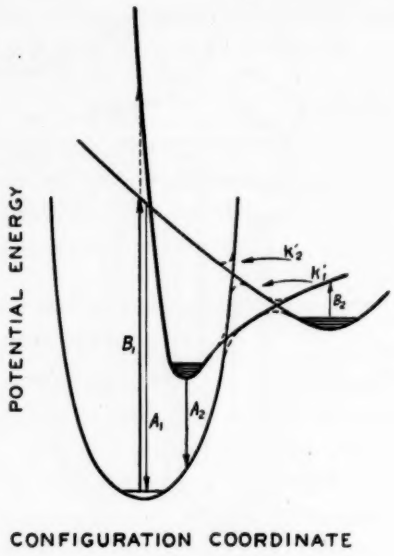

FIG. 3.

tungstate phosphors fell between these limits. The Zn_2SiO_4:Mn phosphor exhibits a slight hysteresis effect and two points of inflection as the efficiency decreases with increasing temperature. Below the rather critical temperature, the efficiencies of most of the phosphors decrease slowly with decreasing temperature.

The pronounced decrease of luminescent efficiency at high temperatures suggests an activated process with a large energy of activation by which excited electrons return to the ground state by a radiationless mechanism. The small decrease in efficiency at low temperatures can be explained by an activated step with a small energy of activation in the actual luminescent process. In other words, two competing processes are active: the radiationless recombination of the excited electron and center, and an activated step in the luminescent process.

To explain the temperature dependence of luminescent efficiency and many other diverse phenomena in the luminescence of solids, the model of potential energy *versus* configuration coordinate shown in Fig. 3 is proposed. The three states—the normal, the metastable, and the emitting states—represented by the contour lines, have different multiplicities: electrons in one state have a large probability of remaining in that state where the contours cross, and optical transitions between the states are to some extent forbidden. The metastable state is often referred to as an electron trap because activation of the electron in this state is necessary before emission can occur. With respect to the states of different multiplicities, the model is similar to the scheme proposed by G. N. Lewis[10] for the phosphorescence of organic molecules.

To calculate the temperature dependence of efficiency with continuous excitation to the metastable state, the following notation is introduced: n_1, n_2, and n_3 are the numbers of electrons in the normal, metastable, and emitting states, respectively; A_1 and A_2 are the transition probabilities for emission before and after trapping; B_1 and B_2 are the transition probabilities for excitation and for optical release from the electron trap; and k_1' and k_2' are the specific rate constants for surmounting the barriers between the metastable and the emitting state and between the metastable and the normal state. The rate constants for the reverse of the last two processes are negligible because of the

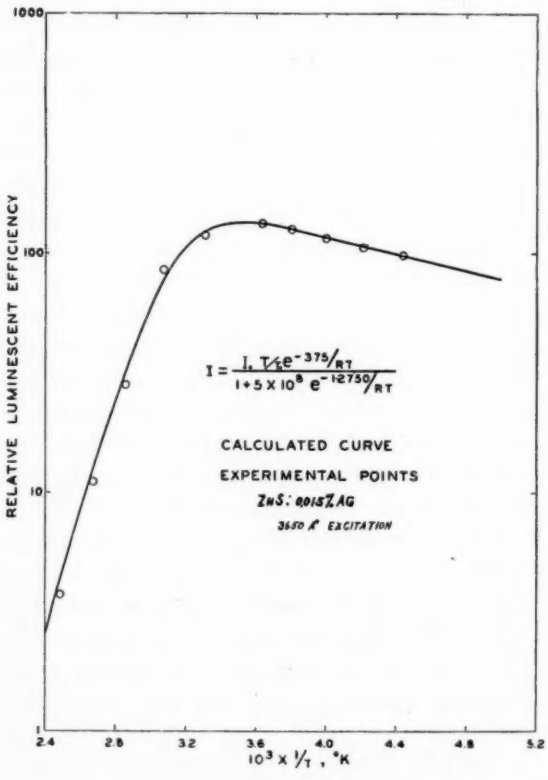

FIG. 4.

[10] G. N. Lewis *et al.*, J. Am. Chem. Soc. **63**, 3005 (1941); **64**, 1774 (1942); and **66**, 2100 (1944).

asymmetric character of the potential barriers. Applying the Stationary State Method, the following conditions result:

$$dn_3/dt = k_1' n_2 + B_2 n_2 - A_2 n_3 = 0,$$

$$dn_2/dt = -k_1' n_2 - k_2' n_2 + B_1 n_1 - A_1 n_2 - B_2 n_2 = 0.$$

Combining these equations, the emission intensity can be written as follows after dividing by the non-temperature-dependent parameters:

$$I = \alpha(k_1' + B_2) \Big/ \left[1 + \frac{(k_1' + B_2)}{A_1} + \frac{k_2'}{A_1}\right].$$

In the absence of infra-red stimulation of suitable frequency to empty the metastable levels optically, the expression is simplified:

$$I = \frac{\alpha k_1'}{1 + k_1'/A_1 + k_2'/A_1}. \qquad (2\text{-}1)$$

According to the Absolute Rate theory,[11] the specific rate constants are of the following form:

$$k' = \kappa \frac{kT}{h} \exp(\Delta S^{\ddagger}/R) \exp(-\Delta H^{\ddagger}/RT). \qquad (2\text{-}2)$$

Substituting (2-2) in (2-1) and assuming that the transmission coefficient for the radiationless process is greater than the transmission coefficient for the activated step in the luminescent process, and that the entropy changes are small, the temperature dependence of the emission intensity takes the form:

$$I = \frac{I_0(T/T_0) \exp(-\Delta H_1^{\ddagger}/RT)}{1 + \beta \exp(-\Delta H_2^{\ddagger}/RT)}, \qquad (2\text{-}3)$$

where β is a constant dependent on A_1.

The experimental points and the curve calculated according to (2-3) are shown in Fig. 4 for the blue-emitting ZnS:Ag crystallized at 1240°C. The logarithm of emission intensity is plotted as a function of the reciprocal of the absolute temperature so that the slope of the straight-line portions of the curve are a measure of the heats of activation for the two competing processes. Similar results have been obtained with ZnS:Cu, ZnS:Mn, and $Cd_3(BO_3)_2$:Mn.

[11] S. Glasstone, K. J. Laidler, and H. Eyring, *The Theory of Rate Processes* (McGraw-Hill Book Company, Inc., New York, 1941).

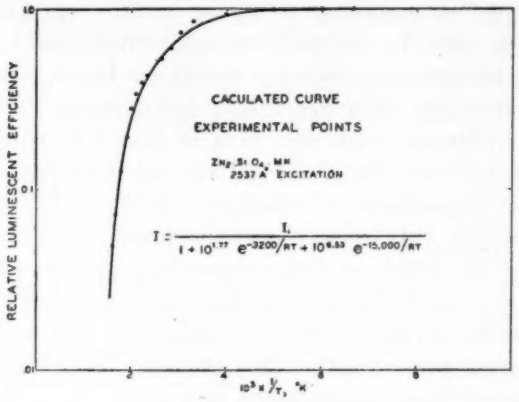

FIG. 5.

Generalizing (2-3) to include several possible mechanisms for the radiationless recombination of the excited electron and center, the following expression results:

$$I = \frac{I_0(T/T_0) \exp(-\Delta H_1^{\ddagger}/RT)}{1 + \sum_{j=2,3,\cdots} \beta_j \exp(-\Delta H_j^{\ddagger}/RT)}. \qquad (2\text{-}4)$$

With Zn_2SiO_4:Mn two possible mechanisms for the radiationless process of returning to the ground state are suspected because of the points of inflection in the region of the curve of luminescent efficiency *versus* temperature where the efficiency is decreasing rapidly with increasing temperature. The experimental points and the calculated curve based on (2-4) are shown in Fig. 5 for Zn_2SiO_4:Mn crystallized at 1200°C. The non-exponential factor for the radiationless process with the smaller heat of activation is unusually small.

In the case of the activated step in the luminescent process, there are also alternative mechanisms active. In fact, as is proven in Part V, there are electron traps of different depths active to different extents in the sulfide phosphors. During continuous excitation the shallower traps participate many times in the luminescent process compared to the deeper traps. Therefore, the depths of the shallow traps are statistically-weighted more than the depths of the deep traps in efficiency data, and the calculated heats of activation for release from the metastable state are only a few hundred calories.

From Fig. 3, it is clear that if the excitation

energy is sufficient to excite to the emitting state, then the electron trap will be bypassed and the luminescent efficiency would not be expected to decrease with decreasing temperature. This is consistent with the data of Schon[12] on the effect of wave-length of excitation on the temperature dependence of efficiency of (Zn, Cd)S:Zn and (Zn, Cd)S:Cu. For monochromatic excitation at 4047A or longer wave-lengths, the efficiency at 85°K is less than the efficiency at 298°K; whereas, for excitation at 3340A or shorter wave-lengths, the efficiency at 85°K is greater than the efficiency at 298°K.

The short wave ultraviolet or high energy corpuscular excitation resulting in a transition directly to the emitting state, in addition, leads to a different mechanism for the radiationless recombination of the excited electron and the center. The rate-determining step now involves surmounting the barrier connecting the emitting and the ground state. This mechanism probably requires a greater energy of activation than is involved in surmounting the barrier between the metastable and the ground state, otherwise it would have competed with the radiationless release from the trap with long wave excitation. This indicates that on excitation directly to the emitting state, the critical temperature, above which the luminescent efficiency decreases rapidly, will occur at a higher temperature than with excitation to the metastable state.

This interpretation was verified by measuring the temperature dependence of luminescent efficiency with excitation by 6 kv electrons. A demountable vacuum chamber was used. The phosphor, deposited on a platinum-plated Nichrome filament, was heated by passing current through the filament and was excited by a 60-cycle scanning electron beam. A 931 photomultiplier tube measured the emission intensity, and a Nichrome-Advance thermocouple measured the temperature of the phosphor. The inherent errors of measuring the temperature of an insulator in a vacuum prevented the results from being reliable to better than 10 percent, but it was concluded that the critical temperatures above which (Zn, Cd)S:Cu phosphors decrease in efficiency are higher with excitation by 6 kv electrons than by 3650A radiation. For example, the phosphor prepared according to the composition: 88 percent ZnS, 12 percent CdS, and 0.008 percent Cu, crystallized at 1220°C, and excited by 3650A ultraviolet has at 360°C only 10 percent the efficiency at 25°C. The same material excited by 6 kv electrons does not decrease to this efficiency until 510°C. This confirms our hypothesis regarding an alternative mechanism for the radiationless process on excitation directly to the emitting state.

[12] M. Schon, Naturwiss. **31**, 169 (1943).

III. PHOSPHORESCENCE

The model shown in Fig. 3 and used to explain the temperature dependence of luminescent efficiency is also consistent with various phosphorescent phenomena. The afterglow of various phosphors may be divided into spontaneous, metastable and recombination phosphorescence. The excited electron during spontaneous phosphorescence does not reach the conduction band but only reaches an excitation level and remains in the field of the center. The rate of emission of photons depends, therefore, only on the concentration of excited electrons and in the case of excited centers of only one kind reduces to monomolecular kinetics with the emission intensity expressed as follows:

$$I = -\alpha \frac{dn}{dt} = \alpha n_0 A e^{-At} \qquad (3\text{-}1)$$

where n and n_0 are, respectively, the numbers of excited electrons at times t and t_0. The transition probability A for spontaneous afterglow is only slightly influenced by temperature and depends on atomic selection rules perturbed by the lattice field.

The essential criterion for metastable afterglow is that the rate-determining step in the luminescent process is the thermal release of an electron from a metastable state or electron trap. If the electron passes through the conduction band on release from the trap, enhanced conductivity will occur. Because during the slow step each electron acts independently, the rate of emission will depend only on the concentration of excited electrons. Metastable phosphorescence requires an activation energy and is, therefore, strongly temperature dependent. In place of the

transition probability A in (3-1), a specific rate constant k' is substituted assuming the traps are of uniform depth:

$$I=-\alpha\frac{dn}{dt}=\alpha n_0 k' e^{-k't}. \qquad (3\text{-}2)$$

The rate constant is of the form (2-2).

If the excited electrons pass through the conduction band, each electron loses its relationship to its "own" center and if the rate-determining step is the migration of the electron through the conduction band, then the recombination of a center and an electron depends both on the concentration of ionized centers and on the concentration of conduction electrons. The decay of emission intensity proceeds by bimolecular kinetics if there are equal numbers of centers and electrons involved:

$$I=-\alpha\frac{dn}{dt}=\frac{\alpha k' n_0^2}{(1+n_0 k' t)^2}. \qquad (3\text{-}3)$$

As in metastable luminescence, k' is again expressed by (2-2).

Following the above introduction on phosphorescence, let us turn to some particular phosphors having interesting afterglow characteristics and interpret these characteristics in terms of our model. The fluorides will be discussed first. These phosphors are prepared from the metal oxides, including about one mole percent Mn, and excess HF acid in platinum apparatus and after drying are crystallized at 700 to 900°C. An alternative preparation is from the metal sulfate and KF.

The measurements of emission spectra and visual efficiencies were made with a spectroradiometer.[13] 6 kv and 1–5 μa/cm^2 d.c. electron excitation was used in these as well as in the phosphorescence measurements. The latter were made with a phosphoroscope[14] capable of automatic changes in sensitivity during the actual afterglow measurements. A 1P21 photo-multiplier picked up the phosphor emission and, after feeding into an oscilloscope, the trace was photographed. Corrections for the filament light and the irreducible ambient light were applied,

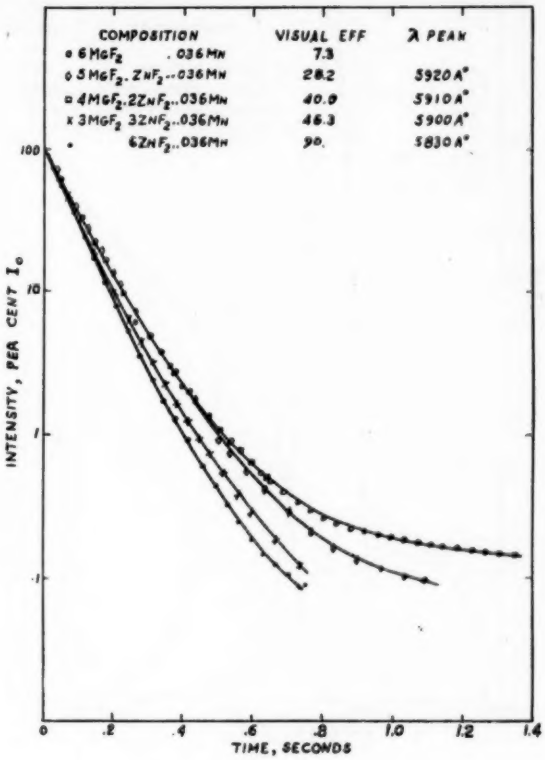

FIG. 6.

and finally the logarithm of intensity was plotted against time.

The (Zn, Mg)F_2:Mn phosphors have the longest, truly exponential afterglow of any of the efficient, known luminescent solids. The average lifetime of the excited state is 0.083±.005 second for ZnF_2:Mn and is 0.092±.005 second for MgF_2:Mn. In Fig. 6 are shown the afterglow curves for representative phosphors in this system. The concave-upward character of the phosphorescent curve is small but real. The emission spectra and relative visual efficiencies of several fluoride phosphors are shown in Fig. 7.

In the region of composition of 88 to 98 mole percent MgF_2 in the (Zn, Mg)F_2:Mn system, marked departure from exponential phosphorescence occurs as shown in Fig. 8. This type of phosphorescence can be accounted for by assuming that when excitation ceases, there are two sources of excited electrons which undergo luminescence by two different rate-determining steps.

In terms of the model shown in Fig. 3 the emitting state is the source of the initial expo-

[13] V. K. Zworykin, J. Opt. Soc. Am. 29, 84 (1939).
[14] R. E. Shrader, private communication.

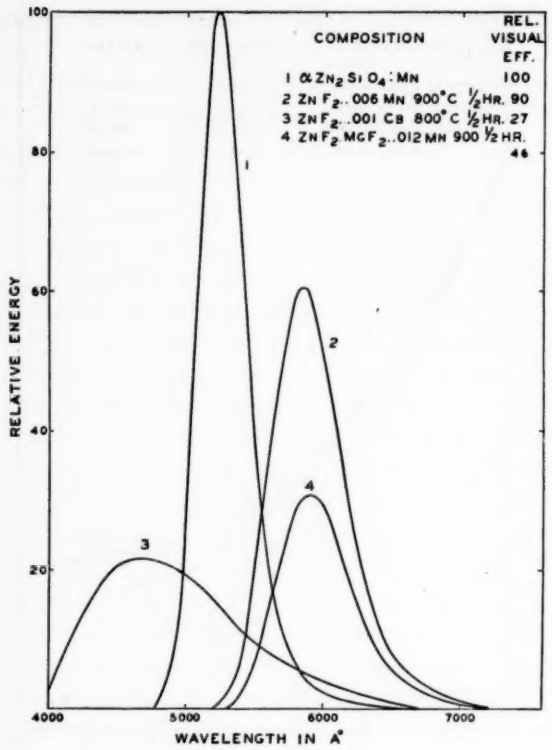

FIG. 7.

nential phosphorescence and the metastable state is the source of the slowly decaying phosphorescent tail. In addition to the notation used in Part II, n_{2_0} and n_{3_0} denote the numbers of electrons in the metastable and emitting states, respectively, when excitation ceases. The following conditions are obvious:

$$\frac{dn_3}{dt}=k_1'n_2-A_2n_3,$$

$$n_2=n_{2_0}\exp(-k_1't).$$

Combining the above and solving for n_3, the emission intensity is:

$$I=\alpha A_2n_3=\alpha A_2\left(\frac{n_{2_0}k_1'}{A_2-k_1'}-1\right)\times\exp(-k_1't)+\alpha n_{3_0}A_2e^{-A_2t}. \quad (3\text{-}4)$$

The application of (3-4) to the long persistent (Zn, Mg)F_2:Mn and to the ZnF_2:Mn is shown in Fig. 9. The long phosphorescence of the former and the slightly concave-upward character of the decay curve of the latter are precisely reproduced by the calculated expressions. The relative numbers of electrons in the metastable and emitting states when the excitation ceases can be determined from (3-4) or from the "light sums." Measurements of the temperature dependence of phosphorescence substantiate the somewhat arbitrary procedure of dividing the afterglow into two parts. The afterglow of ZnF_2:Mn is practically independent of temperature. The long phosphorescent tail of (Zn, Mg)F_2:Mn is latent at −78°C. After excitation by x-rays at this temperature, subsequent heating releases the electrons from the metastable state and light emission results. This is a "glow curve" of the type treated in Part V. The rate of the long-persistent afterglow increases with increasing temperature until at 250°C it equals that of the initial spontaneous afterglow. The heat of activation is about $4.5k$ cal.

$Cd_2P_2O_7$:Mn exhibits exponential phosphorescence with an average lifetime of the excited state of $0.040\pm.003$ second. The phosphate phosphors were prepared by precipitating $CdNH_4PO_4$

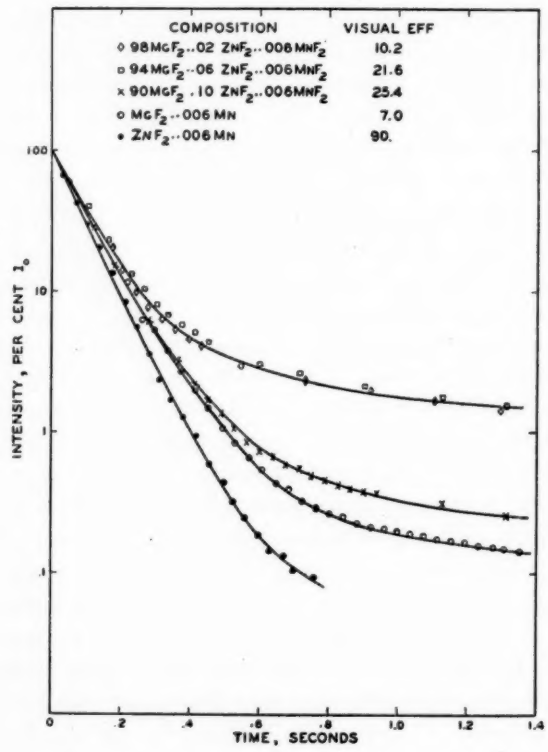

FIG. 8.

from $(NH_4)_2HPO_4$ solution with $Cd(NO_3)_2$, adding the activator as $Mn(NO_3)_2$, and crystallizing at 800 to 1000°C. The afterglow as shown in Fig. 10 depends to some extent on activator concentration and can be precisely reproduced by (3-4). The two curves can be fitted using the same two exponentials, with their individual contributions weighted differently. The initial afterglow may be associated with substitutional Mn and the slow phosphorescence with interstitial Mn.

Fonda[15] reports two-stage afterglow for Zn_2SiO_4:Mn with ultraviolet excitation and indicates that the second process may occur by bimolecular kinetics. In terms of Fig. 3 the data may be interpreted as an initial spontaneous process followed by a series of temperature-dependent monomolecular processes resulting from electron traps of different depths.

It is clear from Fig. 3 that the individual contributions to two-stage afterglow can also be resolved by using different types of excitation. The data of Leverenz[16] for Zn_2SiO_4:Mn indicate

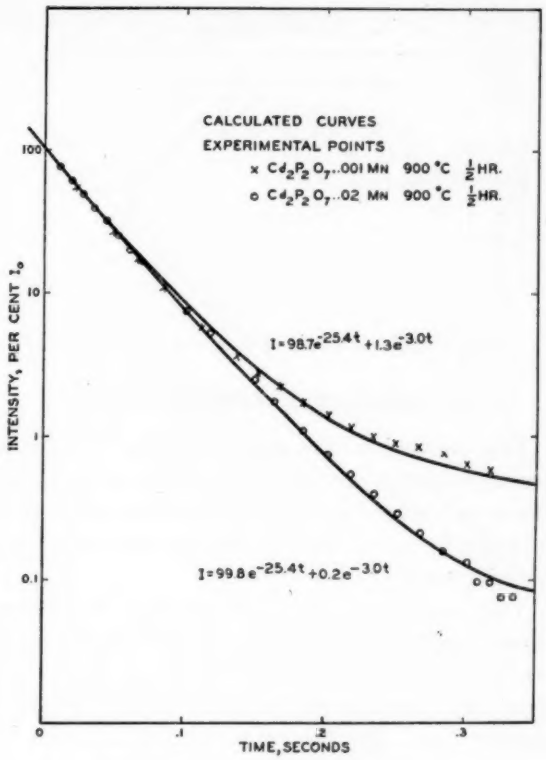

FIG. 10.

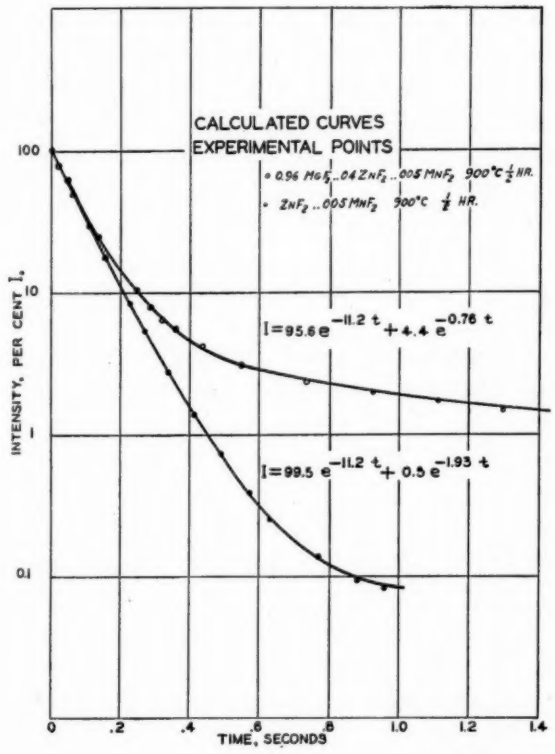

FIG. 9.

that excitation by 6 kv electrons results in the metastable state being bypassed so that even though excitation to the same emission intensity with electrons and ultraviolet can be attained, it is only with the radiation excitation that a temperature-dependent, phosphorescent tail persists. Leverenz explains this effect by localized heating by the cathode rays.

Antonov-Romanovsky[17] reports that KCl:Tl exhibits an initial, exponential afterglow only at low excitation intensities. This indicates a limited concentration of emitting states. The effect of infra-red radiation on the longer phosphorescence of this phosphor results in optical transitions from the metastable state.

An analysis of the data of Shrader[18] for SrS:Sm, Eu indicates that above 375°C a single metastable state with a thermal depth of 0.65 ev is active. This must correspond to the electron trap having an optical depth of 0.95 ev which can be emptied by 1.3μ radiation.

[15] G. R. Fonda, J. App. Phys. **10**, 408 (1939).
[16] H. W. Leverenz, RCA Rev. **7**, 199 (1946).
[17] V. V. Antonov-Romanovsky, J. Phys. U.S.S.R. **6**, 120 (1942); **7**, 153 (1943).
[18] R. E. Shrader, paper 15 at Optical Society of America Meeting at Cleveland (March, 1946).

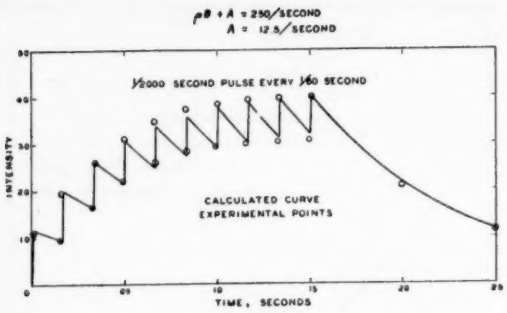

FIG. 11. $\rho B+A=250$/second, $A=12.5$/second.

IV. BUILD-UP OF LUMINESCENCE

The increase in emission intensity with time during initial excitation is referred to as build-up. Data on this property of phosphors have been reported by de Groot[19] for sulfides and by Fonda[15] for willemite.

The simplest build-up mechanism to analyze theoretically involves only a normal state and one excited state. In terms of Fig. 3 this means that the metastable levels participate only slightly and the kinetics are dominated by transitions between the ground state and the emitting state. Applying the notation used in Parts II and III, and introducing B and A as the transition probabilities for excitation and emission, ρ as the energy density of excitation, and n_0 as the total number of centers, the rate of change in the number of excited electrons is:

$$dn_3/dt=\rho B(n_0-n_3)-An_3.$$

Solving for the number of excited electrons:

$$n_3=\frac{\rho Bn_0}{(\rho B+A)}[1-e^{-(\rho B+A)(t-t_0)}]. \quad (4\text{-}1)$$

The emission intensity is therefore:

$$I=\alpha An_3=\frac{\alpha\rho BAn_0}{(\rho B+A)}[1-e^{-(\rho B+A)(t-t_0)}]. \quad (4\text{-}2)$$

On removing the excitation ρ at time t_1, n_3 decreases according to the following:

$$n_3=n_{31}e^{-A(t-t_1)}, \quad (4\text{-}3)$$

where n_{31} is the number of excited electrons at t_1. Substituting the explicit expression for n_{31} obtained from (4-1) in (4-3), the emission intensity during phosphorescence is:

$$I=\frac{\alpha\rho BAn_0}{(\rho B+A)}[1-e^{-(\rho B+A)(t_1-t_0)}]e^{-A(t-t_1)}. \quad (4\text{-}4)$$

The build-up and decay of emission intensity can be calculated for intermittent excitation by introducing the boundary values of n_3 into the solution of the proper differential equation at the beginning and end of each pulse. Introducing the notation:

$$f_m=e^{-(\rho B+A)(t_{m+1}-t_m)},$$

$$g_m=e^{-A(t_{m+1}-t_m)},$$

and noting that the excitation is first turned on at t_0, the emission intensity when the excitation is off is in general:

$$I=\frac{\alpha\rho BAn_0}{(\rho B+A)}(1-f_{m-1}\{1-g_{m-2}\times[1-f_{m-3}\cdots(1-g_1[1-f_0])]\})e^{-A(t-t_m)}, \quad (4\text{-}5)$$

where m denotes the number of times the excitation has either been turned on or off, and in (4-5) m is odd. The general expression for the build-up with pulsed excitation is as follows where m is even:

$$I=\frac{\alpha\rho BAn_0}{(\rho B+A)}(1-e^{-(\rho B+A)(t-t_m)}\{1-g_{m-1}\times[1-f_{m-2}\cdots(1-g_1[1-f_0])]\}). \quad (4\text{-}6)$$

Comparing (4-5) and (4-6), it is interesting to note that the rate constant for build-up may be

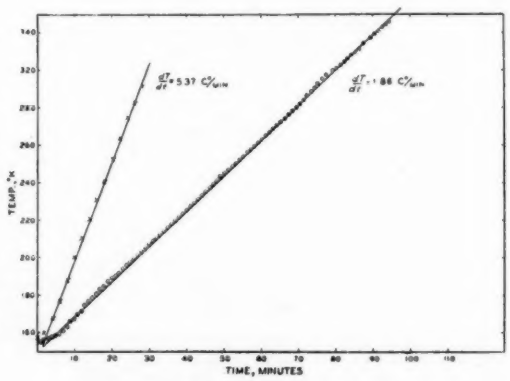

FIG. 12.

[19] W. de Groot, Physica 6, 275 (1939).

strongly dependent on the density of exciting radiation but the rate constant for phosphorescence is not. The latter must be less than or equal to the former. Insofar as the rate constant for build-up depends on excitation intensity, the emission will tend to become independent of the continuous excitation intensity. On the other hand, if $A \gg \rho B$ then the number of excited centers will be small compared to the number of available centers and the emission intensity will be proportional to the excitation intensity.

The data of Fonda[15] indicate that the latter conditions are approximately satisfied for the build-up and initial afterglow of willemite with 2537A excitation. The small contribution of the metastable process is probably responsible for the small differences in the rate constants for build-up and initial phosphorescence.

A better test of (4-5) and (4-6) is the build-up and phosphorescence of ZnF_2:Mn. The calculated curve and experimental points for pulsed build-up and afterglow are shown in Fig. 11. The measurements were made with the phosphoroscope[14] described in Part III. Ten 1/2000 second pulses of electrons were applied at 1/60 second intervals. The average excitation current was 175 $\mu a/cm^2$ during the individual pulses and the voltage was 6 kv. This high excitation intensity, coupled with the long lifetime of the excited state of ZnF_2:Mn, indicates that quite a large fraction of the available centers exist in the excited state. It is, therefore, not surprising that the rate constant for build-up $\rho B+A$ required to fit the data is twenty times the rate constant for phosphorescence A under these conditions of excitation. The slight deviation of the calculated curve from the experimental points is caused by a combination of experimental error and a small contribution from metastable luminescence. The analysis culminating in Eqs. (4-5) and (4-6) predicts at high excitation intensity the dependence of the rate constant for build-up on excitation intensity, the larger rate constant for build-up than for afterglow, and the lack of dependence of the rate constant for phosphorescence on intensity of excitation. The last two characteristics have been verified experimentally in the case of ZnF_2:Mn.

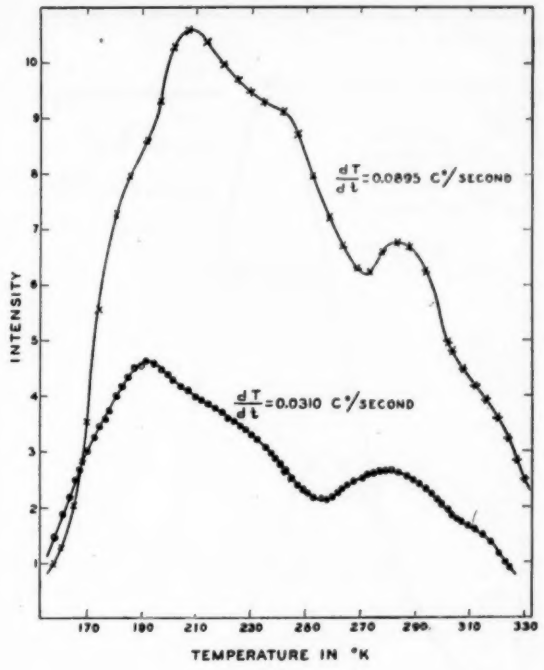

FIG. 13.

V. GLOW CURVES

For a phosphor exhibiting monomolecular, temperature-dependent phosphorescence, the depth of the metastable level is readily calculated from the temperature coefficient of the rate of decay of emission intensity. The afterglow of sulfide phosphors, however, does not vary as a simple function of temperature but tends to have a small irregular temperature dependence. This, coupled with the hyperbolic t^{-n} afterglow, indicates that a more complex type of phosphorescence is active. A possible explanation is that the metastable states or electron traps are not uniform in depth.

"Glow" data are useful in determining the mechanism of complex afterglow. A "glow curve" is obtained by exciting the phosphor, allowing the emission intensity to decay to a low value, and then measuring the emission intensity as the phosphor is heated, preferably at a linear rate. Urbach[20] first reported glow measurements on KCl:Tl, and Randall and Wilkins[21] reported and analyzed glow curves for sulfides assuming various distributions of electron traps. The rates

[20] F. Urbach, Akad. Wiss. Wien **139** IIa, 363 (1930).
[21] J. T. Randall and M. H. F. Wilkins, Proc. Roy. Soc. **A184**, 347, 366, 390 (1945).

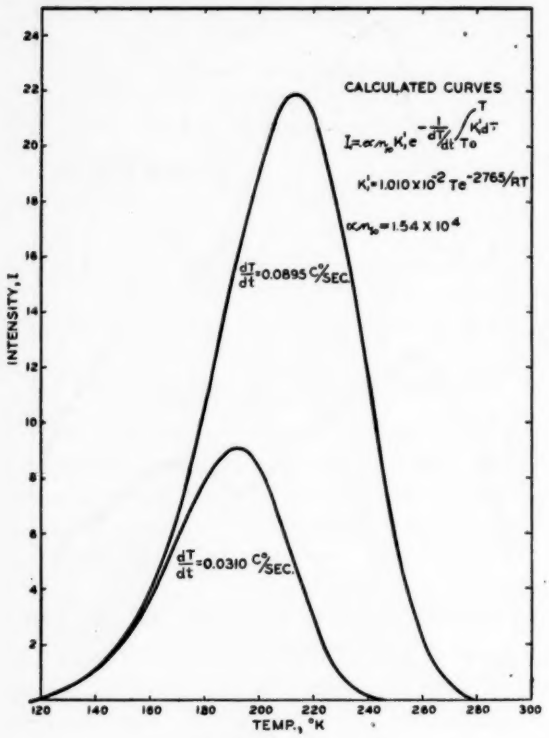
CALCULATED CURVES
$I=\alpha n_0 K_1' e^{-\frac{1}{dT/dt}\int_{T_0}^{T} K_1' dT}$
$K_1'=1.010\times10^{12}\,T e^{-2765/RT}$
$\alpha n_0=1.54\times10^{4}$
$\frac{dT}{dt}$=0.0895 C°/SEC.
$\frac{dT}{dt}$=0.0310 C°/SEC.
INTENSITY, I
TEMP., °K
120 140 160 180 200 220 240 260 280 300
2 4 6 8 10 12 14 16 18 20 22 24

FIG. 14.

of heating used for ZnS:Cu and KCl:Tl varied from 2 to 10°C per second. Such fast heating rates do not allow metastable states of uniform depth to be exclusively operative at one time, but instead electrons from many traps of different depths contribute to the emission intensity.

The glow curves herein reported were obtained with linear heating rates about 100 slower than those previously reported. The apparatus shown in Fig. 2 was adapted to glow measurements. By adjusting the Dewar position and heating current, a constant rate of heating was maintained. Two heating cycles are shown in Fig. 12 and the corresponding glow curves are shown in Fig. 13 for ZnS activated with 0.003 percent Cu and crystallized at 1240°C. The phosphor was excited at 150°K with 3650A; the emission was detected with a 931 photo-multiplier; and the photocurrent was read on an ultra-sensitive d.c. ammeter. Readings of time, temperature, and intensity were taken simultaneously.

In treating the case of metastable states of uniform depth emptying by a monomolecular, rate-determining step, and producing luminescence without retrapping, the following notation is introduced: n_1 and n_{10} as the numbers of electrons in the metastable state at times t and t_0, and k_1' as the specific rate constant for surmounting the potential barrier between the metastable and emitting state. Solving the equation for the rate of decrease of trapped electrons:

$$n_1 = n_{10} \exp\left(-\int_{t_0}^{t} k_1' dt\right). \tag{5-1}$$

Introducing the rate of heating, the emission intensity is:

$$I_1 = -\alpha \frac{dn_1}{dt} = \alpha n_{10} k' \times \exp\left(-\frac{1}{dT/dt}\int_{t_0}^{t} k_1' dT\right). \tag{5-2}$$

Solving (5-1), expanding the logarithmic function, and introducing the rate of heating:

$$\int_{t_0}^{t} k_1' dT = -\ln\left[1-\left(\frac{n_{10}-n_1}{n_{10}}\right)\right] = \frac{dT}{dt}\left[\sum_{j=1}^{\infty}\frac{1}{j}\left(\frac{n_{10}-n_1}{n_{10}}\right)^{j}\right]. \tag{5-3}$$

Assuming that a negligible number of trapped electrons undergo radiationless recombination with the excited center or are retrapped, n_{10} and n_1 can be expressed in terms of the "light sums," so that (5-3) can be solved for k_1' as a function of observables:

$$k_1' = \frac{d}{dT}\left\{\frac{dT}{dt}\left[\sum_{j=1}^{\infty}\frac{1}{j}\left(\frac{\int_{T_0}^{T} I_1 dT}{\int_{T_0}^{\infty} I_1 dT}\right)^{j}\right]\right\}. \tag{5-4}$$

With (5-4) and an experimental glow curve resulting from homogeneous metastable states, both the frequency factor and the heat of activation of the specific rate constant (2-2) can be calculated, although absolute intensities are not measured. Two theoretical monomolecular glow curves calculated from (5-2) are shown in Fig. 14.

In the case of luminescence involving activated,

rate-determining migration through the conduction band, bimolecular kinetics result. The notation is modified as follows: n_2 and n_{20} as the numbers of electrons in the conduction band at times t and t_0, and k_2' as the specific rate constant for the activated bimolecular process. The emission intensity is:

$$I_2 = -\alpha\frac{dn_2}{dt} = \frac{\alpha n^2{}_0 k_2'}{\left[1+\dfrac{n_{20}}{dT/dt}\displaystyle\int_{T_0}^{T} k_2' dT\right]^2}. \quad (5\text{-}5)$$

Assuming that a negligible number of electrons undergo radiationless recombination with the ionized center and that retrapping is again trivial, k_2' is obtained in terms of the "light sum":

$$k_2' = \frac{d}{dT}\left\{\alpha\left(\frac{dT}{dt}\right)^2 \frac{\displaystyle\int_{T_0}^{T} I_2 dT}{\displaystyle\int_{T}^{\infty} I_2 dT \int_{T_0}^{\infty} I_2 dT}\right\}. \quad (5\text{-}6)$$

It is clear from (5-6) that unless absolute intensities are measured only the heat of activation and not the frequency factor of the specific rate constant can be calculated from an experimental glow curve resulting from a bimolecular, rate-determining process. Two theoretical bimolecular glow curves calculated with (5-6) are shown in Fig. 15. These curves, like the monomolecular glow curves of Fig. 14, are not symmetrical. The bimolecular curves are skewed towards the low temperature, whereas the monomolecular curves are skewed toward the high temperature.

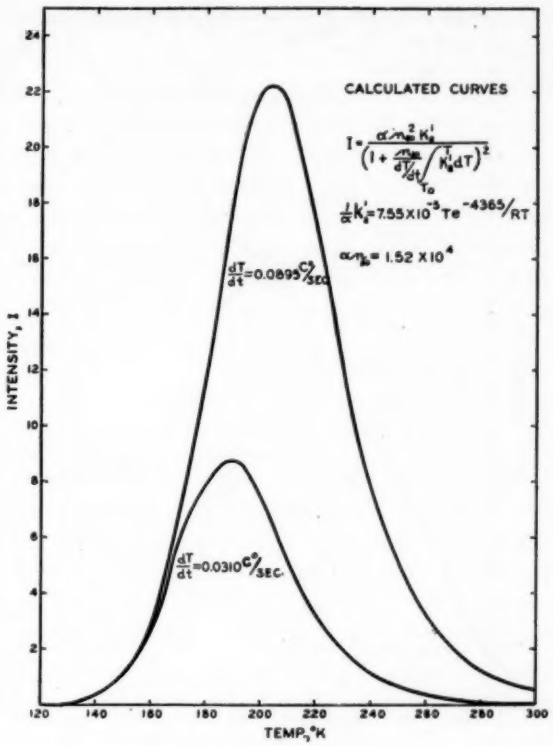
CALCULATED CURVES
$\frac{1}{\alpha}k_1' = 7.55\times10^{-3}Te^{-4365/RT}$
$\alpha n_{20} = 1.52\times10^{4}$
$\frac{dT}{dt}=0.0895^{C°}/_{SEC.}$
$\frac{dT}{dt}=0.0310^{C°}/_{SEC.}$
INTENSITY, I
TEMP, °K
120 140 160 180 200 220 240 260 280 300
2 4 6 8 10 12 14 16 18 20 22 24

FIG. 15.

For the general treatment involving both monomolecular and bimolecular rate-determining processes, the following is the expression for the emission intensity assuming that the electrons in the conduction band and in the metastable state are in equilibrium according to the Boltzmann law:

$$I = \alpha k_1'\left\{\frac{k_1'/k_2' e^{2\epsilon/kT} n_{10}}{n_{10}\left[\exp\displaystyle\int_{t_0}^{t}\left(\frac{k_1'}{e^{-\epsilon/kT}+1}\right)dt - 1\right] + \dfrac{k_1'}{k_2'}e^{2\epsilon/kT}\exp\displaystyle\int_{t_0}^{t}\left(\frac{k_2'}{e^{-\epsilon/kT}-1}\right)dt}\right\}$$

$$+\alpha k_2'\left\{\frac{k_1'/k_2' e^{\epsilon/kT} n_{20}}{n_{20}\left[\exp\displaystyle\int_{t_0}^{t}\left(\frac{k_1' e^{\epsilon/kT}}{e^{\epsilon/kT}+1}\right)dt - 1\right] + \dfrac{k_1'}{k_2'}e^{\epsilon/kT}\exp\displaystyle\int_{t_0}^{t}\left(\frac{k_1' e^{\epsilon/kT}}{e^{\epsilon/kT}+1}\right)dt}\right\}^2, \quad (5\text{-}7)$$

where ϵ is the difference in energy between the conduction band and the metastable state. Because of the complicated nature of (5-7), (5-2), and (5-5) which treat the monomolecular and bimolecular mechanisms separately will be applied to experimental glow curves.

In applying the theoretical expressions for either monomolecular or bimolecular luminescence to experimental glow curves, the following procedure is used: The monomolecular case utilizing (5-1) to (5-4) will be applied first. As shown in the lowest section of Fig. 16, which is

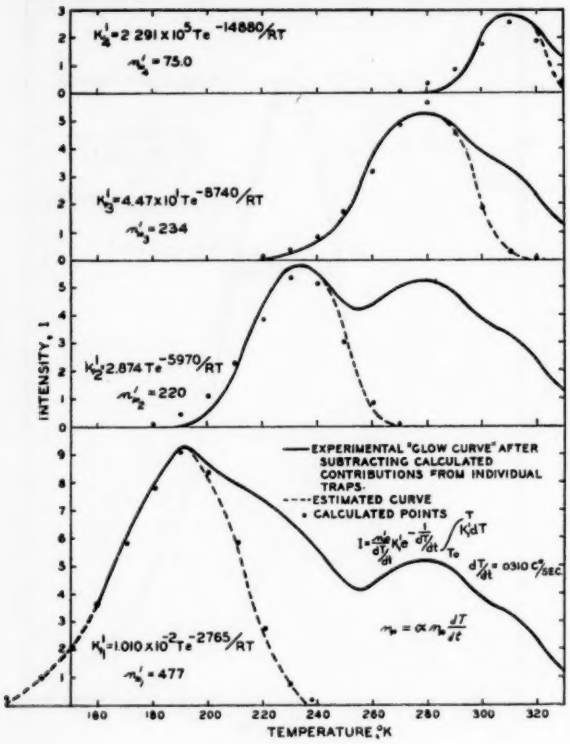

FIG. 16.

based on the glow data shown in Fig. 13, an estimate is made of the high temperature side of the emission intensity contributions from the low temperature peak. By measuring the area under the individual glow peak, a tentative total light sum from the particular metastable state is obtained. The area is also measured up to various temperatures to obtain the partial light sums that are a function of number of electrons that have been released before attaining the temperature in question. The light sums are inserted in (5-4), and a tentative specific rate constant is obtained graphically. The explicit form of the rate constant is substituted in (5-2) and the individual glow peak is calculated and compared with the experimental low temperature side and the estimated high temperature side. The light sums are redetermined to a second approximation, and the above procedure is repeated until the calculated glow peak fits the experimental and estimated curve. Insofar as the experimental, low temperature side of the glow peak is reproduced by the calculated curve, it is concluded that the high temperature side is also fitted. Figure 14 and the lowest section of Fig. 16 show the results of the third approximation.

A similar procedure was also repeated to the third approximation assuming a bimolecular, rate-determining process. The resulting theoretical glow peak is shown in Fig. 15. Because of the dependence of the shape of the build-up of peak emission on the order of the reaction, it is impossible to fit the initial part of the experimental glow curve assuming bimolecular kinetics. It is concluded that either the last remnant of a lower temperature glow peak is contributing or the rate-determining process is predominantly monomolecular.

Comparing (5-2) and (5-5), it is apparent that the emission is a different function of rate of heating for monomolecular and bimolecular processes. The temperature at which the maximum emission occurs depends on the rate of heating. The glow peak for the faster rate of heating can be calculated from the specific rate constant obtained by the analysis of the experimental glow curve at the slower rate. This can be done by assuming either a monomolecular or a bimolecular rate-determining mechanism. In the former case the maximum occurs at 213°K as shown in Fig. 14; in the latter case, the maximum occurs at 203°K as shown in Fig. 15. Because the experimental maximum for the faster rate of heating occurs at 208°K, it would appear that a mixture of monomolecular and bimolecular kinetics are involved. The simultaneous occurrence of photo-conductivity and luminescence favors at least a small bimolecular contribution. However, the shape of the initial portion of the experimental glow curve and the greater likelihood that an electron remains most of the time in a metastable state rather than in the conduction band favors an almost-exclusively monomolecular mechanism.

Having fairly conclusively established that the low temperature peak of the glow curve for ZnS:Cu is caused by a metastable state emptying by predominantly monomolecular kinetics, the remainder of the glow curve can now be analyzed. It is assumed that the remainder of the electron traps also empty by predominantly monomolecular kinetics, that all the traps empty independently, and that retrapping is negligible. Starting with the peak at the low temperature,

each metastable state is treated and subtracted from the experimental curve as shown in Fig. 16. The explicit expression for the specific rate constants and the relative numbers of electrons in the various metastable states are shown in Fig. 16. Summing up the emission contributions, the original glow curve is compared in Fig. 17 with the calculated expression:

$$I=\sum_i \alpha n_{i0} k_i' \exp\left(-\frac{1}{dT/dt}\int_{T_0}^{T} k_i' dT\right). \quad (5\text{-}8)$$

It is clear that, although the experimental and theoretical curves do not coincide precisely, sufficient recalculations would result in complete agreement.

The specific rate constants for the release of electrons from metastable states and the atomic rearrangements are characterized by low frequency factors and heats of activation between 2 and 15 kcal. The low values of the non-exponential part of the specific rate constant, between one and 10^8 per second, can be explained by two effects: Although, as shown in our model in Fig. 3, there is a rearrangement of the center during the release of an electron from a metastable state, it is primarily the electron that undergoes a change of state. Electrons are prone to "tunnel" through potential barriers or at least to pass through the barriers below their maxima. Such a process would have a smaller transmission probability than ordinary chemical reactions. An additional factor that reduces the frequency factor associated with the release of electrons from metastable levels is that the electron on surmounting or passing through the potential barrier undergoes some change in multiplicity. In other words, as shown in Fig. 3 the metastable and emitting states have somewhat different multiplicities, so that, in passing over or through the barrier an alteration of electron spin must occur. This is to some extent forbidden, so that a low transmission coefficient results.[22] Incidentally, it should be pointed out that the presence of two or more metastable states that are emptied by practically the same specific rate constants would, if not resolved, produce the same effect as a single metastable state with a smaller heat of activation and a smaller frequency coefficient. This substantiates the argument that the slowest linear rates of heating that give measurable emission intensities are desired in order to resolve individual metastable levels.

At constant temperature, the phosphorescence of luminescent materials having a number of discrete metastable states, such as the phosphors exhibiting glow curves of the type shown in Fig. 13, should proceed according to a summation of exponential functions:

$$I=\sum_i \alpha n_{i0} k_i' \exp(-k_i' t). \quad (5\text{-}9)$$

An expression of this type for approximately equally weighted metastable states, resulting in a fairly uniform distribution of specific rate constants, provides a markedly concave-upward afterglow that can be approximated by a hyperbolic function. In addition, since each specific rate constant in the summation has its own temperature dependence, the total phosphorescence curve will have a small irregular temperature dependence.

VI. CONCLUDING REMARKS

The purpose of this paper is to demonstrate that apparently unrelated diverse properties of luminescent solids can be quantitatively correlated in terms of a simple configuration coordinate diagram. In addition, deduction from the model shown in Fig. 3 indicates the direction that future experimental work should take.

For example, the lifetimes of the excited states provide some indication of the extent that the

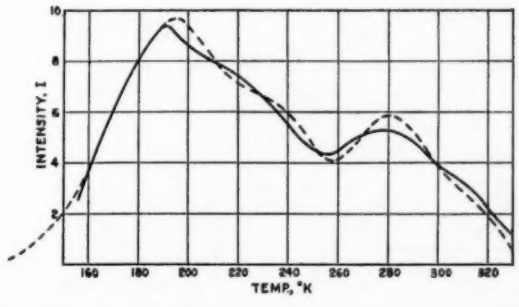

FIG. 17. — experimental "glow curve." -- calculated "glow curve."

$$I=\Sigma_i \alpha n_{i0} k_i' \exp\left(-\frac{1}{dT/dt}\int_{T_0}^{T} k_i' dT\right).$$

[22] C. Zener, Proc. Roy. Soc. **137**, 696 (1932); **140**, 660 (1933).

transitions are forbidden, but to determine the precise differences in multiplicities of the states involved, magnetic susceptibility measurements during different stages of excitation are necessary. ZnF_2:Mn is particularly well-adapted to such an experimental project because of its capacity to be excited to high concentrations of excited centers and to be evaporated and condensed in a vacuum to form thin transparent deposits without the loss of high luminescent efficiency.[23]

The absolute energies of the various excited states are needed to describe the model completely. Photo-conductivity measurements simultaneous with luminescent measurements will reveal the energies of the conducting excited states. Ultraviolet absorption data coupled with photo-conductivity data will reveal the non-conducting "exciton" states. Infra-red stimulation and quenching measurements on excited phosphors provide the optical depths of the metastable states. This information can be correlated with the thermal depths of the metastable states as obtained from the temperature dependence of phosphorescence and from glow data. For example, the heat of activation for release from the metastable state in the case of $(Zn, Mg)F_2$:Mn is about 4.5 kcal. indicating that this phosphor should be stimulated at $<6.3\mu$ if a radiationless process does not interfere.

A useful test of the applicability of the model would be an attempt to correlate for infra-red-sensitive phosphors diverse properties on the basis of a configuration coordinate diagram. With such phosphors some of the electron traps are very deep, and so, pronounced temperature dependence of efficiency is predicted.

This paper does not touch on the efficient mechanism for the transfer of energy from the lattice to the activator with corpuscular excitation. An analysis of this stage of the luminescent process depends on a knowledge of the mechanism of excitation and de-excitation of the activator. Based on the analysis of excitation and de-excitation phenomena presented in this paper, a semi-empirical treatment of the transfer of energy to the activator might be attempted by utilizing experimental results obtained with different types of excitation.

The authors are particularly indebted to Dr. R. E. Shrader of the RCA Laboratories for advice on the experimental work, for the use of apparatus, and in some instances for actual measurements. One of the authors (F.E.W.) would like to express his appreciation to Dr. V. K. Zworykin, Director of Electronic Research of the RCA Laboratories, for permitting him to work independently during this project.

[23] F. E. Williams, J. Opt. Soc. Am. **36**, 353 (1946).

Dependence of Bond Order and of Bond Energy Upon Bond Length

WALTER GORDY
Department of Physics, Duke University, Durham, North Carolina
(Received March 10, 1947)

A simple inverse square relation of the form,

$$N=aR^{-2}+b,$$

(where N is the bond order, R is the bond length, and a and b are constants characteristic of any given pair of atoms) has been found to agree satisfactorily with the available values for bond orders. For CC bonds a and b are found to have the values 6.80 and -1.71, respectively; for CN they are 6.48 and -2.00; for CO they are 5.75 and -1.85. The available data on bond energies suggest a relation of the same form,

$$E=lR^{-2}+m,$$

between bond energy E and bond length R, where l and m represent the characteristic constants of a given atomic pair.

RELATION BETWEEN BOND ORDER AND BOND LENGTH

IT is well known that the length of a bond depends upon its bond order, that a double bond is shorter than a single bond between the same atoms, and that a triple bond is shorter than a double one.

Many researchers have plotted curves to demonstrate that the bond order of CC bonds in hydrocarbons varies uniformly with bond length.[1] Using the recent bond order values determined according to the definition of bond order given by Coulson,[2] I have sought to determine the form of the equation which best represents this relationship, and to test the application of the relation to bonds between atoms other than carbon.

The simple inverse square relation of the form

$$N=aR^{-2}+b \tag{1}$$

seems to agree satisfactorily with the available data. N and R are the bond order and bond length, respectively; a and b are constants characteristic of a given atomic pair. Figure 1 shows a plot of N against $1/R^2$ for CC bonds as well as for BB, NN, and OO bonds. Table I gives sources of the data used. Figure 2 gives a similar plot for bonds between unlike atoms, CN and CO, using the constants listed in Table II. The fractional bond orders are less accurate for the latter bonds than for the CC bonds, as they were determined from an empirical relation of bond order expressed as a function of other bond constants.[3] Nevertheless, the linearity of the relation is evident.

Because experimental values are unavailable I have used the Schomaker-Stevenson rule,[4]

$$R_{AB}=r_A+r_B-\beta|x_A-x_B|,$$

[1] L. Pauling, L. O. Brockway, and H. Y. Beach, J. Am. Chem. Soc. **57**, 2705 (1935); J. J. Fox and A. E. Martin, J. Chem. Soc. 2106 (1938); J. E. Lennard-Jones and C. A. Coulson, Trans. Faraday Soc. **35**, 811 (1939); R. S. Mulliken, C. A. Rieke, and W. G. Brown, J. Am. Chem. Soc. **63**, 41 (1941).

[2] C. A. Coulson, Proc. Roy. Soc. **A169**, 413 (1939). To illustrate Coulson's definition of bond order, suppose that a given electron contributes to all the bonds in the molecule and that its wave function is satisfactorily approximated by a linear combination of the atomic wave functions,

$$\psi=a_1\psi_1+a_2\psi_2\cdots a_k\psi_k,$$

where the coefficients a_1, a_2, etc., are thus normalized

$$a_1^2+a_2^2\cdots a_k^2=1.$$

The contribution of this electron to a bond $r-s$, according to Coulson's definition, is the product $a_r a_s$, of the normalized coefficients in the above equation. The total order of the bond is then

$$N=1+p=1+\sum_n a_r^{(n)}a_s^{(n)},$$

where the summation is taken over all the mobile, or migrating electrons. The unit value here represents the contribution of the σ electrons which are regarded as localized in the given bond.

W. G. Penney (Proc. Roy. Soc. **A158**, 318 (1937)) has given a treatment based on the electron-pair theory which yields results in good agreement with those of Coulson. The fractional "bond order" as defined by Penney and Coulson differs somewhat from the fractional "bond character" used by Pauling (*Nature of the Chemical Bond*, Cornell University Press, Ithaca, New York, 1939). For a discussion of this difference see the paper by Penney referred to above and that by Mulliken, Rieke, and Brown, reference 1.

[3] W. Gordy, J. Chem. Phys. **14**, 305 (1946).

[4] V. Schomaker and D. P. Stevenson, J. Am. Chem. Soc. **63**, 37 (1941).

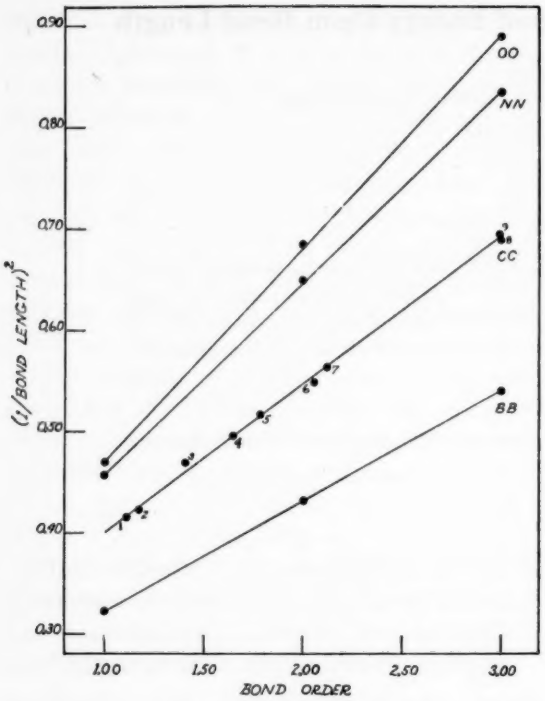

FIG. 1. Plots of bond order *versus* (1/bond length)², from the data given in Table I. The points on the CC curve are for bonds in (1) ethane, (2) propylene, (3) butadiene, (4) graphite, (5) benzene, (6) butadiene, (7) ethylene, (8) acetylene, (9) methyl acetylene.

to determine the lengths of the pure bonds plotted in Fig. 3. The covalent radii values, r_A and r_B, also the electro-negativities, x_A and x_B, are the revised values listed by the author.[5] For single bonds the constant β was determined by Schomaker and Stevenson as 0.09, and for double bonds by the author[5] as 0.06. There are not enough pure triple bonds[6] between unlike atoms to determine the value of β for them in the same way, though from a comparison with the values for single and double bonds it would be expected to be about 0.03 or 0.04. The distances for pure CO and CN triple bonds can be determined from the curves in Fig. 2, and the constant β for triple bonds estimated from them. The value determined in this way is 0.04, and this value is used to compute the triple bond lengths plotted in Fig. 3. Though this does not provide a direct test, the agreement is seen to be very good.

[5] W. Gordy, J. Chem. Phys. **15**, 81 (1947).

[6] There is some evidence that the bond order of the PN bond, also that for the CN bond in HCN, is less than 3. See Fig. 2, also reference 3.

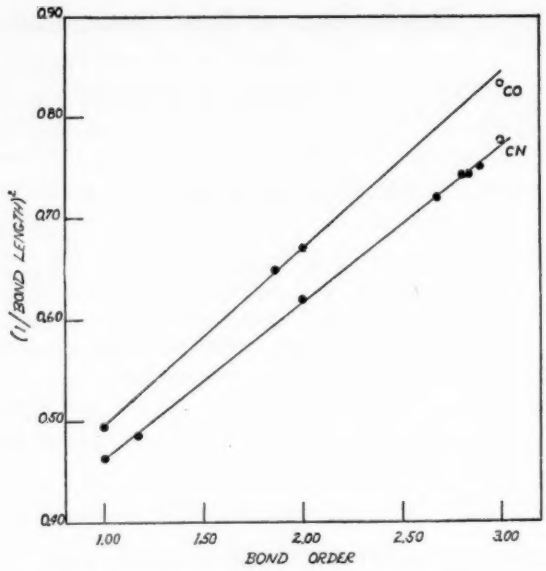

FIG. 2. Plots of bond order *versus* (1/bond length)² for CO and CN bonds, from data listed in Table II. Open circles are for "ideal" triple bonds.

A linear relationship is likewise found between N and $1/R^2$ for single, triple, and double bonds when the sum of the covalent radii as given by

TABLE I.

Compound	Link	Bond order	Bond length
Ideal link	BB	1.00	(1.76)[b]A
Ideal link	BB	2.00	(1.52)[b]
Ideal link	BB	3.00	(1.36)[b]
Ethane	CC	1.118[a]	1.55[c]
Propylene	CC	1.17[a]	(1.54)[d]
Graphite	CC	1.65[a]	1.42[e]
Butadiene	CC	1.41[a]	1.46[f]
		2.06[a]	1.35[f]
Benzene	CC	1.77[a]	1.39[f]
Ethylene	CC	2.124[a]	1.330[g]
Methylacetylene	CC	2.986[a]	1.20[h]
Acetylene	CC	3.00[a]	1.204[i]
Urea hydrogen peroxide	OO	1.00	1.46[j]
Oxygen	OO	2.00	1.208[k]
Ideal link	OO	3.00	(1.06)[b]
Hydrazine	NN	1.00	1.47[l]
Azo-methane	NN	2.00	1.24[m]
Nitrogen	NN	3.00	1.095[k]

[a] From R. S. Mulliken, C. A. Rieke, and W. G. Brown, reference 1.
[b] Added covalent radii, W. Gordy, J. Chem. Phys. **15**, 81 (1947).
[c] L. Pauling and L. O. Brockway, J. Am. Chem. Soc. **59**, 1223 (1937).
[d] This distance, assumed from a comparison with the length of certain other CC bonds, may be slightly large. See Mulliken, Rieke, and Brown, reference 1.
[e] J. D. Bernal, Proc. Roy. Soc. **A106**, 749 (1924).
[f] V. Schomaker and L. Pauling, J. Am. Chem. Soc. **61**, 1769 (1939).
[g] E. H. Eyster, J. Chem. Phys. **6**, 580 (1939).
[h] L. Pauling, H. D. Springhill, and K. J. Palmer, reference 8.
[i] H. Verleger, Physik. Zeits. **38**, 83 (1937).
[j] C. Lu, E. W. Hughes, and P. A. Giguère, J. Am. Chem. Soc. **63**, 1507 (1941).
[k] G. Herzberg, *Molecular Spectra and Molecular Structure* (Prentice-Hall, Inc., New York, 1939), p. 483.
[l] Reference 4.
[m] L. R. Maxwell, J. Opt. Soc. Am. **30**, 374 (1940).

Pauling,[7] without the correction for ionic character, is used for the lengths. I have plotted such curves but do not show them here.

These incomplete tests indicate the applicability of relation (1) to a variety of bond types. There are exceptions. The effective single bond covalent radius of triple bonded carbon is about 0.03A shorter than that of a carbon bound only to single or double bonds.[8] Apparently this is caused by a greater contribution of the *s* orbital to the single bond of the former. For this reason the relation is inapplicable to CC single bonds in methyl acetylene, diacetylene, etc. However, if the observed O−C length in methyl acetylene is increased by 0.03A and that in diacetylene by 0.06A to adjust for this abnormality, the rule gives a satisfactory estimate of the bond orders.

For convenience in estimating bond orders the constants a and b for several bonds are listed in Table III. Bond orders of other links may be estimated from relation (1) in the forms:

$$N=\frac{R^{-2}-R_2^{-2}}{R_2^{-2}-R_1^{-2}}+2,$$

TABLE II.

Compound	Link	Bond order	Bond length
Methylamine	CN	1.00	1.47[b]
Methyl iso-cyanide	CN	1.17[a]	1.44[c]
Methyl iso-cyanide	CN	2.68[a]	1.18[c]
Methyl cyanide	CN	2.81[a]	1.16[d]
Ideal link	CN	2.00[a]	(1.27)[e]
Cyanogen	CN	2.82[a]	1.16[d]
Hydrogen cyanide	CN	2.89[a]	1.154[f]
Ideal link	CN	3.00	(1.132)[g]
Methyl ether	CO	1.00	1.42[h]
Formic acid (monomer)	CO	1.86[a]	1.24[i]
Acetaldehyde	CO	2.00	1.22[j]
Ideal link	CO	3.00	(1.096)[g]

[a] Computed from the relation $k=1.67N\left(\frac{x_Ax_B}{d^2_{AB}}\right)^{3/4}+0.30$. (See W. Gordy, reference 3. This reference also contains the force constant and electro-negativity values used in computing N, except the k_{CN} of cyanogen, which is 17.6.

[b] R. G. Owens and E. F. Barker, J. Chem. Phys. **8**, 229 (1940).

[c] W. Gordy and L. Pauling, J. Am. Chem. Soc. **64**, 2952 (1942).

[d] Reference g, Table I.

[e] Determined from the relation $d_{AB}=r_A+r_B-0.06|x_A-x_B|$. See W. Gordy, J. Chem. Phys. (to be published).

[f] H. Verleger, Physik. Zeits. **38**, 83 (1937).

[g] Determined by the relation: $d_{AB}=r_A+r_B-0.04|x_A-x_B|$.

[h] Reference *l*, Table I.

[i] J. Karle and L. O. Brockway, J. Am. Chem. Soc. **66**, 574 (1944).

[j] D. P. Stevenson, H. D. Burnham, and V. Schomaker, J. Am. Chem. Soc. **61**, 2643 (1939).

[7] L. Pauling, *Nature of the Chemical Bond* (Cornell University Press, Ithaca, New York, 1939), p. 154.

[8] L. Pauling, H. D. Springall, and K. J. Palmer, J. Am. Chem. Soc. **61**, 927 (1939); Mulliken, Rieke, and Brown, reference 1.

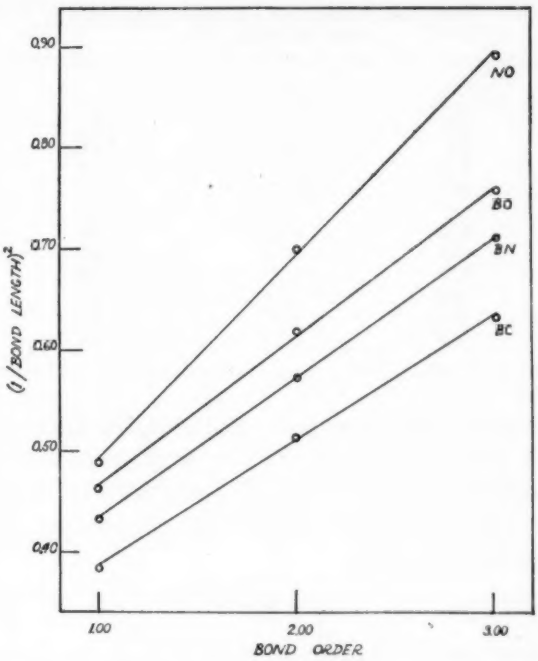

FIG. 3. Plots of bond order *versus* (1/bond length)² for pure bonds with lengths determined by: $R_{AB}=r_A+r_B-\beta|x_A-x_B|$.

$$=\frac{2R^{-2}-R_1^{-2}}{R_3^{-2}-R_1^{-2}}+1,$$

$$=\frac{R^{-2}-R_2^{-2}}{R_3^{-2}=R_2^{-2}},$$

where R is the length of any bond whose order is N, and where R_1, R_2, R_3 are the single, double, and triple bond lengths between the same atomic pair.

Table IV lists some bond orders predicted with the relation using the constants a and b given in Table III. These in turn are used in estimating the bond force constants which are listed in the last column.

RELATION BETWEEN BOND ENERGY AND BOND LENGTH

With the Coulson definition of bond order[2] it can be shown[9] that

$$E=pE_2+(1-p)E_1, \qquad (2)$$

where E is the energy of the bond whose mobile order is p and where E_1 and E_2 are the energies of

[9] J. E. Lennard-Jones and C. A. Coulson, reference 1.

TABLE III. Constants for computing bond order with Eq. (1).

Link	a	b
BB	9.12	−1.94
BC	8.05	−2.11
BN	7.15	−2.10
BO	6.75	−2.14
CC	6.80	−1.71
CN	6.48	−2.00
CO	5.75	−1.85
CS	11.9	−2.59
NN	5.28	−1.41
NO	4.98	−1.45
OO	4.73	−1.22

the pure single and pure double bonds between the same atoms. Since the contribution to the bond order of the localized σ-electrons is unity, the total bond order N is $(1+p)$. Hence, Eq. (2) may be written as

$$E=cN+d \tag{3}$$

where $c=E_2-E_1$ and where $d=2E_1-E_2$. From Eqs. (1) and (3) it follows that

$$E=lR^{-2}+m, \tag{4}$$

where l and m are constants characteristic of a given pair of atoms. If l and m are expressed in terms of the lengths and energies of pure bonds, Eq. (4) becomes

$$E=\frac{R^{-2}-R_2^{-2}}{R_2^{-2}-R_1^{-2}}(E_2-E_1)+E_2,$$

$$=\frac{R^{-2}-R_1^{-2}}{R_3^{-2}-R_1^{-2}}(E_3-E_1)+E_1,$$

$$=\frac{R^{-2}-R_2^{-2}}{R_3^{-2}-R_2^{-2}}(E_3-E_2)+E_2,$$

where the subscripts 1, 2, and 3 refer to pure single, pure double, and pure triple bonds respectively.

Because of the incompleteness of and the uncertainties in the available data on bond energies no very satisfactory test of Eq. (4) is possible at this time. The principal difficulty arises from the uncertainty of all bond energy values of hydrocarbons which is caused by the widely conflicting values obtained by different methods for the heat of sublimation of carbon.[10]

[10] H. A. Skinner, Trans. Faraday Soc. **41**, 645 (1945).

Another difficulty is the fact that energies of like links in different molecules are not equal because of the influence of the different environments. For example, the CH bonds of methane and of acetylene are not of equivalent energy, though in computing the energy of the CC bond of acetylene their equivalence is usually assumed.

In correcting for differences in energy values for CH bonds in different molecules Skinner[10] assumes that the bond energy varies linearly with bond distance; he used the covalent radii additivity rule and the arithmetic mean postulate for bond energies to determine the constants of an ideal C−H link used to establish the slope of the line. The energy difference of CH bonds estimated in this manner may be too large. Fox and Martin[1] showed that this energy difference is approximately $\frac{1}{2}k(\Delta R)$, where ΔR is the difference

TABLE IV. Some predicted bond orders and bond-stretching force constants in resonating structures.

Compound	Link	Bond length	Bond order[g]	Force constant[h] dynes/cm ×10⁻⁵
Urea	CN	1.37[a]	1.45	7.1
	CO	1.25[a]	1.83	11
Glycene	CC	1.52[b]	1.23	4.8
	CN	1.39[b]	1.36	6.7
	CO	1.27[b]	1.72	10
	CO	1.25[b]	1.83	11
Acetamide	CC	1.51[c]	1.27	4.9
	CN	1.38[c]	1.40	6.9
	CO	1.28[c]	1.65	10
Pyridine	CC	1.39[d]	1.81	7.8
	CN	1.37[d]	1.45	7.1
Pyrrole	CC	1.44[d]	1.57	6.5
	CC	1.35[d]	2.03	9.1
	CN	1.42[d]	1.21	5.8
Furan	CC	1.46[d]	1.48	6.0
	CC	1.35[d]	2.03	9.1
	CO	1.41[d]	1.04	5.6
Thiophene	CC	1.44[d]	1.57	6.5
	CC	1.35[d]	2.03	9.1
	CS	1.74[d]	1.36	4.3
Thioacetic acid	CO	1.24[e]	1.89	12
	CS	1.78[e]	1.17	3.6
Tetrachlorethylene	CC	1.38[f]	1.87	8.2

[a] R. W. G. Wyckoff and R. B. Corey, Zeits. f. Krist. **81**, 386 (1936).
[b] G. Albrecht and R. B. Corey, J. Am. Chem. Soc. **61**, 1087 (1939).
[c] F. Senti and D. Harker, J. Am. Chem. Soc. **62**, 2008 (1940).
[d] Reference f, Table I.
[e] W. Gordy, J. Chem. Phys. **14**, 560 (1946).
[f] Reference *l*, Table I.
[g] Predicted from Eq. (1).
[h] Predicted from the relation stated in reference a, Table II.

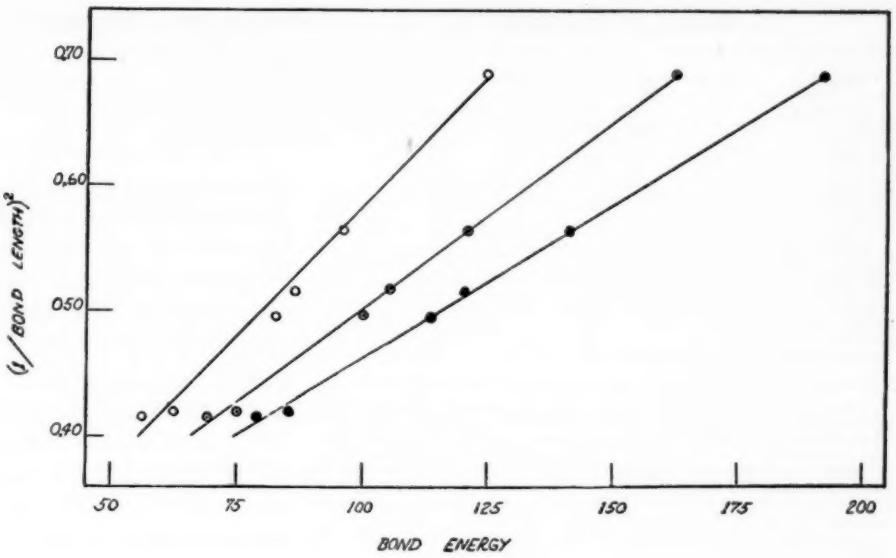

FIG. 4. Plots of bond energy *versus* (1/bond length)² for CC bonds, from bond energy values listed in Table V. The top curve is for $L_C=125$; the middle one, for $L_C=150$; and the bottom one, for $L_C=170$.

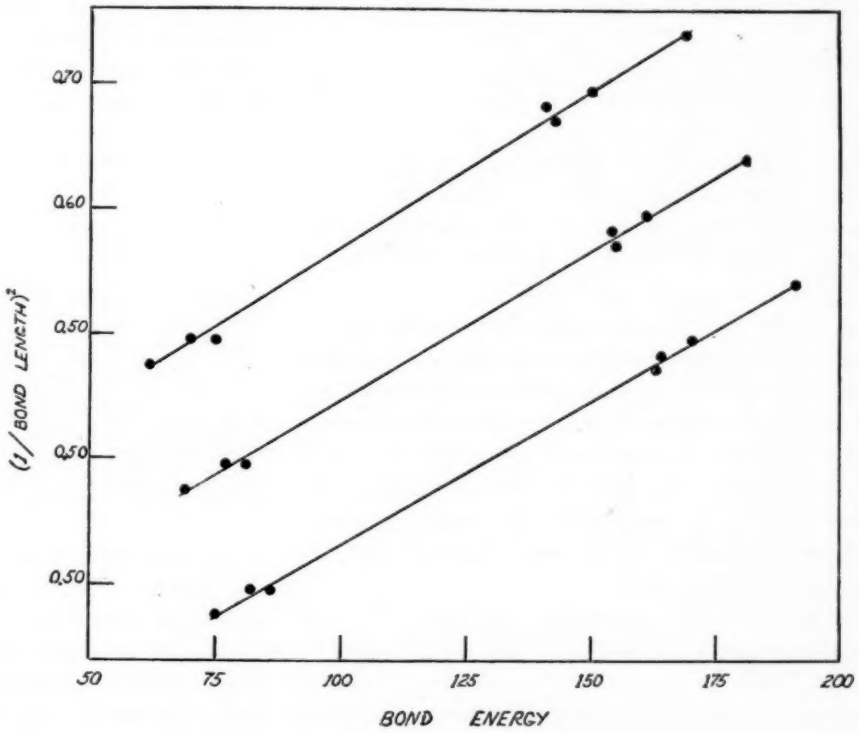

FIG. 5. Plots of bond energy *versus* (1/bond length)² for CO bonds, from bond energy values listed in Table V. The top curve is for $L_C=125$; the middle one, for $L_C=150$; and the bottom one, for $L_C=170$.

in the length of the CH bond and k the average force constant. With this method they estimate the energy difference between CH bonds having the greatest difference in length, $\Delta R=0.04$A as 600 cal. per g mole, whereas the Linnett method gives about 4000 cal. per g mole for this difference.

I have chosen to neglect the differences in the CH bonds in determining energies of other bonds in hydrocarbons listed in Tables V and VII and plotted in Figs. 4 and 5. Because of the uncertainty in the value for the heat of atomization of carbon I have plotted three sets of values corresponding to $L_C=125$, 150, and 170 kg cal. per mole.

Good agreement with relation (4) for both CO and CC bonds is obtained assuming the heat of atomization of carbon as either 150 or 170 kg cal.

TABLE V. Bond energies.[a]

Compound	For $L_C=125$[b]	For $L_C=150$[b]	For $L_C=170$[b]
CC bonds			
Ethane	56.2 kcal./mole	69 kcal./mole	79 kcal./mole
Diamond	62.5	75	85
Graphite	82.5	100	113
Benzene	86.5	105	120
Ethylene	95.8	121	141
Acetylene	124.5	162	192
CO bonds			
Carbon dioxide	169	181	191
Formaldehyde	141	154	164
Acetaldehyde	143	155	163
Glyoxal	150	161	170
Methyl ether	70	77	82
Methyl alcohol	75	81	86
Ethylene oxide	62	69	75

[a] The values for diamond, graphite, and benzene were obtained from Fox and Martin, reference 1. Other values were calculated from the heats of formation compiled by F. R. Bichowsky and F. D. Rossini, *The Thermochemistry of the Chemical Substances* (Reinhold Publishing Corporation, New York, 1936). In determining the CO bond energies of the molecules having CC links, the CC energies were obtained from relation (4) with the constants of Table VI. The CH energies were assumed to be the same as that for the CH in methane.

[b] L_C represents the value assumed for the heat of atomization of carbon.

TABLE VI. Constants for computing bond energies with Eq. (4).

	For $L_C=125$[a]		For $L_C=150$[a]		For $L_C=170$[a]	
Link	l	m	l	m	l	m
CC	240	− 40	335	− 68	410	− 90
CO	396	−125	420	−130	435	−131
CN	337	−109	380	−120	406	−126

[a] L_C represents the value assumed for the heat of atomization of carbon.

per mole, but for $L_C=125$ the agreement for certain CC bonds is not as close. Because relation (4) is not particularly sensitive to changes in L_C, it cannot be used to decide between these values. If the Skinner[10] corrections for deviation in CH bond energies are applied, the agreement with relation (4) is essentially unchanged, though slightly different values are obtained for the constants, l and m.

The diatomic molecules, CO and CC, not plotted, appear to be exceptions to relation (4).

In Table VI values for the constants l and m are given for CO, CC, and CN links. Those for CC and CO were determined from the graphs of Figs. 4 and 5. Those for CN were determined by the bonds of CH_3NH_2, HCN, CH_3CN, and CH_3NC. In Table VII the values of the heats of formation of these molecules as computed with the CN and CC bond energies determined by relation (4), are compared with the observed values.

Since this paper was prepared for publication the recent work of Long and Norrish[11] has appeared and shows that the conflicting values for the heat of sublimation of carbon, mentioned above, originate partly from the failure of some researchers to take into consideration the energy required to raise the carbon atoms from the ^3P-ground-state to the tetravalent ^5S-state in which it usually occurs when in chemical combination. The heat of sublimation, L_1, of carbon atoms into the ^3P-ground-state, they conclude, is near 125 kcal., while L_2, that for the heat of sublimation into free atoms in the ^5S state, is 190 ± 10 kcal. In computing from thermal data bond energy values (as distinct from dissociation energy values) of molecules involving tetravalent carbon, these observers state that it is correct to use the value L_2 rather than the value L_1, as is customary.

TABLE VII. Heats of formation.[a]

	$L_C=125$		$L_C=150$		$L_C=170$	
Compound	obs.[b]	calc.[c]	obs.[b]	calc.[c]	obs.[b]	calc.[c]
HCN	231	231	256	258	276	277
CH_3CN	471	472	521	525	561	566
CH_3NC	450	449	505	496	545	532
CH_3NH_2	475	477	500	504	520	525

[a] From atoms in gaseous state. L_C represents different values assumed for the heat of atomization of carbon.

[b] Determined from the Q_f values of Bichowsky and Rossini, reference a, Table V.

[c] The CN and CC bond energies were calculated with Eq. (4), using the parameter values listed in Table VI. The CH energies were assumed to be the same as that for the CH in methane.

Thus according to their interpretation, since all the bonds plotted above involve tetravalent carbon, it would seem that the proper value for L_C would be about 190 kcal., or L_2. Since this value is not far from one already plotted, $L_C=170$ kcal., an additional curve is not shown. The agreement is still within the possible error of the experimental data.

[11] L. H. Long and R. G. W. Norrish, Proc. Roy. Soc. **A187**, 337 (1946).

The Effect of High Mechanical Stress on Certain Solid Explosives

P. W. BRIDGMAN
The Physics Laboratories, Harvard University, Cambridge, Massachusetts

(Received March 13, 1947)

Eleven different solid explosives have been subjected at room temperature to stresses of the order of those which prevail in the detonating front. Two types of stress were applied. The first consisted of a hydrostatic pressure of 50,000 kg/cm², on which was superposed a shearing stress sufficient to produce shearing deformations of the order of 60 radians. The second type consisted of a hydrostatic pressure of 100,000 kg/cm², with a comparatively small superposed shearing deformation. Seven of the eleven explosives survived stress of the first type without detonation. Only four of the explosives were subjected to the second type of stress; three of these survived without detonation. It is probable that in those cases where detonation occurred secondary effects were responsible, such as striking of sparks by fractured fragments of steel. The general conclusion is drawn that stresses of these magnitudes, without the cooperation of high temperature, cannot be counted on to produce detonation.

Incidentally it was found that yellow ammonium picrate is transformed irreversibly to the red form by the first type of stress. Values were obtained for the plastic flow stress as a function of hydrostatic pressure. The strength increases approximately linearly with pressure.

IN November, 1940, when it seemed probable that the United States would be eventually drawn into the war, I made, at the request of Professor G. B. Kistiakowski, some orienting experiments on the effect of high mechanical stress on various solid explosives. These experiments have not yet been published, and it is perhaps worth while to put a brief account of them in permanent form. The immediate problem was to determine whether detonation could be initiated by the action of stresses alone without the cooperation of high temperature. The particular point of the experiments was that it was possible to reach, in the cold, impressed stresses of the same order of magnitude as those which are supposed to prevail in the detonating front. The application of the results to the ultimate problem of determining the conditions of detonation in the detonating front is obvious.

The following explosives which were provided by Professor Kistiakowski were investigated. Alpha-, beta-, and gamma-T.N.T., alpha- and beta-nitroguanidine, picric acid, ammonium picrate (yellow and red forms), tetryl, cyclonite, and P.E.T.N. (penta-erythritol-tetra-nitrate).

Two types of test were applied. In the first, the explosive was exposed to an average hydrostatic pressure of 50,000 kg/cm², on which was superposed a shearing stress sufficient to produce a drastic shearing deformation of the order of magnitude of 60 radians. This shearing deformation might be several times repeated, with reversal of direction. In the second type of test, average hydrostatic pressure up to 100,000 kg/cm² was applied, but without explicitly applied superposed shearing deformation. The conditions were such, however, that a comparatively small amount of plastic shearing deformation was the incidental accompaniment of the pressure.

The general arrangements for the first type of test were exactly like those which I have previously employed in determining the effect of combined pressure and shear on a large number of substances.[1] The material to be tested is in the

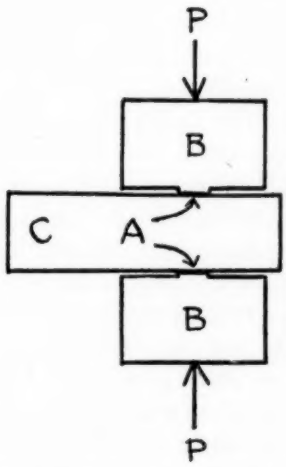

FIG. 1. General scheme of an apparatus for combining shearing stress with pressure.

[1] P. W. Bridgman, Proc. Am. Acad. 71, 387–460, 1937.

FIG. 2. Scale drawing of part of the "piston," modified so as to minimize the possibility of detachment of shearing wedges at the edges.

form of two thin disks, A, placed between the hardened rectangular steel "anvil" block C, and short "pistons," which are cylindrical bosses 0.250 inches in diameter on the cylindrical blocks B. The blocks B are squeezed together in a hydraulic press until an explosion occurs, or until the desired maximum average compressive stress of 50,000 kg/cm² is reached. This application of pressure is accompanied by lateral extrusion of the material of the disks until equilibrium thickness is attained, which is of the order of a few thousandths of an inch. If the desired pressure maximum was successfully reached without explosion, pressure was then released to zero, and then reapplied in steps of 10,000 kg/cm², shearing stress now being applied by rotating the block C between B and B after each pressure increment, and while pressure was maintained constant by a dead weight gauge. The rotation was back and forth through an angle of about 60°. A rotation of 60° gives a shearing deformation on the periphery of a disk 0.250 inch in diameter and 0.002 inch thick (an average thickness) of 65 radians. Rotation was repeated after each pressure increment until detonation occurred or the maximum was reached. The rotating force was also always measured, so that the data exist for a determination of the shearing strength of these materials as a function of hydrostatic pressure.

There were two subdivisions of the first type of test. In the first, exactly the same dimensions of the various steel parts were used as in my previous work. The bosses which constituted the pistons had a height of 0.030 inch. With these dimensions all eleven explosives were tested. All but one of these (red ammonium picrate) survived the initial application of 50,000 kg/cm² without explosion, but only two, alpha- and beta-nitroguanidine, survived the subsequent combination of shearing and pressure, the explosion occurring in most cases at the top pressures. Several repetitions with alpha-T.N.T. under ostensibly identical conditions did not lead to consistent results. The most probable explanation of the capricious results appeared to be that, under the shearing stress, minute steel wedges sheared off the edges of the pistons, struck a spark and so initiated the explosion by the high temperature.

In order to eliminate this factor, the second subdivision of the first type of experiment was made. In this the pistons were redesigned to have a height of only 0.009 inch and with a 45° bevel, as indicated in the figure, in order to eliminate minute shearing failures of the steel at the edges. With this modified arrangement shearing was applied at 50,000 kg/cm² to alpha-T.N.T., tetryl, cyclonite, picric acid, and P.E.T.N. The other explosives were not tried in the modified arrangement, but repeat experiments were made with alpha-T.N.T. and P.E.T.N. The first attempts with these two resulted in explosions and the second attempts did not. The other three successfully withstood the maximum stress without explosion on the first attempt. It is difficult to know whether the capriciousness in the results is to be ascribed to the explosives themselves, or is the result of secondary factors. The existence of such factors is to be recognized. If, for instance, the film of explosive between piston and anvil gets so thin as to allow the steel parts to rub directly on each other, splinters of steel might be detached with high local temperatures. It did indeed seem to be true that explosions occurred in a number of cases when the initial quantity of explosive was less than normal, and therefore the disk unusually thin.

The maximum shearing stress at 50,000 kg/cm² has thus been applied without explosion to seven of the eleven explosives, namely, alpha-T.N.T., tetryl, cyclonite, picric acid, P.E.T.N., and alpha- and beta-nitroguanidine. In view of the capricious character of the results and the fact that one could never have absolute assurance that no sparks were struck, it did not seem worth while to continue to repeat the attempts with the other four in the effort to reach maximum

stress without explosion. In my opinion the probability is that this would have been possible.

The explosions which did occur varied greatly in character; some of them were detonations of extraordinary violence, and some were mild decompositions with a puff of black smoke and a sooty residue.

The yellow ammonium picrate was found to be irreversibly transformed into the red form.

The shearing strength of all these explosives is approximately a linear function of pressure, increasing, if anything, a little more rapidly than linearly with pressure. This is, in general, characteristic of organic substances and in sharp contrast to the metals, the shearing strength of which increases less rapidly than linearly with pressure. Within the limits of repeatability, there is no significant variation in the shearing strength of the different explosives, but all are contained within a range of ± 30 percent. In this range the largest shearing strength was shown by alpha-T.N.T. and the smallest by beta-T.N.T. Under a mean hydrostatic pressure of 50,000 kg/cm^2 the average shearing strength of all these explosives was close to 4000 kg/cm^2. This is not far from the shearing strength of metallic copper at the same pressure. At lower pressures, the shearing strength of copper is, of course, higher than that of the explosives.

In the second type of test Carboloy pistons, pressed directly against each other without the intermediate anvil block, were used. It was not possible in this type of test to apply shearing explicitly, but a small amount of shearing was the incidental accompaniment of the lateral extrusion of the wafer of explosive from between the pistons. The Carboloy pistons were only 0.125 inch in diameter on the face instead of 0.250 as were the steel pistons, and their average height was 0.006 inch. The advantage of the Carboloy over the steel is that much greater pressures can be applied. In preliminary tests a mean pressure of over 150,000 kg/cm^2 on the face of the pistons was applied without completely destructive failure. The first tests with explosives were made with alpha-T.N.T. On the first attempt, there was an explosion with black residue on reaching 57,000 kg/cm^2. On the second attempt there was a similar explosion with black residue on reaching 49,000 kg/cm^2. Neither of these explosions was of sufficient violence to do any perceptible damage to the pistons. On the third attempt, pressure was increased much more slowly than on the first two, waiting several minutes after every increment of 8000. On this third attempt a maximum of 77,000 was reached with no explosion and no apparent alteration in the explosive. The fourth attempt, also with slow application of pressure, reached the full 100,000 kg/cm^2 with no explosion. Similar tests with slow increase of pressure were then made on ammonium picrate (yellow) and alpha-nitroguanidine, reaching the full 100,000 without explosion. Picric acid was then tested. The increase of pressure was not made as slowly as with the three preceding. On reaching 93,000 kg/cm^2 there was an explosion, with black residue, of sufficient violence to destroy the pistons. Since the preparation of new pistons was a matter of some difficulty, the experiment was terminated at this point.

In view of the various possible secondary effects, such as minute local fractures in the metal parts and local elevations of temperature, it would seem legitimate to ascribe a greater significance to the reaching of a given stress condition without explosion than to explosions on other occasions produced by the same or lower stresses. The general conclusion of these experiments would seem to be that mechanical stresses of themselves of the magnitudes of those reached in these experiments cannot be counted on to initiate explosion in explosives of the type of those investigated.

THE JOURNAL OF CHEMICAL PHYSICS VOLUME 15, NUMBER 5 MAY, 1947

On the Behavior of Pure Substances Near the Critical Point

O. K. RICE[1]
University of North Carolina, Chapel Hill, North Carolina
(Received February 25, 1947)

It has been suggested several times that the phenomena of condensation could be understood by considering the vapor as a system in which molecules are associating into clusters, these obeying the ordinary laws of equilibrium. One can also consider the liquid as a system in which bubbles of vapor are forming. The present paper attempts to apply these ideas to phenomena occurring in the neighborhood of the critical point. Only thermodynamic methods are used, in conjunction with some general assumptions concerning the properties of the molecules involved. Some aspects of the surface tension of the liquid near the critical point have been considered in some detail. The highest temperature T_m at which a meniscus can exist is assumed to be the temperature at which the surface tension vanishes at the same time that the condition for equilibrium between liquid and vapor phases is fulfilled. It is concluded that the pressure-volume isotherm at T_m has a finite horizontal region, corresponding to the squeezing out of surface when the surface tension is zero. The slope of the isotherm at T_m in the vapor region outside the horizontal portion is closely related to the slope in the liquid region just to the other side of the horizontal part; these slopes approach zero as the flat part is approached. Above T_m there is still a process which may be called condensation, but no horizontal part to the isotherms. This is in contradiction to conclusions reached by Mayer and Harrison on the basis of their statistical theory of condensation, but is apparently not in real contradiction to the theory.

1. INTRODUCTION

OVER a considerable period of years data have been accumulating which indicate that the phenomena occurring in the neighborhood of the critical point of a pure substance are more complicated than expected from the simple van der Waals theory. This theory would lead one to expect a roughly parabolic shape for the coexistence curve in a pressure-volume diagram, which encloses those sections of the isotherms over which a distinct meniscus can be observed. There is, however, much evidence that this curve actually has a finite horizontal (constant-pressure) portion at the top, instead of being rounded.[2] Some experiments also indicate a tendency for layers of different density to persist at temperatures above that at which the meniscus disappears.[3] Hein stated that, after raising the temperature to obtain density equalization, these density differences would reappear on cooling, though the temperature remained above the critical temperature, which might lead one to believe that they represented equilibrium states. However, Maass and his co-workers said this would not occur, and there is plenty of evidence that complete equilibrium is not attained under these conditions. More recent evidence[4] indicates that a single completely homogeneous phase is obtained either by shaking or by long standing.

It was suggested by Mayer and Harrison,[5] as a result of a statistical mechanical theory of condensation, that the pressure-volume isotherms continue to have a horizontal portion at temperatures slightly above the temperature T_m at which the meniscus disappears, and that the true critical temperature is the temperature above which such a horizontal region does not occur. According to the theory, the isotherms in this region close to the critical temperature should differ from those below the temperature at which the meniscus disappears, in that there should be no break in the slope of the curve as the horizontal portions are approached.

The best experimental data on these properties of the isotherms are not entirely unequivocal. McIntosh, Dacey, and Maass[6] obtained isotherms for ethylene, and the curves which they fitted to their experimental points showed horizontal

[1] On leave 1946–47 at the Clinton Laboratories, Oak Ridge, Tennessee.
[2] See, e.g., E. Schröer, Zeits. f. physik. Chemie **A129**, 79 (1927); **A140**, 241, 379 (1929); S. G. Mason, S. N. Naldrett, and O. Maass, Can. J. Research **B18**, 103 (1940); S. N. Naldrett and O. Maass, *ibid.* **B18**, 118 (1940).
[3] See, e.g., P. Hein, Zeits. f. physik. Chemie **86**, 385 (1914); J. S. Tapp, E. W. R. Steacie, and O. Maass, Can. J. Research **9**, 217 (1933); C. A. Winkler and O. Maass, *ibid.* **9**, 613 (1933). For reviews see A. L. Clark, Chem. Rev. **23**, 1 (1938); O. Maass, *ibid.* **23**, 17 (1938).
[4] Page 120 of article by Naldrett and Maass, Reference 2.
[5] J. E. Mayer and S. F. Harrison, J. Chem. Phys. **6**, 87, 101 (1938).
[6] R. L. McIntosh, J. R. Dacey, and O. Maass, Can. J. Research **B17**, 206, 241 (1939).

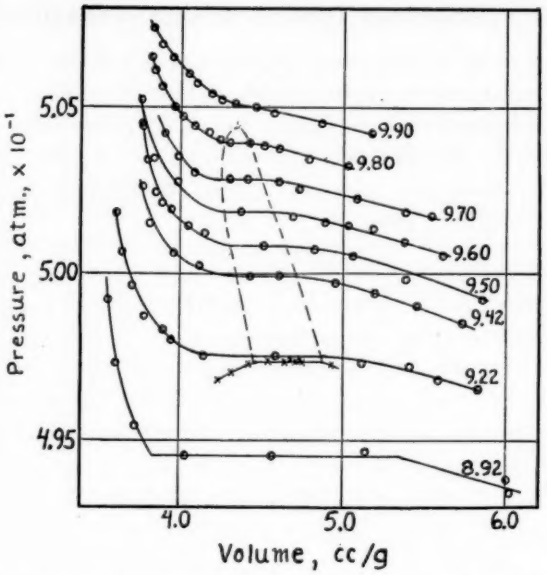

FIG. 1. Isotherms for ethylene, at temperatures indicated on curves, assuming horizontal portions above T_m, as enclosed by the broken line. The crosses are from data of Naldrett and Maass obtained by finding the temperature at which the meniscus disappeared at a fixed specific volume. These have been placed on the pressure-volume diagram by interpolation.

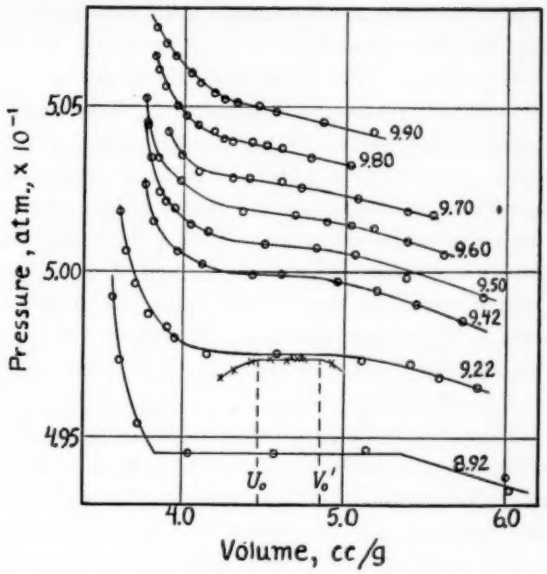

FIG. 2. Isotherms for ethylene, at temperatures indicated on curves, assuming no horizontal portions above T_m. For significance of the crosses see Fig. 1. For U_0 and V_0' see Section 5.

sections. A sudden change of slope was shown at the ends of the horizontal portions. The data, however, do not necessarily demand a sudden change in slope nor even, for that matter, a horizontal portion in the isotherms. In Figs. 1 and 2, we have replotted the data of McIntosh, Dacey, and Maass. In Fig. 1 we have drawn in a set of isotherms showing horizontal sections but no abrupt changes in slope. In Fig. 2 we have drawn in a set of isotherms showing no horizontal sections. Either one of these sets of curves agrees with the experimental results within the limits of experimental error. It is true that the positions of the points on a number of the isotherms seem to indicate a decrease in slope near the critical volume, though it is within the experimental error. On the other hand, as noted before, Naldrett and Maass[4] made the observation that a system, slightly above the temperature at which a meniscus can be observed but still showing layers of different density, finally settles down to a completely homogeneous state. This shows that the two layers, which presumably represent points along the "horizontal" portion of the isotherm, have different free energies; hence the isotherm cannot be exactly horizontal.

It may be mentioned that the isotherms for carbon dioxide, obtained by Michels, Blaisse, and Michels,[7] showed a slope distinctly different from zero only 0.15° above the critical temperature. The pressure measurements were exceedingly accurate, but the non-zero slope was attributed by Mayer and Streeter[8] to small traces of impurities. It is, of course, exceedingly difficult to be sure that the last traces of impurities have been eliminated. By obtaining samples of materials from different sources and purifying by different methods, it might be possible to show by the reproducibility of the data that the impurities have been reduced to a point where they make no further difference. Such a procedure has not as yet been carried out, but Michels, Blaisse, and Michels considered the purity of their material to be adequately confirmed by the fact that the isotherms below the critical point appear to be exactly horizontal. It is, indeed, not obvious that impurities should have more effect just above the critical temperature than just below it.

Mayer and Harrison's theory is highly mathe-

[7] A. Michels, B. Blaisse, and C. Michels, Proc. Roy. Soc. **A160**, 358 (1937). These authors did not observe the meniscus, but their results appear to indicate that the horizontal portion of the isotherm at T_m is of finite length.

[8] J. E. Mayer and S. F. Streeter, J. Chem. Phys. **7**, 1019 (1939).

matical, and the results depend upon assumptions regarding the behavior of certain integrals. These are exceedingly difficult to evaluate because, near the critical point the integrands have large numbers of positive and negative parts, which nearly cancel each other. Further, there are limitations on the range of validity of the theory, which will be discussed later. Under these circumstances it would be an advantage if the phenomena could be considered from a somewhat more pictorial point of view. It will be the purpose of this paper to present such a pictorial theory and to see to what extent the experimental results may be understood on such a basis. The method it is proposed to use is that of associating molecules. Some of the advantages of this method were pointed out by Band,[9] and a somewhat similar treatment was also given by Frenkel.[10] However, in the theory developed by Band the situation near the critical point is not very clear, and Frenkel did not attempt an application in this region. The critical phenomena will receive our particular attention. Actually our procedure will follow more closely one suggested earlier by N. and E. Rashevsky[11] in considering the phenomena exhibited by emulsions. This method is almost entirely thermodynamic, and no formidable mathematical formalism is required.

The work of Mayer and Harrison is based upon the theory of clusters first introduced by Ursell.[12] In this theory a cluster is a mathematical abstraction, which has some resemblance to, but is not identical with, an aggregation of molecules in the usual physical sense. In this paper, we shall deal with real physical clusters of molecules, and since there seems to be no other word which is as descriptive, we shall use the term "cluster" in this sense, occasionally using "aggregation" and "droplet" as synonyms. When we have occasion to refer to a cluster in the sense of Mayer or Ursell, we shall use a modifying term, as "mathematical cluster" or "abstract cluster."

[9] W. Band, J. Chem. Phys. **7**, 324, 927 (1939); T. P. Tseng, S. K. Feng, C. Cheng, and W. Band, *ibid.* **8**; 20 (1940); C. Cheng, T. P. Tseng, S. K. Feng, and W. Band, *ibid.* **9**, 123 (1941).

[10] J. Frenkel, J. Chem. Phys. **7**, 200, 538 (1939).

[11] N. Rashevsky and E. Rashevsky, Zeits. f. Physik **46**, 300 (1927).

[12] H. D. Ursell, Proc. Camb. Phil. Soc. **23**, 685 (1927); J. E. Mayer, J. Chem. Phys. **5**, 67 (1937).

2. ASSOCIATION THEORY OF CONDENSATION

Let us consider one mole of gas in volume V to consist of n_1 single molecules, n_2 pairs of molecules held together by cohesive forces (in simple cases van der Waals forces), n_3 triplets, $\cdots$, n_s clusters of s molecules each, $\cdots$, all in equilibrium with each other. Then

$$\Sigma_s\, sn_s = N \tag{1}$$

where N is Avogadro's number. We let the corresponding concentrations $(n_1/V, n_2/V, n_3/V, \cdots, n_s/V, \cdots)$ be designated as $c_1, c_2, c_3, \cdots, c_s, \cdots$ and the respective chemical potentials (referring to single clusters, rather than to moles of clusters) be denoted by $\mu_1, \mu_2, \mu_3, \cdots, \mu_s, \cdots$. Then, if the gas is sufficiently dilute so that the perfect gas laws may be considered valid

$$\mu_s = s\phi_s + kT \ln c_s, \tag{2}$$

where $s\phi_s$ is the value of μ_s when $c_s = 1$. In particular, of course, ϕ_1 is the value of μ_1 when $c_1 = 1$. To get an expression for ϕ_s we can consider the reaction

s single molecules $(c_1 = 1) \rightarrow$ cluster of s molecules $(c_s = 1)$

and define a quantity β by the equation

$$\beta = \phi_\infty - \phi_1. \tag{3}$$

β, then, is the free energy of condensation, per molecule, of single molecules at unit concentration to form a very large drop. The total free energy of the reactants in the reaction being considered is $s\phi_1$ and that of the products is $s\phi_s$. The reaction involved the condensation of $s-1$ molecules on one molecule, and the free energy would be $\beta(s-1)$, except for surface effects, which would be expected to add a term of the form $\gamma s^{\frac{2}{3}}$. The constant γ is related to, but not exactly equal to the surface tension, and the number of molecules at the surface of the cluster will be in general proportional to $s^{\frac{2}{3}}$. Still a further correction term, which we shall call ϵ_s will be needed to take care of the fact that this proportionality with $s^{\frac{2}{3}}$ will not hold for very small droplets. We thus get

$$s\phi_s = s\phi_1 + \beta(s-1) + \gamma s^{\frac{2}{3}} + \epsilon_s. \tag{4}$$

Substituting $s = 1$, since ϕ_s is then equal to ϕ_1, we see that

$$\epsilon_1 = -\gamma. \tag{5}$$

On the other hand,

$$\lim_{s\to\infty} \epsilon_s = 0. \tag{5a}$$

ϕ_1, β, γ, and ϵ_s will, of course, depend on the temperature.

The condition of equilibrium is that the total free energy F of the system should be a minimum. Hence

$$\delta F = \Sigma_s \mu_s \delta n_s = 0 \tag{6}$$

subject to the condition which follows from Eq. (1) that

$$\Sigma_s s\delta n_s = 0. \tag{7}$$

From Eqs. (6) and (7) we obtain

$$\mu_s + \alpha' s = 0 \tag{8}$$

where α' is a Lagrange multiplier. With Eqs. (2) and (4) this gives

$$c_s = \exp(\beta - \alpha s - \gamma s^{\frac{1}{3}} - \epsilon_s)/kT \tag{9}$$

where $\alpha = \phi_1 + \beta + \alpha'$. In particular, remembering Eq. (5)

$$c_1 = e^{(\beta-\alpha)/kT}, \tag{10}$$

α is determined by Eq. (1), or it may be considered to be determined by Eq. (10), all the other c_s being determined in terms of c_1.

Let us now consider the gas, starting from a highly expanded state, to be gradually compressed. Before compression, with V very large, c_1 will be very small. The quantities β and γ are fixed, so in order for Eq. (10) to hold it will be necessary for α to be large and positive. As V decreases, all c_s and, in particular, c_1 will increase; this means that α must decrease. Eventually α will become zero. If α becomes negative, the terms of Eq. (9) will ultimately increase with s, and as s increases indefinitely become infinite. It is thus seen that when α becomes zero, this is the signal for condensation; condensation saves α from becoming negative, and it can remain zero for the gas phase as the amount of the gas phase decreases. It will be observed that even when α becomes zero c_s will decrease fairly rapidly with s if γ is of reasonable magnitude because of the $\gamma s^{\frac{1}{3}}$ term, ϵ_s being only a correction term. The divergence of the series of c_s values, therefore, occurs suddenly as long as γ itself is positive. At the point of condensation we have

$$c_1 = e^{\beta/kT} \tag{11}$$

which, in view of the interpretation of β as the free energy of condensation of single molecules, is obviously the correct relationship. In fact, this is practically a truism; the interest of the method is in dealing with the phenomena near the critical point.

α may be interpreted as the difference in molecular free energy between the liquid and the vapor. We may build up the vapor, at constant temperature and pressure, by small additions of single unassociated molecules. Between the small additions we allow equilibrium between clusters to be reestablished; since we never depart appreciably from equilibrium the reestablishment of equilibrium takes place with no free energy change. Hence we may write for the free energy of the entire vapor

$$\begin{aligned} F = N\mu_1 &= N\phi_1 + NkT \ln c_1, \\ &= N\phi_1 + N(\beta - \alpha), \\ &= N\phi_\infty - N\alpha. \end{aligned} \tag{12}$$

From Eq. (12) we may obtain another useful relationship. We recall from thermodynamics that

$$(\partial F/\partial p)_T = V. \tag{13}$$

We may also write

$$N(\partial\phi_\infty/\partial p)_T = U, \tag{14}$$

where $U = Nu$ is the molal volume of the condensed phase. Equation (14) follows because $N\phi_\infty$ is the free energy of the condensed phase. From Eq. (12), then, we obtain

$$N(\partial\alpha/\partial p)_T = U - V. \tag{15}$$

3. EFFECT OF GAS IMPERFECTIONS

We have noted that the parameters ϕ_1, β, and ϵ_s will depend on temperature. If we could treat the mixture of clusters of different sizes as though it were a mixture of various species of ideal gases, these quantities would be independent of pressure. Actually they will become dependent on pressure when the pressure becomes high, because of gas imperfections. Gas imperfections will also affect the validity of Eq. (2).

Our considerations will be based on the assumption that even at densities around the

critical density it is possible to distinguish a cluster from its surroundings. However, under these circumstances even the single molecules will be close enough together so that they will exert forces on each other, as well as on the larger clusters. In general, inter-cluster forces will affect the free energy of all the clusters.

The effect of the volume occupied by the molecules themselves may be taken into account by assuming that the c_s represent the concentrations in a free volume rather than in the total volume. The free volume will not necessarily be the same for all size clusters.

In order to formulate these ideas more precisely we recall that

$$\mu_s=\bar{E}_s+p\bar{v}_s-T\bar{s}_s^* \tag{16}$$

where $\bar{E}_s$, $\bar{v}_s$, and $\bar{s}_s$ are the partial molecular energy, volume, and entropy for the clusters with s molecules. In an ideal system we would always have $\bar{E}_s=E_s^0$, $p\bar{v}_s=kT$, and $\bar{s}_s=s_s^0-k\ln c_s$. To take account of the gas imperfections we shall write

$$\bar{E}_s+p\bar{v}_s=E_s^0+kT+s\eta_s \tag{17}$$

where $s\eta_s$ is the energy caused by inter-cluster forces, together with a small correction arising from the deviation of $p\bar{v}_s$ from kT. On the other hand, we shall continue to write

$$\bar{s}_s=s_s^0-k\ln c_s, \tag{18}$$

this equation defining the c_s and thus the free volumes. We thus obtain

$$\mu_s=s\phi_s^*+s\eta_s+kT\ln c_s \tag{19}$$

where ϕ_s^* is a true constant given by

$$s\phi_s^*=E_s^0+kT-Ts_s^0. \tag{20}$$

ϕ_s is given by

$$\phi_s=\phi_s^*+\eta_s. \tag{21}$$

Since the inter-cluster forces become relatively unimportant for large clusters, we may write

$$\eta_\infty=0. \tag{22}$$

β is still given by Eq. (3) though it is no longer constant, since ϕ_1 will depend on pressure, as will all the ϕ_s.

* Here we treat a cluster of s molecules as though it were one large molecule. The superscript zeros just below refer to standard states of unit concentration of clusters which form a hypothetical ideal gas mixture.

Taking note only of the changes in the properties of the quantities involved in them, we may use all the equations of Section 2 unaltered. β and γ, though dependent on pressure, can be considered independent of the index s, all discrepancies being taken care of by ϵ_s.

The free volumes, as noted, may depend on s. In fact, it may readily be seen that the free volumes for large clusters will be smaller than those for small clusters. When the large aggregations are pushed so close together that their edges touch, so that their free volume has essentially vanished, there will still be room in the interstices for the single molecules and smaller clusters. We shall assume for the sake of qualitative considerations that the free volume under any circumstances approaches a limiting value for large s.

It should also be borne in mind that the free lengths which are considered here (and whose cubes will give the free volumes) are small compared to the mean distance through which molecules are free to move in the field of their neighbors. Since the picture we are presenting requires that clusters be distinguishable, the free length can extend no farther than it is possible for a molecule or cluster to move without becoming part of another cluster. Thus a single molecule must be farther from any of its neighbors than the molecules within a cluster, but this distance does not represent a particularly large free length.

4. THE SURFACE TENSION NEAR THE CRITICAL POINT

Something about the dependence of γ on the pressure may be learned from a thermodynamic relationship. First we may note, as shown in Appendix I, that (assuming spherical clusters) 0.23γ may be taken as the actual surface tension expressed as energy per surface molecule. We may then write[13]

$$0.23(\partial\gamma/\partial p)_T=\Delta u_\sigma \tag{23}$$

where Δu_σ is the excess volume required by a molecule at the surface above that required by a molecule inside a cluster or inside the liquid. Since the molecules at the surface are less strongly bound than those inside, they should have greater

[13] G. N. Lewis and M. Randall, *Thermodynamics* (McGraw-Hill Book Company, Inc., New York, 1923), p. 248.

freedom of motion normal to the surface and should be less closely packed.[14] Both of these effects would tend to make Δu_σ positive, and γ will increase with increasing pressure. We may expect Δu_σ to be of the order of magnitude of, but probably less than, u.

The surface tension is small in the neighborhood of the critical temperature. The temperature at which the surface tension is zero when liquid is in equilibrium with vapor we shall call T_m. This is, we assume, the highest temperature at which a meniscus can be observed. The pressure at T_m at which liquid and vapor are in equilibrium we shall call p_m.

We may obtain an approximate relation between T_m and the value of β at T_m and under the pressure p_m. This results from forming an estimate of the surface tension, 0.23γ, and setting it equal to zero. We may write $0.23\gamma = \Delta E_\sigma + p\Delta u_\sigma - T\Delta s_\sigma$, where ΔE_σ is the excess of energy and Δs_σ is the excess of entropy per molecule at the surface. Setting this equal to zero, we have

$$\Delta E_\sigma + p_m \Delta u_\sigma - T_m \Delta s_\sigma = 0. \tag{24}$$

We shall now attempt rough estimates of Δs_σ and ΔE_σ. When a molecule comes to the surface, its translational entropy increases because of the lack of constraint on the side away from the liquid. We might expect the force caused by a given displacement normal to the surface to be about halved, which would mean that the average vibration frequency would be lowered by a factor of $2^{\frac{1}{3}}$. The corresponding increase in entropy would be $\frac{1}{2}k \ln 2$. Since the vibrations parallel to the surface would be somewhat affected, too, and since the density at the surface is less than in the interior of the liquid, it will, perhaps, be a fair estimate to say that the entropy increases by $k \ln 2$. The energy increase, ΔE_σ, might be expected to be of the order of $\frac{1}{4}\Delta E_v$, where ΔE_v is the energy of vaporization per molecule, because a molecule at the surface has about three-fourths as many nearest neighbors as one in the interior of the liquid, so the vaporization process might be said to have proceeded to an extent of about one-fourth. However, because of the lower density at the surface, the transfer of a molecule to the surface is equivalent to a greater fraction of the vaporization than this. It seems about right[15] to set $\Delta E_\sigma = 0.4\Delta E_v$. This is not based on data near the critical point, but it should not cause much error to use it.

The molecule which enters the surface will be under the influence of vapor molecules outside the surface to about the same extent as a single molecule is under the influence of forces arising from neighboring molecules and clusters. Therefore, it is reasonable to set for the ΔE_v under these circumstances

$$\Delta E_v = \bar{E}_1 - E_\infty$$

where E_∞ is the energy per molecule of a large cluster. Using Eq. (17) with $s=1$

$$\Delta E_v = E_1^0 + kT + \eta_1 - p\bar{v}_1 - E_\infty. \tag{25}$$

Now

$$\begin{aligned}\beta &= \phi_\infty - \phi_1 \\ &= \phi_\infty - \phi_1^* - \eta_1.\end{aligned}$$

Since ϕ_∞ is a free energy term we may write

$$\phi_\infty = E_\infty + pu - Ts_\infty.$$

Also

$$\phi_1^* = E_1^0 + kT - Ts_1^0.$$

Therefore, if we set $\Delta s_v^0 = s_1^0 - s_\infty$

$$\begin{aligned}\beta &= E_\infty - E_1^0 - \eta_1 + pu - kT + T\Delta s_v^0 \\ &= -\Delta E_v + pu - p\bar{v}_1 + T\Delta s_v^0.\end{aligned} \tag{26}$$

From its definition, we can set Δs_v^0 equal to $k \ln(1/u_f)$, where u_f is the free volume per molecule in the condensed phase, that is, in a large cluster. u_f may be estimated in terms of u, the actual volume per molecule of the condensed phase near the critical point.

As has been pointed out by Eyring and Hirschfelder,[16] the free volume of a liquid is best calculated as the cube of a free length, and the free length may be assumed in first approximation to increase at the same rate as the linear expansion. Thus if we let l_f be the free length near the critical point we may say that $u^{\frac{1}{3}} - l_f$ is roughly the length which is not free, and we may identify $u^{\frac{1}{3}} - l_f$ with the cube root of the volume at the melting point. The ratio of the volume at

[14] Compare H. Eyring, J. Walter, and A. E. Stearn in *Surface Chemistry* (edited by F. R. Moulton, A. A. A. S., 1943), p. 88.

[15] W. D. Harkins, Zeits. f. physik. Chemie **A139**, 647 (1928) (see especially p. 665).

[16] H. Eyring and J. O. Hirschfelder, J. Phys. Chem. **41**, 249 (1937).

the critical point to that at the melting point is, therefore, $u/(u^{\frac{1}{3}}-l_f)^3$, and this is known to be about 3. This gives $l_f=0.306u^{\frac{1}{3}}$ or $u_f=l_f^3=0.03u$. Hence $\Delta s_v^0\sim -k\ln(0.03u)$. The effect of communal entropy is neglected in this rough calculation.

We set this value of Δs_v^0 in Eq. (26), solve for ΔE_v, set $\Delta E_\sigma=0.4\Delta E_v$ in Eq. (24), and insert also in Eq. (24) our estimated value of Δs_σ. This gives at $T=T_m$ and $p=p_m$

$$\beta=-kT_m\ln(0.17u)+p_mu-p_m\bar{v}_1+2.5p_m\Delta u_\sigma. \quad (27)$$

As noted above, Δu_σ will be of the order of u. p_mu will be considerably less than kT; since the single molecules feel the attractive forces less than the molecules within a large cluster, $p_m\bar{v}_1$ should be larger than p_mu, but it cannot be as great as kT. Therefore, the last three terms in Eq. (27) may be reasonably neglected in the applications we shall make, and we shall use

$$\beta\sim -kT_m\ln(0.17u). \quad (28)$$

The estimates of Δs_σ and Δu_σ, which we have made in the above discussion, can be checked roughly from experimental data. Δs_σ is equal to $-(\partial\gamma_\sigma/\partial T)_p$ where $\gamma_\sigma\sim 0.23\gamma$ is the free energy per molecule at the surface. $(\partial\gamma_\sigma/\partial T)_p$ is closely related to the Eötvös constant, which is equal to $-d(U^{\frac{1}{3}}\gamma_0)/dT$ where γ_0 is the ordinary surface tension and U is the molal volume of the liquid. If we transform this to $d(u^{\frac{1}{3}}\gamma_0)/dT$, the quantity obtained will be almost the same as $(\partial\gamma_\sigma/\partial T)_p$, since $u^{\frac{1}{3}}$ is roughly the area occupied by a molecule. The Eötvös constant is usually of the order of 2 erg mole$^{-\frac{1}{3}}$ deg.$^{-1}$, which makes $d(u^{\frac{1}{3}}\gamma_0)/dT$ about -2.8×10^{-16} erg molecule$^{-\frac{1}{3}}$ deg.$^{-1}$. Comparing this with the value of the Boltzmann constant, $k=1.37\times10^{-16}$ erg deg.$^{-1}$, we see that our estimate of Δs_σ as $k\ln 2$ is of the right order of magnitude.

Turning now to Δu_σ, we may estimate this quantity if we are willing to admit that a change of volume at the surface has the same effect on the entropy as a change of volume in general. We then set $\Delta s_\sigma/\Delta u_\sigma=(\partial S/\partial U)_T$. Since $(\partial S/\partial U)_T=(\partial p/\partial T)_u$, it may be estimated from Fig. 1 or 2 to be slightly over 1 atmos. per deg. for liquid ethylene. Taking Δs_σ as $k\ln 2$, we find Δu_σ to be about 10^{-22} cc per molecule, which is obviously of the same order of magnitude as u.

Measurements of the surface tensions of methyl ether and of propylene have been carried close to the critical temperature, T_c (which may or may not be identical with our T_m), by Winkler and Maass.[17] They found that the surface tension was not a linear function of T_c-T, but that the slope of the curve, surface tension *vs.* temperature, became considerably smaller near the critical point. The values seemed to follow either the rule suggested by Ferguson[18] (specializing an equation of van der Waals) that the surface tension should be proportional to $(T_c-T)^{6/5}$ or that suggested by Katayama[18] that it should be proportional to $(T_c-T)(U^{-\frac{1}{3}}-V^{-\frac{1}{3}})^{\frac{1}{3}}$. Ferguson's formula would lead to a slope which is zero, though only weakly, at T_c, while Katayama's formula would still give a finite slope if T_c is the same as T_m, since the molal volume of the liquid, U, and of the vapor, V, are not equal at this point. It is difficult to give a suggestion as to the exact significance of these formulas;[19] however, there are at least two factors which would contribute to a decrease in the slope of the surface tension *vs.* temperature curve near the critical point.

In the first place, the surface tension which is being measured is the surface tension between the saturated liquid and its vapor. We must write

$$\begin{aligned} d\gamma_\sigma/dT&=(\partial\gamma_\sigma/\partial T)_p+(\partial\gamma_\sigma/\partial p)_T dp/dT \\ &=-\Delta s_\sigma+\Delta u_\sigma dp/dT. \end{aligned} \quad (29)$$

Since dp/dT near the critical point is of the same order of magnitude as $(\partial p/\partial T)_v$, and this is roughly equal to $\Delta s_\sigma/\Delta u_\sigma$, it is seen that the two terms in Eq. (29) will be of the same order of magnitude, and since they are of opposite sign, $d\gamma_\sigma/dT$ should be smaller near the critical point than it would be far removed from it where dp/dT is very small.

Furthermore, near the critical point the vapor is full of droplets, and the liquid will also be full

[17] C. A. Winkler and O. Maass, Can. J. Research 9, 65 (1933).

[18] See N. K. Adam, *The Physics and Chemistry of Surfaces* (Oxford University Press, New York, 1941), third edition, pp. 165.

[19] R. H. Fowler, Proc. Roy. Soc. **A159**, 229 (1937); R. H. Fowler and E. A. Guggenheim, *Statistical Thermodynamics* (The Cambridge University Press, New York, 1939), pp. 445, have discussed these formulas and their application in the neighborhood of the critical point. This discussion, however, is based upon the assumptions that the co-existence curve has the rounded top of the van der Waals theory and that the density of the liquid remains constant to the surface.

of bubbles. This means that an increase in the extent of the boundary between the two phases is greater than the actual increase in the true surface. This can be visualized by considering what happens when one slices a piece of Swiss cheese. If a cut made through the liquid intersects some bubbles, an increase in true surface area will only result from the part which does not go through the bubbles. This will result in an apparently lower surface energy in this temperature region, hence a flatter approach to $\gamma_\sigma = 0$.

None of these considerations indicate that γ will not go through zero and become negative. A negative surface tension cannot be observed but is important for our considerations.

As soon as the surface tension vanishes, there will be a tendency for the formerly nearly spherical droplets to spread out in such forms as to have the greatest possible surface, such as sheets or filaments. The question as to whether a filament will be more stable than a flat surface is a fairly complicated one, however. The molecules in a filament have considerably more freedom of motion than those on a surface, but they also have fewer neighbors. It is, therefore, difficult to say whether the entropy term should be expected to overtake the energy term at a higher or lower temperature than for the flat surface. However, if a filament became stable at a temperature lower than that at which the surface tension of a flat surface vanished, we might expect the system to tend at this temperature suddenly to go over to filaments, causing what would appear to be a sudden drop to a state of zero surface tension. This certainly does not seem to be the case.

The considerations for wide-spread disks with sharp edges should be qualitatively the same as for filaments. However, it is possible to have flat disks with bulges around the edge, thus avoiding sharp corners. Furthermore it is quite possible that filaments become stable only slightly above the temperature at which the surface tension for flat surfaces vanishes. In any event filaments and disks are wasteful of space. It may, therefore, be expected that they will be suppressed when the system is fairly highly compressed.

Even if filaments and thin films are avoided, it does appear that as soon as the surface tension becomes negative there will be a tendency for the proliferation of surfaces in the form of bulges and protuberances. The surface of a cluster will probably be practically proportional to its volume; since the $s^{\frac{1}{3}}$ term in Eq. (4) will thus be replaced by a term proportional, or nearly proportional, to s, the effect of surface tension will largely disappear. However, the larger the cluster the greater will be the number of possible configurations it may take on account of folding and distortion of the surface. This may be expected to introduce a term of the form s^a, where a is a fairly small number, into the partition function for the cluster, and hence a term $NkTa \ln s$ into the free energy expression. Some of these considerations have been mentioned by Mayer and Streeter.[8]

It may be noted that since γ decreases with decreasing pressure, the effects of negative surface tension will already appear at $T = T_m$ on the vapor side of the isotherm where $p < p_m$. But even the system of bulges and protuberances will be wasteful of space, certainly of free space, and so as p approaches p_m this particular effect of negative surface will be suppressed, both because there is less space and because the surface tension becomes less negative.

5. THE PHENOMENA AT TEMPERATURE T_m

On the basis of the discussion of the preceding sections, we shall now attempt a description of the phenomena which take place in the neighborhood of the critical point. We have seen (just preceding Eq. (11)) that, when γ is positive, very large clusters suddenly come into equilibrium when α vanishes, and we interpret this as the normal type of condensation. However, at T_m, where γ becomes zero, the large droplets may come in gradually, and the process $\alpha \to 0$ needs reinterpretation. For large value of s, Eq. (9) becomes

$$c_s = e^{(\beta - \alpha s)/kT_m} = c_1 e^{-\alpha(s-1)/kT_m}. \tag{30}$$

We shall for the moment neglect the free energy term $NkTa \ln s$ mentioned at the end of the preceding section.

We shall assume that the free volume approaches a definite value V_f for large s. Then,

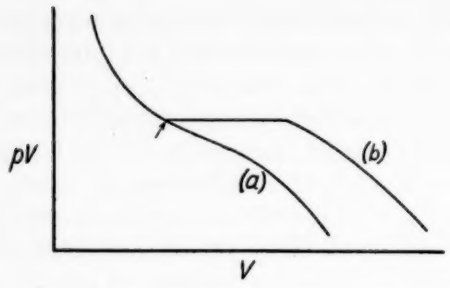

FIG. 3.

if α is sufficiently small so that most of the molecules are contained in large clusters we may define a total net concentration $C=N/V_f$, and write

$$C\cong\Sigma_s sc_s. \tag{31}$$

Using Eq. (30)

$$C=e^{\beta/kT_m}(1-e^{-\alpha/kT_m})^{-2}e^{-\alpha/kT_m}. \tag{32}$$

If α/kT_m is very small, this becomes approximately

$$C=e^{\beta/kT_m}(kT_m/\alpha)^2 \tag{33}$$

which, solved for α, gives

$$\alpha=kT_m(e^{\beta/kT_m}/C)^{\frac{1}{2}}. \tag{34}$$

As $\alpha\to 0$, the system approaches a state in which $e^{\beta/kT_m}=c_1$ is vanishingly small compared to C. This can only happen if V_f approaches zero. Since V_f is a free volume, it is possible for this situation to occur while the total volume V is still finite. There will be a volume, which we shall call V_0', so small that large clusters can no longer move independently, and at this point V_f is zero. When the system is compressed to still lower values of V, the large aggregation itself is being compressed. As we have remarked above, this large aggregation will contain many internal surfaces. If the surface tension is zero (i.e., at temperature T_m), there will be no resistance to the further change in volume and hence no free energy, or pressure, change until these surfaces are squeezed out.

Another expression for the quantity $C=N/V_f$ may be obtained directly from the determination of V_f as a function of V. This problem is very similar to the one previously discussed, which led to Eq. (27). $V_f^{\frac{1}{3}}$ may be taken as the free length, which may be set equal to $V^{\frac{1}{3}}-V'^{\frac{1}{3}}$, where V' is the volume which would be occupied if the system were compressed, without change in the density or total amount of material in the large clusters, until the free volume just vanished. If the large clusters neither evaporated nor accumulated material and were incompressible, V' would be equal to V_0'. Actually V' is a function of V and approaches V_0' as V approaches V_0'.

From the identity,

$$x-y=(x^{\frac{1}{3}}-y^{\frac{1}{3}})(x^{\frac{2}{3}}+x^{\frac{1}{3}}y^{\frac{1}{3}}+y^{\frac{2}{3}}),$$

we may write, if $V-V'$ is small compared to V,

$$V_f^{\frac{1}{3}}=(V-V')/3V'^{\frac{2}{3}}. \tag{35}$$

Hence

$$C=27NV'^2(V-V')^{-3}. \tag{36}$$

From Eq. (34) then,

$$\alpha=kT_me^{\beta/2kT_m}(V-V')^{\frac{1}{2}}/(27N)^{\frac{1}{2}}V'. \tag{37}$$

If we neglect the variation of β, we may use Eq. (28) to get a rough evaluation. This gives

$$\alpha/kT_m\sim 0.5(V-V')^{\frac{1}{2}}/V_0'^{\frac{1}{2}}. \tag{38}$$

In this we have set $V'=U=V_0'$ in the denominator.

The above equations are all predicated on the assumption that γ is zero and remains zero. Actually, as we have noted before, γ will depend on the volume; but for $V>V_0'$ the value of γ will only decrease below zero, so the system will still act as though it had zero surface tension, as far as Eq. (30) and the quantities based on it are concerned; that is, the effect of γ may be included in α.

Equation (15) may be used to find the rate at which α changes as the volume is increased beyond V_0'. For a small range of such volumes $U-V$ will not vary too much and may be set equal to U_0-V_0', where U_0 is the value of U when $V=V_0'$. At the critical point for ethylene we see from Fig. 2 that $V_0'-U_0$ is about $0.1V_0$. An increase in volume until $V-V_0'$ is about $0.2V_0'$ lowers the pressure by 0.1 atmos., and from Eq. (15), using $V-U=0.1U\sim 0.1\times 4$ cc/g, we find that α/kT changes from zero to about 0.5×10^{-4}. A rough evaluation of $V-V'$ may

then be made from Eq. (38), and we estimate[20] that when $V-V_0'$ is about $0.2V_0'$ then $V-V'$ is about $0.002V_0'$.

Since the change in $V-V'$ is so much less than $V-V_0'$, it appears that over this range $dV'\cong dV$. It would seem that over as great a range in $V-V_0'$ as this, the effect could only be ascribed to expansion of the large clusters as the pressure is decreased, so that they continue almost to fill the space available. This would be further aided as γ became negative, by the tendency of the large clusters to take shapes which have a large surface. Just at $V=V_0'$ the large clusters resemble the liquid phase; the large clusters themselves will contain bubbles of gas, as the liquid itself must. The expansion of the liquid is a combination of the expansibility (inverse of compressibility) of true liquid and the bubbles contained in it; and it appears that the expansibility of the vapor is the combined expansibility of the gas substance and the droplets contained therein, the droplets in turn containing gas within themselves, and so on. If, however, rather than considering the clusters and bubbles, which are complex entities, we should desire to fix our attention on what we might call "true" liquid (liquid without bubbles) and "true" vapor (the part composed of single molecules and small clusters), then we could not exclude the possibility that the expansibility of liquid and vapor are caused by changes in the relative amounts of "true" liquid and "true" vapor. We cannot eliminate this possibility because our equations deal only in free volumes, and we cannot estimate very exactly what the actual molecular density of true vapor may be. In any event, since there is no discontinuity at the point where $\gamma=0$ and $\alpha=0$, it seems natural, though perhaps still a little speculative, to set the coefficient of compressibility of the large

[20] The estimate of $V-V'$ is based, it will be recalled, upon the assumption that the free energy term $NkTa$ ln$s$ mentioned at the end of Section 4 could be neglected; that is, we assume $a=0$. If a were 1, then Eq. (33) would be replaced by $C=2e^{\beta/kT_m}(kT_m/\alpha)^3$. The final result would be that when $V-U=0.2U$ and α/kT is about 10^{-4}, we would get a very much smaller value for $V-V'$. Our conclusions, then, would hold *a fortiori*, and this would be true for any value of $a>0$. There seems to be no reason to suppose that a would be less than zero. We may also remark that (as can be readily seen from the calculations in Section 6) the value of γ remains so small that it would not change our conclusions even if the $s^{\frac{1}{3}}$ term remained in the expression for the free energy.

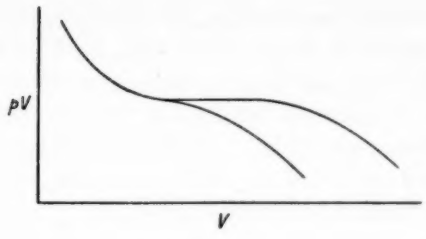

FIG. 4.

clusters in the vapor phase at $V=V_0'$ equal to the coefficient of compressibility of liquid at $U=U_0$, or $V_0'^{-1}(\partial V'/\partial P)_T=U_0^{-1}(\partial U/\partial p)_T$, which gives, at $V=V_0'$

$$(\partial V/\partial p)_T\cong(V_0'/U_0)(\partial U/\partial p)_T. \qquad (39)$$

In other words, the slope of the isotherm to the right of the horizontal portion at T_m is determined by, and is approximately equal to, the slope on the left. If these ideas are correct, the situation may be illustrated graphically as shown in Fig. 3. Suppose that, if we could have a liquid which did not vaporize, it would follow an isotherm of the form illustrated in Fig. 3(a). It is in equilibrium with vapor at the point indicated by the arrow. Just at T_m, this point coincides with the condition of zero surface tension. The curve splits apart, so to speak, at this pressure and, as shown in Fig. 3(b), the section at lower pressures is simply transferred to large volumes, only slightly distorted. The amount of distortion will increase, of course, at larger volumes.

However, if this much is correct we can draw a further conclusion. Since β will certainly not vary rapidly at $V=V_0'$, we may use Eq. (38) to find $(\partial\alpha/\partial V)_T$:

$$(\partial\alpha/\partial V)_T\cong 0.75(V-V')^{\frac{1}{3}}V_0'^{-\frac{1}{3}}(1-dV'/dV).$$

Combining this with Eq. (15) we obtain

$$(\partial p/\partial V)_T\cong 0.75N(V-V')^{\frac{1}{3}}V_0'^{-\frac{1}{3}} \times(U-V)^{-1}(1-dV'/dV). \qquad (40)$$

This will vanish at $V=V_0'$, since $(V-V')^{\frac{1}{3}}$ then becomes zero. This, in itself, would not be of great importance, since it vanishes to a low order; and it can be readily shown that if V' were constant the value of $(\partial p/\partial V)_T$ would actually become quite large when V was only slightly greater than V_0'. However, since V' does in-

crease with V, the value of $(\partial p/\partial V)_T$ does not increase nearly this rapidly, and, if dV'/dV does actually approach 1 as $V \rightarrow V_0'$, then we see that $(\partial p/\partial V)_T$ becomes zero to a higher order. We may thus expect Fig. 3 to be replaced by Fig. 4, and the curve at T_m will be quite smooth.[21] This is indeed indicated by Fig. 2.

In the calculations of this section we have assumed that the free volume of a large cluster is not affected by the presence of the small clusters. In other words, we assume, for example, that the reaction, 2 clusters ($s=2000$)$\rightleftarrows$1 cluster ($s=4000$), comes to the same equilibrium as if the space occupied by the small clusters were empty. This will be true if the large clusters can move around throughout the space without thereby affecting the freedom of motion of the small clusters. This should be approximately the case, because the small clusters do not form a very densely packed molecular system. Even though the free volumes of individual cluster sizes may be very small, as indicated at the end of Section 3, it is rather the actual spacing of the individual molecules of the small clusters which is important here. For, if a certain amount of association or dissociation among the small clusters is forced by motion of the large clusters, this may still take place without appreciably affecting the total free energy of all the molecules in the small clusters, since all sizes of cluster are in equilibrium with each other. Any residual effect on the collective free energy of the small clusters caused by the occurrence of association or dissociation among the large clusters is probably proportional to the surface of the large clusters, and is properly taken into account in the surface tension term.

6. THEORY OF EVAPORATION

Frenkel[10] has pointed out that a general theory of heterophase fluctuations can be adapted to the formation of bubbles in a liquid, as well as to the formation of droplets in a vapor. So we may expect to be able to develop a theory of evaporation, complementary to the theory of condensation, in which evaporation will be preceded by the appearance of bubbles in the liquid. Since the same liquid and vapor are involved in the two cases, there will be a relationship between the parameters, and on this account it seems worth while to develop the bubble theory of evaporation in some detail.

The bubbles are in some respects similar to the "holes" in liquids which have been considered before,[22] but are not the same thing since they are defined by the number, t, of gas molecules contained within the bubble. Such bubbles will appear in appreciable numbers, for reasons we shall see, only very close to the critical point; the "holes" which are usually discussed may be a real property of a liquid, and any contribution they may make to the molecular free energy, in addition to the effect of the bubbles, is included in the quantity we have called ϕ_∞. Both the holes and the bubbles lower ϕ_∞ from the value it would have if they did not exist—otherwise neither holes nor bubbles could occur. The bubbles affect ϕ_∞ simply by lowering the mole fraction of true liquid in the mixture.

The molecular free energy of a gas bubble consisting of an infinite number of molecules is given by $\phi_\infty - \alpha$. This follows from Eq. (12) since an infinitely large bubble is nothing but a vapor phase. We assume that the relation continues to hold for finite bubbles, where the liquid is the stable phase and α is negative; in fact, the negative values of α may be considered to be defined in this way.

The chemical potential μ_t of a gas bubble containing t molecules will have a term $t(\phi_\infty - \alpha)$. There will also be a contribution from a surface term proportional to $t^{\frac{2}{3}}$. However, the molecules at the surface will actually be supplied by the liquid rather than the vapor. If we are to express this term in terms of the quantity γ which we have previously defined, we must multiply t by the ratio of the density of the liquid, $1/u = N/U$, to the density of the gas, $1/v = N/V$. The term is, therefore, $\gamma(tv/u)^{\frac{2}{3}}$. To this we must add a correction term ϵ_t for small bubbles. Finally, there will be a term arising from the mobility of the bubble. This may be obtained if we fix our attention on a single arbitrarily chosen molecule in the bubble, assuming that it can

[21] The free energy term $NkTa \ln s$ mentioned at the end of Section 4 could conceivably upset this conclusion. If a were equal to 1, for example, α would be proportional to $V-V'$ instead of $(V-V')^{\frac{2}{3}}$, and $(\partial\alpha/\partial V)_T$ would be proportional to $1-dV'/dV$ instead of $(V-V')^{\frac{2}{3}}(1-dV'/dV)$. If, however, dV'/dV approaches 1 at $V=V_0'$, as would seem even more probable if a were greater than zero, the conclusion would still hold. Were a greater than 1, it would be necessary for $1-dV'/dV$ to approach zero, in order to avoid an infinity. However, if the droplets nearly fill the volume, it seems unlikely that the many configurations of the large droplets, which would result in the term $NkTa \ln s$, could be realized on account of the interference of their neighbors. I, therefore, believe that the discussion based on Eq. (40) gives the best account of the true situation.

[22] See S. Glasstone, K. J. Laidler, and H. Eyring, *Theory of Rate Processes* (McGraw-Hill Book Company, Inc., New York, 1941), p. 477.

wander at will through its portion of the volume of the liquid, namely c_t^{-1}, in addition to its space within the bubble, namely, its free volume v_f'. If c_t is defined as the proper kind of effective concentration, we may say that the free volume of the selected molecule is $c_t^{-1}+v_f'$. The other molecules in the bubble, being constrained to move with the chosen molecule, have only the free volume v_f'. The fact that the chosen molecule has the free volume $c_t^{-1}+v_f'$ instead of v_f' means that we must add to the chemical potential a term $-kT\ln[(c_t^{-1}+v_f')/v_f']$. Summarizing

$$\mu_t = t\phi_\infty - t\alpha + \gamma(tv/u)^{\frac{1}{3}} + \epsilon_t - kT\ln[(c_t^{-1}+v_f')/v_f']. \quad (41)$$

The total change in free energy produced by an arbitrary variation of the numbers of bubbles n_t will be given by

$$\delta F = \Sigma_t u_t \delta n_t - \phi_\infty \delta N_0$$

where N_0 is the total number of molecules in bubbles and $-\delta N_0$, therefore, is the change in the total number of molecules not in bubbles. Obviously

$$\delta N_0 = \Sigma_t t\delta n_t.$$

Setting this into the expression for δF and setting it equal to zero, we obtain

$$\Sigma_t \delta n_t(\mu_t - t\phi_\infty) = 0.$$

Since there is now no restriction on the δn_t's, we may set the coefficient of each one equal to zero. This gives

$$v_f'/(c_t^{-1}+v_f') = \exp[t\alpha - \gamma(tv/u)^{\frac{1}{3}} - \epsilon_t]/kT \quad (42)$$

as the equation which determines c_t.

The quantity on the left-hand side of Eq. (42) obviously cannot become greater than 1. As long as α is negative and γ is positive (since ϵ_t is a correction to the term $\gamma(tv/u)^{\frac{1}{3}}$ which cannot change its sign), the right-hand side is less than 1. This is true even if $\alpha=0$, but as soon as α becomes positive the terms with large t become greater than 1 and, in fact, the expression diverges. The pressure at which α becomes positive is, therefore, the vapor pressure, in agreement with conclusions reached from the study of the condensation process.

It is of interest to note that, if γ is appreciable and v/u large, the exponential quantities on the right-hand side of Eq. (42) are very small even when $\alpha=0$. This means that c_t must be very small; in other words, except close to the critical point, where γ is small and v/u near 1, there will be practically no bubbles.

At $T=T_m$ the two quantities γ and α are zero together when the volume of the liquid U is equal to U_0, the value at the low volume end of the flat part of the isotherm; but for $U<U_0$, the terms in α and γ are of the same sign since α is less than 0 and γ greater than zero. As $U\to U_0$ and $p\to p_m$, therefore, the right-hand side of Eq. (42) increases, and the expressions for all values of t approach 1 simultaneously. We thus get a gradual approach to a condition of big bubbles, that is, a foam.

Let us now consider the situation when the liquid has been compressed to 0.1 atmos. above p_m. The rate of change of α will be about the same as on expansion of the gas phase; α will go to about -0.5×10^{-4}. By comparing Eqs. (23) and (15) we see that the change of γ will be about 50 times as great as that of α; γ/kT will become about 3×10^{-3}. If the terms other than $t\alpha$ are negligible in the exponent of Eq. (42), and provided that v_f' is small enough, the maximum value of tc_t occurs at $t=t_{\max}=|kT_m/\alpha|$, or, about 3, indicating that the surface tension will have a large but not an overwhelming effect, and the effect will be smaller the less the amount of the compression above p_m. For the purpose of evaluating c_t, a correction to the approximate equation

$$v_f'/(c_t^{-1}+v_f') = e^{t\alpha/kT_m}$$

could be made by multiplying the right-hand side by $e^{-\gamma(t_{\max}v/u)^{\frac{1}{3}}/kT_m}$. This would give us an expression from which c_t could be found, provided v_f' were known. Actually we shall be content with an inequality, and since $c_t = 1/c_t^{-1} > 1/(c_t^{-1}+v_f')$ we write

$$c_t > v_f'^{-1} e^{t\alpha/kT_m} e^{-\gamma(t_{\max}v/u)^{\frac{1}{3}}/kT_m}. \quad (43)$$

We shall now consider a quantity C_0, analogous to the quantity C of Section 5. C_0 is defined as the number of molecules in bubbles per unit free volume for the motion of bubbles in the liquid. It may be approximately obtained as

$\int_0^\infty tc_t dt$. Therefore, from Eq. (43), since $\alpha<0$,

$$C_0>v_f'^{-1}e^{-\gamma(t_{\max}v/u)^{\frac{1}{3}}/kT_m}(kT_m/\alpha)^2. \quad (44)$$

By reasoning similar to that which resulted in Eq. (36), we may write

$$C_0=\frac{27N_0(fN_0v)^2}{(U-fN_0v)^3}. \quad (45)$$

Here N_0v is the total volume of the bubbles, and fN_0v is the total volume of the liquid at which the free volume U_f of the bubbles would vanish, assuming N_0 and v constant. f will be slightly greater than 1, since it is only necessary that the bubbles touch in order for U_f to vanish. It will be recognized that use of Eq. (45) may not be entirely consistent with our definition of C_0 in terms of effective concentrations c_t which are set up so that the sum $c_t^{-1}+v_f'$ gives the effective free volume of a chosen molecule in a bubble. If we use Eq. (45), it might, for example, be supposed that it would be better to add free lengths, using $(c_t^{-\frac{1}{3}}+v_f'^{\frac{1}{3}})^3$ instead of $c_t^{-1}-v_f'$ in Eq. (41); but changes of this sort would still allow us to insert Eq. (45) into the inequality (44).

We may write for the total volume of the liquid, including the bubbles,

$$U=(N-N_0)u'+N_0v \quad (46)$$

where u' is the molecular volume of the liquid aside from the bubbles. The denominator of Eq. (45) becomes $Nu'-N_0(fv-v+u')$. This is zero when $U=U_0$. Suppose at some smaller value of U the value of N_0 has become $N_0-\delta N_0$. If v and u' do not change, the denominator becomes $\delta N_0(fv-v+u')$. Therefore, Eq. (45) becomes

$$C_0=\frac{27f^2N_0^3v^3}{v(fv-v+u')^3(\delta N_0)^3} \quad (47)$$

and using (44) we obtain

$$\left(\frac{\delta N_0}{N_0}\right)^3<27e^{\gamma(t_{\max}v/u)^{\frac{1}{3}}/kT_m}\times\frac{v_f'}{v}\cdot\frac{f^2v^3}{(fv-v+u')^3}\left(\frac{\alpha}{kT_m}\right)^2. \quad (48)$$

Since $v\sim u'$ and $f\sim 1$, and since v_f' will be smaller than v, we may write

$$\delta N_0/N_0<3e^{\gamma(t_{\max}v/u)^{\frac{1}{3}}/3kT_m}|\alpha/kT_m|^3. \quad (49)$$

For the case we have considered, namely $p-p_m=0.1$ atmos., we find that this gives $\delta N_0/N_0<0.01$. It is clear that this will be insufficient to account for the decrease in volume caused by an increase in pressure of 0.1 atmos. For smaller values of $p-p_m$ the discrepancy would be still greater. In this calculation we have neglected changes in u' and v. The result shows that this is not permissible, and we see that the high compressibility of the liquid is a result of the intrinsic compressibility of the true liquid part and of the bubbles, but is not to be ascribed merely to the squeezing out of the bubbles. In this respect the liquid phase is very similar to the vapor phase.

We are now in a position to consider a little more closely the nature of the process by which the surface is decreased as the spongy mass of liquid and vapor is squeezed from molecular density $1/v_0'$ to molecular density $1/u_0$ across the flat part of the isotherm at T_m. As we approach the density $1/v_0'$ from the low density side we have droplets of average density approximately $1/u_0$ dispersed in a medium consisting of single molecules and smaller droplets which is of considerably lower density. The droplets or clusters themselves consist of material of higher density in which bubbles are dispersed; in fact, in view of the negative surface tension when the density is less than $1/v_0'$, the bubbles probably form a continuous matrix within the drops. On the other hand, as we approach the density $1/u_0$ from the high density side we have bubbles of density $1/v_0'$ dispersed in a medium of considerably higher density; these bubbles, in turn, consist of material of lower density with droplets dispersed inside them. To go from the state existing at the low density side of the horizontal part of the isotherm to that existing at the high density side thus requires an exceedingly complex rearrangement of interior surfaces. The general picture which we have developed as to the nature of the phenomena which take place in the neighborhood of the critical point has some points of resemblance to, and some differences from, descriptions which have been previously

given.[23] As far as I am aware, the connection of these ideas with the equations of the theory of associating systems has not been brought out.

We conclude this section with a remark on the experiments of Mason, Naldrett, and Maass.[2] These writers state that only a very small portion of the apparently horizontal section of the coexistence curve ("coexistence" meaning that there is a stable meniscus) is absolutely flat, although a considerable section is horizontal to within about 0.001°C. This is based on the behavior of the meniscus in vigorously shaken tubes whose total molal volumes lie between U_0 and V_0'. One would naturally expect that for any volume in this range the meniscus would stand near the center of the tube and simply fade out as the temperature was increased. Actually, it was found that for an appreciable range of volumes greater than U_0 the meniscus appeared to disappear through the bottom of the tube, as though there were evaporation of the liquid. Of course this occurred over an extremely minute range of temperature. Also, for an appreciable range of volumes less than V_0' the meniscus seemed to disappear through the top of the tube. Maass and Naldrett interpreted this as meaning that the "critical range" of volumes, though finite, in contradiction to the van der Waals theory, was somewhat smaller than one would suppose from the appearance of the coexistence curve. However, if the isotherm of T_m is truly horizontal over a region, it is possible to have material of any density along the isotherm in equilibrium with material of any other density. This allows the possibility of an apparent shortening of the horizontal portion. For it may be that sufficient gradients of temperature or pressure are set up in the tubes in the process of shaking so that the state finally approached is one in which the densities of the two phases in equilibrium (or nearly in equilibrium) are close to the middle, rather than exactly at the ends of the horizontal part of the coexistence curve. If the coexistence curve is really geometrically flat only over a small region near the center of the apparently horizontal portion, it presumably means that the isotherm is geometrically flat only over the same region.

[23] See, e.g., Wo. Ostwald, Kolloid Zeits. **64**, 50 (1933); J. Frenkel, Acta Physicochimica U.R.S.S. **8**, 261 (1938). The illustrations of Ostwald's are especially suggestive but do not reproduce the situation existing at the critical point in its full complication. Many of Ostwald's considerations have to do with phenomena which are not equilibrium phenomena.

7. PHENOMENA AT TEMPERATURES ABOVE T_m

At the temperature T_m the horizontal part of the isotherm corresponds to the squeezing out of the holes and the decrease in the total surface of the spongy but connected mass of liquid which is formed when $\alpha=0$. Above T_m the liquid has a negative surface tension, and in order to cause the spongy mass to disappear it will be necessary to increase the pressure. The isotherms, therefore, slope upward toward lower values of V just above the region where the isotherm is horizontal at T_m.

At volumes somewhat greater than this critical region the clusters will, since the surface tension is negative, have a wrinkled surface. As the volume is decreased, there will be a tendency for these to smooth out and for the bubbles inside the clusters to be squeezed out, in order to make the best use of the space. This tendency will be resisted by the negative surface tension. The net result will be that the spongy mass will form at a larger volume than is the case at T_m. This will happen when the free energy increase caused by formation of a single connected large particle is less than the increase which would be occasioned by the decrease in surface necessary in order to keep the individual large clusters separated from each other.

It would not be expected that the slope would be uniform over any great range of volumes in the region in which the spongy mass occurred. The surface would act somewhat like a spring, the force tending to uncoil it, increasing as it is squeezed up. (Since the compression of the spongy mass is only a continuation of the compression of the clusters at larger volumes, the first point at which the spongy mass occurs does not correspond to a completely uncoiled spring; if this were the case one might expect one point, a point of inflection, at which the isotherm was horizontal.) This effect of "coiling the spring" will be counteracted to some extent by the very fact that the pressure does increase as the volume is decreased, for this would tend to cause the surface tension to become less negative. Also it

is difficult to see to just how greatly the compressibility of the liquid itself would be involved. So it is apparent that the exact shape of the isotherm is determined by a rather complex interplay of forces as soon as the temperature T_m is passed. It is clear, however, that there will be a critical region in which we may speak in a rough way of the vapor being changed, on compression, into the liquid.

Some discussion of the way in which an isotherm approaches the critical region may be of interest. The discussion resulting in Eqs. (9) and (10) will remain largely unchanged. But, as we have noted, when the surface tension is negative we may expect the extent of the surface to be proportional to s instead of $s^{\frac{2}{3}}$. In place of the term $\gamma s^{\frac{2}{3}}$ in Eq. (9) we will, therefore, write $\gamma\nu s$, where ν is a further proportionality factor, related to the fraction of molecules at the surface and, therefore, dependent on the volume. (In the light of the discussion at the end of Section 4, γ may be expected to depend on the average curvature of the surface, but this will not affect our considerations.) Equation (10) will remain unchanged. We see now that the expression for c_s diverges when $\alpha+\nu\gamma$, rather than α itself, becomes less than zero. $\alpha+\nu\gamma$ will also replace α in Eq. (37). We shall be interested in finding $[\partial(\alpha+\nu\gamma)/\partial V]_T$ rather than $(\partial\alpha/\partial V)_T$, and comparing it with $[\partial(\alpha+\nu\gamma)/\partial p]_T$ rather than with $(\partial\alpha/\partial p)_T$. $[\partial(\alpha+\nu\gamma)/\alpha p]_T$ cannot, however, be evaluated in the same way as $(\partial\alpha/\partial p)_T$; in fact, T_m will be the last temperature at which an equation like Eq. (15) will hold. This may be seen in the following way. Equation (12) will hold as before, but ϕ_∞ is not the actual free energy of an infinitely large cluster, since ϕ_∞ does not include the surface energy. Actually we should write for the actual free energy $\phi_\infty+\nu\gamma$, and we can put Eq. (12) in the form

$$F=N(\phi_\infty+\nu\gamma)-N(\alpha+\nu\gamma).$$

When $\alpha+\nu\gamma$ is zero, we have $F=N(\phi_\infty+\nu\gamma)$. But now this relation corresponds to one definite volume, since there is no horizontal place in the isotherm. At this pressure the large cluster fills the space, and its volume becomes equal to the total volume V. Hence when $\alpha+\nu\gamma=0$, instead of Eqs. (13) and (14) we have

$$N[\partial(\phi_\infty+\nu\gamma)/\partial p]_T=V=(\partial F/\partial p)_T$$

and

$$[\partial(\alpha+\nu\gamma)/\partial p]_T=0.$$

Thus, instead of Eq. (40) we get an indeterminate expression; if it could be evaluated this would presumably give a finite, non-zero value of $(\partial p/\partial T)_V$.

Equation (15) can hold only because below and at T_m, as the pressure on the vapor is increased, the density of the large clusters approaches a value different from that of the whole system as the point is approached at which a two-phase system is in equilibrium; even at T_m the system cannot be compressed until the volume is down to the value U_0. Above T_m the large clusters approach a specific volume equal to that of the whole system and on further compression no phase change occurs, but the properties of the system, including the pressure, gradually change. Obviously $N[\partial(\phi_\infty+\nu\gamma)/\partial p]$ cannot, when $\alpha+\nu\gamma=0$, be set equal to any smaller volume than the total volume of the system, since such a smaller volume corresponds to a higher pressure. On the other hand, Eq. (14) must hold at T_m, since between V and U it is impossible to produce any change in the pressure on the large clusters. Actually, however, no discontinuity is involved, as the isotherm at T_m can equally well be considered to be the limiting case for those above or those below T_m.

8. RELATION TO MAYER AND HARRISON'S STATISTICAL THEORY

As we noted in Section 1, Mayer and Harrison came to the conclusion that not only is there a critical region above the temperature T_m, but that there should be a series of isotherms above that temperature, which would still have a portion which was exactly horizontal. These isotherms would further have the property that there was no apparent discontinuity in slope at the ends of these flat portions of the isotherms. According to our conclusions, the last horizontal isotherm occurs at T_m. It is desirable to reconcile these apparently contradictory conclusions.[24]

Mayer and Harrison's theory is based upon the setting up of the partition function for the

[24] In the discussion which follows we shall use the notation of J. E. Mayer and M. Goeppert Mayer, *Statistical Mechanics* (John Wiley and Sons, Inc., New York, 1940), Chapters 13 and 14.

condensing vapor in terms of certain "cluster integrals," b_l, where l is a running subscript which takes values from 1 to N, where N is the number of molecules in the system, and it is based upon the assumption that the b_l's are independent of the volume of the system. The cluster integrals are in turn expressed in terms of irreducible integrals, $\beta_\mathbf{k}$, where $\mathbf{k}$ is a running subscript which goes from 1 to $l-1$. The $\beta_\mathbf{k}$ are independent of l; that is, the same set of $\beta_\mathbf{k}$ serves to evaluate all the b_l. (Since the $\beta_\mathbf{k}$ will always be written with a subscript, they need not be confused with β used in the earlier sections of this paper.)

It is shown that for large l we may write b_l in the form

$$b_l = f(l, \beta) b_0{}^l \tag{50}$$

where

$$b_0 = \rho^{-1} \exp \sum_{\mathbf{k}=1}^{\infty} \beta_\mathbf{k} \rho_\mathbf{k} \tag{51}$$

and

$$f(l, \beta) = \rho l^{-5/2} (2\pi \sum_{\mathbf{k}=1}^{\infty} \mathbf{k}^2 \beta_\mathbf{k} \rho^\mathbf{k})^{-\frac{1}{2}}. \tag{52}$$

ρ is the solution of the equation

$$\sum_{\mathbf{k}=1}^{\infty} \mathbf{k} \beta_\mathbf{k} \rho^\mathbf{k} = 1. \tag{53}$$

This holds as long as there is a real positive root of Eq. (53) and $\Sigma \mathbf{k}^2 \beta_\mathbf{k} \rho^\mathbf{k}$ converges. These conditions, however, can hold only at relatively high temperatures, where the $\beta_\mathbf{k}$ are not too large. At low temperatures $\sum_{\mathbf{k}=1}^{\infty} \mathbf{k} \beta_\mathbf{k} x^\mathbf{k}$ diverges as x increases from $x=0$ before reaching the value 1. In this case Eq. (52) does not hold, but $f(l, \beta)$ will still not vary faster than as a power of l. Also, we must then define b_0 by

$$b_0 = \lim_{l \to \infty} \rho^{-1} \exp \sum_{\mathbf{k}=1}^{l} \beta_\mathbf{k} \rho^\mathbf{k} \tag{54}$$

where ρ is the limit of ρ' as $l \to \infty$, with ρ' the root of the equation,

$$\sum_{\mathbf{k}=1}^{l} \mathbf{k} \beta_\mathbf{k} \rho'^\mathbf{k} = 1.$$

The limiting value, ρ, then, will obviously coincide with the value of x which just causes the series to diverge.

Condensation occurs when a certain parameter Z, which may be shown to be equal to $v^{-1} \exp(-\sum_{\mathbf{k}=1}^{\infty} \beta_\mathbf{k} v^{-\mathbf{k}})$ where v is the volume per molecule, becomes equal to or greater than b_0. The value of v at which this occurs is called v_s, and it is shown that $v_s = \rho^{-1}$. The sum $\sum_{l=1}^{\infty} v b_l Z^l$, which appears in the partition function, may readily be seen to diverge as soon as $Z b_0$ becomes greater than 1.

It is proved that

$$(\partial p / \partial v)_T = -(kT/v^2)[1 - \sum_{\mathbf{k}=1}^{\infty} \mathbf{k} \beta_\mathbf{k} v^{-\mathbf{k}}] \tag{55}$$

provided $v > v_s$. At v_s the isotherm becomes horizontal. However, the slope of the isotherm may or may not approach zero as v decreases toward v_s. To get this information about the isotherm from Eq. (55), it is necessary to know something about the $\beta_\mathbf{k}$ as functions of T. Mayer and Harrison make the assumption that[25]

$$\beta_\mathbf{k} = f(\mathbf{k}, T) \beta_0{}^\mathbf{k} (|\beta_0| / \beta_0)^{\mathbf{k}+1} \tag{56}$$

where β_0 is a function of T and $f(\mathbf{k}, T)$ is a positive factor and, at least, for large $\mathbf{k}$ a smooth function of $\mathbf{k}$, such that

$$\lim_{\mathbf{k} \to \infty} \mathbf{k}^{-1} \ln f(\mathbf{k}, T) = 0. \tag{57}$$

According to Eq. (57), the factor $f(\mathbf{k}, T)$ may not increase with $\mathbf{k}$ as rapidly as a constant raised to the $\mathbf{k}$th power, but it may contain a factor of the form $\mathbf{k}^a$, where a is a constant, and a factor of the form $e^{-\gamma \mathbf{k}^{\frac{2}{3}}}$, where γ is a surface tension term.[26]

---

[25] Mayer and Harrison did not actually apply Eq. (56) for $\beta_0 < 0$, and they did not have the factor $(|\beta_0|/\beta_0)^{\mathbf{k}+1}$ in their equation. This factor simply has the effect of making all the terms in the series have the same sign as β_0. Even if Eq. (56) is not strictly applicable for values of β_0 very close to or less than zero, I believe that it may be used in order to see how the series behaves when the $\beta_\mathbf{k}$'s change sign.

[26] It may be questioned whether we are allowed to identify the γ of this section with the γ we have used previously. Mayer and Harrison identified their γ with the surface tension (within a constant factor) by an argument which essentially assumed that a mathematical cluster was the same thing as a physical cluster. Since this would be strictly true only for a dilute gas, it would appear that their γ is identified with the surface tension of a cluster under these conditions, rather than under conditions existing near the critical point.

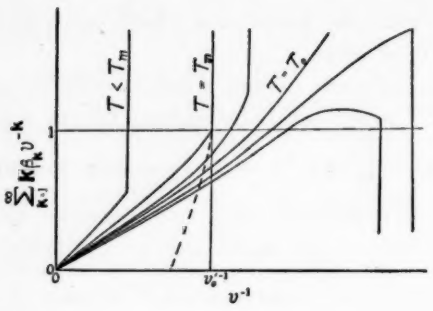

FIG. 5.

It is known that at very low temperatures all the β_k are positive. In general they will be expected to decrease with the temperature, and some or all will become negative. The assumption is made that β_0 decreases with the temperature and eventually becomes negative. It is also implied that the smaller the value of $\mathbf{k}$ the more positive the corresponding values of β_k; in other words, as the temperature increases, the β_k become negative in order, starting with those with large values of $\mathbf{k}$.

The β_k are integrals whose integrands have large numbers of positive and negative parts. There is no doubt that the positive parts predominate at low temperatures. Their behavior as the temperature increases is not so clear, and it is possible that Eq. (56) may not continue to hold. The β_k's, for example, could have, at least in some range of temperatures, alternating positive and negative values. Nevertheless, we shall accept the assumptions formulated in Eqs. (56) and (57) and those described in the accompanying paragraphs. I believe, however, that the validity of Mayer and Harrison's conclusions is limited, because the region in which the b_l's are volume independent is limited in a way which will become clear as the discussion proceeds.

On the basis of Eq. (56) we may write

$$\sum_{k=1}^{\infty} k\beta_k v^{-k} = \sum_{k=1}^{\infty} k f(\mathbf{k}, T)(\beta_0/v)^k(|\beta_0|/\beta_0)^{k+1}. \quad (58)$$

As the volume decreases the sum diverges when $\beta_0/v > 1$. When the temperature is low and β_0 is strongly positive this occurs at a small value of v^{-1}, as is indicated by the first curve ($T < T_m$) in Fig. 5. Because $f(\mathbf{k}, T)$ will be largely determined by the factor $e^{-\gamma k^{\frac{1}{3}}}$, and, since γ decreases rapidly with T, the actual value of the sum when divergence sets in increases with T. There will be a temperature T_0 at which $\beta_0 = 0$. In this case, the series will not diverge, but its value will continue to increase with v^{-1} because of the early terms in the series, which are positive. Above T_0 the series will diverge with negative sign. The negative terms will also cause the value of the sum to increase at a less rapid rate; finally, at high T, it will decrease before the divergence occurs.

At low values of T the divergence of $\sum_{k=1}^{\infty} k\beta_k v^{-k}$ occurs before it is equal to 1; by Eq. (55), then, $(\partial p/\partial v)_T$ is still negative for values of v very slightly greater than v_s, which is, of course, the value of v at which the divergence occurs. This corresponds to the break in the slope of the isotherm in ordinary condensation. The temperature at which the point of divergence of the sum coincides with its reaching the value 1 is the last temperature at which the ordinary type of condensation occurs, and we identify it with our previously defined T_m. We see from Eq. (55) that above $T = T_m$ the slope of the isotherm approaches zero as the point of condensation is approached. According to Mayer and Harrison, then, we have a smooth approach to a horizontal stretch of the isotherm.

However, as Mayer and Harrison pointed out, and as we have already noted, these calculations break down as soon as the b_l's become volume dependent. The b_l's become volume dependent as soon as one of the mathematical clusters which contribute appreciably to the partition function contains an appreciable fraction of all the molecules. As soon as the vapor is all condensed, and all the molecules are in one mathematical cluster, the breakdown will occur. The volume involved will be the volume of the liquid phase. But, as we have seen, at the temperature T_m the system has been coagulated into one spongy mass at the large volume end of the horizontal part of the isotherm. One cannot identify the true physical clusters with the mathematical clusters of Mayer and Harrison's theory; however, there is enough resemblance between them so that it seems reasonable to conclude that when the spongy mass is formed the cluster integrals of Mayer and Harrison's theory become volume dependent.

This happens at still larger values of v when T is greater than T_m. Thus only the portion of the curves to the left of the broken line in Fig. 5 will be susceptible of physical interpretation. This will not include the region above T_m, in which Mayer and Harrison believed the isotherms to be horizontal.

At first it might appear that a situation such as is described in the preceding paragraph is automatically excluded by the theory of Mayer and Harrison. For the sum $\sum vb_lZ^l$ which appears in the partition function will not be expected to diverge until v has reached the value which makes $\sum \mathbf{k}\beta_k v^{-\mathbf{k}}=1$. Therefore, we should expect that terms for which $l\sim N$, the total number of molecules, would not contribute appreciably to the sum, and since it is these terms which are volume dependent, it would appear that this volume dependence would not have an appreciable effect. However, actually it may become quite important. As we approach the point at which the series would normally diverge, any influence which changes the character of the higher terms can cause the series to diverge sooner because of these terms alone. A b_l for which l is large may be expected to be extremely sensitive to such influences because b_0 occurs to the lth power in Eq. (50).

If, on account of the variation of b_l with the volume, the series $\Sigma\, vb_lZ^l$ is to diverge at a larger value of v and hence a smaller value of Z than is normally to be expected, this can only result because b_l has attained a larger absolute value than its asymptotic value for large v. b_l is a complex sum and product of integrals, each of which has an integrand with many positive and negative parts. It is, therefore, difficult to decide *a priori* whether it is possible for its absolute value to increase as the system is compressed. Mayer, in a private communication, states his belief that it will not happen; however, it cannot be proved either way, and I believe that the experimental results and the considerations of this paper lend strength to the inference that b_l does actually, at least ultimately, increase as v is decreased. (b_l may decrease, passing through zero, and finally passing its asymptotic absolute value on the negative side.) If this were not true, it could be reconciled with Section 7 only by the supposition that it is possible to compress a system with negative surface tension, when the spongy mass is formed, for at least a short range without increasing the pressure, and, therefore, without decreasing the total surface. Such a situation is geometrically possible, with condensation of some of the less dense portions into the denser portions of the material. It would, presumably, however, involve an increase in the average curvature of the surface, that is, an approach to sharper edges and corners. In the region where the surface tension is negative this process has presumably gone as far as is profitable in the normal proliferation of the surface. Therefore, further increase in curvature would be resisted, and would not be expected to occur unless forced by an increase in pressure, which is just what we wished to avoid.

As Mayer has pointed out in a private communication, wherever the sum $\sum vb_lZ^l$ does diverge, and from whatever cause it may diverge, a phase transition of some order will occur. For the divergence of the sum at a given v means that beyond that v the partition function must be expressed by a new analytic function. This means that at least some derivation of the partition function, and hence some derivative of p with respect to v, must be discontinuous. It seems probable, however, that above T_m this is a transition of higher order and that at least $(\partial p/\partial v)_T$ is continuous though $(\partial^2 p/\partial v^2)_T$ may not be.

It is not, perhaps, absolutely certain that the theory of Mayer and Harrison will not break down even slightly to the left of the broken line in Fig. 5. This, however, would mean a transition of higher order at some temperatures below T_m just before the first order transition of ordinary condensation. Such an occurrence does not seem indicated by the theory of the present paper. Discounting the possibility, then, and assuming that Eq. (55) can be used up to the broken line, certain further conclusions can be drawn. Then, according to the discussion at the end of Section 5, at T_m the isotherm should diverge at a value of $\sum_{k=1}^{\infty} \mathbf{k}\beta_k v^{-\mathbf{k}}$ just equal to 1, as shown in Fig. 5, since by Eq. (55) this will make $(\partial p/\partial V)_T=0$ at the point of divergence in agreement with Eq. (40). Furthermore, we see that $(\partial p/\partial V)_T$ approaches

zero as $V-V_0'$. This will be consistent with Eq. (40) only if $V-V'$ is proportional to $(V-V_0')^{4/3}$, which makes $1-dV'/dV$ proportional to $(V-V_0')^{\frac{1}{3}}$.

9. CONCLUSIONS

The net result of our discussion is that, apparently in agreement with experiment, the isotherm at the highest temperature T_m at which a meniscus is distinguishable has a horizontal portion. Above T_m there is a critical region, in which a transition from vapor to liquid takes place over a finite range of volumes, but where the isotherms never have zero slope. To get a final check on this, more experimental data are needed, and particular attention needs to be paid to possible effects of impurities. More surface tension measurements, correlated as well as possible with the other phenomena which occur at the critical point would also be valuable. It should be remarked that in order to compare any experimental results with the theory, it is necessary that the measurements should be made under equilibrium conditions. It seems to be true that near the critical point it is especially difficult to attain equilibrium and various kinds of hysteresis effects are common. These non-equilibrium phenomena are of considerable interest in themselves, but the theory presented here makes no attempt to explain them.

Our results appear not to be in contradiction to the more exact mathematical theory of Mayer and Harrison. Their equations are exact for the range over which they hold, whereas our discussion involves a number of assumptions and approximations. However, it seems to be reasonable to assume that the methods used in this paper can penetrate into a region where Mayer's equations break down.

It would seem best, on the basis of the results obtained, to define the critical temperature as being identical with T_m.

I wish to thank Dr. G. E. Boyd and Dr. L. D. Roberts for some interesting and helpful discussions. I also wish to thank Dr. J. E. Mayer for reading the manuscript and making several suggestions.

APPENDIX

The number of molecules on the surface of a large spherical cluster can be calculated roughly if we assume the molecules are themselves spherical and in close-packed array. Neither assumption is exactly correct, but the result will suffice for our purpose.

Let r be the radius of the cluster and let a be the distance between the centers of nearest neighbors. Let τ be the total volume of the cluster, σ its total surface area, s the number of molecules in it, and n the number of molecules at the surface. The volume per molecule in a close-packed array is $2^{-\frac{1}{2}}a^3$. Hence

$$\tau=2^{-\frac{1}{2}}sa^3=(4/3)\pi r^3.$$

From this we get

$$s^{\frac{1}{3}}=3.28(r/a)^2.$$

Let us suppose that the sphere is sufficiently large so that its surface is practically a plane and that the molecules form a two-dimensional hexagonal close-packed array on the surface. The area per molecule on such a surface is $(3/4)^{\frac{1}{2}}a^2$. Hence

$$\sigma=(3/4)^{\frac{1}{2}}na^2=4\pi r^2.$$

So

$$n=14.5(r/a)^2.$$

Hence

$$n=4.4s^{\frac{1}{3}},$$

or

$$s^{\frac{1}{3}}=0.23n.$$

The Effect of Pressure on Surface Tension

O. K. RICE[1]
University of North Carolina, Chapel Hill, North Carolina
(Received February 25, 1947)

The thermodynamic formula for the change of surface tension with pressure is interpreted for a one-component system and for a two-component system consisting of an inert gas over a liquid. In the latter case the effect of pressure on surface tension can be attributed in part to absorption of gas at the surface of the liquid and in part to an intrinsic decrease in density of the liquid in the neighborhood of the surface. The equations are interpreted in terms of the Gibbs adsorption isotherm. The adsorption of gas at the liquid surface has been estimated in several cases from data in the literature.

THE variation of surface tension with pressure has been shown by Lewis and Randall[2] to be given by the equation

$$(\partial\gamma/\partial p)_{\sigma,T}=(\partial V/\partial\sigma)_{p,T}. \qquad (1)$$

Here V is the total volume of the system and σ the total surface area, so $(\partial V/\partial\sigma)_{p,T}$ is the increase in volume produced by increasing the surface by unit area. This equation holds, as Lewis and Randall noted, for any system in which the total amount of any component remains fixed, regardless of the number of components present. γ, itself, is defined in terms of a constant pressure, as well as a constant temperature, process, namely

$$\gamma=(\partial F/\partial\sigma)_{p,T} \qquad (2)$$

where F is the total Gibbs free energy of the system.

In a one-component system consisting of a liquid in equilibrium with its vapor it is not possible for the pressure to vary. Equation (1) will be applicable, nevertheless, if we can imagine the equilibrium between liquid and vapor to be frozen. In this case $(\partial V/\partial\sigma)_{p,T}$ is a measure of the difference of density of the liquid at its surface and in the bulk of the material. Since the liquid is almost certainly less dense near the surface than it is in bulk, $(\partial V/\partial\sigma)_{p,T}$ should be positive, and the surface tension should increase with pressure. This cannot, of course, be verified experimentally; conceptually, however, it is of importance and has some applications in the study of the equilibrium between liquid and vapor, as is shown in the preceding article.[3]

About the only available experiments on the effect of high pressure on the surface tension of a gas-liquid interface are those done by Kundt.[4] The pressure was exerted by an inert gas over the liquid, and it was found that the surface tension was appreciably lowered. This is in contrast to the effect to be expected in a one-component system. Adam[5] has remarked upon the importance of the gas itself in this effect, and the amount of lowering of the surface tension depends upon the nature of the gas used.

Some similar effects have been observed on the surface tension of water and mercury, when these liquids are in contact with a relatively low pressure of vapor of different substances in the region above the surface. In these cases, the effect has been quite properly ascribed to the adsorption of the vapor at the surface, and the ordinary Gibbs adsorption equation has been applied.[6]

It seems almost certain that the phenomena with inert gases at high pressures have a similar origin. The surface is a favorable place for there to be some accumulation of gas. The gas is attracted to the liquid by van der Waals forces, and at the surface it is not necessary to disturb the intermolecular attractions of the liquid. If there is, thus, an excess concentration of gas molecules in the surface over that of gas molecules dissolved in the liquid, this excess (which we designate as Γ, the amount adsorbed per unit

[1] On leave 1946–47 at the Clinton Laboratories, Oak Ridge, Tennessee.
[2] G. N. Lewis and M. Randall, *Thermodynamics* (McGraw-Hill Book Company, Inc., New York, 1923), p. 248.
[3] O. K. Rice, J. Chem. Phys. **15**, 314 (1947).
[4] Kundt, Ann. d. Physik **12**, 538 (1881); *Int. Crit. Tab.* **4**, 475.
[5] N. K. Adam, *The Physics and Chemistry of Surfaces* (Oxford University Press, 1941), third edition, p. 165.
[6] See reference 5, pp. 130ff.

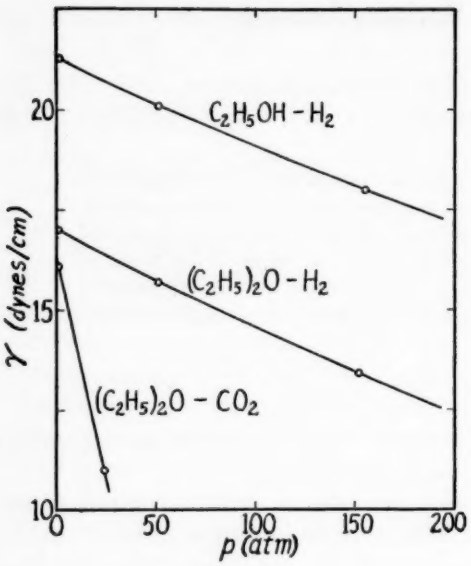

FIG. 1.

surface) must be removed from the gas phase when the surface is increased. This will result in a considerable lowering of the volume and will usually be the principal contribution to $(\partial V/\partial\sigma)_{p,T}$ in such a two-component system. If the gas may be considered to be ideal, it will be equal to $-\Gamma kT/p$, where T is the absolute temperature, k is Boltzmann's constant, and Γ is expressed in molecules per unit surface.

In addition there will be the intrinsic change of volume, due to decreased density of the surface, discussed in connection with one-component systems. If this change in volume is ΔV_σ per unit surface, we may write Eq. (1) in the form

$$(\partial\gamma/\partial p)_\sigma=(\partial V/\partial\sigma)_p=-\Gamma kT/p+\Delta V_\sigma. \quad (3)$$

If the gas is not ideal, we may set

$$(\partial\gamma/\partial p)_\sigma=-(\Gamma kT/p)(pV)_{\text{obs.}}/(pV)_{\text{i. d.}}+\Delta V_\sigma \quad (4)$$

where $(pV)_{\text{obs.}}$ is the observed value of pV, which may be obtained readily from tables, and $(pV)_{\text{i. d.}}$ is its ideal value.

The results may be interpreted in terms of the Gibbs adsorption isotherm. In fact, Eq. (1) may be readily thrown into the form of Gibbs equation. We let there be a total number of moles, $n_1, n_2, \cdots, n_i, \cdots$ of the respective components in the two-phase system. The chemical potentials are given by the usual equations

$$\mu_i=(\partial F/\partial n_i)_{p,T,\sigma,n_1,\cdots n_{i-1},n_{i+1},\cdots} \quad (5)$$

and we may define quantities $\bar{v}_1, \bar{v}_2, \cdots \bar{v}_i, \cdots$ by the equations

$$\bar{v}_i=(\partial V/\partial n_i)_{p,T,\sigma,n_1,\cdots,n_{i-1},n_{i+1},\cdots} \quad (6)$$

$\bar{v}_i$ is not the partial molal volume of either phase, since n_i is the total number of moles in both phases, but is a kind of average partial molal volume. By differentiating Eq. (5) with respect to p, noting that

$$(\partial F/\partial p)_{T,\sigma,n_1,\cdots,n_i,\cdots}=V,$$

we have

$$(\partial\mu_i/\partial p)_{T,\sigma,n_1,\cdots,n_i,\cdots}=\bar{v}_i. \quad (7)$$

The quantity $(\partial V/\partial\sigma)_{p,T}$ which appears in Eq. (1) is the volume change caused by a unit increase in surface, when $n_1, n_2, \cdots, n_i, \cdots$ are not changed. In order to restore the volume to its original value, maintaining the pressure and the composition of each phase constant, we add $\Gamma_1, \Gamma_2, \cdots, \Gamma_n, \cdots$ moles, per unit surface increase, of the various components. We may then write

$$(\partial V/\partial\sigma)_{p,T}=-\Gamma_1\bar{v}_1-\Gamma_2\bar{v}_2-\cdots-\Gamma_i\bar{v}_i-\cdots. \quad (8)$$

Inserting Eq. (8) in Eq. (1), and applying Eq. (7) we obtain

$$d\gamma=-\Gamma_1 d\mu_1-\Gamma_2 d\mu_2-\cdots-\Gamma_i d\mu_i-\cdots \quad (9)$$

which is the general form of the Gibbs equation for constant temperature. The proof is not general, because it takes into account only such changes of the μ's as may be caused by the total pressure. In this respect it supplements proofs of Gibbs equation which assume that the pressure remains constant. It is possible, however, to give a proof which is perfectly general.[7]

For a two-component ideal system of gas above liquid it is clear that $\Gamma_1\bar{v}_1$ in Eq. (8) corresponds exactly to $\Gamma kT/p$ in Eq. (3), if the gas is assigned the subscript 1, and it is equally clear that $-\Gamma_2\bar{v}_2$ can be equated to ΔV_σ. The correspondence between Eq. (3) and the Gibbs equation is thus brought out.

Equation (4) makes it possible to attempt to calculate the amount of gas adsorbed at the surface. In Fig. 1 we have plotted the data of Kuntz for hydrogen above ethyl alcohol, hydro-

[7] See reference 5, pp. 109ff.

gen above diethyl ether, and carbon dioxide above diethyl ether. We have used this curve to determine $(\partial\gamma/\partial p)_{\sigma,T}$. It is possible to obtain $(pV)_{\text{obs.}}$ for hydrogen from either the Landolt-Börnstein Tables, or the International Critical Tables. For carbon dioxide we have used Eq. (3), which should suffice at 10 atmospheres.

The values of $(\partial\gamma/\partial p)_{\sigma,T}$ for the case with hydrogen, when converted to cc per cm², turn out to be 2 to 3×10^{-8}. This is unquestionably of the same order of magnitude as ΔV_σ. If, as in Table I, we set $\Delta V_\sigma=0$, we can obtain only the order of magnitude of Γ. Γ may be considerably larger than the value given, but it is, in any case, sufficiently small so that we may say that in no case is a complete monomolecular layer very closely approached.

That carbon dioxide should have a much greater effect than hydrogen is entirely to be expected, on account of the large van der Waals attraction between it and the surface of the ethyl ether. Adam noted this but had a slightly different, though related, explanation.

The calculations suggest that it would be of interest to perform experiments with helium as the inert gas. Helium would probably be less adsorbed than hydrogen, and in this case ΔV_σ might be the predominant term so that $\partial\gamma/\partial p$ would become positive. Unfortunately, it does not seem possible to separate the two effects, though the approach to saturation (possibly hinted at in the results discussed) might throw some light on the matter. For this purpose measurements at higher pressures would be needed.

TABLE I. Surface tensions at various pressures and 21°C.

	p atm.	$\partial\gamma/\partial p$ dynes/cm atm.	$(pV)_{\text{obs.}}/(pV)_{\text{i. d.}}$	$\Gamma\times10^{-16}(\Delta V_\sigma=0)$ molecules/cm²
C_2H_5OH with H_2	10	0.0256	1.006	0.00063
	50	.0220	1.031	.0026
	100	.0205	1.061	.0048
	150	.0192	1.092	.0065
$(C_2H_5)_2O$ with H_2	10	0.0272	1.006	0.00067
	50	.0242	1.031	.0029
	100	.0230	1.061	.0054
	150	.0218	1.092	.0074
$(C_2H_5)_2O$ with CO_2	10	0.222		0.0055

Letters to the Editor

THIS section will accept reports of new work, provided these are terse and contain few figures, and especially few halftone cuts. The Editorial Board will not hold itself responsible for opinions expressed by the correspondents. Contributions to this section should not exceed 600 words in length and must reach the office of the Managing Editor not later than the 15th of the month preceding that of the issue in which the letter is to appear. No proof will be sent to the authors. The usual publication charge ($4.00 per page) will not be made and no reprints will be furnished free.

Chemisorption of Gases*

SOL WELLER**
Central Experiment Station, U. S. Bureau of Mines, Pittsburgh, Pennsylvania
April 10, 1947

THE question occasionally arises of the appropriateness of including the amount of chemisorbed gas (i.e., that for which the heat of adsorption is comparable with the heats of chemical reactions) when applying the Brunauer-Emmett-Teller (B.E.T.) theory[1] of gas adsorption to an adsorption isotherm. If the first layer of adsorbed gas is chemisorbed, two cases may be distinguished: either the first layer is reversibly adsorbed and partakes in the B.E.T. equilibria, or under the experimental conditions (temperature and time) it is practically irreversibly adsorbed. The latter situation will be favored with short equilibration time and at temperatures so low that the energy required for desorption is much greater than the thermal energy (RT).

If the first layer is irreversibly adsorbed, it does not take part in the equilibrium relations of the B.E.T. theory, and for the purposes of the theory it may be considered to form part of the solid surface. The theory will then apply to the balance of the adsorbed gas, i.e., to the total adsorption minus the chemisorption. If the solid surface is uniform and is completely covered by the chemisorbed gas, the total adsorption, expressed as the statistical number of layers of gas adsorbed, will in this case be given by

$$n=\frac{v}{v_m}=1+\frac{cx}{(1-x)[1+(c-1)x]}, \tag{1}$$

where $c=p_0(a_2/b_2)e^{(E_2-E_L)/RT}$, E_2 = heat of adsorption for the second layer, $E_3=E_4=\cdots=E_L$.

On the other hand, the case in which the chemisorbed gas does participate in the statistical equilibria is included in the B.E.T. theory without any special treatment. In this situation, if E_1, the heat of adsorption of the first (chemisorbed) layer, is unique and $E_2=E_3=\cdots=E_L$, the simple B.E.T. theory applies and the total adsorption is given by

$$n=\frac{v}{v_m}=\frac{cx}{(1-x)[1+(c-1)x]}, \tag{2}$$

where $c=p_0(a_1/b_1)e^{(E_1-E_L)/RT}$. However, the high value of E_1 implies strong binding between the chemisorbed layer and the solid surface, and it is exactly in this situation that one expects E_2 as well as E_1 to be unique and different from E_L. The reasonable assumption that $E_1\neq E_2\neq E_3=E_4=\cdots=E_L$ leads to an interesting result. This case was worked out by Brunauer, Emmett, and Teller.[1] It can be shown that the number of adsorbed layers is expressible in the form

$$n=\frac{v}{v_m}=\frac{cx[(1-x)^2+kx(2-x)]}{(1-x)[(1-x)(1+cx)+ckx^2]}, \tag{3}$$

where $c=p_0(a_1/b_1)e^{(E_1-E_L)/RT}$ and $k=p_0(a_2/b_2)e^{(E_2-E_L)/RT}$. Now if E_1 is very large, as it is for chemisorption, c is also large and $cx\gg1$ for all values of x usually studied (e.g., $x>.05$). In this case, the term 1 may be neglected in comparison with cx in the denominator of Eq. (3), and Eq. (3) becomes

$$n=\frac{v}{v_m}=\frac{(1-x)^2+kx(2-x)}{(1-x)(1-x+kx)}=\frac{1-2x+x^2+kx-kx^2+kx}{1-2x+x^2+kx-kx^2},$$

or

$$n=\frac{v}{v_m}=1+\frac{kx}{(1-x)[1+(k-1)x]}.[2] \tag{4}$$

It will be seen that Eq. (4) is identical with Eq. (1), and k has exactly the same significance in Eq. (4) as does c in Eq. (1). This means that when both physical adsorption and chemisorption occur, and if the approximation that E_1 and E_2 are unique and $E_3=E_4=\cdots=E_L$ is good, then the total adsorption is given by Eq. (2) or Eq. (4) regardless of whether or not the chemisorption is reversible.

* Published by permission of the Director, Bureau of Mines, U. S. Department of the Interior.
** Physical chemist, Bureau of Mines, Central Experiment Station, Pittsburgh, Pennsylvania.
[1] Brunauer, Emmett, and Teller, J. Am. Chem. Soc. **60**, 309 (1938).
[2] Equations (1) and (4) involve the implicit assumption that the packing of adsorbed molecules is the same in the first layer as in subsequent layers. If this is not true, the term unity on the right of the equation will be replaced by v_m'/v_m, where v_m' and v_m are, respectively, the volumes of "chemisorbed" and "physically adsorbed" gas required to form a monolayer.

Errata: On the Dissociation Energies of CO, N_2, NO, and CN

[J. Chem. Phys. **14**, 568 (1946)]
J. G. VALATIN
Institute of Experimental Physics, University for Technical and Economic Sciences, Budapest, Hungary

STYLISTIC changes made by the kindness and courtesy of the editors have accidentally altered the meaning of the original text.

The second sentence of the paper should read: "Their paper shows that even the correlation of those authors leads to contradictions with such a non-crossing rule for the excited states who consider . . ." instead of: "Their paper shows that even their correlation leads to contradictions with such a non-crossing rule for the excited states since they consider. . . ."

In the 13th line of the text "Moreover" should be replaced by "On the other hand"; in the 15th line "other" by "some."

Molecular Association in Hydrogen Fluoride Vapor

H. A. Benesi and C. P. Smyth
Frick Chemical Laboratory, Princeton University, Princeton, New Jersey
March 24, 1947

DENSITY measurements[1-4] of hydrogen fluoride vapor have shown the existence of strong molecular association in a region of temperature and pressure extending some distance above the boiling point. Simons and Hildebrand[2] and Long, Hildebrand, and Morrell[4] were able to calculate the densities on the assumption of the existence of a single equilibrium $6HF \rightleftharpoons (HF)_6$, although some indication of the formation of lower polymers at low degrees of association was also obtained. Briegleb,[5] on the other hand, concluded that the association was of the type, $HF+(HF)_n \rightleftharpoons (HF)_{n+1}$, and calculated from the data of Fredenhagen[3] values of the equilibrium constants for the cases $n=1, 2, \cdots 8$. Hildebrand and his co-workers considered the hexamer to be stabilized by linking of the two ends of the chain to form a hexagonal ring, and Pauling[6] calculated that the additional bond obtained by ring formation would make a ring containing six or more hydrogen fluorides more stable than its chain analog. Electron diffraction measurements[7] indicated that the molecules were zig-zag chains of different lengths, mostly trimers, tetramers, and pentamers. However, it was recognized that there was a slight possibility that ring structures might have dissociated into chains during the course of the measurements, which were made as a molecular beam passed into a vacuum.

Dielectric constant measurements[8] in a region of temperature and pressure where molecular association was negligible gave a dipole moment 1.91×10^{-18} for the monomeric hydrogen fluoride molecule. A polymeric molecule in the form of a plane ring or a puckered ring with the fluorines at the corners and the hydrogens in the edges would have zero dipole moment. An extended rectilinear chain or an extended zig-zag chain with the hydrogens in the fluorine-fluorine lines, as indicated by electron diffraction, would have a larger moment than the monomer. Measurement of the dielectric constant of the vapor and calculation of its polarization, P, which, for hydrogen fluoride with its very small molar refraction is approximately proportional to the square of the dipole moment, can thus give evidence of the presence or absence of any considerable amount of ring formation.

The apparatus previously used[8] in the determination of the hydrogen fluoride dipole moment was employed after slight alterations. The insertion of a second nickel reservoir and an additional Bourdon gauge facilitated the purification of the hydrogen fluoride by fractional distillation. The purity of the carefully purified sample used in the measurements was checked by determination of its liquid vapor pressure. As the effect of the deviation from the ideal gas law for each kind of molecule was insignificant in comparison with the effect of the molecular association, the polarization, P, was calculated from the dielectric constant, ϵ, by means of the simple equation

$$P=RT(\epsilon-1)/p(\epsilon+2),$$

in which R is the gas constant, T, the absolute temperature, and p, the pressure.

Two curves were run for polarization as a function of pressure, one at 26.0° and the other at 38°C, temperatures at which the association had been established by previous investigations.[4] At both temperatures, the polarization values at pressures below 100 mm showed no measurable variation with change of pressure, in agreement with the indications given by the density measurements.[4] These polarization values were consistent with those previously found by Hannary and Smyth.[8] For pressures above 120 mm at 26.0° and 160 mm at 38.0°, the polarization rose rapidly with increasing pressure, the rise being more rapid at the lower temperature and continuing with increasing pressure up to the highest pressures observed, 551 mm at 26.0° and 707 mm at 38°. The large increase in polarization brought about by molecular association shows that ring structures, which would decrease the polarization, cannot predominate and the presence of more or less extended chains, which, because of their large dipole moments, increase the polarization, is clearly indicated.

A detailed discussion of the quantitative data will be given when the measurements now being carried out in this laboratory are completed.

[1] T. E. Thorpe and F. J. Hambly, J. Chem. Soc. **55**, 163 (1889).
[2] J. Simons and J. H. Hildebrand, J. Am. Chem. Soc. **46**, 2183 (1924).
[3] K. Fredenhagen, Zeits. f. anorg. allgem. Chemie **218**, 161 (1934).
[4] R. W. Long, J. H. Hildebrand, and W. E. Morrell, J. Am. Chem. Soc. **65**, 182 (1943).
[5] G. Briegleb, Zeits. f. physik. Chemie **51B**, 9 (1941).
[6] L. Pauling, *The Nature of the Chemical Bond* (Cornell University Press, Ithaca, New York, 1940), p. 298.
[7] S. H. Bauer, J. Y. Beach, and J. H. Simons, J. Am. Chem. Soc. **61**, 19 (1939).
[8] N. B. Hannay and C. P. Smyth, J. Am. Chem. Soc. **68**, 171 (1946).

The Mechanism of Nitrogen Pentoxide Decomposition

Richard A. Ogg, Jr.
Department of Chemistry, Stanford University, Stanford University, California
April 15, 1947

CONSIDERATIONS of reaction mechanism discussed below suggested a probable serious error in the previously accepted value for the heat of formation of nitrogen pentoxide. Accordingly, the heat of solution of this substance in water has been redetermined. Extremely pure samples were obtained by resubliming in a stream of ozonized oxygen the product from nitric acid-phosphorus pentoxide reaction. The calorimetric procedure amounted to direct comparison of the desired heat of solution with the heat of neutralization of dilute aqueous nitric acid and sodium hydroxide. The results of four duplicate determinations (respective values 20.0, 20.8, 20.2, and 19.8 kilocalories) give as an average value (at 25°C)

$$N_2O_5(c)+H_2O(l)\rightarrow 2HNO_3(aq) \quad \Delta H=-20.2 \text{ kcal.}$$

The considerably smaller value of 16.7 kcal. found by Berthelot[1] is scarcely surprising in view of the difficulties in purification of this notoriously reactive and unstable substance. Using the above new value, and other requisite thermochemical data[2] of relatively modern origin, one finds

the heat of formation of $N_2O_5(c)$ to be 9.6 kcal. per mole, and for the following reaction (at 25°C)

$$N_2O_5(g) \rightarrow NO(g)+NO_2(g)+O_2(g)$$

$$\Delta H = +25.5 \text{ kcal.} \quad \Delta E = \Delta H - 2RT = +24.3 \text{ kcal.}$$

It is proposed that the apparently first-order decomposition of N_2O_5 is in reality a chemically complex process involving the transient intermediate NO_3—a well-recognized substance which plays an important role in related reactions.[3] Steps of the suggested mechanism follow, with indicated rate constants.

(1) $N_2O_5 \rightarrow NO_3+NO_2$ k_1
(2) $NO_3+NO_2 \rightarrow N_2O_5$ k_2
(3) $NO_3+NO_2 \rightarrow NO_2+O_2+NO$ k_3
(4) $NO+N_2O_5 \rightarrow 3NO_2$—rapid

The rate constant k_2 would be expected to be similar in magnitude to that for the corresponding recombination of NO_2 radicals—known to have at most a very small activation energy.[3] However, it will appear that reaction (3) is endothermic, and hence has appreciable activation energy. Consequently, at relatively low temperatures (~25°C), $k_3 \ll k_2$. By the usual "steady-state" treatment one finds

$$-\frac{d(N_2O_5)}{dt} = 2\frac{d(NO)}{dt} = 2\frac{k_1k_3}{k_2+k_3}(N_2O_5) \sim 2\frac{k_1}{k_2}k_3(N_2O_5).$$

The apparent first-order rate constant is thus in reality the product of an *equilibrium* constant (k_1/k_2) and a *second-order* rate constant (k_3). Hence no "falling off" of constants at low pressures is to be expected. The exhaustive experimental tests[3] have shown this to be the case—a fact for which no reasonable explanation could be offered on the basis of the collisional activation theory of first-order reactions.

The proposed quasi-equilibrium dissociation of N_2O_5 is supported by the observations of Ramsperger and Tolman[4] that at extremely low concentrations the ratio of final to initial pressures falls considerably *below* the value 2.5 corresponding to the reaction $N_2O_5 \rightarrow 2NO_2+\frac{1}{2}O_2$. The data of these authors allow one to estimate rough values of the equilibrium constants for the dissociation $N_2O_5 \rightleftarrows NO_3+NO_2$. If the corresponding entropy change is assumed to be similar to those for N_2O_4 and N_2O_3 dissociation, the dissociation energy is estimated very approximately as some 18–22 kcal. per mole (compare 14.0 and 9.7 for N_2O_4 and N_2O_3, respectively[5]).

The revised thermochemical values supply the strongest support of the proposed mechanism. Denoting reaction energies as "E," activation energies as "Q," and experimental values by the subscript "Ex," since

$$k_{Ex} = 2(k_1/k_2)k_3, \quad Q_{Ex} = E_1+Q_3.$$

However, if (3) is endothermic by amount E_3, $Q_3 \geqq E_3$ and hence $Q_{Ex} \geqq E_1+E_3$. Adding (1) and (3) and applying Hess' Law

$$N_2O_5 \rightarrow NO+NO_2+O_2-E_1-E_3.$$

From the above new data, $E_1+E_3 = 24.3$ kcal.—as compared with $Q_{Ex} = 24.6$ kcal. The near identity of these values suggests that Q_3 exceeds E_3 by very little. If E_1 is taken roughly as ~20 kcal., Q_3 is thus ~5 kcal.—a value sufficient to ensure the inequality $k_3 \ll k_2$.

[1] M. Berthelot, Ann. Chim. Phys. (5) **4**, 8 (1875).
[2] F. R. Bichowsky and F. D. Rossini, *Thermochemistry of Chemical Substances* (Reinhold Publishing Corporation, New York, 1936).
[3] L. S. Kassel, *Kinetics of Homogeneous Gas Reactions* (Chemical Catalogue Company, New York, 1932).
[4] H. C. Ramsperger and R. C. Tolman, Proc. Nat. Acad. Sci. **16**, 6 (1930).
[5] F. H. Verhoek and F. Daniels, J. Am. Chem. Soc. **53**, 1250 (1931).

The Detection of Radioactive Persulfate Fragments in Emulsion Polymerized Styrene

WENDELL V. SMITH AND HERBERT N. CAMPBELL
General Laboratories of the United States Rubber Company, Passaic, New Jersey
February 4, 1947

PRICE and co-workers[1] have shown that fragments of organic peroxide catalysts are chemically combined with polystyrene polymerized in oil phase. It is a much more difficult problem to demonstrate by chemical analysis the presence in the polymer of fragments of the inorganic peroxides normally used as catalysts in emulsion polymerization because of the high molecular weights of the polymers produced in emulsion in the absence of chain transfer agents. However, by the use of potassium persulfate prepared from radioactive S^{35} it has now been found that fragments (containing sulfur) of the potassium persulfate used as a catalyst in the emulsion polymerization of styrene are chemically combined with the polystyrene.

Radioactive potassium persulfate was prepared by electrolysis of potassium sulfate in sulfuric acid containing radioactive S^{35}. The radioactive S^{35} was received as a trace constituent of potassium chloride supplied by the Clinton Laboratories of the Monsanto Chemical Company.

The active potassium persulfate was used as a catalyst in polymerizing styrene in a soap emulsion. The polystyrene produced was purified by precipitating it from the emulsion with methyl alcohol, then dissolving in benzene and reprecipitating with methyl alcohol, the dissolving and reprecipitating being done three successive times. The polystyrene was then examined for radioactivity with a Geiger counter of the end window type.[2]

The background count was 2.5 counts per sec. A 0.1-mg sample of the potassium persulfate dried from solution in an aluminum dish gave a count of 480 $sec.^{-1}$. A sample of 50 mg of the purified polystyrene gave a count of 65.9 $sec.^{-1}$. An additional purification of the polystyrene by precipitating from benzene with methyl alcohol left the activity substantially unchanged, i.e., the count obtained was 65.3 $sec.^{-1}$.

Thus, sulfur containing fragments of the persulfate must be chemically combined with the polystyrene. We are now endeavoring to obtain the quantitative relation between persulfate fragments and number of polymer molecules.

[1] C. C. Price, R. W. Kell, and E. Krebs, J. Am. Chem. Soc. **64**, 1103 (1942); C. C. Price and B. E. Tate, J. Am. Chem. Soc. **65**, 517 (1943).
[2] P. E. Yankwich, G. K. Rollefson, and T. H. Norris, J. Chem. Phys. **14**, 131 (1946); F. C. Henriques, Jr., G. B. Kistiakowsky, C. Margnetti, and W. G. Schneider, Ind. Eng. Chem. Anal. Ed. **18**, 349 (1946).

A Bond Energy Relation for Multiple Bonds

H. J. BERNSTEIN
Division of Chemistry, National Research Council, Ottawa, Canada
February 26, 1947

MAKING use of the notion of preserved tetrahedral angles and circularly bent single bonds constituting multiple bonds,[1] the following energy relation is obtained, *viz.*,

$$E=E_1(1+p)\left[1-c\left(\frac{R_1}{R}\right)^2\left(\frac{R_1-R}{R_1}\right)\right] \qquad (1)$$

where p is the bond order and equal to 0, 1, 2 for single, double, and triple bonds, respectively; E_1 is the single bond energy, R_1 is the single bond distance, and c is a constant.

Using Pauling's[2] values for the multiple bond energies of the CC and CN bonds, the observed and calculated values of the double bond energies and of the CC bond energy in benzene are compared.

	Single bond	Double bond	Triple bond	Benzene
CC cal. (Obs.)†	58.6	100	123	86
CC cal. (calc. from (1))	58.6*	99	123*	87.2[a]
R in A	1.55	1.33	1.21	1.39
CN cal. (Obs.)	48.6	94	144	
CN cal. (calc. from (1))	48.6*	96.5	144*	
R in A	1.47	1.27	1.15	

† Bond energies and bond distances from Pauling, reference 2.
* These more reliable values were used to calculate the constant of Eq. (1).
[a] The bond order for benzene was taken as $p=2/3$[3]; the calculated bond order from Eq. (1) and the value 86 cal. is 0.64 which is intermediate to the values .667 and .623 given by Coulson, Proc. Roy. Soc. **169**, 413 (1939) and Penney, Proc. Roy. Soc. **A158**, 306 (1937), respectively.

Equation (1) which involves two constants reproduces the data to within ±2.5 percent in the worst cases and with better accuracy in the single to double bond range. Until more reliable bond energies are known it is probably just as accurate and certainly more expedient to use this expression rather than one involving more constants.[3]

Where a bond distance or a bond order is known the order or distance may be calculated from the relation $R=R_1[2/3+1/3(1/3)^{p/2}]$ for first row atoms[1] and the corresponding bond energies evaluated from Eq. (1).

[1] H. J. Bernstein, J. Chem. Phys. **15**, 284 (1947), see appendix.
[2] L. Pauling, *The Nature of the Chemical Bond* (Cornell University Press, Ithaca, New York, 1939).
[3] J. L. Kavanau, J. Chem. Phys. **15**, 77 (1947). In this paper a three constant expression for the bond energy as a function of bond order is given in the form $E=E_0\left[1-\left(1-\frac{1+p}{A}\right)^B\right]$ where E_0, A, B are constants and p is the bond order.

Errata: "Vibrational Frequencies of the Isotopic Water Molecules; Equilibria with the Isotopic Hydrogens"

[J. Chem. Phys. **11**, 101 (1943)]
W. F. LIBBY
Institute for Nuclear Studies and Department of Chemistry, University of Chicago, Chicago, Illinois

IN applying their elegantly simplified method[1] for calculating isotopic equilibria to the water-hydrogen equilibria, Drs. Goeppert-Mayer and Bigeleisen discovered certain discrepancies in the above paper. The errors were arithmetical.

Table XI, Frequencies and anharmonicities of hydrogen molecules:

Multiply all anharmonicities by two.

Table XII, H_0^0 values:

Change values for hydrogen molecules to 6208, 5389, 4411, 4030, 3610, 5084 in the order given previously.

Table XIII, $(F-H_0^0)/T$ values:

HDO, DTO, T_2O up by 0.05, 0.11, and 0.29, respectively, at all temperatures (e.g., for HDO at 25°C change −39.80 to −39.75).

Table XIV, Moments of inertia:

Change value for HDO from 16.6 to 16.2.

These changes cause up to 5 percent correction on three of the nine equilibrium constants. The corrected values are:

TABLE XV. Equilibrium constants.

	Equilibrium	20°C	100°C	200°C	300°C	400°C	500°C
(5)	$\frac{(HDO)}{(H_2O)(D_2O)}$	3.89	3.96	3.97	3.97	3.97	4.00
(8)	$\frac{(HTO)^2}{(H_2O)(T_2O)}$	3.44	3.63	3.83	3.86	3.95	4.00
(9)	$\frac{(DTO)^2}{(D_2O)(T_2O)}$	3.59	3.69	3.74	3.78	3.83	3.86

The equilibria (1) and (2), (3), (4), (6), and (7) for the partition of the hydrogen isotopes between the water and hydrogen molecules are unchanged.

[1] J. Bigeleisen and M. G. Mayer, J. Chem. Phys. **15**, 261 (1947).